Spring 2022

Efficient Estimation of Signals via Non-Convex Approaches

Sheng Xu
Yale University Graduate School of Arts and Sciences, xusheng920821@gmail.com

Abstract

Efficient Estimation of Signals via Non-Convex Approaches

Sheng Xu

2022

This dissertation aims to highlight the importance of methodological development and the need for tailored algorithms in non-convex statistical problems. Specifically, we study three non-convex estimation problems with novel ideas and techniques in both statistical methodologies and algorithmic designs.

Chapter 2 discusses my work with Zhou Fan on estimation of a piecewise-constant image, or a gradient-sparse signal on a general graph, from noisy linear measurements. We propose and study an iterative algorithm to minimize a penalized least-squares objective, with a penalty given by the "ℓ_0-norm" of the signal's discrete graph gradient. The method uses a non-convex variant of the proximal gradient descent, applying the alpha-expansion procedure to approximate the proximal mapping in each iteration and using a geometric decay of the penalty parameter across iterations to ensure convergence. Under a cut-restricted isometry property for the measurement design, we prove global recovery guarantees for the estimated signal. For standard Gaussian designs, the required number of measurements is independent of the graph structure, and improves upon worst-case guarantees for total-variation (TV) compressed sensing on the 1-D line and 2-D lattice graphs by polynomial and logarithmic factors, respectively. The method empirically yields lower mean-squared recovery error compared with TV regularization in the regimes of moderate undersampling and moderate to high signal-to-noise, for several examples of changepoint signals and gradient-sparse phantom images.

Chapter 3 discusses my work with Zhou Fan and Sahand Negahban on a tree-projected gradient descent for estimating gradient-sparse parameters. We consider estimating a gradient-sparse parameter $\boldsymbol{\theta}^* \in \mathbb{R}^p$, having strong gradient-sparsity $s^* := \|\nabla_G \boldsymbol{\theta}^*\|_0$ on an underlying graph G. Given observations $Z_1, \ldots, Z_n$ and a smooth, convex loss function $\mathcal{L}$ for which our parameter of interest $\boldsymbol{\theta}^*$ minimizes the population risk $\mathbb{E}[\mathcal{L}(\boldsymbol{\theta}; Z_1, \ldots, Z_n)]$, we propose to estimate $\boldsymbol{\theta}^*$ by a projected gradient descent algorithm that iteratively and approximately projects gradient steps onto spaces of vectors having small gradient-sparsity over low-degree spanning trees of G. We show that, under suitable restricted strong convexity and smoothness assumptions for the loss, the resulting estimator achieves the squared-error risk $\frac{s^*}{n} \log(1 + \frac{p}{s^*})$ up to a multiplicative constant that is independent of G. In contrast, previous polynomial-time algorithms have only been shown to achieve this guarantee

in more specialized settings, or under additional assumptions for G and/or the sparsity pattern of $\nabla_G \boldsymbol{\theta}^*$. As applications of our general framework, we apply our results to the examples of linear models and generalized linear models with random designs.

Chapter 4 discusses my joint work with Zhou Fan, Roy R. Lederman, Yi Sun, and Tianhao Wang on maximum likelihood for high-noise group orbit estimation. Motivated by applications to single-particle cryo-electron microscopy (cryo-EM), we study several problems of function estimation in a low SNR regime, where samples are observed under random rotations of the function domain. In a general framework of group orbit estimation with linear projection, we describe a stratification of the Fisher information eigenvalues according to a sequence of transcendence degrees in the invariant algebra, and relate critical points of the log-likelihood landscape to a sequence of method-of-moments optimization problems. This extends previous results for a discrete rotation group without projection. We then compute these transcendence degrees and the forms of these moment optimization problems for several examples of function estimation under $\mathsf{SO}(2)$ and $\mathsf{SO}(3)$ rotations. For several of these examples, we affirmatively resolve numerical conjectures that 3^{rd}-order moments are sufficient to locally identify a generic signal up to its rotational orbit, and also confirm the existence of spurious local optima for the landscape of the population log-likelihood. For low-dimensional approximations of the electric potential maps of two small protein molecules, we empirically verify that the noise-scalings of the Fisher information eigenvalues conform with these theoretical predictions over a range of SNR, in a model of $\mathsf{SO}(3)$ rotations without projection.

Efficient Estimation of Signals via Non-Convex Approaches

A Dissertation
Presented to the Faculty of the Graduate School
of
Yale University
in Candidacy for the Degree of
Doctor of Philosophy

By
Sheng Xu

Dissertation Directors: Zhou Fan and Sahand Negahban

May, 2022

Contents

List of Figures

List of Tables

Acknowledgements

First and foremost, I would like to express my sincere gratitude to my terrific Ph.D. advisors Professor Zhou Fan and Professor Sahand Negahban. I was so fortunate to be Zhou's first student at Yale. I have learned many deep insights from the discussion with him in our regular weekly meetings for over three years. Impressed by his passion, perseverance, and diligence, I have learned to put high standard on my own research. It has always been pleasant to work with Sahand. My research life became more delightful and creative because of his humor and fantastic ideas. Without their tremendous support, encouragement, patience, and mentorship, the work in this dissertation would not have been possible.

I am deeply grateful to Professor Andrew R. Barron, for his kindness, time, and efforts to be on my thesis committee, and his support and guidance throughout my Ph.D. studies. My thanks also go to other professors at Yale, in particular Xiaohong Chen, Joseph Chang, Forrest Crawford, John W. Emerson, Anna Gilbert, John Lafferty, Roy R. Lederman, Peter C. B. Phillips, David Pollard, Fredrik Sävje, Jas Sekhon, Dan Spielman, Sekhar Tatikonda, Van H. Vu, Yihong Wu, Hongyu Zhao, Harrison Huibin Zhou for their advice and mentorship. I would also thank professors outside Yale: Yi Sun at University of Chicago, Brian Caffo, Nilanjan Chatterjee, Constantine Frangakis, Hongkai Ji, Michael Rosenblum, Daniel Scharfstein, Mei-Cheng Wang at Johns Hopkins, and Fang Han at University of Washington. Thanks to my past and current collaborators: Lin Chen, Wayne Yuan Gao, Ming Li, Huitong Qiu, and Wen-Xin Zhou.

I would also express my gratitude to our department and Ph.D. program. I am grateful to all the staff, especially Joann DelVecchio and Karen Kavanaugh. I have also benefitted hugely from my excellent fellow students, in particular Colleen Chan, Chao Gao, Soham Jana, Zifan Li, Yu Lu, Curtis McDonald, Ganlin Song, Tianhao Wang, Ruitu Xu, Xin Xu, Dana Xiaoqian Yang, Anderson Ye Zhang, Mingrui Zhang, and Xinyi Zhong. Further I would like to thank my academic friends outside Yale, including but not limited to Shizhe Chen, Yilun Chen, Junrui Di, Lihua Lei, Chen Lian, Song Mei, Zhichao Jiang, Tianchen Qian, Zhihao Tang, Feng Ruan, Zhuoran Yang, Yuting Ye,

Haoyu Zhang, Ruixiang Zhang, Ruofei Zhao, Yiqiao Zhong, Daisy Yuxin Zhu, and Ziquan Zhuang.

I am fortunate to have met Haoran here at Yale, whose love and support have brightened my day through the journey.

Finally, I would like to thank my family. My parents and family are always supportive and have their faith in me. I could not have made any achievement without their unconditional love and support.

Chapter 1

Introduction

Modern scientific research often involves developing efficient statistical methods to extract actionable knowledge from complex datasets. Implementing those methods naturally requires designing reliable, scalable, and robust learning algorithms in high dimensions. With the rapid advances of modeling tools and the proliferation of empirical success, non-convex optimization has received considerable attention. Yet, a plethora of non-convex problems cannot be solved, or at least efficiently solved, by convex relaxation or off-the-shelf first-order algorithms. As a consequence, more in-depth analyses are crucial for methodological development in those complex problems and the resulting methods should be tailored to achieve the desired efficiency.

Despite the large ambient dimensions in many applications, the structure of interest in the data is often low-dimensional or sparse intrinsically. This idea of parsimony dates back to the Ancient Greece. Philosopher and polymath Aristotle wrote "Nature operates in the shortest way possible."(Gibbs and Hiroshi, 1996) This remarkable heuristic rule of thumb still sheds light on the imposition of structural constraints on the learning models in modern statistics. Such constraints, which naturally involve non-convex formulations, not only reflect the scientific domain knowledge, but are often critical to interpret statistical models and prevent the problems from being ill-posed. Examples include compressed sensing (Donoho, 2006; Baraniuk, 2007; Candès and Wakin, 2008), sparse regression (Fan and Li, 2001; Zhang, 2010), sparse PCA (d'Aspremont et al., 2004; Zou et al., 2006; Cai et al., 2013), and low-rank matrix completion (Candès and Recht, 2009; Candès and Tao, 2010; Davenport and Romberg, 2016). Because of computational barriers of non-convex optimization, convex relaxation has been widely used. However, such modification has limitations. For instance, in the absence of certain stability conditions, the popular LASSO method for sparse

regression may yield inconsistent estimators (Zhao and Yu, 2006; Meinshausen and Bühlmann, 2006). For compressed sensing, ℓ_1 or total variation relaxation suffers from poor scalability (Donoho and Tanner, 2006; Needell and Ward, 2013b). These results suggest the tremendous value of studying non-convex optimization directly.

In many other applications, the natural objective of the learning problem is non-convex. Notable examples include Gaussian mixture models (Dasgupta, 1999), deep neural networks (LeCun et al., 2015; Schmidhuber, 2015), and tensor decompositions (Kolda and Bader, 2009; Sidiropoulos et al., 2017). While vanilla procedures such as gradient descent achieve statistical accuracy and computational efficiency simultaneously in certain non-convex estimation problems (Chen and Candès, 2015; Candès et al., 2015; Ma et al., 2018; Du et al., 2019), the success relies on two key geometrical properties of the associated non-convex objective functions: a reasonably large basin of attraction around the global solution and/or benign global optimization landscape (Chi et al., 2019). However, those benign structures amenable to computation do not necessarily carry over to other problems and simple first-order methods may get stuck in suboptimal local minima. Dauphin et al. (2014) further argue that the existence of saddle points is more notorious for learning tasks and often gives the illusory impression of reaching a spurious local minimum. Therefore, delicate landscape analyses are essential to developing efficient methods and designing scalable algorithms.

In my dissertation, I will investigate two main non-convex statistical estimation problems. In Chapter 2 and Chapter 3, we study estimation of piecewise-constant or gradient-sparse signals. We propose iterative, approximate, and polynomial-time algorithms to directly solve non-convex objectives and improve estimation guarantees upon existing convex approaches under suitable conditions. In Chapter 4, motivated by applications to single-particle cryo-electron microscopy, we study group orbit estimation with potential linear projections. To understand both local and global behaviors of maximum likelihood estimation procedures, we describe the geometry of the Fisher information matrix and log-likelihood landscape and their relation to the algebraic structure of the underlying rotational group.

Chapter 2

Iterative Alpha Expansion for Estimating Gradient-Sparse Signals

2.1 Introduction

Consider an unknown signal $\mathbf{x}_* \in \mathbb{R}^p$ observed via n noisy linear measurements

$$\mathbf{y} = \mathbf{A}\mathbf{x}_* + \mathbf{e} \in \mathbb{R}^n.$$

We study the problem of estimating $\mathbf{x}_*$, under the assumption that its coordinates correspond to the p vertices of a given graph $G = (V, E)$, and $\mathbf{x}_*$ is gradient-sparse. By this, we mean that

$$\|\nabla \mathbf{x}_*\|_0 \equiv \sum_{(i,j)\in E} \mathbf{1}\{x_{*,i} \neq x_{*,j}\} \tag{2.1}$$

is much smaller than the total number of edges $|E|$. Special cases of interest include the 1-D line graph, where variables have a sequential order and $\mathbf{x}_*$ has a changepoint structure, and the 2-D lattice graph, where coordinates of $\mathbf{x}_*$ represent pixels of a piecewise-constant image.

This problem has been studied since early pioneering works in compressed sensing (Candès et al., 2006a,b; Donoho, 2006). Among widely-used approaches for estimating $\mathbf{x}_*$ are those based on constraining or penalizing the total-variation (TV) semi-norm (Rudin et al., 1992), which may be

defined (anisotropically) for a general graph as

$$\|\nabla \mathbf{x}\|_1 \equiv \sum_{(i,j)\in E} |x_i - x_j|.$$

These are examples of ℓ_1-analysis methods (Elad et al., 2007; Candès et al., 2011; Nam et al., 2013), which regularize the ℓ_1-norm of a general linear transform of $\mathbf{x}$ rather than of its coefficients in an orthonormal basis. Related fused-lasso methods have been studied for different applications of regression and prediction in Tibshirani et al. (2005); Rinaldo (2009); Tibshirani (2011); Padilla et al. (2017). Other graph-based regularization methods were studied in Krishnamuthy et al. (2013); Li et al. (2018); Kim and Gao (2019), and generalizations to trend-filtering methods that regularize higher-order discrete derivatives of $\mathbf{x}$ were studied in Kim et al. (2009); Wang et al. (2016).

The reconstruction error of TV-regularization depends on the structure of the graph (Needell and Ward, 2013b,a; Cai and Xu, 2015). More generally, the error of ℓ_1-analysis methods with sparsifying transform ∇ depends on sparse conditioning properties of the pseudo-inverse $\nabla^\dagger$ (Candès et al., 2011). For direct measurements $\mathbf{A} = \mathbf{I}$, these and related issues were discussed in Hütter and Rigollet (2016); Dalalyan et al. (2017); Fan and Guan (2018), which showed in particular that TV-regularization may not achieve the same recovery guarantees as analogous ℓ_0-regularization methods on certain graphs including the 1-D line. In this setting of $\mathbf{A} = \mathbf{I}$, different computational approaches also exist to approximately minimize an ℓ_0-regularized objective on general graphs (Boykov et al., 1999; Kleinberg and Tardos, 2002; Xu et al., 2011).

Motivated by this line of work, our current paper studies an alternative to TV-regularization in the more difficult setting of indirect linear measurements, where $\mathbf{A} \neq \mathbf{I}$. Our procedure is based similarly on the idea of minimizing a possibly non-convex objective

$$F(\mathbf{x}) = \frac{1}{2}\|\mathbf{y} - \mathbf{A}\mathbf{x}\|_2^2 + \lambda \sum_{(i,j)\in E} c(x_i, x_j) \tag{2.2}$$

for an edge-associated cost function c. We will focus attention in this work on the specific choice of an ℓ_0-regularizer

$$c(x_i, x_j) = \mathbf{1}\{x_i \neq x_j\}, \tag{2.3}$$

which matches (2.1), although the algorithm may be applied with more general choices of metric

edge cost. For the above ℓ_0 edge cost, the resulting objective takes the form

$$F(\mathbf{x}) = \frac{1}{2}\|\mathbf{y} - \mathbf{A}\mathbf{x}\|_2^2 + \lambda\|\nabla\mathbf{x}\|_0.$$

For $\mathbf{A} = \mathbf{I}$, Fan and Guan (2018) analyzed the alpha-expansion algorithm of Boykov et al. (1999) for minimizing this objective, and showed that it can achieve statistically rate-optimal estimation guarantees. We review this method in Section 2.2. Its algorithmic idea is specific to $\mathbf{A} = \mathbf{I}$, where the objective (2.2) decomposes as a sum of terms involving only individual variables x_i and pairs (x_i, x_j), and this idea does not easily extend to indirect linear measurements. In this work, we instead study an approach of applying this method to minimize $F(\mathbf{x})$ using a non-convex and non-smooth variant of proximal gradient descent: For parameters $\gamma \in (0, 1)$ and $\eta > 0$, we iteratively compute $\mathbf{x}_{k+1}$ from $\mathbf{x}_k$ via

$$\begin{aligned}
\mathbf{a}_{k+1} &\leftarrow \mathbf{x}_k - \eta\mathbf{A}^\mathsf{T}(\mathbf{A}\mathbf{x}_k - \mathbf{y}) \\
\mathbf{x}_{k+1} \text{“} &\leftarrow \text{”} \operatorname*{argmin}_{\mathbf{x}} \frac{1}{2}\|\mathbf{x} - \mathbf{a}_{k+1}\|_2^2 + \lambda_k \sum_{(i,j)\in E} c(x_i, x_j) \\
\lambda_{k+1} &\leftarrow \lambda_k \cdot \gamma
\end{aligned}$$

The update for $\mathbf{x}_{k+1}$ is carried out approximately, using the alpha-expansion idea. We call this algorithm ITALE, for ITerative ALpha Expansion.

There are two important differences between ITALE and standard proximal gradient methods for convex problems (Beck and Teboulle, 2009; Parikh and Boyd, 2014). First, since the edge cost $c(x_i, x_j)$ is non-convex, the minimization problem for updating $\mathbf{x}_{k+1}$ is also non-convex. That such an algorithm should converge is not as evident as for proximal gradient methods applied with convex penalties. Second, to ensure that the algorithm indeed converges, we must start with a large initialization for the penalty $\lambda_{\max}$ and geometrically decay this penalty across iterations. This is the case even if we were only interested in one final tuning parameter λ in the objective (2.2). This type of penalty decay was studied previously in a convex setting by Xiao and Zhang (2013), but the purpose there was to improve the convergence rate rather than to ensure convergence.

In practice, for γ sufficiently close to 1, we directly interpret the sequence of ITALE iterates $\mathbf{x}_k$ as approximate minimizers of the objective function (2.2) for penalty parameters $\lambda = \lambda_k/\eta$ along a regularization path. We comment more on this approach in Section 2.2. We select the iterate k using cross-validation on the prediction error for $\mathbf{y}$, and we use the final estimate $\hat{\mathbf{x}}^{\text{ITALE}} = \mathbf{x}_k$.

Despite $F(\mathbf{x})$ being non-convex and non-smooth, we provide global recovery guarantees for ITALE. For example, under exact gradient-sparsity $\|\nabla \mathbf{x}_*\|_0 = s_*$, if $\mathbf{A}$ consists of

$$n \gtrsim s_* \log(1 + |E|/s_*) \tag{2.4}$$

linear measurements with i.i.d. $\mathcal{N}(0, 1/n)$ entries, then the ITALE iterate $\mathbf{x}_k$ for the ℓ_0-regularizer (2.3) and a penalty value $\lambda_k \asymp \|\mathbf{e}\|_2^2/s_*$ satisfies, with high probability,

$$\|\mathbf{x}_k - \mathbf{x}_*\|_2 \lesssim \|\mathbf{e}\|_2. \tag{2.5}$$

More generally, we provide recovery guarantees when $\mathbf{A}$ satisfies a certain cut-restricted isometry property, described in Definition 2.3.1 below. Note that (2.5) is the optimal worst-case error guarantee for deterministic measurement errors $\mathbf{e}$, which is the typical setting studied in the compressed sensing literature (Candès et al., 2006b,a; Blumensath and Davies, 2009; Needell and Tropp, 2009) and also the setting that we study in this work.

Even for i.i.d. Gaussian design, we are not aware of previous polynomial-time algorithms which provably achieve this guarantee for either the 1-D line or the 2-D lattice. In particular, connecting with the previous discussion, similar existing results for TV-regularization in noisy or noiseless settings require $n \gtrsim s_*(\log|E|)^3$ Gaussian measurements for the 2-D lattice and $n \gtrsim \sqrt{|E|s_*}\log|E|$ measurements for the 1-D line (Needell and Ward, 2013b; Cai and Xu, 2015). Applying thresholding or ℓ_1-regularization instead to a representation of $\mathbf{x}_*$ in a spanning tree wavelet basis, as proposed and studied in Padilla et al. (2017), would reduce this requirement for n to be optimal up to a logarithmic factor. The requirement for n in ITALE is instead optimal up to a constant factor, for any bounded-degree graph.

Figure 2.1 compares in simulation $\hat{\mathbf{x}}^{\mathrm{ITALE}}$ using the ℓ_0-regularizer (2.3) with $\hat{\mathbf{x}}^{\mathrm{TV}}$ (globally) minimizing the TV-regularized objective

$$F^{\mathrm{TV}}(\mathbf{x}) = \frac{1}{2}\|\mathbf{y} - \mathbf{A}\mathbf{x}\|_2^2 + \lambda\|\nabla \mathbf{x}\|_1. \tag{2.6}$$

The example depicts a synthetic image of a human chest slice, previously generated by Gong et al. (2017) using the XCAT digital phantom (Segars et al., 2010). The design $\mathbf{A}$ is an undersampled and reweighted Fourier matrix, using a sampling scheme described in Section 2.3 and similar to that proposed in Krahmer and Ward (2014) for TV-regularized compressed sensing. In a low-noise setting, a detailed comparison of the recovered images reveals that $\hat{\mathbf{x}}^{\mathrm{ITALE}}$ provides a sharper reconstruction

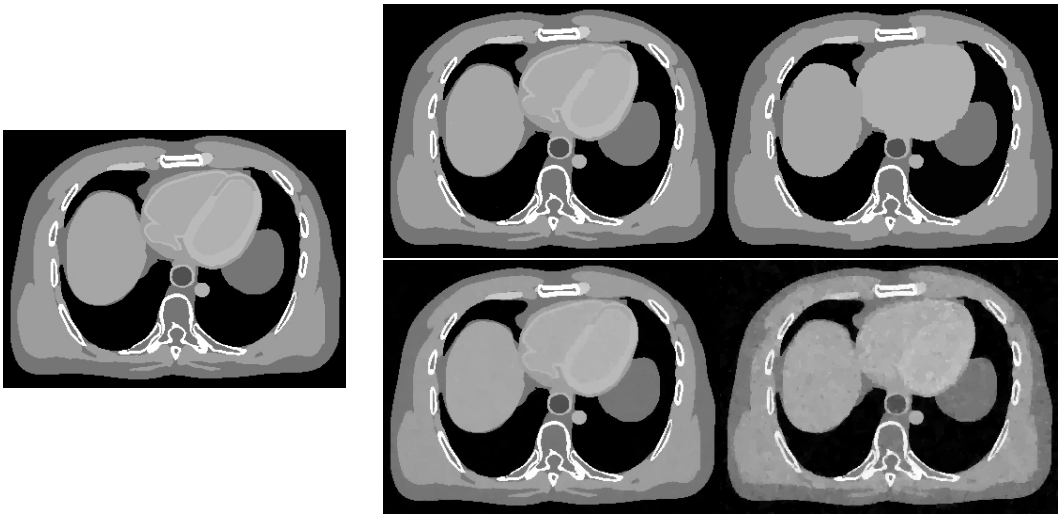

Figure 2.1: Left: Original image slice from the XCAT digital phantom. Top row: $\hat{\mathbf{x}}^{\text{ITALE}}$ from 20% undersampled and reweighted Fourier measurements, in low noise ($\sigma = 4$, left) and medium noise ($\sigma = 16$, right) settings. Bottom row: $\hat{\mathbf{x}}^{\text{TV}}$ for the same measurements. The iterate k in ITALE and tuning parameter λ for TV were both selected using 5-fold cross-validation on the squared prediction error for $\mathbf{y}$.

than $\hat{\mathbf{x}}^{\text{TV}}$. As noise increases, $\hat{\mathbf{x}}^{\text{TV}}$ becomes blotchy, while $\hat{\mathbf{x}}^{\text{ITALE}}$ begins to lose finer image details. Quantitative comparisons of recovery error are provided in Section 2.4.2 and are favorable towards ITALE in lower noise regimes.

ITALE is similar to some methods oriented towards ℓ_0-regularized sparse regression and signal recovery (Tropp and Gilbert, 2007; Zhang, 2011; Bertsimas et al., 2016), including notably the Iterative Hard Thresholding (IHT) (Blumensath and Davies, 2009) and CoSaMP (Needell and Tropp, 2009) methods in compressed sensing. We highlight here several differences:

- For sparsity in an orthonormal basis, forward stepwise selection and orthogonal matching pursuit provide greedy "ℓ_0" approaches to variable selection, also with provable guarantees (Tropp and Gilbert, 2007; Zhang, 2011; Elenberg et al., 2018). However, such methods do not have direct analogues for gradient-sparsity in graphs, as one cannot select a single edge difference $x_i - x_j$ to be nonzero without changing other edge differences.

- IHT and CoSaMP enforce sparsity of $\mathbf{x}_{k+1}$ in each iteration by projecting to the s largest coordinates of $\mathbf{a}_{k+1}$, for user-specified s. In contrast, ITALE uses a Lagrangian form that penalizes (rather than constrains) $\|\nabla \mathbf{x}_{k+1}\|_0$. This is partly for computational reasons, as we are not aware of fast algorithms that can directly perform such a projection step onto the (non-convex) set $\{\mathbf{x} : \|\nabla \mathbf{x}\|_0 \leq s\}$ for general graphs. This Lagrangian form complicates the theoretical convergence analysis, as it requires establishing simultaneous control of the gradient

sparsity $\|\nabla \mathbf{x}_k\|_0$ and the error $\|\mathbf{x}_k - \mathbf{x}_*\|_2$ in each iteration.

- In contrast to general-purpose mixed-integer optimization procedures studied in Bertsimas et al. (2016), each iterate of ITALE (and hence also the full algorithm, for a polynomial number of iterations) is provably polynomial-time in the input size $(n, p, |E|)$ (Fan and Guan, 2018). On our personal computer, for the $p = 360 \times 270 = 97200$ image of Figure 2.1, computing the 60 iterates constituting a full ITALE solution path required about 20 minutes, using the optimized alpha-expansion code of Boykov and Kolmogorov (2004).

While our theoretical focus is on ℓ_0-regularization, we expect that for certain regimes of undersampling and signal-to-noise, improved empirical recovery may be possible with edge costs $c(x_i, x_j)$ interpolating between the ℓ_0 and ℓ_1 penalties. These are applicable in the ITALE algorithm and would be interesting to investigate in future work.

2.2 Model and algorithm

Let $G = (V, E)$ be a given connected graph on the vertices $V = \{1, \ldots, p\}$, with undirected edge set E. We assume throughout that $p \geq 3$. For a signal vector $\mathbf{x}_* \in \mathbb{R}^p$, measurement matrix $\mathbf{A} \in \mathbb{R}^{n \times p}$, and measurement errors $\mathbf{e} \in \mathbb{R}^n$, we observe

$$\mathbf{y} = \mathbf{A}\mathbf{x}_* + \mathbf{e} \in \mathbb{R}^n. \tag{2.7}$$

Denote by $\nabla \in \{-1, 0, 1\}^{|E| \times p}$ the discrete gradient matrix on the graph G, defined by

$$\nabla \mathbf{x} = \big(x_i - x_j : \ (i, j) \in E\big) \in \mathbb{R}^{|E|}.$$

Here, we may fix an arbitrary ordering of the vertex pair (i, j) for each edge. We study estimation of $\mathbf{x}_*$, assuming that $\mathbf{x}_*$ has (or is well-approximated by a signal having) small exact gradient sparsity $\|\nabla \mathbf{x}_*\|_0$.

Our proposed algorithm is an iterative approach called ITALE, presented as Algorithm 1. It is based around the idea of minimizing the objective (2.2). In this objective, the cost function $c : \mathbb{R}^2 \to \mathbb{R}$ must satisfy the metric properties

$$c(x, y) = c(y, x) \geq 0, \qquad c(x, x) = 0 \Leftrightarrow x = 0, \qquad c(x, z) \leq c(x, y) + c(y, z), \tag{2.8}$$

but is otherwise general. Importantly, c may be non-smooth and non-convex. The algorithm alternates between constructing a surrogate signal $\mathbf{a}_{k+1}$ in line 3, denoising this surrogate signal in line 4, and geometrically decaying the penalty parameter λ_k used for the denoiser in line 5. We discuss these steps in more detail below.

The surrogate signal $\mathbf{a}_{k+1}$ that is computed in line 3 may be written as

$$\begin{aligned}\mathbf{a}_{k+1} &= \mathbf{x}_k - \eta \mathbf{A}^\mathsf{T}(\mathbf{A}\mathbf{x}_k - \mathbf{y}) \\ &= \mathbf{x}_* + (\mathbf{I} - \eta \mathbf{A}^\mathsf{T}\mathbf{A})(\mathbf{x}_k - \mathbf{x}_*) + \eta \mathbf{A}^\mathsf{T}\mathbf{e}.\end{aligned}$$

This is a noisy version of the true signal $\mathbf{x}_*$, with two sources of noise $(\mathbf{I} - \eta \mathbf{A}^\mathsf{T}\mathbf{A})(\mathbf{x}_k - \mathbf{x}_*)$ and $\eta \mathbf{A}^\mathsf{T}\mathbf{e}$. Line 4 denoises this signal by applying the alpha-expansion graph cut procedure from Boykov et al. (1999) to approximately solve the minimization problem

$$\min_{\mathbf{x} \in \mathbb{R}^p} \frac{1}{2}\|\mathbf{x} - \mathbf{a}_{k+1}\|_2^2 + \lambda_k \sum_{(i,j) \in E} c(x_i, x_j).$$

This sub-routine is denoted as AlphaExpansion$(\mathbf{a}_{k+1}, \lambda_k, \delta)$, and is described in Algorithm 2 for completeness. At a high level, the alpha-expansion method encodes the above objective function in the structure of an edge-weighted augmented graph, and iterates over global moves that swap the signal value on a subset of vertices for a given new value, by finding a minimum graph cut. The original alpha-expansion algorithm of Boykov et al. (1999) is in the setting of a discrete Potts model. To apply this to a continuous signal domain, we restrict coordinate values of $\mathbf{x}$ to a discrete grid

$$\delta\mathbb{Z} = \{k\delta : k \in \mathbb{Z}\}$$

for a small user-specified parameter $\delta > 0$.

The geometric decay of λ_k in line 5 may be understood by examining the two sources of error $(\mathbf{I} - \eta \mathbf{A}^\mathsf{T}\mathbf{A})(\mathbf{x}_k - \mathbf{x}_*)$ and $\eta \mathbf{A}^\mathsf{T}\mathbf{e}$ in $\mathbf{a}_{k+1}$. Assuming that $\mathbf{I} - \eta \mathbf{A}^\mathsf{T}\mathbf{A}$ has a small operator norm when restricted to gradient-sparse vectors, the first error term decays geometrically across iterations, whereas the second error term is fixed in every iteration. When $\mathbf{e} \neq 0$, this suggests choosing λ_k to also decay geometrically up to a final positive constant $\lambda_* > 0$, after which we may fix $\lambda_k = \lambda_*$ and run the iterations to convergence. In this approach, the best choice for λ_* would depend on the size of $\eta \mathbf{A}^\mathsf{T}\mathbf{e}$, and this may be set in practice using cross-validation.

We do not directly use this approach, because this requires a separate run for each different value

Algorithm 1 Iterative Alpha Expansion

Input: $\mathbf{y} \in \mathbb{R}^n$, $\mathbf{A} \in \mathbb{R}^{n \times p}$, and parameters $\gamma \in (0,1)$, $\lambda_{\max} > \lambda_{\min} > 0$, and $\eta, \delta > 0$.

Initialize $\mathbf{x}_0 \leftarrow \mathbf{0}$, $\lambda_0 \leftarrow \lambda_{\max}$
for $k = 0, 1, 2, \ldots, K$ until $\lambda_K < \lambda_{\min}$ **do**
  $\mathbf{a}_{k+1} \leftarrow \mathbf{x}_k - \eta \mathbf{A}^\mathsf{T}(\mathbf{A}\mathbf{x}_k - \mathbf{y})$
  $\mathbf{x}_{k+1} \leftarrow \text{AlphaExpansion}(\mathbf{a}_{k+1}, \lambda_k, \delta)$
  $\lambda_{k+1} \leftarrow \lambda_k \cdot \gamma$
end for

Output: $\mathbf{x}_1, \ldots, \mathbf{x}_K$

Algorithm 2 AlphaExpansion$(\mathbf{a}, \lambda, \delta)$ subroutine

Input: $\mathbf{a} \in \mathbb{R}^p$, cost function $c : \mathbb{R}^2 \to \mathbb{R}$, parameters $\lambda, \delta > 0$.

Let $a_{\min}, a_{\max}$ be the minimum and maximum values of $\mathbf{a}$. Initialize $\mathbf{x} \in \mathbb{R}^p$ arbitrarily.
loop
  for each $z \in \delta\mathbb{Z} \cap [a_{\min}, a_{\max}]$ **do**
    Construct the following edge-weighted augmentation $G_{z,\mathbf{x}}$ of the graph G:
      Introduce a source vertex s and a sink vertex t, connect s to each $i \in \{1, \ldots, p\}$ with weight $\frac{1}{2}(a_i - z)^2$, and connect t to each $i \in \{1, \ldots, p\}$ with weight $\frac{1}{2}(a_i - x_i)^2$ if $x_i \neq z$, or weight ∞ if $x_i = z$.
      for each edge $\{i, j\} \in E$ **do**
        if $x_i = x_j$ **then**
          Assign weight $\lambda c(x_i, z)$ to $\{i, j\}$.
        else
          Introduce a new vertex $v_{i,j}$, and replace edge $\{i, j\}$ by the three edges $\{i, v_{i,j}\}$, $\{j, v_{i,j}\}$, and $\{t, v_{i,j}\}$, with weights $\lambda c(x_i, z)$, $\lambda c(x_j, z)$, and $\lambda c(x_i, x_j)$ respectively.
        end if
      end for
    Find the minimum s-t cut (S, T) of $G_{z,\mathbf{x}}$ such that $s \in S$ and $t \in T$.
    For each $i \in \{1, \ldots, p\}$, update $x_i \leftarrow z$ if $i \in T$, and keep x_i unchanged if $i \in S$.
  end for
  If $\mathbf{x}$ was unchanged for each z above, then return $\mathbf{x}$.
end loop

Output: $\mathbf{x}$

of λ_* to perform the cross-validation. Instead, Algorithm 1 performs only a single proximal gradient step for each λ_k, starting from a value $\lambda_{\max} > \lambda_*$ that oversmooths the surrogate signal and ending at a value $\lambda_{\min} < \lambda_*$ that undersmooths the surrogate signal (when $\mathbf{e} \neq 0$). For γ sufficiently close to 1, we directly interpret each iterate $\mathbf{x}_k$ as an approximate minimizer of the objective (2.2) for a different penalty $\lambda \equiv \lambda_k/\eta$. We apply cross-validation to select the iterate $\mathbf{x}_k$ that represents the final estimate $\hat{\mathbf{x}}^{\text{ITALE}}$, and this corresponds to selecting a penalty λ in (2.2). Thus, Algorithm 1 computes an estimate for each tuning parameter along a regularization path, in a single pass of the proximal gradient descent. We find that this works well in practice and yields substantial savings in computational cost, and our theoretical analysis will also be for the algorithm in this form.

We make a few additional remarks regarding parameter tuning in practice:

- Using conservative choices for $\lambda_{\max}$ (large), γ (close to 1), and δ (small) increases the total

runtime of the procedure, but does not degrade the quality of recovery. In our experiments, we fix $\gamma = 0.9$ and set δ in each iteration to yield 300 grid values for $\delta\mathbb{Z} \cap [a_{\min}, a_{\max}]$ in Algorithm 2.

- We do not specify $\lambda_{\min}$. Instead, we monitor the gradient sparsity $\|\nabla \mathbf{x}_k\|_0$ across iterations, and terminate the algorithm when $\|\nabla \mathbf{x}_K\|_0$ exceeds a certain fraction (e.g. 50%) of the total number of edges $|E|$.

- The parameter η should be matched to the scaling and restricted isometry properties of the design matrix $\mathbf{A}$. For sub-Gaussian and Fourier designs scaled by $1/\sqrt{n}$ as in Propositions 2.3.2 and 2.3.3 below, we set $\eta = 1$.

- The most important tuning parameter is the iterate k for which we take the final estimate $\hat{\mathbf{x}}^{\mathrm{ITALE}} = \mathbf{x}_k$. In our examples, we apply 5-fold cross-validation on the mean-squared prediction error for $\mathbf{y}$ to select k. Note that η should be rescaled by the number of training samples in each fold, i.e. for 5-fold cross-validation with training sample size $0.8n$, we set $\eta = 1/0.8$ instead of $\eta = 1$ in the cross-validation runs.

2.3 Recovery guarantees

We provide in this section theoretical guarantees on the recovery error $\|\hat{\mathbf{x}}^{\mathrm{ITALE}} - \mathbf{x}_*\|_2$, where $\hat{\mathbf{x}}^{\mathrm{ITALE}} \equiv \mathbf{x}_k$ for a deterministic (non-adaptive) choice of iterate k. Throughout this section, ITALE is assumed to be applied with the ℓ_0 edge cost $c(x_i, x_j) = \mathbf{1}\{x_i \neq x_j\}$.

2.3.1 cRIP condition

Our primary assumption on the measurement design $\mathbf{A}$ will be the following version of a restricted isometry property.

Definition 2.3.1. *Let $\kappa > 0$, and let $\rho : [0, \infty) \to [0, \infty)$ be any function satisfying $\rho'(s) \geq 0$ and $\rho''(s) \leq 0$ for all $s > 0$. A matrix $\mathbf{A} \in \mathbb{R}^{n \times p}$ satisfies the (κ, ρ)-**cut-restricted isometry property** (cRIP) if, for every $\mathbf{x} \in \mathbb{R}^p$ with $\|\nabla \mathbf{x}\|_0 \geq 1$, we have*

$$\left(1 - \kappa - \sqrt{\rho(\|\nabla \mathbf{x}\|_0)}\right) \|\mathbf{x}\|_2 \leq \|\mathbf{A}\mathbf{x}\|_2 \leq \left(1 + \kappa + \sqrt{\rho(\|\nabla \mathbf{x}\|_0)}\right) \|\mathbf{x}\|_2.$$

This definition depends implicitly on the structure of the underlying graph G, via its discrete gradient matrix ∇. Examples of the function ρ are given in the two propositions below.

This condition is stronger than the usual RIP condition in compressed sensing (Candès et al., 2006a,b) in two ways: First, Definition 2.3.1 requires quantitative control of $\|\mathbf{A}\mathbf{x}\|_2$ for *all* vectors $\mathbf{x} \in \mathbb{R}^p$, rather than only those with sparsity $\|\nabla \mathbf{x}\|_0 \leq s$ for some specified s. We use this in our analysis to handle regularization of $\|\nabla \mathbf{x}\|_0$ in Lagrangian (rather than constrained) form. Second, approximate isometry is required for signals with small gradient-sparsity $\|\nabla \mathbf{x}\|_0$, rather than small sparsity $\|\mathbf{x}\|_0$. This requirement is similar to the D-RIP condition of Candès et al. (2011) for general sparse analysis models, and is also related to the condition of Needell and Ward (2013b) that $\mathbf{A}\mathcal{H}^{-1}$ satisfies the usual RIP condition, where $\mathcal{H}^{-1}$ is the inverse Haar-wavelet transform on the 2-D lattice.

Despite this strengthening of the required RIP condition, the following shows that Definition 2.3.1 still holds for sub-Gaussian designs $\mathbf{A}$. For a random vector $\mathbf{a}$, we denote its sub-Gaussian norm as $\|\mathbf{a}\|_{\psi_2} = \sup_{\mathbf{u}:\|\mathbf{u}\|_2=1} \sup_{k \geq 1} \; k^{-1/2}\mathbb{E}[|\mathbf{u}^\mathsf{T}\mathbf{a}|^k]^{1/k}$, and say that $\mathbf{a}$ is sub-Gaussian if $\|\mathbf{a}\|_{\psi_2} \leq K$ for a constant $K > 0$.

Proposition 2.3.2. *Let $\mathbf{A} \in \mathbb{R}^{n \times p}$ have i.i.d. rows $\mathbf{a}_i/\sqrt{n}$, where $\mathrm{Cov}[\mathbf{a}_i] = \mathbf{\Sigma}$ and $\|\mathbf{a}_i\|_{\psi_2} \leq K$. Suppose that the largest and smallest eigenvalues of $\mathbf{\Sigma}$ satisfy $\sigma_{\max}(\mathbf{\Sigma}) \leq (1+\kappa)^2$ and $\sigma_{\min}(\mathbf{\Sigma}) \geq (1-\kappa)^2$ for a constant $\kappa \in (0,1)$. Then for any $k > 0$ and some constant $C > 0$ depending only on K, κ, k, with probability at least $1 - |E|^{-k}$, the matrix $\mathbf{A}$ satisfies (κ, ρ)-cRIP for the function*

$$\rho(s) = \frac{Cs \log(1 + |E|/s)}{n}.$$

Here, κ depends on the condition number of the design covariance, and $\rho(s)$ does not depend on the structure of the graph other than its total number of edges. The proof is a standard union bound argument, which we defer to Appendix A.2 of the online supplementary material.

For large 2-D images, using Fourier measurements with matrix multiplication implemented by an FFT can significantly reduce the runtime of Algorithm 1. As previously discussed in Lustig et al. (2007); Needell and Ward (2013b); Krahmer and Ward (2014), uniform random sampling of Fourier coefficients may not be appropriate for reconstructing piecewise-constant images, as these typically have larger coefficients in the lower Fourier frequencies. We instead study a non-uniform sampling and reweighting scheme similar to that proposed in Krahmer and Ward (2014) for total-variation compressed sensing, and show that Definition 2.3.1 also holds for this reweighted Fourier matrix.

For $p = N_1 N_2$ and N_1, N_2 both powers of 2, let $\mathcal{F} \in \mathbb{C}^{p \times p}$ be the 2-D discrete Fourier matrix on the lattice graph G of size $N_1 \times N_2$, normalized such that $\mathcal{F}\mathcal{F}^* = \mathbf{I}$. We define this as the Kronecker

product $\mathcal{F} = \mathcal{F}^1 \otimes \mathcal{F}^2$, where $\mathcal{F}^1 \in \mathbb{C}^{N_1 \times N_1}$ is the 1-D discrete Fourier matrix with entries

$$\mathcal{F}^1_{jk} = \frac{1}{\sqrt{N_1}} \cdot e^{2\pi \mathbf{i} \cdot \frac{(j-1)(k-1)}{N_1}},$$

and $\mathcal{F}^2 \in \mathbb{C}^{N_2 \times N_2}$ is defined analogously. (Thus rows closer to $N_1/2 + 1$ in $\mathcal{F}^1$ correspond to higher frequency components.) Let $\mathcal{F}^*_{(i,j)}$ denote row (i, j) of $\mathcal{F}$, where we index by pairs $(i, j) \in \{1, \ldots, N_1\} \times \{1, \ldots, N_2\}$ corresponding to the Kronecker structure. We define a sampled Fourier matrix as follows: Let ν_1 be the probability mass function on $\{1, \ldots, N_1\}$ given by

$$\nu_1(i) \propto \frac{1}{C_0 + \min(i - 1, N_1 - i + 1)}, \qquad C_0 \geq 1. \tag{2.9}$$

Define similarly ν_2 on $\{1, \ldots, N_2\}$, and let $\nu = \nu_1 \times \nu_2$. For a given number of measurements n, draw $(i_1, j_1), \ldots, (i_n, j_n) \overset{iid}{\sim} \nu$, and set

$$\tilde{\mathbf{A}} = \frac{1}{\sqrt{n}} \begin{pmatrix} \mathcal{F}^*_{(i_1,j_1)} / \sqrt{\nu(i_1, j_1)} \\ \vdots \\ \mathcal{F}^*_{(i_n,j_n)} / \sqrt{\nu(i_n, j_n)} \end{pmatrix} \in \mathbb{C}^{n \times p}. \tag{2.10}$$

Proposition 2.3.3. *Let G be the 2-D lattice graph of size $N_1 \times N_2$, where N_1, N_2 are powers of 2 and $1/K < N_1/N_2 < K$ for a constant $K > 0$. Set $p = N_1 N_2$ and let $\tilde{\mathbf{A}}$ be the matrix defined in (2.10). Then for some constants $C, t_0 > 0$ depending only on K, and for any $t > t_0$, with probability at least $1 - e^{-(\log n)(\log p)^3} - p^{-t}$, $\tilde{\mathbf{A}}$ satisfies the (κ, ρ)-cRIP with $\kappa = 0$ and*

$$\rho(s) = Cts \frac{(\log p)^8 \log n}{n}.$$

The proof follows closely the ideas of (Rudelson and Vershynin, 2008, Theorem 3.3), and we defer this to Appendix A.2 of the online supplementary material.

This proposition pertains to the complex analogue of Definition 2.3.1, where $\tilde{\mathbf{A}}, \mathbf{x}$ are allowed to be complex-valued, and $\| \cdot \|_2$ denotes the complex ℓ_2-norm. For a real-valued signal $\mathbf{x}_* \in \mathbb{R}^p$, Algorithm 1 may be applied to $\tilde{\mathbf{y}} = \tilde{\mathbf{A}}\mathbf{x}_* + \mathbf{e} \in \mathbb{C}^n$ by separating real and imaginary parts of $\tilde{\mathbf{y}}$ into a real vector $\mathbf{y} \in \mathbb{R}^{2n}$. The corresponding $\mathbf{A} \in \mathbb{R}^{2n \times p}$ satisfies $\|\mathbf{A}\mathbf{x}\|_2^2 = \|\tilde{\mathbf{A}}\mathbf{x}\|_2^2$, so the same cRIP condition holds (in the real sense) for $\mathbf{A}$.

2.3.2 Recovery error bounds

To illustrate the idea of analysis, we first establish a result showing that ITALE can yield exact recovery in a setting of no measurement noise. We require $\mathbf{x}_*$ to be gradient-sparse with coordinates belonging exactly to $\delta\mathbb{Z}$, as the ITALE output has this latter property. Discretization error will be addressed in our subsequent result.

Theorem 2.3.4. *Suppose* $\mathbf{e} = \mathbf{0}$ *and* $\mathbf{x}_* \in (\delta\mathbb{Z})^p$*, and denote* $s_* = \max(\|\nabla\mathbf{x}_*\|_0, 1)$*. Suppose* $\sqrt{\eta}\cdot\mathbf{A}$ *satisfies* (κ,ρ)*-cRIP, where* $\kappa \in [0, \sqrt{3/2}-1)$*. Set* $t(\kappa) = 1-4\kappa-2\kappa^2 \in (0,1]$*, and choose tuning parameters*

$$(1-t(\kappa)/4)^2 < \gamma < 1, \qquad \lambda_{\max} > \|\mathbf{x}_*\|_2^2.$$

For some constants $C, c > 0$ *depending only on* κ*, if* $\rho(s_*) \le c$*, then each iterate* $\mathbf{x}_k$ *of Algorithm 1 satisfies*

$$\|\mathbf{x}_k - \mathbf{x}_*\|_2 \le C\sqrt{\lambda_{\max} s_*}\cdot\gamma^{k/2}. \tag{2.11}$$

In particular, $\mathbf{x}_k = \mathbf{x}_*$ *for all sufficiently large* k*.*

Thus, in this noiseless setting, the iterates exhibit linear convergence to the true signal $\mathbf{x}_*$. The required condition $\rho(s_*) \le c$ translates into a requirement of

$$n \gtrsim s_* \log(1 + |E|/s_*)$$

measurements for $\mathbf{A}$ having i.i.d. $\mathcal{N}(0, 1/n)$ entries, by Proposition 2.3.2, or

$$n \gtrsim s_* (\log p)^8 \log\log p$$

weighted Fourier measurements for the 2-D lattice graph, as defined in Proposition 2.3.3. For these designs, (κ,ρ)-cRIP holds for $\sqrt{\eta}\cdot\mathbf{A}$ where $\kappa = 0$ and $\eta = 1$.

Proof of Theorem 2.3.4. Denote

$$s_k = \|\nabla\mathbf{x}_k\|_0, \qquad \mathbf{r}_k = \mathbf{x}_k - \mathbf{x}_*.$$

As shown in (Fan and Guan, 2018, Lemma S2.1) (see also (Boykov et al., 1999, Theorem 6.1)), the

output $\mathbf{x}_{k+1}$ of the sub-routine AlphaExpansion$(\mathbf{a}_{k+1}, \lambda_k, \delta)$ has the deterministic guarantee

$$\frac{1}{2}\|\mathbf{x}_{k+1} - \mathbf{a}_{k+1}\|_2^2 + \lambda_k \|\nabla \mathbf{x}_{k+1}\|_0 \leq \min_{\mathbf{x} \in (\delta\mathbb{Z})^p} \left(\frac{1}{2}\|\mathbf{x} - \mathbf{a}_{k+1}\|_2^2 + 2\lambda_k \|\nabla \mathbf{x}\|_0 \right). \tag{2.12}$$

Applying this optimality condition (2.12) to compare $\mathbf{x}_{k+1}$ with $\mathbf{x}_* = \mathbf{x}_k - \mathbf{r}_k$, we obtain

$$\|\mathbf{x}_{k+1} - \mathbf{a}_{k+1}\|_2^2 + 2\lambda_k s_{k+1} \leq \|\mathbf{x}_k - \mathbf{r}_k - \mathbf{a}_{k+1}\|_2^2 + 4\lambda_k s_*. \tag{2.13}$$

Let $\mathcal{S}_k$ be the partition of $\{1, \ldots, p\}$ induced by the piecewise-constant structure of $\mathbf{x}_k$: Each element of $\mathcal{S}_k$ corresponds to a connected subgraph of G on which $\mathbf{x}_k$ takes a constant value. Let $\mathcal{S}_{k+1}, \mathcal{S}_*$ similarly be the partitions induced by $\mathbf{x}_{k+1}, \mathbf{x}_*$, and denote by $\mathcal{S}$ the common refinement of $\mathcal{S}_k, \mathcal{S}_{k+1}, \mathcal{S}_*$. Defining the boundary

$$\partial\mathcal{S} = \{(i,j) \in E : \ i, j \text{ belong to different elements of } \mathcal{S}\},$$

observe that each edge $(i,j) \in \partial S$ must be such that at least one of $\mathbf{x}_k$, $\mathbf{x}_{k+1}$, or $\mathbf{x}_*$ takes different values at its two endpoints. Then

$$|\partial\mathcal{S}| \leq s_* + s_k + s_{k+1}. \tag{2.14}$$

Let $\mathbf{P} : \mathbb{R}^p \to \mathbb{R}^p$ be the orthogonal projection onto the subspace of signals taking a constant value over each element of $\mathcal{S}$, and let $\mathbf{P}^\perp = \mathbf{I} - \mathbf{P}$. Then $\mathbf{x}_{k+1}, \mathbf{x}_k, \mathbf{r}_k$ all belong to the range of $\mathbf{P}$, so an orthogonal decomposition yields

$$\begin{aligned}
\|\mathbf{x}_{k+1} - \mathbf{a}_{k+1}\|_2^2 &= \|\mathbf{x}_{k+1} - \mathbf{P}\mathbf{a}_{k+1}\|_2^2 + \|\mathbf{P}^\perp \mathbf{a}_{k+1}\|_2^2, \\
\|\mathbf{x}_k - \mathbf{r}_k - \mathbf{a}_{k+1}\|_2^2 &= \|\mathbf{x}_k - \mathbf{r}_k - \mathbf{P}\mathbf{a}_{k+1}\|_2^2 + \|\mathbf{P}^\perp \mathbf{a}_{k+1}\|_2^2.
\end{aligned}$$

Applying this, the definition (in the noiseless setting $\mathbf{e} = \mathbf{0}$)

$$\mathbf{a}_{k+1} = \mathbf{x}_k - \eta \mathbf{A}^\mathsf{T}(\mathbf{A}\mathbf{x}_k - \mathbf{y}) = \mathbf{x}_k - \eta \mathbf{A}^\mathsf{T}\mathbf{A}\mathbf{r}_k,$$

and the condition $\mathbf{P}\mathbf{x}_k = \mathbf{x}_k$ to (2.13), we obtain

$$\|\mathbf{x}_{k+1} - \mathbf{x}_k + \eta \mathbf{P}\mathbf{A}^\mathsf{T}\mathbf{A}\mathbf{r}_k\|_2^2 \leq \|\eta \mathbf{P}\mathbf{A}^\mathsf{T}\mathbf{A}\mathbf{r}_k - \mathbf{r}_k\|_2^2 + \lambda_k(4s_* - 2s_{k+1}).$$

Applying the triangle inequality and $\mathbf{x}_{k+1} - \mathbf{x}_k = \mathbf{r}_{k+1} - \mathbf{r}_k$,

$$\left(\|\mathbf{r}_{k+1}\|_2 - \|\mathbf{r}_k - \eta\mathbf{P}\mathbf{A}^\mathsf{T}\mathbf{A}\mathbf{r}_k\|_2\right)_+^2 \le \|\mathbf{r}_k - \eta\mathbf{P}\mathbf{A}^\mathsf{T}\mathbf{A}\mathbf{r}_k\|_2^2 + \lambda_k(4s_* - 2s_{k+1}). \tag{2.15}$$

We derive from this two consequences: First, lower-bounding the left side by 0 and rearranging,

$$\lambda_k s_{k+1} \le \frac{1}{2}\|\mathbf{r}_k - \eta\mathbf{P}\mathbf{A}^\mathsf{T}\mathbf{A}\mathbf{r}_k\|_2^2 + 2\lambda_k s_* \le \|\mathbf{r}_k\|_2^2 + \|\sqrt{\eta}\mathbf{A}\mathbf{P}\|_{\mathrm{op}}^2 \cdot \|\sqrt{\eta}\mathbf{A}\mathbf{r}_k\|_2^2 + 2\lambda_k s_*. \tag{2.16}$$

The condition (2.14) and definition of $\mathbf{P}$ imply, for any $\mathbf{u} \in \mathbb{R}^p$, that $\|\nabla(\mathbf{P}\mathbf{u})\|_0 \le s_* + s_k + s_{k+1}$. The definition of $\mathbf{r}_k$ implies $\|\nabla\mathbf{r}_k\|_0 \le s_* + s_k$. Setting

$$\tau_k = \kappa + \sqrt{\rho(s_* + s_k + s_{k+1})}, \qquad \zeta_k = \kappa + \sqrt{\rho(s_* + s_k)}$$

we deduce from the (κ, ρ)-cRIP condition for $\sqrt{\eta}\cdot\mathbf{A}$ that

$$\|\sqrt{\eta}\mathbf{A}\mathbf{P}\|_{\mathrm{op}}^2 = \sup_{\mathbf{u}\in\mathbb{R}^p:\|\mathbf{u}\|_2=1} \|\sqrt{\eta}\mathbf{A}\mathbf{P}\mathbf{u}\|_2^2 \le (1+\tau_k)^2, \qquad \|\sqrt{\eta}\mathbf{A}\mathbf{r}_k\|_2^2 \le (1+\zeta_k)^2\|\mathbf{r}_k\|_2^2. \tag{2.17}$$

Note that since $\rho(s)$ and $\sqrt{\rho(s)}$ are both nonnegative and concave by Definition 2.3.1, we have

$$\rho'(s) \le (\rho(s) - \rho(0))/s \le \rho(s)/s, \qquad \frac{d}{ds}[\sqrt{\rho(s)}] \le (\sqrt{\rho(s)} - \sqrt{\rho(0)})/s \le \sqrt{\rho(s)}/s.$$

The function

$$f_k(s) = \left(1 + \kappa + \sqrt{\rho(s_* + s_k + s)}\right)^2$$

is also increasing and concave, and by the above, its derivative at $s = 0$ satisfies

$$f_k'(0) \le d_k/(s_* + s_k), \qquad d_k \equiv 2(1+\kappa)\sqrt{\rho(s_* + s_k)} + \rho(s_* + s_k).$$

Thus

$$(1+\tau_k)^2 = f_k(s_{k+1}) \le f_k(0) + f_k'(0)\cdot s_{k+1} \le (1+\zeta_k)^2 + d_k s_{k+1}/s_*. \tag{2.18}$$

Applying this and (2.17) to (2.16), we get

$$\begin{aligned}\lambda_k s_{k+1} &\le \left(1 + (1+\tau_k)^2(1+\zeta_k)^2\right)\|\mathbf{r}_k\|_2^2 + 2\lambda_k s_* \\ &\le \left(1 + (1+\zeta_k)^4 + (1+\zeta_k)^2 d_k s_{k+1}/s_*)\right)\|\mathbf{r}_k\|_2^2 + 2\lambda_k s_*.\end{aligned}$$

Rearranging gives

$$\Big(\lambda_k - (1+\zeta_k)^2 d_k \|\mathbf{r}_k\|_2^2/s_*\Big)\cdot s_{k+1} \le (1+(1+\zeta_k)^4)\cdot\|\mathbf{r}_k\|_2^2 + 2\lambda_k s_*. \tag{2.19}$$

Second, applying the (κ,ρ)-cRIP condition for $\sqrt{\eta}\cdot\mathbf{A}$ again, we have for every $\mathbf{u}\in\mathbb{R}^p$

$$\begin{aligned}\Big|\mathbf{u}^\mathsf{T}(\eta\mathbf{P}\mathbf{A}^\mathsf{T}\mathbf{A}\mathbf{P}-\mathbf{P})\mathbf{u}\Big| &= \Big|\|\sqrt{\eta}\mathbf{A}\mathbf{P}\mathbf{u}\|_2^2 - \|\mathbf{P}\mathbf{u}\|_2^2\Big| \\ &\le \max\Big(|1-(1-\tau_k)^2|, |1-(1+\tau_k)^2|\Big)\|\mathbf{P}\mathbf{u}\|_2^2 = (2\tau_k+\tau_k^2)\|\mathbf{P}\mathbf{u}\|_2^2,\end{aligned}$$

So $\|\eta\mathbf{P}\mathbf{A}^\mathsf{T}\mathbf{A}\mathbf{P}-\mathbf{P}\|_{\mathrm{op}} \le 2\tau_k+\tau_k^2$. Then, as $\mathbf{r}_k = \mathbf{P}\mathbf{r}_k$, we get from (2.15) that

$$\Big(\|\mathbf{r}_{k+1}\|_2 - (2\tau_k+\tau_k^2)\|\mathbf{r}_k\|_2\Big)_+^2 \le (2\tau_k+\tau_k^2)^2\|\mathbf{r}_k\|_2^2 + \lambda_k(4s_* - 2s_{k+1}).$$

Taking the square-root and applying $\sqrt{x+y}\le\sqrt{x}+\sqrt{y}$,

$$\|\mathbf{r}_{k+1}\|_2 \le (4\tau_k+2\tau_k^2)\|\mathbf{r}_k\|_2 + \sqrt{\lambda_k(4s_*-2s_{k+1})_+}$$

Applying the definitions of τ_k and $t(\kappa)$,

$$4\tau_k+2\tau_k^2 \le 1 - t(\kappa) + 4(1+\kappa)\sqrt{\rho(s_*+s_k+s_{k+1})} + 2\rho(s_*+s_k+s_{k+1}).$$

Thus

$$\|\mathbf{r}_{k+1}\|_2 \le \Big[1 - t(\kappa) + 4(1+\kappa)\sqrt{\rho(s_*+s_k+s_{k+1})} + 2\rho(s_*+s_k+s_{k+1})\Big]\cdot\|\mathbf{r}_k\|_2 + \sqrt{4\lambda_k s_*}. \tag{2.20}$$

We now claim by induction on k that, if $\rho(s_*)\le c_0$ for a sufficiently small constant $c_0>0$, then

$$s_k \le \frac{90}{t(\kappa)^2}s_*, \qquad \|\mathbf{r}_k\|_2 \le \frac{4\sqrt{\lambda_k s_*}}{t(\kappa)} \tag{2.21}$$

for every k. For $k=0$, these are satisfied as $s_0=0$ and $\lambda_0=\lambda_{\max}\ge\|\mathbf{r}_0\|_2^2 = \|\mathbf{x}_*\|_2^2$. Assume inductively that these hold for k. Note that for any $t\ge 1$, nonnegativity and concavity yield $\rho(ts_*)\le t\rho(s_*)$. In particular, assuming (2.21) and applying $\kappa<\sqrt{3/2}-1$ and $\rho(s_*)\le c_0$, we get for small enough c_0 that $(1+\zeta_k)^2<2$. Then applying (2.21) to (2.19), we get for a constant

$C \equiv C(\kappa) > 0$ not depending on c_0 that

$$(1 - C\sqrt{c_0})\,\lambda_k s_{k+1} \le \left(\frac{80}{t(\kappa)^2} + 2\right)\lambda_k s_*.$$

Then for small enough c_0,

$$s_{k+1} \le (1 - C\sqrt{c_0})^{-1}\,\frac{82}{t(\kappa)^2} s_* < \frac{90}{t(\kappa)^2} s_*.$$

Applying (2.21) and this bound to (2.20), for sufficiently small c_0, we have

$$\|\mathbf{r}_{k+1}\|_2 \le \left(1 - \frac{3}{4}t(\kappa)\right)\|\mathbf{r}_k\|_2 + \sqrt{4\lambda_k s_*} \le \left(\frac{4}{t(\kappa)} - 1\right)\sqrt{\lambda_k s_*}.$$

Applying $\sqrt{\lambda_k} = \sqrt{\lambda_{k+1}/\gamma} \le \sqrt{\lambda_{k+1}}(1 - t(\kappa)/4)^{-1}$, we obtain from this

$$\|\mathbf{r}_{k+1}\|_2 \le 4\sqrt{\lambda_{k+1} s_*}/t(\kappa).$$

This completes the induction and establishes (2.21) for every k.

The bound (2.11) follows from (2.21), the definition of $\mathbf{r}_k$, and $\lambda_k = \lambda_{\max}\gamma^k$. Since $\mathbf{x}_k, \mathbf{x}_* \in (\delta\mathbb{Z})^p$, for k large enough such that the right side of (2.11) is less than δ^2, we must have $\mathbf{x}_k = \mathbf{x}_*$. □

We now extend this result to a robust recovery guarantee in the presence of measurement and discretization error. In this setting, ITALE is not guaranteed to converge to a global minimizer of the non-convex objective (2.2). Instead, we provide a direct bound on the estimation error of a suitably chosen ITALE iterate. The proof is an extension of the above argument, which we defer to Appendix A.1 of the online supplementary material.

Theorem 2.3.5. *Suppose $\sqrt{\eta}\cdot\mathbf{A}$ satisfies (κ,ρ)-cRIP, where $\kappa \in [0, \sqrt{3/2} - 1)$. Choose tuning parameters $\gamma, \lambda_{\max}$ as in Theorem 2.3.4. Then for some constants $C, C', c > 0$ depending only on κ, the following holds: Let $\mathbf{x} \in (\delta\mathbb{Z})^p$ be any vector satisfying $\rho(s) \le c$ where $s \equiv \max(\|\nabla\mathbf{x}\|_0, 1)$. Let D be the maximum vertex degree of G, and define*

$$E(\mathbf{x}) = \left(1 + \sqrt{D\rho(s)}\right)\cdot\left(\|\mathbf{x} - \mathbf{x}_*\|_2 + \frac{\|\mathbf{x} - \mathbf{x}_*\|_1}{\sqrt{s}}\right) + \sqrt{\eta}\cdot\|\mathbf{e}\|_2.$$

Suppose $\lambda_{\max} \ge CE(\mathbf{x})^2/s \ge \lambda_{\min}$, and let k_* be the last iterate of Algorithm 1 where $\lambda_{k_*} \ge CE(\mathbf{x})^2/s$. Then $\hat{\mathbf{x}} \equiv \mathbf{x}_{k_*}$ satisfies

$$\|\hat{\mathbf{x}} - \mathbf{x}_*\|_2 \le C' E(\mathbf{x}).$$

Here, $\mathbf{x} \in (\delta\mathbb{Z})^p$ is any deterministic vector that approximates $\mathbf{x}_*$ and satisfies $\|\nabla\mathbf{x}\|_0 \leq s$, and the theorem should be interpreted for $\mathbf{x}$ being the best such approximation to $\mathbf{x}_*$. The quantity $E(\mathbf{x})$ above is the combined measurement error and approximation error of $\mathbf{x}_*$ by $\mathbf{x}$. For any $\mathbf{A}$ scaled such that it satisfies (κ, ρ)-cRIP with $\eta = 1$, and for G with maximum degree $D \lesssim 1$, we get

$$\|\hat{\mathbf{x}} - \mathbf{x}_*\|_2 \lesssim \|\mathbf{x}_* - \mathbf{x}\|_2 + \frac{\|\mathbf{x}_* - \mathbf{x}\|_1}{\sqrt{s}} + \|\mathbf{e}\|_2. \tag{2.22}$$

This guarantee is similar to those for compressed sensing of sparse signals in Candès et al. (2006b); Needell and Tropp (2009); Blumensath and Davies (2009). Note that, as in these works, we are assuming a setting of deterministic and possibly adversarial measurement error $\mathbf{e}$.

If $\mathbf{x}_*$ has exact gradient-sparsity $\|\nabla\mathbf{x}_*\|_0 \leq s$, then also $\mathbf{x} \in (\delta\mathbb{Z})^p$ obtained by entrywise rounding to $\delta\mathbb{Z}$ satisfies $\|\nabla\mathbf{x}\|_0 \leq s$. Hence, applying (2.22) with this $\mathbf{x}$ and choosing $\delta \ll \|\mathbf{e}\|_2/p$ further ensures

$$\|\hat{\mathbf{x}} - \mathbf{x}_*\|_2 \lesssim \|\mathbf{e}\|_2$$

i.e. the discretization error is negligible in the above bound. It is clear that this is the rate-optimal error bound for worst-case error $\mathbf{e}$, as may be seen by taking $\mathbf{e} = \mathbf{A}\mathbf{1}$ where $\mathbf{1}$ is the all-1's vector. The required number of measurements is the same as in Theorem 2.3.4 for the noiseless setting, which is $n \gtrsim s_* \log(1 + |E|/s_*)$ for i.i.d. Gaussian designs. This is the claim (2.5) stated in the introduction.

When $\mathbf{x}_*$ is not exactly gradient-sparse, the error (2.22) depends also on the errors $\|\mathbf{x}_* - \mathbf{x}\|_2$ and $\|\mathbf{x}_* - \mathbf{x}\|_1$ of the approximation by a gradient-sparse vector $\mathbf{x}$. This dependence is similar to the guarantees of Needell and Ward (2013b) for TV-regularization, although we note that Needell and Ward (2013b) provided bounds in terms of $\nabla\mathbf{x}_* - \nabla\mathbf{x}$ rather than $\mathbf{x}_* - \mathbf{x}$.

2.4 Simulations

We compare $\hat{\mathbf{x}}^{\mathrm{ITALE}}$ using the ℓ_0 edge cost (2.3) to $\hat{\mathbf{x}}^{\mathrm{TV}}$ minimizing the TV-regularized objective (2.6), for several signals on the 1-D and 2-D lattice graphs. We used software developed by Boykov and Kolmogorov (2004), to implement the alpha-expansion sub-routine of Algorithm 2. For convenience, we further made an R package `ITALE` to realize Algorithm 1. To minimize the TV-regularized objective (2.6), we used the generalized lasso path algorithm from Tibshirani (2011) in the 1-D examples and the FISTA algorithm from Beck and Teboulle (2009) in the 2-D examples. All parameters were set as described in Section 2.2 for ITALE.

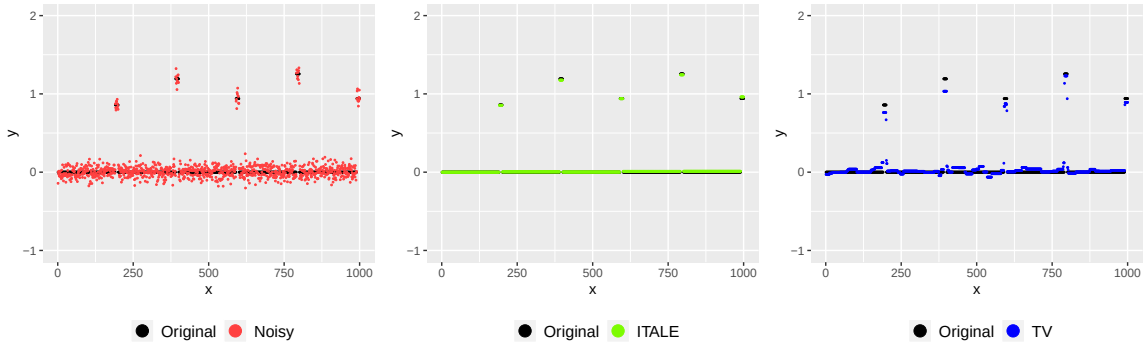

Figure 2.2: Left: True spike signal $\mathbf{x}_*$ (black) and a depiction of $\mathbf{x}_* + \mathbf{A}^\mathsf{T}\mathbf{e}/n$ (red) under low noise $\sigma = 1$ for i.i.d. measurements $A_{ij} \sim \mathcal{N}(0,1)$ with 15% undersampling. Middle and right: True signal (black), $\hat{\mathbf{x}}^{\text{ITALE}}$ (green), and $\hat{\mathbf{x}}^{\text{TV}}$ (blue) for one simulation.

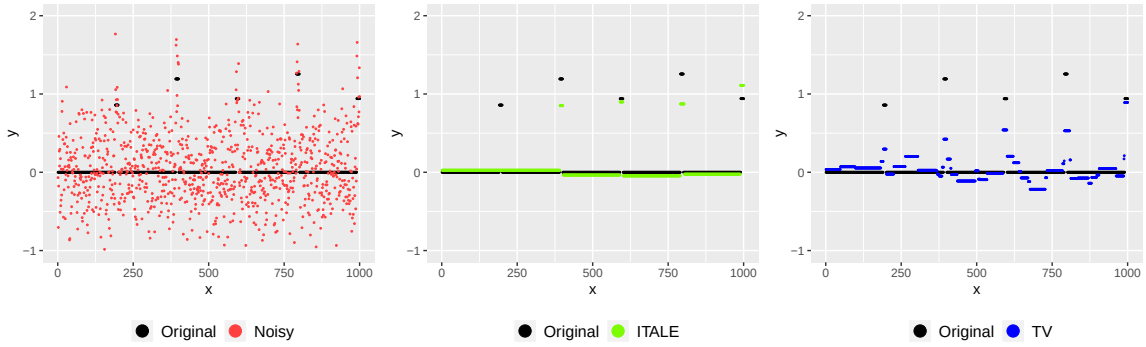

Figure 2.3: Same setting as Figure 2.2, for noise level $\sigma = 6$.

2.4.1 1-D changepoint signals

We tested ITALE on two simulated signals for the linear chain graph, with different changepoint structures: the "spike" signal depicted in Figures 2.2 and 2.3, and the "wave" signal depicted in Figure 2.4 and 2.5. The two signals both have $p = 1000$ vertices with $s_* = 9$ break points. The spike signal consists of short segments of length 10 with elevated mean, while the breaks of the wave signal are equally-spaced.

We sampled i.i.d. random Gaussian measurements $A_{ij} \sim \mathcal{N}(0,1)$. The measurement error $\mathbf{e}$ was generated as i.i.d. Gaussian noise $e_k \sim \mathcal{N}(0, \sigma^2)$. To provide an intuitive understanding of the tested signal-to-noise, we plot $\mathbf{x}_* + \mathbf{A}^\mathsf{T}\mathbf{e}/n$ in red in Figures 2.2 to 2.5, corresponding to two different tested noise levels. Recall that ITALE denoises $\mathbf{a}_{k+1} = \mathbf{x}_* + (\mathbf{I} - \mathbf{A}^\mathsf{T}\mathbf{A}/n)(\mathbf{x}_k - \mathbf{x}_*) + \mathbf{A}^\mathsf{T}\mathbf{e}/n$ in each iteration (corresponding to $\eta = 1/n$ for this normalization of $\mathbf{A}$), so that $\mathbf{x}_* + \mathbf{A}^\mathsf{T}\mathbf{e}/n$ represents the noisy signal in an ideal setting if $\mathbf{x}_k \equiv \mathbf{x}_*$ is a perfect estimate from the preceding iteration.

Tables 2.1 and 2.2 display the root-mean-squared estimation errors RMSE $= \sqrt{\|\hat{\mathbf{x}} - \mathbf{x}_*\|_2^2/p}$,

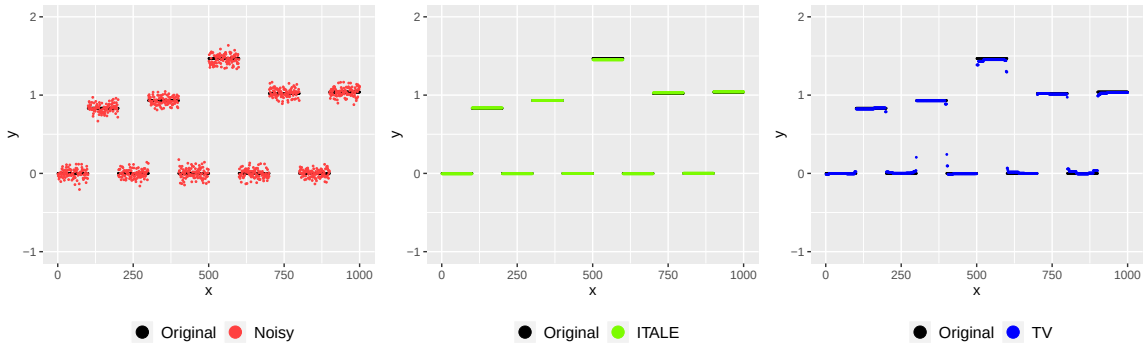

Figure 2.4: Left: True wave signal $\mathbf{x}_*$ (black) and a depiction of $\mathbf{x}_* + \mathbf{A}^\mathsf{T}\mathbf{e}/n$ (red) under low noise $\sigma = 1$ for i.i.d. measurements $A_{ij} \sim \mathcal{N}(0, 1)$ with 15% undersampling. Middle and right: True signal (black), $\hat{\mathbf{x}}^{\text{ITALE}}$ (green), and $\hat{\mathbf{x}}^{\text{TV}}$ (blue) for one simulation.

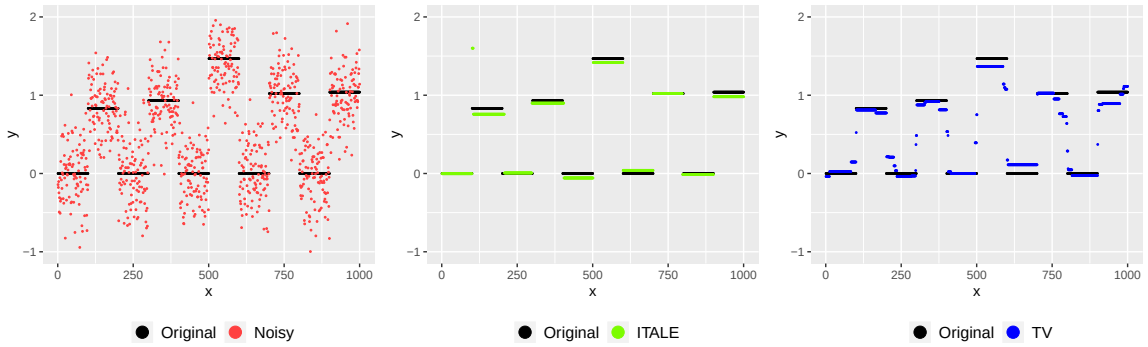

Figure 2.5: Same setting as Figure 2.4, for noise level $\sigma = 6$.

Table 2.1: RMSE for the 1-D spike signal, averaged over 20 simulations.

n/p		$\sigma = 0$	$\sigma = 1$	$\sigma = 2$	$\sigma = 3$	$\sigma = 4$	$\sigma = 5$	$\sigma = 6$	$\sigma = 7$
10%	ITALE	**0.000**	**0.014**	**0.060**	**0.090**	**0.144**	**0.173**	**0.199**	**0.216**
	TV	**0.000**	0.047	0.092	0.129	0.160	0.189	0.213	0.228
15%	ITALE	**0.000**	**0.009**	**0.023**	**0.049**	**0.076**	**0.104**	**0.133**	**0.153**
	TV	**0.000**	0.030	0.060	0.088	0.114	0.136	0.158	0.175
20%	ITALE	**0.000**	**0.007**	**0.015**	**0.032**	**0.056**	**0.076**	**0.099**	**0.123**
	TV	**0.000**	0.022	0.045	0.067	0.089	0.109	0.128	0.146
30%	ITALE	**0.000**	**0.006**	**0.012**	**0.021**	**0.031**	**0.049**	**0.065**	**0.079**
	TV	**0.000**	0.017	0.035	0.052	0.070	0.087	0.104	0.120
40%	ITALE	**0.000**	**0.005**	**0.010**	**0.015**	**0.025**	**0.041**	**0.051**	**0.063**
	TV	**0.000**	0.014	0.028	0.043	0.057	0.071	0.085	0.098
50%	ITALE	**0.000**	**0.005**	**0.010**	**0.015**	**0.023**	**0.033**	**0.040**	**0.051**
	TV	**0.000**	0.013	0.026	0.038	0.051	0.064	0.075	0.088

for undersampling ratio n/p from 10% to 50%, and a range of noise levels σ that yielded RMSE values between 0 and roughly 0.2. Each reported error value is an average across 20 independent simulations. In these results, the iterate k in ITALE and penalty parameter λ in TV were both selected using 5-fold cross-validation. Best-achieved errors over all k and λ are reported in Appendix A.3 of the online supplementary material, and suggest the same qualitative conclusions. Standard deviations of the best-achieved errors are also reported in Appendix A.3; those for cross-validation are similar and omitted for brevity.

In the spike example, ITALE yielded lower RMSE in all of the above settings of undersampling and signal-to-noise. Figures 2.2 and 2.3 display one instance each of the resulting estimates $\hat{\mathbf{x}}^{\text{ITALE}}$ and $\hat{\mathbf{x}}^{\text{TV}}$ at 15% undersampling, illustrating some of their differences and typical features. Under optimal tuning, $\hat{\mathbf{x}}^{\text{TV}}$ returns an undersmoothed estimate even in a low-noise setting where ITALE can often correctly estimate the changepoint locations. With higher noise, ITALE begins to miss changepoints and oversmooth.

In the wave example, with undersampling ranging between 15% and 50%, ITALE yielded lower RMSE at most tested noise levels. Figures 2.4 and 2.5 depict two instances of the recovered signals at 15% undersampling. For 10% undersampling, the component $(\mathbf{I} - \mathbf{A}^\mathsf{T}\mathbf{A}/n)(\mathbf{x}_k - \mathbf{x}_*)$ of the effective noise was sufficiently high such that ITALE often did not estimate the true changepoint structure, and TV usually outperformed ITALE in this case. The standard deviations of RMSE reported in Appendix A.3 indicate that the ITALE estimates are a bit more variable than the TV estimates in all tested settings, but particularly so in this 10% undersampling regime.

Table 2.2: RMSE for the 1-D wave signal, averaged over 20 simulations.

n/p		$\sigma = 0$	$\sigma = 1$	$\sigma = 2$	$\sigma = 3$	$\sigma = 4$	$\sigma = 5$	$\sigma = 6$	$\sigma = 7$
10%	ITALE	0.036	0.040	0.118	0.150	0.198	0.236	0.262	0.315
	TV	**0.000**	**0.032**	**0.064**	**0.093**	**0.120**	**0.143**	**0.168**	**0.189**
15%	ITALE	**0.000**	**0.009**	**0.025**	**0.059**	0.090	0.111	0.143	0.176
	TV	**0.000**	0.023	0.046	0.068	**0.089**	**0.109**	**0.127**	**0.144**
20%	ITALE	**0.000**	**0.007**	**0.017**	**0.039**	**0.061**	**0.079**	**0.103**	**0.121**
	TV	**0.000**	0.019	0.037	0.056	0.074	0.092	0.108	0.124
30%	ITALE	**0.000**	**0.006**	**0.012**	**0.019**	**0.035**	**0.051**	**0.065**	**0.085**
	TV	**0.000**	0.014	0.028	0.042	0.056	0.070	0.084	0.097
40%	ITALE	**0.000**	**0.005**	**0.011**	**0.018**	**0.027**	**0.037**	**0.052**	**0.064**
	TV	**0.000**	0.012	0.024	0.037	0.049	0.061	0.073	0.085
50%	ITALE	**0.000**	**0.005**	**0.010**	**0.016**	**0.024**	**0.033**	**0.044**	**0.055**
	TV	**0.000**	0.011	0.022	0.033	0.043	0.054	0.065	0.075

Table 2.3: RMSE for the Shepp-Logan phantom, averaged over 20 simulations.

n/p		$\sigma = 0$	$\sigma = 4$	$\sigma = 8$	$\sigma = 12$	$\sigma = 16$	$\sigma = 20$	$\sigma = 24$	$\sigma = 28$
10%	ITALE	**0.001**	**0.006**	**0.012**	**0.018**	**0.028**	**0.036**	**0.051**	0.071
	TV	0.005	0.011	0.021	0.031	0.040	0.049	0.057	**0.064**
15%	ITALE	**0.000**	**0.003**	**0.011**	**0.013**	**0.018**	**0.028**	**0.034**	**0.042**
	TV	0.001	0.009	0.016	0.024	0.031	0.038	0.046	0.053
20%	ITALE	**0.000**	**0.002**	**0.009**	**0.012**	**0.014**	**0.024**	**0.028**	**0.034**
	TV	**0.000**	0.007	0.014	0.020	0.027	0.033	0.039	0.045
30%	ITALE	**0.000**	**0.002**	**0.006**	**0.011**	**0.013**	**0.015**	**0.021**	**0.028**
	TV	**0.000**	0.006	0.012	0.017	0.022	0.027	0.032	0.036
40%	ITALE	**0.000**	**0.001**	**0.005**	**0.010**	**0.012**	**0.013**	**0.015**	**0.021**
	TV	**0.000**	0.005	0.010	0.015	0.019	0.023	0.028	0.032
50%	ITALE	**0.000**	**0.001**	**0.004**	**0.008**	**0.011**	**0.013**	**0.014**	**0.017**
	TV	**0.000**	0.005	0.009	0.013	0.018	0.022	0.025	0.028

2.4.2 2-D phantom images

Next, we tested ITALE on three 2-D image examples, corresponding to piecewise-constant digital phantom images of varying complexity: the Shepp-Logan digital phantom depicted in Figure 2.6, a digital brain phantom from Fessler and Hero (1994) depicted in Figure 2.7, and the XCAT chest slice from Gong et al. (2017) as previously depicted in Figure 2.1.

Each image $\mathbf{x}_*$ was normalized to have pixel value in $[0, 1]$. We sampled a random Fourier design matrix as specified in (2.10), fixing the constant $C_0 = 10$ in the weight distribution (2.9) for this design. This value of C_0 yielded the best recovery across several tested values for both ITALE and TV. The measurement error $\mathbf{e}$ was generated as i.i.d. Gaussian noise $e_k \sim \mathcal{N}(0, \sigma^2)$, applied to the measurements $\mathcal{F}^*_{(i,j)}\mathbf{x}_*/\sqrt{\nu(i,j)}$ before the $1/\sqrt{n}$ normalization. Tables 2.3, 2.4, and 2.5 display the average RMSE of the estimates $\hat{\mathbf{x}}^{\text{ITALE}}$ and $\hat{\mathbf{x}}^{\text{TV}}$ across 20 independent simulations of $\mathbf{e}$, with tuning parameters selected by 5-fold cross-validation. Best-achieved errors and standard deviations

Table 2.4: RMSE for the brain phantom, averaged over 20 simulations.

n/p		$\sigma = 0$	$\sigma = 8$	$\sigma = 16$	$\sigma = 24$	$\sigma = 32$	$\sigma = 40$	$\sigma = 48$	$\sigma = 56$
10%	ITALE	0.003	**0.002**	**0.011**	**0.027**	**0.044**	**0.062**	0.081	0.097
	TV	**0.002**	0.014	0.028	0.041	0.054	0.066	**0.078**	**0.088**
15%	ITALE	**0.000**	**0.001**	**0.007**	**0.018**	**0.030**	**0.044**	**0.059**	**0.073**
	TV	0.001	0.011	0.022	0.032	0.043	0.053	0.062	**0.073**
20%	ITALE	**0.000**	**0.001**	**0.005**	**0.011**	**0.025**	**0.035**	**0.047**	**0.060**
	TV	**0.000**	0.010	0.019	0.028	0.038	0.047	0.055	0.062
30%	ITALE	**0.000**	**0.001**	**0.003**	**0.008**	**0.015**	**0.026**	**0.033**	**0.043**
	TV	**0.000**	0.008	0.015	0.023	0.030	0.037	0.046	0.052
40%	ITALE	**0.000**	**0.001**	**0.002**	**0.006**	**0.010**	**0.020**	**0.026**	**0.034**
	TV	**0.000**	0.007	0.013	0.020	0.026	0.032	0.038	0.044
50%	ITALE	**0.000**	**0.000**	**0.002**	**0.004**	**0.008**	**0.014**	**0.022**	**0.028**
	TV	**0.000**	0.006	0.012	0.018	0.023	0.029	0.035	0.040

Table 2.5: RMSE for the XCAT chest slice phantom, averaged over 20 simulations.

n/p		$\sigma = 0$	$\sigma = 4$	$\sigma = 8$	$\sigma = 12$	$\sigma = 16$	$\sigma = 20$	$\sigma = 24$	$\sigma = 28$
10%	ITALE	0.063	0.065	0.070	0.075	0.082	0.091	0.099	0.108
	TV	**0.009**	**0.019**	**0.032**	**0.043**	**0.053**	**0.061**	**0.068**	**0.073**
15%	ITALE	**0.002**	**0.007**	**0.024**	0.036	0.055	0.070	0.079	0.088
	TV	0.005	0.014	**0.024**	**0.034**	**0.042**	**0.050**	**0.057**	**0.063**
20%	ITALE	**0.002**	**0.005**	**0.014**	**0.023**	**0.032**	0.045	0.062	0.076
	TV	**0.002**	0.011	0.020	0.028	0.036	**0.043**	**0.050**	**0.055**
30%	ITALE	**0.002**	**0.004**	**0.011**	**0.018**	**0.025**	**0.031**	**0.041**	0.050
	TV	**0.002**	0.008	0.016	0.023	0.030	0.036	0.042	**0.047**
40%	ITALE	0.002	**0.003**	**0.009**	**0.015**	**0.020**	**0.027**	**0.033**	**0.040**
	TV	**0.001**	0.007	0.014	0.020	0.026	0.031	0.036	0.042
50%	ITALE	0.002	**0.003**	**0.008**	**0.013**	**0.018**	**0.023**	**0.028**	**0.033**
	TV	**0.001**	0.006	0.012	0.018	0.023	0.028	0.033	0.037

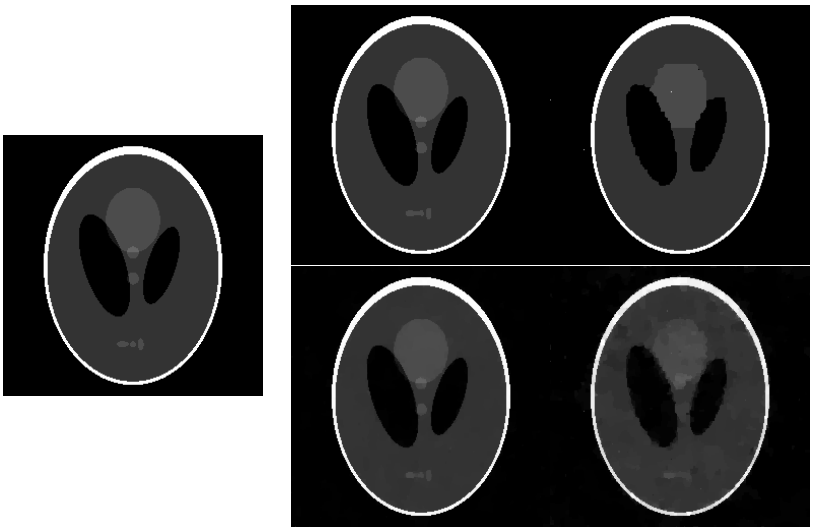

Figure 2.6: Left: Original Shepp-Logan phantom. Top row: $\hat{\mathbf{x}}^{\mathrm{ITALE}}$ from 15% undersampled and reweighted Fourier measurements, in low noise ($\sigma = 4$, left) and medium noise ($\sigma = 16$, right) settings. Bottom row: $\hat{\mathbf{x}}^{\mathrm{TV}}$ for the same measurements.

are reported in Appendix A.3.

For the simpler Logan-Shepp and brain phantom images, which exhibit stronger gradient-sparsity, ITALE yielded lower RMSE in nearly all tested undersampling and signal-to-noise regimes. For the XCAT chest phantom, with undersampling ranging between 15% and 50%, ITALE yielded lower RMSE at a range of tested noise levels, and in particular for those settings of higher signal-to-noise. With 10% undersampling for the XCAT phantom, ITALE was not able to recover some details of the XCAT image even with no measurement noise, and RMSE was higher than TV at all tested noise levels. Results of Appendix A.3 indicate that this is partially due to sub-optimal selection of the tuning parameter using 5-fold cross-validation, caused by the further reduction of undersampling from 10% to 8% in the size of the training data in each fold.

Examples of recovered signals $\hat{\mathbf{x}}^{\mathrm{ITALE}}$ and $\hat{\mathbf{x}}^{\mathrm{TV}}$ are depicted for the Shepp-Logan and brain phantoms in Figures 2.6 and 2.7, at 15% and 20% undersampling for two low-noise and medium-noise settings. The qualitative comparisons are similar to those in the 1-D simulations, and to those previously depicted for the XCAT chest slice in Figure 2.1: As measurement noise increases, ITALE begins to lose finer details, while TV begins to yield an undersmoothed and blotchy image. These observations are also similar to previous comparisons that have been made for algorithms oriented towards ℓ_0 versus TV regularization for direct measurements $\mathbf{A} = \mathbf{I}$, in Xu et al. (2011); Fan and Guan (2018); Kim and Gao (2019).

Figure 2.7: Left: Original brain phantom. Top row: $\hat{\mathbf{x}}^{\mathrm{ITALE}}$ from 20% undersampled reweighted Fourier measurements, in low noise ($\sigma = 16$, left) and medium noise ($\sigma = 40$, right) settings. Bottom row: $\hat{\mathbf{x}}^{\mathrm{TV}}$ for the same measurements.

2.5 Conclusion

We have studied recovery of piecewise-constant signals over arbitrary graphs from noisy linear measurements. We have proposed an iterative algorithm, ITALE, to minimize an ℓ_0-edge-penalized least-squares objective. Under a cut-restricted isometry property for the measurement design, we have established global recovery guarantees for the estimated signal, in noisy and noiseless settings.

In the field of compressed sensing, for signals exhibiting sparsity in an orthonormal basis, ℓ_1-regularization (Donoho, 2006; Candès et al., 2006b,a) and discrete iterative algorithms (Tropp and Gilbert, 2007; Needell and Tropp, 2009; Blumensath and Davies, 2009) constitute two major approaches for signal recovery. It has been observed that for recovering piecewise-constant signals, regularizing the signal gradient in a sparse analysis framework can yield better empirical recovery than regularizing signal coefficients in such a basis. Whereas ℓ_1-regularization extends naturally to the sparse analysis setting, iterative algorithms have received less attention. By applying the alpha-expansion idea for MAP estimation in discrete Markov random fields, ITALE provides a computationally tractable approach for "iterative thresholding" recovery of gradient-sparse signals, with provable recovery guarantees.

In contrast to sparse signal recovery over an orthonormal basis, the comparison of ℓ_1 versus ℓ_0 regularization for gradient-based sparsity is graph-dependent. Using an ℓ_0-based approach, we es-

tablish signal recovery guarantees on the 1-D and 2-D lattice graphs with numbers of measurements optimal up to a constant factor, which were not previously available for TV-regularization. This difference is closely connected to slow and fast rates of convergence for lasso and best-subset regression for correlated regression designs (Bühlmann et al., 2013; Zhang et al., 2014; Dalalyan et al., 2017). ITALE provides a polynomial-time approach for ℓ_0-regularization in a special graph-based setting, and we believe it is an interesting question whether similar algorithmic ideas may be applicable to other classes of sparse regression problems.

Acknowledgments

We would like to thank Brian Caffo for pointing us to the XCAT digital phantom, Feng Ruan for helpful discussions, and the anonymous reviewers for suggestions that helped improve our paper. This research was supported in part by NSF grant DMS-1916198. I would thank Professor Zhou Fan for his excellent supervision on this work. The paper was published by the Journal of the Royal Statistical Society: Series B on January, 2021 (Xu and Fan, 2021).

Chapter 3

Tree-Projected Gradient Descent for Estimating Gradient-Sparse Parameters

3.1 Introduction

We study estimation of a piecewise-constant or gradient-sparse parameter vector on a given graph. This problem may arise in statistical changepoint detection (Killick et al., 2012; Fryzlewicz, 2014), where an unknown vector on a line graph has a sequential changepoint structure. In image denoising (Rudin et al., 1992) and compressed sensing (Candès et al., 2006a; Donoho, 2006), this vector may represent a gradient-sparse image on a 2D or 3D lattice graph, as arising in medical X-rays and CT scans. For applications of epidemic tracking and anomaly detection on general graphs and networks, this vector may indicate regions of infected or abnormal nodes (Arias-Castro et al., 2011).

We consider the following general framework: Given observations $Z_1^n := (Z_1, \dots, Z_n) \in \mathcal{Z}^n$ with distribution $\mathcal{P}$, we seek to estimate a parameter $\boldsymbol{\theta}^* \in \mathbb{R}^p$ associated to $\mathcal{P}$. The coordinates of $\boldsymbol{\theta}^*$ are identified with the vertices of a known graph $G = (V, E)$, where the number of vertices is $|V| = p$. Denoting by $\nabla_G : \mathbb{R}^p \to \mathbb{R}^{|E|}$ the discrete gradient operator

$$\nabla_G \boldsymbol{\theta} = \big(\theta_i - \theta_j : (i,j) \in E\big), \tag{3.1}$$

we assume that the gradient sparsity $s^* := \|\nabla_G \boldsymbol{\theta}^*\|_0$ is small relative to the total number of edges

in G. For example, when G is a line or lattice graph, s^* measures the number of changepoints or the total boundary size between the constant pieces of an image, respectively. For a given convex and differentiable loss function $\mathcal{L} : \mathbb{R}^p \times \mathcal{Z}^n \to \mathbb{R}$, we assume that $\boldsymbol{\theta}^*$ is related to the data distribution $\mathcal{P}$ as the minimizer of the population risk,

$$\boldsymbol{\theta}^* = \operatorname*{argmin}_{\boldsymbol{\theta} \in \mathbb{R}^p} \mathbb{E}_{\mathcal{P}} \left[\mathcal{L}(\boldsymbol{\theta}; Z_1^n) \right].$$

Important examples include linear and generalized linear models for $Z_i = (\mathbf{x}_i, y_i)$, where $\boldsymbol{\theta}^*$ is the vector of regression coefficients and $\mathcal{L}$ is the usual squared-error or negative log-likelihood loss.

Our main result implies that, under suitable restricted strong convexity and smoothness properties of the loss (Negahban et al., 2012) and subgaussian assumptions on the noise, a polynomial-time projected gradient descent algorithm yields an estimate $\widehat{\boldsymbol{\theta}}$ which achieves the squared-error guarantee

$$\|\widehat{\boldsymbol{\theta}} - \boldsymbol{\theta}^*\|_2^2 \leq C \cdot \frac{s^*}{n} \log \left(1 + \frac{p}{s^*}\right) \tag{3.2}$$

with high probability. Here, $C > 0$ is a constant independent of the graph G, and depends only on the loss $\mathcal{L}$ and distribution $\mathcal{P}$ via their convexity, smoothness, and subgaussian constants.

Despite the simplicity of the guarantee (3.2) and its similarity to results for estimating *coordinate-sparse* parameters $\boldsymbol{\theta}^* \in \mathbb{R}^p$, to our knowledge, our work is the first to establish this guarantee in polynomial time for estimating *gradient-sparse* parameters on general graphs, including the 1D line. In particular, (3.2) is not necessarily achieved by convex approaches which constrain or regularize the ℓ_1 (total-variation) relaxation $\|\nabla_G \boldsymbol{\theta}^*\|_1$, for the reason that an ill-conditioned discrete gradient matrix $\nabla_G \in \mathbb{R}^{|E| \times p}$ contributes to the restricted convexity and smoothness properties of the resulting convex problem (Hütter and Rigollet, 2016; Fan and Guan, 2018). We discuss this further below, in the context of related literature.

Our work instead analyzes an algorithm that iteratively and approximately computes the projected gradient update

$$\boldsymbol{\theta}_t \approx \operatorname*{argmin}_{\boldsymbol{\theta} \in \mathbb{R}^p : \|\nabla_{T_t} \boldsymbol{\theta}\|_0 \leq S} \|\boldsymbol{\theta} - \boldsymbol{\theta}_{t-1} + \eta \cdot \nabla \mathcal{L}(\boldsymbol{\theta}_{t-1}; Z_1^n)\|_2 \tag{3.3}$$

over a sequence of low-degree spanning trees $T_1, T_2, \ldots$ of G.[1] To obtain a polynomial-time algorithm, we approximate each projection onto the non-convex space $\{\boldsymbol{\theta} \in \mathbb{R}^p : \|\nabla_{T_t} \boldsymbol{\theta}\|_0 \leq S\}$ by discretizing

1. Here, $\nabla \mathcal{L}(\boldsymbol{\theta}_{t-1}; Z_1^n)$ is the gradient of $\mathcal{L}(\boldsymbol{\theta}; Z_1^n)$ with respect to $\boldsymbol{\theta}$ at $\boldsymbol{\theta}_{t-1}$, and $\nabla_{T_t} \boldsymbol{\theta}$ is the discrete gradient operator (3.1) over the edges in T_t instead of G.

the signal domain $\mathbb{R}^p$ and applying a dynamic-programming recursion over T_t to compute the discrete projection. For graphs G that do not admit spanning trees of low degree, we apply an idea of Padilla et al. (2017) and construct T_t using a combination of edges in G and additional edges representing backtracking paths along a depth-first-search traversal of G.

Our algorithm and analysis rely on an important insight from Jain et al. (2014), which is to perform each projection using a target sparsity-level S that is larger than the true gradient-sparsity s^* by a constant factor. This idea was applied in Jain et al. (2014) to provide a statistical analysis of iterative thresholding procedures such as IHT, CoSaMP, and HTP for estimating coordinate-sparse parameters (Blumensath and Davies, 2009; Needell and Tropp, 2009; Foucart, 2011). A key ingredient in our proof, Lemma 3.3.6 below, is a combinatorial argument which compares the errors of approximating any vector $\mathbf{u}$ by vectors $\mathbf{u}^S$ and $\mathbf{u}^*$ that are gradient-sparse over a tree, with two different sparsity levels S and s^*. This extends a central lemma of Jain et al. (2014) from the simpler setting of coordinate-sparsity to a setting of gradient-sparsity on trees.

3.1.1 Related literature

Existing literature on this and related problems is extensive, and we provide here a necessarily partial overview.

Convex approaches: Estimating a piecewise-constant vector $\boldsymbol{\theta}^*$ in both the direct-measurements model $y_i = \theta_i^* + e_i$ and the indirect linear model $y_i = \mathbf{x}_i^\top \boldsymbol{\theta}^* + e_i$ has been of interest since early work on the fused lasso (Tibshirani et al., 2005; Rinaldo, 2009) and compressed sensing (Candès et al., 2006b,a; Donoho, 2006). A natural and commonly-used approach is to constrain or penalize the total-variation semi-norm $\|\nabla_G \boldsymbol{\theta}^*\|_1$ (Rudin et al., 1992). Statistical properties of this approach have been extensively studied, including estimation guarantees over signal classes of either bounded variation or bounded exact gradient-sparsity (Mammen and van de Geer, 1997; Hütter and Rigollet, 2016; Sadhanala et al., 2016; Dalalyan et al., 2017; Lin et al., 2017; Ortelli and van de Geer, 2018); exact or robust recovery guarantees in compressed sensing contexts (Needell and Ward, 2013a,b; Cai and Xu, 2015); and correct identification of changepoints or of the discrete gradient support (Harchaoui and Lévy-Leduc, 2010; Sharpnack et al., 2012). Extensions to higher-order trend-filtering methods have been proposed and studied in (Kim et al., 2009; Wang et al., 2016; Sadhanala et al., 2017; Guntuboyina et al., 2017). These works have collectively considered settings of both direct and indirect linear measurements, for the 1D line, 2D and 3D lattices, and more general graphs.

In the above work, statistical guarantees analogous to (3.2) have only been obtained under

restrictions for either G or $\boldsymbol{\theta}^*$, which we are able to remove using a non-convex approach. Hütter and Rigollet (2016) established a guarantee analogous to (3.2) when certain compatibility and inverse-scaling factors of G are $O(1)$; a sufficient condition is that G has constant maximum degree, and the Moore-Penrose pseudo-inverse $\nabla_G^\dagger$ has constant $\ell_1 \to \ell_2$ operator norm. This notably does not include the 1D line or 2D lattice. Dalalyan et al. (2017), Lin et al. (2017), and Guntuboyina et al. (2017) developed complementary results, showing that (3.2) can hold for the 1D line provided that the s^* changepoints of $\boldsymbol{\theta}^*$ have minimum spacing $\gtrsim p/(s^*+1)$. An extension of this to tree graphs was proven in Ortelli and van de Geer (2018). Roughly speaking, $\nabla_G^\dagger$ is an effective design matrix for an associated sparse regression problem, and the spacing condition ensures that the *active* variables in the regression model are weakly correlated, even if the full design $\nabla_G^\dagger$ has strong correlations.

Synthesis approach: A separate line of work focuses on the *synthesis* approach, which uses a sparse representation of $\boldsymbol{\theta}^*$ in an orthonormal basis or more general dictionary. Such methods include wavelet approaches in 1D (Daubechies, 1988; Donoho and Johnstone, 1994, 1995), curvelet and ridgelet frames in 2D (Candès, 1998; Candès and Donoho, 2000, 2004), and tree-based wavelets for more general graphs (Gavish et al., 2010; Sharpnack et al., 2013). Elad et al. (2007) and Nam et al. (2013) compare and discuss differences between the synthesis and analysis approaches. Note that in general, an s^*-gradient-sparse signal $\boldsymbol{\theta}^*$ may not admit a $O(s^*)$-sparse representation in an orthonormal basis. For example, $\boldsymbol{\theta}^*$ having s^* changepoints on the line may have up to $s^* \log_2 p$ non-zero coefficients in the Haar wavelet basis, and (3.2) would be inflated by an additional log factor using Haar wavelets.

3.1.2 Our contributions

In contrast to this first line of work on convex methods, our current work is most closely related to a third line of literature on methods that penalize or constrain the exact non-convex gradient-sparsity $\|\nabla_G \boldsymbol{\theta}^*\|_0$, rather than its convex ℓ_1 relaxation (Mumford and Shah, 1989; Boykov et al., 1999; Boysen et al., 2009; Fan and Guan, 2018). This direct method enables theoretical guarantees that remove the spectral conditions on the graph G as well as the minimum spacing requirements of the work alluded to above.

Our results extend those of Fan and Guan (2018), which established similar guarantees to (3.2) for direct measurements $y_i = \theta_i^* + e_i$. Our projected gradient algorithm is similar to the proximal-gradient method recently studied in Xu and Fan (2021), which considered indirect linear measurements $y_i = \mathbf{x}_i^\top \boldsymbol{\theta}^* + e_i$ in a compressed sensing context. In contrast to Xu and Fan (2021), which

considered deterministic measurement errors and a restrictive RIP-type condition on the measurement design, we provide guarantees in the statistical setting of random noise, with much weaker conditions for the regression design, and for a general convex loss. These statistical guarantees are based on a novel tree-projection algorithm that approximates the graph at every iteration. The analysis leverages a new bound that controls the approximation error of tree projections, which is presented in Lemma 3.3.6.

3.2 Tree-projected gradient descent algorithm

Our proposed algorithm, tree-projected gradient descent (tree-PGD), consists of two main steps:

1. For a specified vertex degree $d_{\max} \geq 2$ and iteration count $\tau \geq 1$, we construct a sequence of trees $T_1, \ldots, T_\tau$ on the same vertices as G, such that each tree T_t has maximum degree $\leq d_{\max}$, and any gradient-sparse vector on G remains gradient-sparse on T_t.

2. For a specified step size $\eta > 0$ and sparsity level $S > 0$, we compute iterates $\boldsymbol{\theta}_1, \ldots, \boldsymbol{\theta}_\tau$ where each $\boldsymbol{\theta}_t$ solves the projected gradient-descent step (3.3) over a discretized domain—see (3.5) and (3.6) below.

For simplicity, we initialize the algorithm at $\boldsymbol{\theta}_0 = 0$. The main tuning parameter is the projection sparsity S, which controls the bias-variance trade-off and the gradient sparsity of the final estimate $\widehat{\boldsymbol{\theta}} = \boldsymbol{\theta}_\tau$. The additional parameters of the algorithm are $d_{\max}$, τ, η, and the discretization (3.5) specified by $(\Delta_{\min}, \Delta_{\max}, \delta)$. We discuss these two steps in detail below.

For our theoretical guarantees, it is sufficient to choose $d_{\max} = 2$ and to fix the same tree in every iteration. However, we observe in Section 3.5 that using both larger values of $d_{\max}$ and a different random tree in each iteration can yield substantially lower recovery error in practice, so we will state our algorithm and theory to allow for these possibilities.

3.2.1 Tree construction

We construct a tree T on the vertices $V = \{1, \ldots, p\}$ by the following procedure.

1. Compute any spanning tree $\tilde{T}$ of G. If $\tilde{T}$ has maximum degree $\leq d_{\max}$, then set $T = \tilde{T}$.

2. Otherwise, let $\mathcal{O}_{DFS}$ be the ordering of unique vertices and edges visited in any depth-first-search (DFS) traversal of $\tilde{T}$. For each vertex v whose degree exceeds $d_{\max}$ in $\tilde{T}$, keep its first

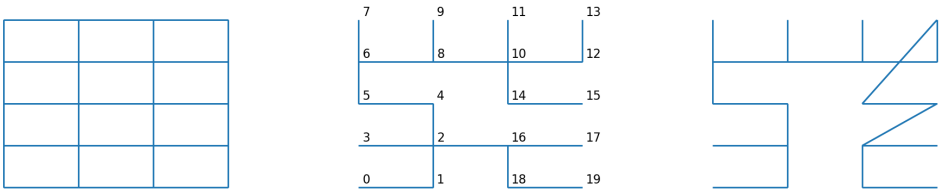

Figure 3.1: An illustration of the tree construction method. Left: Original lattice graph G. Middle: A spanning tree $\tilde{T}$ of G, with vertices numbered in DFS ordering. Right: The final tree T with $d_{\max} = 3$, which changes edge $(2, 16)$ to $(15, 16)$, and edge $(10, 14)$ to $(13, 14)$, thus replacing the two edges adjacent to the degree-4 vertices of T.

$d_{\max}$ edges in this ordering, and delete its remaining edges from $\tilde{T}$. Note that the deleted edges are between v and its children.

3. For each such deleted edge (v, w) where w is a child of v, let w' be the vertex preceding w in the ordering $\mathcal{O}_{DFS}$, and add to $\tilde{T}$ the edge (w', w). Let T be the final tree.

This procedure is illustrated in Figure 3.1. We repeat this construction to obtain each tree $T_1, \ldots, T_\tau$.

If G itself has maximum degree $\leq d_{\max}$, then Steps 2 and 3 above are not necessary, and the guarantee (3.4) below may be trivially strengthened to $\|\nabla_T \boldsymbol{\theta}\|_0 \leq \|\nabla_G \boldsymbol{\theta}\|_0$. For graphs G of larger maximum degree, the idea in Steps 2 and 3 above and the associated guarantee (3.4) are drawn from Lemma 1 of Padilla et al. (2017), which considered the case of a line graph for T (where $d_{\max} = 2$).

Lemma 3.2.1. *Let $G = (V, E)$ be any connected graph with p vertices, and let T be as constructed above. Then T is a tree on V with maximum degree $\leq d_{\max}$. Furthermore, for any $\boldsymbol{\theta} \in \mathbb{R}^p$,*

$$\|\nabla_T \boldsymbol{\theta}\|_0 \leq 2\|\nabla_G \boldsymbol{\theta}\|_0. \tag{3.4}$$

The computational complexity for constructing T is $O(|E|)$.

3.2.2 Projected gradient approximation

The exact minimizer of (3.3) is the projection of $\mathbf{u}_t := \boldsymbol{\theta}_{t-1} - \eta \cdot \nabla \mathcal{L}(\boldsymbol{\theta}_{t-1}; Z_1^n)$ onto the space of S-gradient-sparse vectors over T_t. This space is a union of $\binom{p-1}{S}$ linear subspaces, and naively iterating over these subspaces is intractable for large S. We instead propose to approximate the projection by taking a discrete grid of values

$$\Delta := \{\Delta_{\min}, \Delta_{\min} + \delta, \Delta_{\min} + 2\delta, \ldots, \Delta_{\max} - \delta, \Delta_{\max}\} \tag{3.5}$$

and performing the minimization over $\boldsymbol{\theta} \in \Delta^p$. Thus, our tree-PGD algorithm sets

$$\boldsymbol{\theta}_t = \underset{\boldsymbol{\theta} \in \Delta^p : \|\nabla_{T_t} \boldsymbol{\theta}\|_0 \leq S}{\operatorname{argmin}} \|\boldsymbol{\theta} - \boldsymbol{\theta}_{t-1} + \eta \cdot \nabla \mathcal{L}(\boldsymbol{\theta}_{t-1}; Z_1^n)\|_2 \tag{3.6}$$

Each $\boldsymbol{\theta}_t$ may be computed by a dynamic-programming recursion over T_t.[2]

In detail, fix any target vector $\mathbf{u} \in \mathbb{R}^p$ and a tree T on the vertices $\{1, \ldots, p\}$. To compute

$$\underset{\boldsymbol{\theta} \in \Delta^p : \|\nabla_T \boldsymbol{\theta}\|_0 \leq S}{\operatorname{argmin}} \|\boldsymbol{\theta} - \mathbf{u}\|_2, \tag{3.7}$$

pick any vertex $o \in \{1, \ldots, p\}$ with degree 1 in T as the root. For each vertex v of T, let T_v be the sub-tree consisting of v and its descendants. Let $|T_v|$ be the number of vertices in T_v and $\mathbf{u}_{T_v} \in \mathbb{R}^{|T_v|}$ be the coordinates of $\mathbf{u}$ belonging to T_v. Define $f_v : \Delta \times \{0, 1, \ldots, S\} \to \mathbb{R}$ by

$$f_v(c, s) = \min \Big\{ \|\boldsymbol{\theta} - \mathbf{u}_{T_v}\|_2^2 : \boldsymbol{\theta} \in \Delta^{|T_v|},\ \|\nabla_{T_v} \boldsymbol{\theta}\|_0 \leq s,\ \theta_v = c \Big\}. \tag{3.8}$$

This is the minimum over vectors $\boldsymbol{\theta}$ on T_v that are s-gradient-sparse and take value $c \in \Delta$ at v. These values $f_v(c, s)$ may be computed recursively from the leaves to the root, as follows.

1. For each leaf vertex v of T and each $(c, s) \in \Delta \times \{0, 1, \ldots, S\}$, set $f_v(c, s) = (c - u_v)^2$.

2. For each vertex v of T with children $(w_1, \ldots, w_k)$, given $f_w(c, s)$ for all $w \in \{w_1, \ldots, w_k\}$ and $(c, s) \in \Delta \times \{0, 1, \ldots, S\}$:

   (a) For each $s \in \{0, 1, \ldots, S\}$ and $w \in \{w_1, \ldots, w_k\}$, compute $m_w(s) = \min_{c \in \Delta} f_w(c, s)$.

   (b) For each $(c, s) \in \Delta \times \{0, 1, \ldots, S\}$ and $w \in \{w_1, \ldots, w_k\}$, compute $g_w(c, s) = \min\{f_w(c, s), m_w(s - 1)\}$, where this is taken to be $f_w(c, s)$ if $s = 0$.

   (c) For each $(c, s) \in \Delta \times \{0, 1, \ldots, S\}$, set

$$f_v(c, s) = (c - u_v)^2 + \min_{\substack{s_1, \ldots, s_k \geq 0 \\ s_1 + \ldots + s_k = s}} \Big(g_{w_1}(c, s_1) + \ldots + g_{w_k}(c, s_k) \Big). \tag{3.9}$$

The following then produces the vector $\boldsymbol{\theta}$ which solves (3.7).

3. For the root vertex o, set $\theta_o = \operatorname{argmin}_{c \in \Delta} f_o(c, S)$ and $S_o = S$.

2. For the case where T_t is a line graph, an alternative non-discretized algorithm with complexity $O(p^2 S)$ is presented in (Auger and Lawrence, 1989).

4. For each other vertex v, given θ_v and S_v: Let $w_1, \ldots, w_k$ be the children of v and let $s_1, \ldots, s_k$ be the choices which minimized (3.9) for $f_v(\theta_v, S_v)$. For each $i = 1, \ldots, k$, if $g_{w_i}(\theta_v, s_i) = f_{w_i}(\theta_v, s_i)$, then set $\theta_{w_i} = \theta_v$ and $S_{w_i} = s_i$. If $g_{w_i}(\theta_v, s_i) = m_{w_i}(s_i - 1)$, then set $\theta_{w_i} = \operatorname{argmin}_{c \in \Delta} f_{w_i}(c, s_i - 1)$ and $S_{w_i} = s_i - 1$.

The update $\boldsymbol{\theta}_t$ in (3.6) is computed by applying this algorithm to $\mathbf{u} \equiv \mathbf{u}_t = \boldsymbol{\theta}_{t-1} - \eta \cdot \nabla \mathcal{L}(\boldsymbol{\theta}_{t-1}; Z_1^n)$.

Lemma 3.2.2. *This algorithm minimizes (3.7). Letting $d_{\max}$ be the maximum vertex degree of T and $|\Delta|$ be the cardinality of Δ, its computational complexity is $O(d_{\max} p |\Delta| (S + d_{\max})^{d_{\max}-1})$.*

3.2.3 Total complexity for the linear model

Let us compute the total complexity of this tree-PGD algorithm, under parameter settings that yield a rate-optimal statistical guarantee for the linear model discussed in Section 3.4.1. We set $d_{\max}$ as a small integer and S as a constant multiple of s^*. Evaluating $\nabla \mathcal{L}(\boldsymbol{\theta}_{t-1}; Z_1^n)$ in the linear model requires two matrix-vector multiplications of complexity $O(np)$, where n is the sample size. Let us assume that the number of graph edges is $|E| = O(p)$, and that the entries of $\boldsymbol{\theta}^*$ and the noise $\mathbf{e}$ are both of constant order. Then Corollary 3.4.2 indicates that we may take $\Delta_{\max} - \Delta_{\min} = O(\sqrt{p})$, $\delta = O(\sqrt{s^*/np})$, and $\tau = O(\log np)$. Under these settings, the total complexity of tree-PGD is $O\Big(\big(np + p^2\sqrt{n}(s^*)^{d_{\max}-3/2}\big) \log np\Big)$. Setting $d_{\max} = 2$ (i.e. taking $T_1, \ldots, T_\tau$ to be line graphs) yields the lowest complexity.

3.3 Main theorem

We introduce the following notation which identifies gradient-sparse vectors, partitions of the vertices $\{1, \ldots, p\}$, and subspaces of $\mathbb{R}^p$.

Definition 3.3.1. *Let T be a connected graph on the vertices $V = \{1, \ldots, p\}$, and let $\boldsymbol{\theta} \in \mathbb{R}^p$. The* **partition induced by $\boldsymbol{\theta}$ over** *T is the partition of V whose sets are the connected components of $\{(i,j) \in T : \theta_i = \theta_j\}$ in T. For such a partition $\mathcal{P}$ having k sets, the* **subspace associated to** *$\mathcal{P}$ is the dimension-k subspace of vectors in $\mathbb{R}^p$ taking a constant value over each set. The* **boundary of $\mathcal{P}$ over** *T, denoted by $\partial_T \mathcal{P}$, is the set of edges $(i,j) \in T$ where i, j belong to different sets of $\mathcal{P}$.*

Thus, the sets of the partition $\mathcal{P}$ induced by $\boldsymbol{\theta}$ over T are the "pieces" of the graph T where $\boldsymbol{\theta}$ takes a constant value. If $\mathcal{P}$ is induced by $\boldsymbol{\theta}$ over T, and K is the associated subspace, then $\boldsymbol{\theta} \in K$. Furthermore, $\partial_T \mathcal{P}$ is exactly the edge set where $\nabla_T \boldsymbol{\theta}$ is non-zero, and $\|\nabla_T \boldsymbol{\theta}\|_0 = |\partial_T \mathcal{P}|$.

We introduce two properties for the loss, defined for pairs of connected graphs (T_1, T_2) on the same vertices V. We will apply these to consecutive pairs of trees generated by tree-PGD.

Definition 3.3.2 (cRSC and cRSS)**.** *A differentiable function $f : \mathbb{R}^p \to \mathbb{R}$ satisfies cut-restricted strong convexity (cRSC) and smoothness (cRSS) with respect to (T_1, T_2), at sparsity level S and with convexity and smoothness constants $\alpha, L > 0$, if the following holds: For any partitions $\mathcal{P}_1, \mathcal{P}_2$ of $\{1, \dots, p\}$ where $|\partial_{T_1}\mathcal{P}_1| \le S$ and $|\partial_{T_2}\mathcal{P}_2| \le S$, and any $\boldsymbol{\theta}_1, \boldsymbol{\theta}_2 \in K := K_1 + K_2$ where K_1, K_2 are the subspaces associated to $\mathcal{P}_1, \mathcal{P}_2$,*

$$f(\boldsymbol{\theta}_2) \ge f(\boldsymbol{\theta}_1) + \langle \boldsymbol{\theta}_2 - \boldsymbol{\theta}_1, \nabla f(\boldsymbol{\theta}_1)\rangle + \frac{\alpha}{2}\|\boldsymbol{\theta}_2 - \boldsymbol{\theta}_1\|_2^2, \tag{3.10}$$

$$f(\boldsymbol{\theta}_2) \le f(\boldsymbol{\theta}_1) + \langle \boldsymbol{\theta}_2 - \boldsymbol{\theta}_1, \nabla f(\boldsymbol{\theta}_1)\rangle + \frac{L}{2}\|\boldsymbol{\theta}_2 - \boldsymbol{\theta}_1\|_2^2. \tag{3.11}$$

Definition 3.3.3 (cPGB)**.** *A differentiable function $f : \mathbb{R}^p \to \mathbb{R}$ has a cut-projected gradient bound (cPGB) of $\Phi(S)$ with respect to (T_1, T_2), at a point $\boldsymbol{\theta}^* \in \mathbb{R}^p$ and sparsity level S, if the following holds: For any partitions $\mathcal{P}_1, \mathcal{P}_2$ of $\{1, \dots, p\}$ where $|\partial_{T_1}\mathcal{P}_1| \le S$ and $|\partial_{T_2}\mathcal{P}_2| \le S$, letting K_1, K_2 be their associated subspaces and $\mathbf{P}_K$ be the orthogonal projection onto $K := K_1 + K_2$,*

$$\|\mathbf{P}_K \nabla f(\boldsymbol{\theta}^*)\|_2 \le \Phi(S). \tag{3.12}$$

To provide some interpretation, the below lemma gives an example for this function Φ in the important setting where $\mathbf{w}^\mathsf{T}\nabla\mathcal{L}(\boldsymbol{\theta}^*; Z_1^n)$ is subgaussian for any $\mathbf{w} \in K$.

Lemma 3.3.4. *Let $S \ge 1$, let T_1, T_2 be trees on $\{1, \dots, p\}$, and let $\boldsymbol{\theta}^* \in \mathbb{R}^p$. Suppose, for any subspace K as defined in Definition 3.3.3 and any $\mathbf{w} \in K$, that $\mathbf{w}^\top\nabla\mathcal{L}(\boldsymbol{\theta}^*; Z_1^n)$ is σ^2/n-subgaussian.*[3] *Then for any $k > 0$ and a constant $C_k > 0$ depending only on k, with probability at least $1 - p^{-k}$, the loss $\mathcal{L}(\cdot\,; Z_1^n)$ has the cPGB*

$$\Phi(S) = C_k\sigma\sqrt{\tfrac{S}{n}\log\left(1 + \tfrac{p}{S}\right)}$$

with respect to (T_1, T_2), at $\boldsymbol{\theta}^*$ and sparsity level S.

The following is our main result, which provides a deterministic estimation guarantee when tree-PGB is applied with an appropriate choice of the projection sparsity $S = \kappa s^*$. This result yields the same type of guarantee for any choice of $d_{\max} \ge 2$ and any sequence of trees.

3. This means that for any $t > 0$, $\mathbb{P}[|\mathbf{w}^\top\nabla\mathcal{L}(\boldsymbol{\theta}^*; Z_1^n)| > t] \le 2e^{-nt^2/(2\sigma^2)}$.

Theorem 3.3.5. *Suppose $\|\nabla_G \boldsymbol{\theta}^*\|_0 \leq s^*$, where $s^* > 0$. Set $S = \kappa s^*$ in tree-PGD for a constant $\kappa > 1$. Let $\tau \geq 1$ and $d_{\max} \geq 2$, let $T_1, \ldots, T_\tau$ be the sequence of trees generated by tree-PGD, and denote $T_0 = T_1$ and $S' = S + 2s^* + \max(\sqrt{S}, d_{\max})$. Suppose, for all $1 \leq t \leq \tau$, that*

1. *$\mathcal{L}(\cdot\,; Z_1^n)$ satisfies cRSC and cRSS with respect to (T_{t-1}, T_t), at sparsity level S' and with convexity and smoothness constants $\alpha, L > 0$.*
2. *$\mathcal{L}(\cdot\,; Z_1^n)$ has the cPGB $\Phi(S')$ with respect to (T_{t-1}, T_t), at the point $\boldsymbol{\theta}^*$ and sparsity level S'.*

Define

$$\gamma = \sqrt{\tfrac{(d_{\max}-1)(2s^*+\sqrt{S}+1)+1}{S-2s^*-\sqrt{S}}}, \quad \Gamma = (1+\gamma)\sqrt{1-\tfrac{\alpha}{L}}, \quad \Lambda = \tfrac{1}{1-\Gamma}\left(\tfrac{4(1+\gamma)}{\alpha}\cdot\Phi(S') + \delta\sqrt{p}\right),$$

and suppose κ is large enough such that $S > \sqrt{S} + 2s^*$ and $\Gamma < 1$. Take $\eta = \frac{1}{L}$, $\boldsymbol{\theta}_0 = 0$, and $-\Delta_{\min}, \Delta_{\max} \geq \frac{1}{L}\|\nabla\mathcal{L}(\boldsymbol{\theta}^*; Z_1^n)\|_\infty + 3\|\boldsymbol{\theta}^*\|_2 + 2\Lambda$ in tree-PGD. Then the τ^{th} iterate $\boldsymbol{\theta}_\tau$ of tree-PGD satisfies

$$\|\boldsymbol{\theta}_\tau - \boldsymbol{\theta}^*\|_2 \leq \Gamma^\tau \cdot \|\boldsymbol{\theta}^*\|_2 + \Lambda.$$

Note that since $\gamma \to 0$ as $\kappa \to \infty$, for any value $\alpha/L \in (0, 1]$, there is a choice of constant $\kappa \equiv \kappa(\alpha, L)$ sufficiently large to ensure $\Gamma < 1$.

3.3.1 Proof overview

The proof of Theorem 3.3.5 adopts an induction argument. For simplicity, let us suppose here that $\boldsymbol{\theta}_t$ exactly minimizes (3.3). Then for each iteration, we wish to prove

$$\|\boldsymbol{\theta}_t - \boldsymbol{\theta}^*\|_2 \leq \Gamma \cdot \|\boldsymbol{\theta}_{t-1} - \boldsymbol{\theta}^*\|_2 + \tfrac{4(1+\gamma)}{\alpha}\cdot\Phi(S'). \tag{3.13}$$

The proof of (3.13) contains two main steps. First, we construct a subspace K which contains $\boldsymbol{\theta}_t$ and $\boldsymbol{\theta}^*$ and write $\|\boldsymbol{\theta}_t - \boldsymbol{\theta}^*\|_2 \leq \|\mathbf{P}_K\mathbf{u}_t - \boldsymbol{\theta}_t\|_2 + \|\mathbf{P}_K\mathbf{u}_t - \boldsymbol{\theta}^*\|_2$. Using the following key lemma, we show that there exists such a subspace K for which $\|\mathbf{P}_K\mathbf{u}_t - \boldsymbol{\theta}_t\|_2 \leq \gamma\|\mathbf{P}_K\mathbf{u}_t - \boldsymbol{\theta}^*\|_2$, and the vectors in K have gradient-sparsity not much larger than $S + s^*$.

Lemma 3.3.6. *Let T be a tree on the vertices $\{1, \ldots, p\}$ with maximum vertex degree $d_{\max}$. Let $s^* > 0$ and $S = \kappa s^*$, where $\kappa > 1$ and $S > \sqrt{S} + s^*$. Let $\mathbf{u} \in \mathbb{R}^p$ be arbitrary, let $\mathbf{u}^* \in \mathbb{R}^p$ be any*

vector satisfying $\|\nabla_T \mathbf{u}^*\|_0 \leq s^*$*, and set*

$$\mathbf{u}^S = \underset{\boldsymbol{\theta} \in \mathbb{R}^p : \|\nabla_T \boldsymbol{\theta}\|_0 \leq S}{\operatorname{argmin}} \|\mathbf{u} - \boldsymbol{\theta}\|_2.$$

Denote by (K^S, K^*) *the subspaces associated to the partitions induced by* $(\mathbf{u}^S, \mathbf{u}^*)$ *over* T*. Then there exists a partition* $\mathcal{P}$ *of* $\{1, \ldots, p\}$ *with associated subspace* K*, such that* K *contains* $K^S + K^*$*,*

$$|\partial_T \mathcal{P}| \leq S + s^* + \sqrt{S}, \tag{3.14}$$

and the orthogonal projection $\mathbf{P}_K \mathbf{u}$ *of* $\mathbf{u}$ *onto* K *satisfies*

$$\|\mathbf{P}_K \mathbf{u} - \mathbf{u}^S\|_2^2 \leq \frac{(d_{\max} - 1)(s^* + \sqrt{S} + 1) + 1}{S - s^* - \sqrt{S}} \|\mathbf{P}_K \mathbf{u} - \mathbf{u}^*\|_2^2. \tag{3.15}$$

Then, in the second step, we bound $\|\mathbf{P}_K \mathbf{u}_t - \boldsymbol{\theta}^*\|_2$ by introducing $\mathbf{v} = \operatorname{argmin}_{\boldsymbol{\theta} \in K} \mathcal{L}(\boldsymbol{\theta}; Z_1^n)$. Using a property of the gradient mapping (Lemma B.3.2) and the cRSC and cRSS conditions, we show that $\|\mathbf{P}_K \mathbf{u}_t - \mathbf{v}\|_2 \leq \sqrt{1 - \alpha/L} \cdot \|\boldsymbol{\theta}_{t-1} - \mathbf{v}\|_2$. Applying the triangle inequality, this implies $\|\mathbf{P}_K \mathbf{u}_t - \boldsymbol{\theta}^*\|_2 \leq \sqrt{1 - \alpha/L} \cdot \|\boldsymbol{\theta}_{t-1} - \boldsymbol{\theta}^*\|_2 + 2\|\mathbf{v} - \boldsymbol{\theta}^*\|_2$. Finally, we show that $\|\mathbf{v} - \boldsymbol{\theta}^*\|_2 \leq (2/\alpha)\Phi(S')$ using the cRSC and cPGB properties of the loss, and combining gives (3.13).

The use of Lemma 3.3.6 is inspired by an analogous argument of Jain et al. (2014) for coordinate-sparse parameter estimation. However, the analysis for coordinate-sparsity is simpler, due to a key structural property that if $\mathbf{u}^S$ and $\mathbf{u}^*$ are the best (coordinate-) S-sparse and s^*-sparse approximations of $\mathbf{u}$, then the sparse subspace of $\mathbf{u}^*$ is contained inside that of $\mathbf{u}^S$. This nested subspace structure does not hold for gradient-sparsity, and thus our proofs of both Lemma 3.3.6 and Theorem 3.3.5 follow different arguments from those of Jain et al. (2014).

3.4 Examples

3.4.1 Gradient-sparse linear regression

Consider the example of $Z_i = (\mathbf{x}_i, y_i)$ satisfying a linear model

$$y_i = \mathbf{x}_i^\top \boldsymbol{\theta}^* + e_i \tag{3.16}$$

for independent design vectors $\mathbf{x}_i \in \mathbb{R}^p$ and mean-zero residual errors e_i. Let us write this as $\mathbf{y} = \mathbf{X}\boldsymbol{\theta}^* + \mathbf{e}$ where $\mathbf{y} = (y_1, \ldots, y_n)$, $\mathbf{e} = (e_1, \ldots, e_n)$, and $\mathbf{X} \in \mathbb{R}^{n \times p}$ is the random design matrix

with rows $\mathbf{x}_i^\top$. Then $\boldsymbol{\theta}^*$ is the minimizer of $\mathbb{E}[\mathcal{L}(\boldsymbol{\theta}; Z_1^n)]$ for the squared-error loss

$$\mathcal{L}(\boldsymbol{\theta}; Z_1^n) = \frac{1}{2n}\|\mathbf{y} - \mathbf{X}\boldsymbol{\theta}\|_2^2.$$

The gradient of the loss is given by $\nabla\mathcal{L}(\boldsymbol{\theta}; Z_1^n) = \mathbf{X}^\top(\mathbf{X}\boldsymbol{\theta} - \mathbf{y})/n$.

We assume that

$$\mathrm{Cov}(\mathbf{x}_i) = \boldsymbol{\Sigma}, \qquad \lambda_{\max}(\boldsymbol{\Sigma}) = \lambda_1, \qquad \lambda_{\min}(\boldsymbol{\Sigma}) = \lambda_p, \qquad \|\mathbf{x}_i\|_{\psi_2}^2 \le D\lambda_p \tag{3.17}$$

$$\mathbb{E}[e_i] = 0, \qquad \|e_i\|_{\psi_2}^2 \le \sigma^2 \tag{3.18}$$

for constants $\lambda_1, \lambda_p, D, \sigma^2 > 0$, where $\|\cdot\|_{\psi_2}$ denotes the scalar or vector subgaussian norm. Then the cRSC, cRSS, and cPGB conditions hold according to the following proposition.

Proposition 3.4.1. *Suppose (3.17) and (3.18) hold, and let $S' \ge 1$. Define*

$$g(S') = S'\log(1 + \tfrac{p}{S'}). \tag{3.19}$$

Let $T_1, \dots, T_\tau$ be the trees generated by tree-PGD, and let $T_0 = T_1$. For any $k > 0$, and some constants $C_1, C_2, C_3 > 0$ depending only on k and D, if

$$n \ge C_1 g(S')$$

then with probability at least $1 - \tau \cdot p^{-k}$, for every $1 \le t \le \tau$,

1. *$\mathcal{L}(\cdot; Z_1^n)$ satisfies cRSC and cRSS with respect to (T_{t-1}, T_t) at sparsity level S' and with convexity and smoothness constants $\alpha = \lambda_p/2$ and $L = 3\lambda_1/2$.*
2. *$\mathcal{L}(\cdot; Z_1^n)$ has the cPGB*
$$\Phi(S') = C_2\sigma\sqrt{\lambda_1 g(S')/n}$$
with respect to (T_{t-1}, T_t), at $\boldsymbol{\theta}^*$ and sparsity level S'.
3. *$\|\nabla\mathcal{L}(\boldsymbol{\theta}^*; Z_1^n)\|_\infty \le C_3\sigma\sqrt{(\lambda_1 \log p)/n}$.*

Applying this and Theorem 3.3.5, we obtain the following immediate corollary.

Corollary 3.4.2. *Suppose (3.17) and (3.18) hold, and $\|\nabla_G\boldsymbol{\theta}^*\|_0 \le s^*$ and $\|\boldsymbol{\theta}^*\|_2 \le c_0\sqrt{p}$ for some $s^* \ge 1$ and $c_0 > 0$. Set $S = c_1(\lambda_1/\lambda_p)^2 s^*$, $\eta = 2/(3\lambda_1)$, $\omega = \sigma\lambda_1^{3/2}/\lambda_p^2$, $-\Delta_{\min} = \Delta_{\max} =$*

$c_2(\sqrt{p}+\omega\sqrt{(s^*\log p)/n})$, $\delta = \omega\sqrt{s^*/np}$, *and* $\tau = c_3\log(np/\omega^2 s^*)$ *in tree-PGD, for sufficiently large constants* $c_1 > 0$ *depending on* $d_{\max}, D$ *and* $c_2, c_3 > 0$ *depending on* $d_{\max}, D, c_0$.

Then for any $k > 0$ *and some constants* $C_1, C_2 > 0$ *depending only on* $k, d_{\max}, D$, *if* $n \geq C_1(\lambda_1/\lambda_p)^2 s^* \log(1 + p/s^*)$, *then with probability at least* $1 - \tau \cdot p^{-k}$,

$$\|\boldsymbol{\theta}_\tau - \boldsymbol{\theta}^*\|_2^2 \leq C_2 \cdot \frac{\sigma^2\lambda_1^3}{\lambda_p^4} \cdot \frac{s^*}{n} \log\Big(1 + \frac{p}{s^*}\Big).$$

3.4.2 Gradient-sparse GLM

Consider the example of $Z_i = (\mathbf{x}_i, y_i)$ satisfying a generalized linear model (GLM)

$$P(y_i|\mathbf{x}_i, \boldsymbol{\theta}^*, \phi) = \exp\Big\{\frac{y_i\mathbf{x}_i^\mathsf{T}\boldsymbol{\theta}^* - b(\mathbf{x}_i^\mathsf{T}\boldsymbol{\theta}^*)}{\phi}\Big\} \cdot h(y_i, \phi)$$

for independent design vectors $\mathbf{x}_i \in \mathbb{R}^p$. Here $\phi > 0$ is a constant scale parameter, and h and b are the base measure and cumulant function of the exponential family, where $\mathbb{E}(y_i|\mathbf{x}_i) = b'(\mathbf{x}_i^\top\boldsymbol{\theta}^*)$. Then $\boldsymbol{\theta}^*$ minimizes the population risk $\mathbb{E}[\mathcal{L}(\boldsymbol{\theta}; Z_1^n)]$ for the negative log-likelihood loss

$$\mathcal{L}(\boldsymbol{\theta}; Z_1^n) = \frac{1}{n}\sum_{i=1}^n \Big(b(\mathbf{x}_i^\top\boldsymbol{\theta}) - y_i\mathbf{x}_i^\top\boldsymbol{\theta}\Big).$$

The gradient of this loss is $\nabla\mathcal{L}(\boldsymbol{\theta}; Z_1^n) = \frac{1}{n}\sum_{i=1}^n (b'(\mathbf{x}_i^\top\boldsymbol{\theta}) - y_i)\mathbf{x}_i$.

Let us assume that (3.17) holds for the design vectors $\mathbf{x}_i$. Setting $e_i = y_i - b'(\mathbf{x}_i^\top\boldsymbol{\theta}^*)$, let us assume also that for some constants $\alpha_b, L_b, D_1, D_2 > 0$ and $\beta \in [1, 2]$,

$$\frac{\alpha_b}{2}(x_2 - x_1)^2 \leq b(x_2) - b(x_1) - b'(x_1)(x_2 - x_1) \leq \frac{L_b}{2}(x_2 - x_1)^2 \quad \text{for all } x_1, x_2 \in \mathbb{R}, \tag{3.20}$$

$$\mathbb{P}(|e_i| > \zeta) \leq D_1\exp(-D_2\zeta^\beta) \quad \text{for all } \zeta > 0. \tag{3.21}$$

Then the cRSC, cRSS, and cPGB conditions hold according to the following proposition.

Proposition 3.4.3. *Suppose that (3.17), (3.20), and (3.21) hold. Let* $S' \geq 1$ *and* $g(S')$ *be as in (3.19). Let* $T_1, \ldots, T_\tau$ *be the trees generated by tree-PGD, and let* $T_0 = T_1$. *For any* $k > 0$ *and some constants* $C_1, C_2, C_3 > 0$ *depending only on* k, D, D_1, D_2, β, *if* $n \geq C_1 g(S')$, *then with probability at least* $1 - \tau \cdot p^{-k}$, *for every* $1 \leq t \leq \tau$,

1. $\mathcal{L}(\cdot\,; Z_1^n)$ *satisfies cRSC and cRSS with respect to* (T_{t-1}, T_t) *at sparsity levels* S' *with convexity and smoothness constants* $\alpha = \frac{\alpha_b\lambda_p}{2}$ *and* $L = \frac{3L_b\lambda_1}{2}$.

Noise std. dev. σ	1.0	1.5	2.0	2.5	3.0
Fixed line	0.0372	0.0373	0.0383	0.0388	0.0407
Random, $d_{\max} = 2$	0.0005	0.0009	0.0020	0.0040	0.0058
Random, $d_{\max} = 3$	0.0003	0.0008	0.0014	0.0028	0.0052
Random, $d_{\max} = 4$	0.0003	0.0007	0.0013	0.0032	0.0055
Total variation	0.0006	0.0013	0.0023	0.0036	0.0052

Table 3.1: MSE $\frac{1}{p}\|\widehat{\boldsymbol{\theta}} - \boldsymbol{\theta}^*\|_2^2$ for recovering the image of Figure 3.2 (under best tuning of S), averaged across 20 independent simulations. For tree-PGD, using a different random tree T_t per iteration yields a sizeable improvement over using a fixed line graph across all iterations, and small improvements are observed for increasing $d_{\max}$. Average MSE for the total-variation penalized estimate is provided for comparison (under best tuning of λ).

2. $\mathcal{L}(\cdot\,; Z_1^n)$ *has the cPGB*

$$\Phi(S') = \begin{cases} C_2\sqrt{\lambda_1/n} \cdot g(S')^{1/\beta} & \text{if} \quad 1 < \beta \leq 2 \\ C_2 \log n \sqrt{\lambda_1/n} \cdot g(S') & \text{if} \quad \beta = 1 \end{cases}$$

with respect to (T_{t-1}, T_t)*, at* $\boldsymbol{\theta}^*$ *and sparsity level* S'*.*

3. $\|\nabla \mathcal{L}(\boldsymbol{\theta}^*; Z_1^n)\|_\infty \leq \begin{cases} C_3(\log p)^{1/\beta}\sqrt{\lambda_1/n} & \text{if} \quad 1 < \beta \leq 2 \\ C_3(\log n)(\log p)\sqrt{\lambda_1/n} & \text{if} \quad \beta = 1 \end{cases}$

Under suitable settings of the tree-PGD parameters, similar to Corollary 3.4.2 and which we omit for brevity, when $n \geq C' s^* \log(1 + p/s^*)$, this yields the estimation rate

$$\|\boldsymbol{\theta}_\tau - \boldsymbol{\theta}^*\|_2^2 \leq C \cdot \frac{(s^* \log(1 + p/s^*))^{2/\beta}}{n}$$

in models where $1 < \beta \leq 2$, and this rate with an additional $(\log n)^2$ factor in models where $\beta = 1$. (Here, these constants C, C' depend on $\lambda_1, \lambda_p, D, D_1, D_2, \beta$.)

We note that this result may be established under a relaxed condition (3.20) that only holds over a sufficiently large bounded region for x_1, x_2, following a more delicate analysis and ideas of Negahban et al. (2012). For simplicity, we will not pursue this direction in this work.

3.5 Simulations

Theorem 3.3.5 applies for any choices of trees $T_1, \ldots, T_\tau$ in tree-PGD, with any maximum degree $d_{\max} \geq 2$. We perform a small simulation study in the linear model (3.16) to compare the empirical estimation accuracy of tree-PGD using different tree constructions.

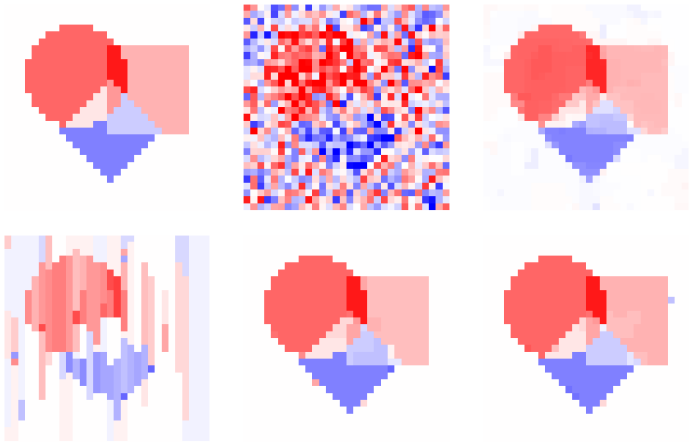

Figure 3.2: Top-left: True image $\boldsymbol{\theta}^*$, with values between -0.5 (blue) and 0.9 (red). Top-middle: Noisy image $\frac{1}{n}\mathbf{X}^\top\mathbf{y}$, for $\mathbf{y} = \mathbf{X}\boldsymbol{\theta}^* + \mathbf{e}$ with Gaussian design and noise standard deviation $\sigma = 1.5$. Top-right: Best total-variation penalized estimate $\widehat{\boldsymbol{\theta}}$. Bottom row: Best tree-PGD estimate $\widehat{\boldsymbol{\theta}}$ for a fixed line graph T_t in every iteration (zig-zagging vertically through G, bottom left), a different random tree with $d_{\max} = 2$ in each iteration (bottom middle), and a different random tree with $d_{\max} = 4$ in each iteration (bottom right).

We recover the image $\boldsymbol{\theta}^*$ depicted in Figure 3.2 on a 30×30 lattice graph G, using $n = 500$ linear measurements with $\mathbf{x}_i \sim \mathcal{N}(0, \mathbf{I})$ and $e_i \sim \mathcal{N}(0, \sigma^2)$. For $\sigma = 1.5$, a noisy image $\frac{1}{n}\mathbf{X}^\top\mathbf{y} = \boldsymbol{\theta}^* + (\frac{1}{n}\mathbf{X}^\top\mathbf{X} - \mathbf{I})\boldsymbol{\theta}^* + \frac{1}{n}\mathbf{X}^\top\mathbf{e}$ is also depicted.

Tree construction: We applied tree-PGD in two settings: First, we constructed T_t using a deterministic DFS over G, fixed across all iterations. This resulted in T_t being a line graph that zig-zags vertically through G. Second, we constructed T_t using a different spanning tree $\tilde{T}_t$ generated by random DFS in each iteration. The DFS procedure started at a uniform random node and, at each forward step, chose a uniform random unvisited neighbor. We tested restricting to $d_{\max} = 2$ or $d_{\max} = 3$ for T_t, or letting $T_t = \tilde{T}_t$ (corresponding to $d_{\max} = 4$). In all experiments, we used $\tau = 80$, $\eta = 1/5$, and $(\Delta_{\min}, \Delta_{\max}, \delta) = (-0.6, 1.0, 0.05)$.

Results for a single experiment at $\sigma = 1.5$ are depicted in Figure 3.2, and average MSE across 20 experiments for varying σ are reported in Table 3.1. These results correspond to the best choices $S = \kappa s^*$ across a range of tested values. Estimation accuracy is substantially better using different and random trees than using the same fixed line graph. We observe small improvements using $d_{\max} = 3$ or $d_{\max} = 4$ over random line graphs with $d_{\max} = 2$, especially in the higher signal-to-noise settings. For comparison, we display in Figure 3.2 and Table 3.1 also the total-variation (TV) regularized estimate $\widehat{\boldsymbol{\theta}} = \operatorname{argmin}_{\boldsymbol{\theta}} \frac{1}{2n}\|\mathbf{y} - \mathbf{X}\boldsymbol{\theta}\|_2^2 + \lambda\|\nabla_G\boldsymbol{\theta}\|_1$ and its average MSE, corresponding to the best choices of λ. We observe that tree-PGD, which targets the exact gradient-sparsity rather

than a convex surrogate, is more accurate in high signal-to-noise settings, and becomes less accurate in comparison with TV as signal strength decreases. This agrees with previous observations made in similar contexts in Hastie et al. (2017); Mazumder et al. (2017); Fan and Guan (2018).

3.6 Discussion

We have shown linear convergence of gradient descent with projections onto the non-convex space of gradient-sparse vectors on a graph. Our results show that this method achieves strong statistical guarantees in regression models, without requiring a matching between the underlying graph and design matrix. We do this by introducing a careful comparison between gradient-sparse approximations at different sparsity levels, which generalizes previous results for coordinate-sparse vectors.

Our theory is presented in such a way that allows the approximation trees to vary at each iteration. However, this is not required and the tree can be fixed with $d_{\max} = 2$ at the start of the algorithm. Nevertheless, we observe experimentally that using a different random tree in each iteration substantially improves the practical performance. Our intuition for the improvement with random trees is that the gradient-sparsity of the signal on the original graph G may be better captured by the average sparsity with respect to a randomly chosen sub-tree of G, than by the sparsity with respect to any fixed sub-tree. By using a different random tree in each iteration, the algorithm is better targeting this average sparsity. This observation will be studied in future work.

Another interesting direction for future work is to explore the connections between this work and computationally tractable sparse linear regression problems with highly correlated designs. For instance, some work (Bühlmann et al., 2013; Dalalyan et al., 2017) discuss various ways to overcome correlated designs. In our setting, the tree projection step enables a computationally efficient method, and it is of interest to understand more general settings where one may overcome the correlated structure of the problem using a computationally efficient procedure.

Acknowledgement

This research was supported in part by NSF Grant DMS-1916198 and DMS-1723128. I would thank Professor Zhou Fan and Professor Sahand Negahban for their excellent supervision on this work. The paper was published at the Conference on Learning Theory, 2020 (Xu et al., 2020). Zhou Fan and Sahand Negahban provided joint advising on this work, with joint meetings of the three of us weekly.

Chapter 4

Maximum Likelihood for High-Noise Group Orbit Estimation

4.1 Introduction

We study several problems of function estimation in low dimensions, where the function is observed under random and unknown rotations of its domain. Let $f : \mathcal{X} \to \mathbb{R}$ be a function on the domain $\mathcal{X}$, and let G be a rotational group acting on $\mathcal{X}$. Denote by $f_{\mathfrak{g}}(x) = f(\mathfrak{g}^{-1} \cdot x)$ the rotation of f by $\mathfrak{g} \in \mathsf{G}$. We seek to estimate f from many independently rotated observations of the whole function $f_{\mathfrak{g}}$ in white noise,

$$f_{\mathfrak{g}}(x)\,\mathrm{d}x + \sigma\,\mathrm{d}W(x),$$

which we will refer to as the "samples". The rotations $\mathfrak{g}$ are unknown, and we assume them to be uniformly random across samples.[1] Each rotated sample is observed in standard Gaussian white noise $\mathrm{d}W(x)$ on $\mathcal{X}$, scaled by the noise level $\sigma > 0$.

In classical settings of function estimation without rotations of the domain, many such samples may first be averaged. Thus it is equivalent to study estimation from a single mean sample, commonly assumed to have low noise $\sigma^2 \ll \|f\|_{L_2}^2$. In this work, we instead focus on a setting where each

1. When there is no projection, the case of non-uniform rotations can be reduced to our uniform case by applying an additional uniformly random rotation to each sample. However, it is known in several settings that estimation can become easier for non-uniform rotations Abbe et al. (2019); Sharon et al. (2020).

individual sample has high noise $\sigma^2 \gtrsim \|f\|_{L_2}^2$, so that the information from many rotated samples must be combined to obtain an accurate estimate of f.

Our primary motivation is a formulation of this problem that models molecular reconstruction in single-particle cryo-electron microscopy (cryo-EM) Dubochet et al. (1988); Henderson et al. (1990); Frank (2006). In this application, $f : \mathbb{R}^3 \to \mathbb{R}$ is the electric potential of an unknown molecular structure. Tomographic projections of this potential are measured for many samples of the molecule, each in a different and unknown rotated orientation, typically with a high level of measurement noise. The molecular structure is determined by estimating this electric potential f from the rotated and projected samples, and then fitting an atomic model Bendory et al. (2020a); Singer and Sigworth (2020). A brief introduction to cryo-EM and a discussion of its relation to the problems studied in this work are presented in Appendix C.6.

Among computational procedures for solving this reconstruction problem, regularized versions of maximum likelihood estimation (MLE), as implemented via expectation-maximization or stochastic gradient descent, are very commonly used Sigworth (1998); Scheres et al. (2007); Scheres (2012); Punjani et al. (2017). However, theoretical properties of these approaches are not well-understood for the cryo-EM application Bendory et al. (2020a).

In this work, we study the properties of maximum likelihood estimation for a basic model of the cryo-EM reconstruction problem, as well as several simpler statistical models with qualitative similarities, which may be of independent interest while building up to the complexity of cryo-EM:

- (Continuous multi-reference alignment, Section 4.3.) Estimating a function on the unit circle $\mathcal{X} = \mathcal{S}^1$, under $\mathsf{SO}(2)$ rotations of the circle Bandeira et al. (2020); Bendory et al. (2020b).

- (Spherical registration, Section 4.4.1.) Estimating a function on the unit sphere $\mathcal{X} = \mathcal{S}^2$, under $\mathsf{SO}(3)$ rotations of the sphere (Bandeira et al., 2017, Section 5.4).

- (Unprojected cryo-EM, Section 4.4.2.) Estimating a function on $\mathbb{R}^3$ under $\mathsf{SO}(3)$ rotations about the origin, without tomographic projection (Bandeira et al., 2017, Appendix B). Such a problem arises in a related application of cryo-ET, discussed in Appendix C.6.1.

- (Cryo-EM, Section 4.4.3.) Estimating a function on $\mathbb{R}^3$ under $\mathsf{SO}(3)$ rotations about the origin, with tomographic projection (Bandeira et al., 2017, Section 5.5).

4.1.1 Group orbit recovery and related literature

Classical work on function estimation has explored the rich interplay between the complexity of infinite-dimensional function classes, the statistical difficulty of estimation, and the role of regularization Ibragimov and Has'minskii (1981); Tsybakov (2008); Johnstone (2017).

In this paper, we instead study connections between the statistical and computational difficulty of estimation and the algebraic structure of the underlying rotational group. We will focus attention on several examples of *finite-dimensional* function spaces, and study the unregularized MLE that marginalizes over the random rotations. Our main results describe the geometry of the Fisher information matrix and log-likelihood landscape and their relation to the invariant polynomial algebra of the group action.

Passing to a Gaussian sequence form by a choice of function basis, our problem may be restated as an *orbit recovery problem* Bandeira et al. (2017); Abbe et al. (2018) of estimating an unknown coefficient vector $\theta_* \in \mathbb{R}^d$ from noisy observations, rotated by elements of a subgroup $\mathsf{G} \subset \mathsf{O}(d)$ acting on the coefficients in this basis. A body of recent literature has studied both specific and general instances of this orbit recovery problem Perry et al. (2019); Bandeira et al. (2020, 2017); Abbe et al. (2018); Pumir et al. (2019); Brunel (2019); Fan et al. (2020); Sharon et al. (2020); Romanov et al. (2021). When G is a discrete cyclic group acting by cyclic rotations of coordinates (a.k.a. discrete multi-reference alignment), Perry et al. (2019) first proved that the optimal squared error for estimating generic signals $\theta_* \in \mathbb{R}^d$ in high noise is significantly larger than that in the model without latent rotations, scaling as σ^6 rather than σ^2. This analysis was extended to non-generic signals for continuous multi-reference alignment in Bandeira et al. (2020) and to general group actions in Abbe et al. (2018); Bandeira et al. (2017).

For a general subgroup $\mathsf{G} \subseteq \mathsf{O}(d)$, Bandeira et al. (2017) obtained a number of results on method-of-moments estimators that are inspirational for our current work. These results showed that the squared error for estimating generic signals up to a finite list of group orbits scales as σ^{2K}, where K is the smallest integer for which the transcendence degree $\mathrm{trdeg}(\mathcal{R}^{\mathsf{G}})$ of the algebra $\mathcal{R}^{\mathsf{G}}$ of G-invariant polynomials on $\mathbb{R}^d$ coincides with the transcendence degree $\mathrm{trdeg}(\mathcal{R}^{\mathsf{G}}_{\leq K})$ of only G-invariant polynomials with degree $\leq K$. Bandeira et al. (2017) placed cryo-EM and other examples of function estimation in this context and stated a number of results and conjectures on the values of K in these specific examples.

For discrete subgroups G, Fan et al. (2020) connected these results to the MLE and the Fisher information, showing that for generic θ_* and high noise σ^2, the Fisher information matrix $I(\theta_*)$

has exactly $\mathrm{trdeg}(\mathcal{R}^{\mathsf{G}}_{\leq k}) - \mathrm{trdeg}(\mathcal{R}^{\mathsf{G}}_{\leq k-1})$ eigenvalues scaling as σ^{-2k} for each $k = 1, \ldots, K$. Fan et al. (2020) studied also the geometric properties of the global maximum likelihood optimization landscape in different signal-to-noise regimes, in particular relating this landscape for high noise to a sequence of moment optimization problems.

The results of Fan et al. (2020) were proven using a series expansion of the log-likelihood function in powers of σ^{-1}. An extension of this series expansion was obtained by Katsevich and Bandeira in Katsevich and Bandeira (2020), for a more general class of high-noise Gaussian mixture models. These results of Katsevich and Bandeira (2020) enable our current analyses of orbit recovery models with a linear projection.

4.1.2 Contributions

The main contributions of our paper are three-fold:

1. We build upon the analyses in Fan et al. (2020); Katsevich and Bandeira (2020) to provide a structural characterization of the Fisher information matrix and log-likelihood landscape, in the high-noise regime, for orbit recovery problems with a possibly continuous group action and/or a linear projection.

   For generic $\theta_* \in \mathbb{R}^d$, we show that the Fisher information matrix has rank $\mathrm{trdeg}(\mathcal{R}^{\mathsf{G}})$ and eigenvalues described by a sequence of transcendence degrees $\mathrm{trdeg}(\mathcal{R}^{\mathsf{G}}_{\leq k})$, analogously to the unprojected discrete group setting of Fan et al. (2020). Under technical conditions, local optima of the log-likelihood are in correspondence with local optima in a sequence of moment optimization problems, whose properties relate to the forms of the subalgebras $\mathcal{R}^{\mathsf{G}}_{\leq k}$.

2. We analyze the forms of the terms of the log-likelihood expansion and derive the associated transcendence degrees, for several examples of function estimation on the circle $\mathcal{S}^1$, the sphere $\mathcal{S}^2$, and $\mathbb{R}^3$.

   For each example, assuming that the bandlimit of the function basis exceeds a small constant, we establish precise values of $\mathrm{trdeg}(\mathcal{R}^{\mathsf{G}}_{\leq k})$ for $k = 1, 2, 3$ and prove that $\mathrm{trdeg}(\mathcal{R}^{\mathsf{G}}_{\leq K}) = \mathrm{trdeg}(\mathcal{R}^{\mathsf{G}})$ for $K = 3$. This implies, as in the simpler multi-reference alignment model of Perry et al. (2019), that 3^{rd}-order moments are sufficient to locally identify a generic signal up to its rotational orbit, and the squared error of the MLE scales as σ^6 in high noise. This provides a positive resolution to (Bandeira et al., 2017, Conjectures 5.6 and B.1), and also (Bandeira

et al., 2017, Conjecture 5.11) for the cryo-EM model under a mild additional assumption of $S \geq 4$ "shells".

3. We empirically study the accuracy of this finite-dimensional theory for describing the noise-scalings of the Fisher information matrices of two small proteins: a rotavirus VP6 trimer and hemoglobin. We do this by computing the observed Fisher information matrices from simulated samples in a $\mathsf{SO}(3)$-rotational model without tomographic projection based on existing cryo-EM maps of these proteins.

   Our simulations suggest that the secondary structures of both proteins, up to a spatial resolution of approximately 7-8 Angstroms, may be well-captured by a basis approximation of dimension $d \approx 4000$. At this resolution, the theoretically predicted σ^{-2}, σ^{-4}, and σ^{-6} scalings of individual eigenvalues of the Fisher information matrices are empirically observed over a range of SNR. However, we discuss also some limitations of this body of theory for capturing higher-resolution phenomena at lower levels of noise.

Section 4.2 will introduce the orbit recovery model and describe our general results in this context. Sections 4.3 and 4.4 will apply these results to examples of function estimation. Section 4.5 describes our numerical simulations for the above two protein molecules.

Notation

We use the conventions $\langle u, v \rangle = \sum_i \overline{u_i} v_i$ for the complex inner product, $\|u\|$ for the (real or complex) ℓ_2-norm, $\|M\|$ for the $\ell_2 \to \ell_2$ operator norm for matrices, and $\mathbf{i} = \sqrt{-1}$ for the imaginary unit.

For a measure space (X, μ), $L_2(X, \mathbb{C})$ is the L_2-space of functions $f : X \to \mathbb{C}$ with inner-product $\int_X \overline{f(x)} g(x) \mu(\mathrm{d}x)$. We write $L_2(X) = L_2(X, \mathbb{R})$ for the analogous L_2-space of real-valued functions. $\mathcal{S}^1$ and $\mathcal{S}^2$ are the unit circle and unit sphere.

For differentiable $f : \mathbb{R}^d \to \mathbb{R}^k$, $\mathrm{d}f(x) \in \mathbb{R}^{k \times d}$ is its derivative or Jacobian at x. For twice-differentiable $f : \mathbb{R}^d \to \mathbb{R}$, $\nabla f(x) = \mathrm{d}f(x)^\top \in \mathbb{R}^d$ is its gradient, and $\nabla^2 f(x) \in \mathbb{R}^{d \times d}$ is its Hessian. We will write $\mathrm{d}_x, \nabla_x, \nabla_x^2$ to clarify that the variable of differentiation is x. For a subset of coordinates y, we write $\nabla_y f(x)$ and $\nabla_y^2 f(x)$ as the components of this gradient and Hessian in y.

For a smooth manifold $\mathcal{M}$ and twice-differentiable $f : \mathcal{M} \to \mathbb{R}$, we write $\nabla f(x)|_{\mathcal{M}}$ and $\nabla^2 f(x)|_{\mathcal{M}}$ for its gradient and Hessian evaluated in any choice of local chart at $x \in \mathcal{M}$. We will often not

make the choice of chart explicit when referring to properties of $\nabla f(x)|_{\mathcal{M}}$ and $\nabla^2 f(x)|_{\mathcal{M}}$ that do not depend on the specific choice of chart.

4.2 The general orbit recovery model in high noise

4.2.1 Model and likelihood

Let $\theta_* \in \mathbb{R}^d$ be an unknown signal of interest. Let $\mathsf{G} \subseteq \mathsf{O}(d)$ be a known compact subgroup of the orthogonal group of dimension d. We denote by Λ the unique Haar probability measure on G, satisfying

$$\Lambda(\mathsf{G}) = 1, \qquad \Lambda(g \cdot S) = \Lambda(S \cdot g) = \Lambda(S) \text{ for all } g \in \mathsf{G} \text{ and } S \subseteq \mathsf{G}.$$

In the *unprojected orbit recovery model*, we observe n noisy and rotated samples of θ_*, given by

$$Y_i = g_i \cdot \theta_* + \sigma \varepsilon_i \in \mathbb{R}^d, \qquad i = 1, \dots, n \tag{4.1}$$

where $g_1, \dots, g_n \overset{iid}{\sim} \Lambda$ are Haar-uniform random elements of G, and $\varepsilon_1, \dots, \varepsilon_n \overset{iid}{\sim} \mathcal{N}(0, \mathrm{Id}_{d\times d})$ are Gaussian noise vectors independent of $g_1, \dots, g_n$. The signal θ_* is identifiable only up to an arbitrary rotation in G, i.e. it is identifiable up to its orbit

$$\mathcal{O}_{\theta_*} = \{g \cdot \theta_* : g \in \mathsf{G}\}.$$

Our goal is to estimate $\mathcal{O}_{\theta_*}$ from the observed rotated samples $Y_1, \dots, Y_n$.

In the *projected orbit recovery model*, we consider an additional known linear map[2] $\Pi : \mathbb{R}^d \to \mathbb{R}^{\tilde{d}}$. We observe n samples

$$Y_i = \Pi(g_i \cdot \theta_*) + \sigma \varepsilon_i \in \mathbb{R}^{\tilde{d}}, \qquad i = 1, \dots, n \tag{4.2}$$

where $g_1, \dots, g_n \overset{iid}{\sim} \Lambda$ as before, and $\varepsilon_1, \dots, \varepsilon_n \overset{iid}{\sim} \mathcal{N}(0, \mathrm{Id}_{\tilde{d}\times\tilde{d}})$ are Gaussian noise vectors in the projected dimension $\tilde{d}$. Our goal is again to estimate $\mathcal{O}_{\theta_*}$ from $Y_1, \dots, Y_n$.

The unprojected and projected orbit recovery models are both Gaussian mixture models, where the distribution of mixture centers is the law of $g \cdot \theta_* \in \mathbb{R}^d$ or of $\Pi(g \cdot \theta_*) \in \mathbb{R}^{\tilde{d}}$ induced by the uniform law $g \sim \Lambda$ over G. This mixture distribution may be continuous if $\mathsf{G} \subseteq \mathsf{O}(d)$ is a continuous

2. Here Π is a linear operator, typically not invertible, which may not necessarily be an orthogonal projection. The terminology here is borrowed from the example of the tomographic projection in cryo-EM.

subgroup. In both models, we denote the negative sample log-likelihood as

$$R_n(\theta) = -\frac{1}{n}\sum_{i=1}^{n} \log p_\theta(Y_i),$$

where $p_\theta(Y_i)$ is the Gaussian mixture density for Y_i, marginalizing over the unknown rotation $g_i \sim \Lambda$. This density is given in the projected setting by

$$p_\theta(y) = \int_{\mathsf{G}} \frac{1}{(2\pi\sigma^2)^{\tilde{d}/2}} \exp\left(-\frac{\|y - \Pi(g\cdot\theta)\|^2}{2\sigma^2}\right) \mathrm{d}\Lambda(g), \tag{4.3}$$

and in the unprojected setting by the same expression with $\Pi = \mathrm{Id}$ and $\tilde{d} = d$. The maximum likelihood estimator (MLE) of θ_* is $\hat{\theta}_n = \mathrm{argmin}_{\theta\in\mathbb{R}^d} R_n(\theta)$. Since R_n satisfies the rotational invariance $R_n(\theta) = R_n(g\cdot\theta)$ for all $g \in \mathsf{G}$, the MLE is also only defined up to its orbit $\mathcal{O}_{\hat{\theta}_n}$.

Remark 4.2.1 (Identifiability of the orbit)**.** *The parameter θ_* is identifiable up to the distribution of the mixture centers $g\cdot\theta_*$ or $\Pi(g\cdot\theta_*)$. In the unprojected model, the equality in law $g\cdot\theta \overset{L}{=} g\cdot\theta'$ over $g\sim\Lambda$ holds if and only if $\mathcal{O}_\theta = \mathcal{O}_{\theta'}$, so θ_* is identifiable exactly up to its orbit.*

In projected models, there may be further non-identifiability. For instance, under the tomographic projection arising in cryo-EM, we have $\Pi(g\cdot\theta) \overset{L}{=} \Pi(g\cdot\theta')$ when θ' represents the mirror reflection of θ Bendory et al. (2020a). Thus in this setting there may be two distinct orbits which cannot be further identified, and θ_* is recovered only up to chirality.

In general, the number of distinct orbits with the same image under Π depends on the interaction between the structures of G and Π and can be infinite. For example, for the trivial group $\mathsf{G} = \{\mathrm{Id}\}$ and the projection $\Pi : \mathbb{R}^d \to \mathbb{R}^{d-k}$ that removes the last k coordinates of θ, $\mathcal{O}_\theta = \{\theta\}$ and $\Pi(\mathcal{O}_\theta) = \Pi(\mathcal{O}_{\theta_*})$ for any θ sharing the same first $d-k$ coordinates as θ_*.

We use the equivalence notation

$$\Pi(\mathcal{O}_\theta) \equiv \Pi(\mathcal{O}_{\theta_*})$$

to mean that $\Pi(\mathcal{O}_\theta) = \Pi(\mathcal{O}_{\theta_*})$ as subsets of $\mathbb{R}^{\tilde{d}}$, and in addition, $\Pi(g\cdot\theta) \overset{L}{=} \Pi(g\cdot\theta_*)$ under the Haar-uniform law $g\sim\Lambda$. Thus θ_* is identifiable up to this equivalence. We will restrict attention to projected models where

$$\text{there are a finite number of orbits } \mathcal{O}_\theta \text{ such that } \Pi(\mathcal{O}_\theta) \equiv \Pi(\mathcal{O}_{\theta_*}), \text{ for generic } \theta_* \in \mathbb{R}^d. \tag{4.4}$$

An equivalent algebraic characterization is provided in Proposition 4.2.4(b) below.

We denote the negative *population* log-likelihood function by

$$R(\theta) = \mathbb{E}[R_n(\theta)] = -\mathbb{E}[\log p_\theta(Y)], \tag{4.5}$$

where the expectation is taken under the true model $Y \sim p_{\theta_*}$.[3] This population log-likelihood is minimized at $\theta \in \mathcal{O}_{\theta_*}$ in the unprojected model, and at $\{\theta : \Pi(\mathcal{O}_\theta) \equiv \Pi(\mathcal{O}_{\theta_*})\}$ in projected models.

4.2.2 Invariant polynomials and the high-noise expansion

For sufficiently high noise σ^2, it is informative to study $R(\theta)$ via a series expansion of the Gaussian density of (4.3) in powers of σ^{-1}, as developed in Fan et al. (2020); Katsevich and Bandeira (2020). We review this expansion in this section.

Let $\mathcal{R}^{\mathsf{G}}$ be the (real) algebra of all G-invariant polynomial functions $p : \mathbb{R}^d \to \mathbb{R}$. These are the polynomials that satisfy

$$p(\theta) = p(g \cdot \theta) \text{ for all } \theta \in \mathbb{R}^d \text{ and } g \in \mathsf{G}.$$

For each integer $k \geq 0$, let $\mathcal{R}^{\mathsf{G}}_{\leq k}$ be the subalgebra generated by the G-invariant polynomials having total degree at most k. These are the polynomials $p \in \mathcal{R}^{\mathsf{G}}$ that may be expressed as $p(\theta) = q(p_1(\theta), \ldots, p_j(\theta))$ for some polynomial q and some $p_1, \ldots, p_j \in \mathcal{R}^{\mathsf{G}}$ each having degree $\leq k$.

Examples of polynomials in $\mathcal{R}^{\mathsf{G}}_{\leq k}$ include the entries of the symmetric moment tensors

$$T_k(\theta) = \int_{\mathsf{G}} (g \cdot \theta)^{\otimes k} \, \mathrm{d}\Lambda(g) \in \mathbb{R}^{d \times \ldots \times d},$$

which are the k^{th}-order mixed moments of the distribution of Gaussian mixture centers $g \cdot \theta$. Conversely, all degree-k G-invariant polynomials are affine linear combinations of entries of $T_1, \ldots, T_k$, so $\mathcal{R}^{\mathsf{G}}_{\leq k}$ is generated by $T_1, \ldots, T_k$. The subalgebra $\mathcal{R}^{\mathsf{G}}_{\leq k}$ may be intuitively understood as containing all information in the moments of orders 1 to k for the Gaussian mixture defined by θ.

For the projected model with projection Π, we define analogously the projected moment tensors

$$\widetilde{T}_k(\theta) = \int_{\mathsf{G}} (\Pi \cdot g \cdot \theta)^{\otimes k} \mathrm{d}\Lambda(g) \in \mathbb{R}^{\tilde{d} \times \ldots \times \tilde{d}},$$

which are again the mixed moments of the Gaussian mixture centers $\Pi \cdot g \cdot \theta$. We then define

$$\widetilde{\mathcal{R}}^{\mathsf{G}}_{\leq k} = \text{subalgebra of } \mathcal{R}^{\mathsf{G}} \text{ generated by the entries of } \widetilde{T}_1, \ldots, \widetilde{T}_k.$$

3. $R(\theta)$ depends implicitly on θ_*, but we will omit this dependence in the notation.

Since each entry of $\widetilde{T}_k$ is a G-invariant polynomial of degree k, we have $\widetilde{\mathcal{R}}^{\mathsf{G}}_{\leq k} \subseteq \mathcal{R}^{\mathsf{G}}_{\leq k}$, but equality does not necessarily hold.

We denote by $\langle \cdot, \cdot \rangle$ the Euclidean inner-product in the vectorization of these tensor spaces $\mathbb{R}^{d \times \ldots \times d}$ and $\mathbb{R}^{\tilde{d} \times \ldots \times \tilde{d}}$, and by $\| \cdot \|^2_{\mathrm{HS}}$ the corresponding squared Euclidean norm. We will use the following general form of the large-σ series expansion of the population log-likelihood $R(\theta)$. We explain how the results of Katsevich and Bandeira (2020) yield this form in Appendix C.1.

Theorem 4.2.1. *Let $\mathsf{G} \subseteq \mathsf{O}(d)$ be any compact subgroup. Fix any $\theta_* \in \mathbb{R}^d$ and any integer $K \geq 0$.*

(a) In the unprojected orbit recovery model, $R(\theta)$ admits an expansion

$$R(\theta) = C_0 + \sum_{k=1}^{K} \frac{1}{\sigma^{2k}} \Big(s_k(\theta) + q_k(\theta) \Big) + q(\theta). \tag{4.6}$$

Here $C_0 \in \mathbb{R}$, $q_k \in \mathcal{R}^{\mathsf{G}}_{\leq k-1}$ is a polynomial of degree at most $2k$, and $s_k \in \mathcal{R}^{\mathsf{G}}_{\leq k}$ is the polynomial

$$s_k(\theta) = \frac{1}{2(k!)} \| T_k(\theta) - T_k(\theta_*) \|^2_{\mathrm{HS}}. \tag{4.7}$$

The remainder $q(\theta)$ is G-invariant and satisfies, for all $\theta \in \mathbb{R}^d$ with $\|\theta\| \leq \sigma$,

$$|q(\theta)| \leq \frac{C_K (1 \vee \|\theta\|)^{2K+2}}{\sigma^{2K+2}}, \quad \|\nabla q(\theta)\| \leq \frac{C_K (1 \vee \|\theta\|)^{2K+1}}{\sigma^{2K+2}}, \quad \|\nabla^2 q(\theta)\| \leq \frac{C_K (1 \vee \|\theta\|)^{2K}}{\sigma^{2K+2}}. \tag{4.8}$$

(b) In the projected orbit recovery model, $R(\theta)$ admits an expansion

$$R(\theta) = C_0 + \sum_{k=1}^{K} \frac{1}{\sigma^{2k}} \Big(\tilde{s}_k(\theta) + \big\langle \widetilde{T}_k(\theta), P_k(\theta) \big\rangle + q_k(\theta) \Big) + q(\theta). \tag{4.9}$$

Here $C_0 \in \mathbb{R}$, $q_k \in \widetilde{\mathcal{R}}^{\mathsf{G}}_{\leq k-1}$ is a polynomial of degree at most $2k$, all entries of P_k are polynomials of degree at most k belonging to $\widetilde{\mathcal{R}}^{\mathsf{G}}_{\leq k-1}$, P_k satisfies $P_k(\theta_*) = 0$, and $\tilde{s}_k \in \widetilde{\mathcal{R}}^{\mathsf{G}}_{\leq k}$ is the polynomial

$$\tilde{s}_k(\theta) = \frac{1}{2(k!)} \| \widetilde{T}_k(\theta) - \widetilde{T}_k(\theta_*) \|^2_{\mathrm{HS}}. \tag{4.10}$$

The remainder $q(\theta)$ is G-invariant and satisfies (4.8) for all $\theta \in \mathbb{R}^d$ with $\|\theta\| \leq \sigma$.

The above constants C_0, C_K, the coefficients of the polynomials $q_k(\theta)$ and $P_k(\theta)$, and the forms of the functions $q(\theta)$ may all depend on $\theta_*, \mathsf{G}, d, \tilde{d}$, and the projection Π.

The exact forms of $q_k(\theta)$ and $P_k(\theta)$ can be explicitly derived—see (Fan et al., 2020, Section 4.2)

for these derivations in the unprojected setting—but we will not require them in what follows. Our arguments will only require the forms of the "leading" terms $s_k(\theta)$ and $\tilde{s}_k(\theta)$ defined in (4.7) and (4.10).

4.2.3 Fisher information in high noise

Consider the Fisher information matrix

$$I(\theta_*) = \nabla^2 R(\theta)\big|_{\theta=\theta_*}.$$

In this section, we characterize the scaling dependence of the eigenvalues of $I(\theta_*)$ on the noise level σ^2, for high noise and generic $\theta_* \in \mathbb{R}^d$. This generalizes the analogous result (Fan et al., 2020, Theorem 4.14) for the unprojected model and a discrete group.

Definition 4.2.2. *A subset $S \subseteq \mathbb{R}^d$ is* generic *if $\mathbb{R}^d \setminus S$ is contained in the zero set of some non-zero analytic function $\psi : \mathbb{R}^d \to \mathbb{R}^k$, for some $k \geq 1$.*

If $S \subseteq \mathbb{R}^d$ is generic, then $\mathbb{R}^d \setminus S$ has zero Lebesgue measure Mityagin (2020). We say that a statement holds for generic $\theta_* \in \mathbb{R}^d$ if it holds for all θ_* in some generic subset.

Our characterization of $I(\theta_*)$ is in terms of the number of distinct "degrees-of-freedom" captured by the moments of the Gaussian mixture model up to each order k. This is formalized by the notion of the transcendence degrees of the subalgebras $\mathcal{R}^{\mathsf{G}}_{\leq k}$ and $\widetilde{\mathcal{R}}^{\mathsf{G}}_{\leq k}$.

Definition 4.2.3. *For any subalgebra $\mathcal{A} \subseteq \mathcal{R}^{\mathsf{G}}$, its* transcendence degree $\mathrm{trdeg}(\mathcal{A})$ *is the maximum size of any algebraically independent (over $\mathbb{R}$) subset $S \subseteq \mathcal{A}$.*

Geometrically, this coincides with the maximum number of linearly independent gradient vectors of the polynomials in $\mathcal{A}$, evaluated at any generic point $\theta \in \mathbb{R}^d$.

For the full invariant algebra $\mathcal{R}^{\mathsf{G}}$, if $\mathsf{G} \subseteq \mathsf{O}(d)$ is a discrete subgroup as studied in Fan et al. (2020), then $\mathrm{trdeg}(\mathcal{R}^{\mathsf{G}}) = d$. More generally,

$$\mathrm{trdeg}(\mathcal{R}^{\mathsf{G}}) = d - \max_{\theta \in \mathbb{R}^d} \dim(\mathcal{O}_\theta),$$

where $\max_{\theta \in \mathbb{R}^d} \dim(\mathcal{O}_\theta)$ is the dimension[4] of a generic orbit. We will mostly consider group actions where this orbit dimension equals the group dimension $\dim(\mathsf{G})$, so that $\mathrm{trdeg}(\mathcal{R}^{\mathsf{G}}) = d - \dim(\mathsf{G})$. In

4. This is formally defined as $\dim(\mathcal{O}_\theta) = \dim(\mathsf{G}) - \dim(\mathsf{G}_\theta)$ where $\mathsf{G}_\theta = \{g \in \mathsf{G} : g \cdot \theta = \theta\}$ is the stabilizer subgroup of θ, and $\dim(\mathsf{G}), \dim(\mathsf{G}_\theta)$ are their dimensions as Lie subgroups of $\mathsf{O}(d)$.

particular, for the function estimation examples to be discussed in Sections 4.3 and 4.4, we will have $\mathrm{trdeg}(\mathcal{R}^{\mathsf{G}}) = d-1$ for an action of $\mathsf{G} = \mathsf{SO}(2)$, and $\mathrm{trdeg}(\mathcal{R}^{\mathsf{G}}) = d-3$ for an action of $\mathsf{G} = \mathsf{SO}(3)$.

It was shown in Bandeira et al. (2017) that the order of moments needed to locally identify the orbit of a generic signal $\theta_* \in \mathbb{R}^d$ coincides with the order needed to capture all $\mathrm{trdeg}(\mathcal{R}^{\mathsf{G}})$ degrees-of-freedom of the invariant algebra. We will denote this order as K in the unprojected model, and $\widetilde{K}$ in the projected model. These are defined formally by the following proposition, whose proof we defer to Appendix C.1.

Proposition 4.2.4. *For any compact subgroup* $\mathsf{G} \subseteq \mathsf{O}(d)$*,*

(a) There is a smallest integer $K < \infty$ *for which* $\mathrm{trdeg}(\mathcal{R}^{\mathsf{G}}_{\leq K}) = \mathrm{trdeg}(\mathcal{R}^{\mathsf{G}})$*.*

(b) Π *satisfies (4.4) if and only if there is a smallest integer* $\widetilde{K} < \infty$ *for which* $\mathrm{trdeg}(\widetilde{\mathcal{R}}^{\mathsf{G}}_{\leq \widetilde{K}}) = \mathrm{trdeg}(\mathcal{R}^{\mathsf{G}})$*.*

In the unprojected model, let us now denote

$$d_0 = \max_{\theta \in \mathbb{R}^d} \dim(\mathcal{O}_\theta), \qquad d_k = \mathrm{trdeg}\, \mathcal{R}^{\mathsf{G}}_{\leq k} - \mathrm{trdeg}\, \mathcal{R}^{\mathsf{G}}_{\leq k-1} \text{ for } k = 1, \ldots, K \tag{4.11}$$

to decompose the total dimension of θ_* as $d = d_0 + d_1 + \ldots + d_K$. In the projected model, assuming the condition (4.4), let us similarly denote

$$\tilde{d}_0 = \max_{\theta \in \mathbb{R}^d} \dim(\mathcal{O}_\theta), \qquad \tilde{d}_k = \mathrm{trdeg}\, \widetilde{\mathcal{R}}^{\mathsf{G}}_{\leq k} - \mathrm{trdeg}\, \widetilde{\mathcal{R}}^{\mathsf{G}}_{\leq k-1} \text{ for } k = 1, \ldots, \widetilde{K} \tag{4.12}$$

to decompose the total dimension as $d = \tilde{d}_0 + \tilde{d}_1 + \ldots + \tilde{d}_{\widetilde{K}}$. The following result expresses the spectral properties of the Fisher information matrix in terms of these decompositions.

Theorem 4.2.5. *For any generic* $\theta_* \in \mathbb{R}^d$*, some* $\sigma_0 \equiv \sigma_0(\theta_*, \mathsf{G}, \Pi)$*, and all* $\sigma > \sigma_0$*:*

(a) In the unprojected orbit recovery model,

1. *The Fisher information matrix* $I(\theta_*)$ *has rank exactly* $\mathrm{trdeg}(\mathcal{R}^{\mathsf{G}}) = d - d_0$*. Defining* K *by Proposition 4.2.4(a), for some* (θ_*, G)*-dependent constants* $C, c > 0$ *(independent of* σ*) and each* $k = 1, \ldots, K$*,*

   $$\text{exactly } d_k \text{ eigenvalues of } I(\theta_*) \text{ belong to } [c\sigma^{-2k}, C\sigma^{-2k}].$$

2. *For any* $k = 1, \ldots, K$*, any polynomial* $p \in \mathcal{R}^{\mathsf{G}}_{\leq k}$*, and some* $(p, \theta_*, \mathsf{G})$*-dependent constant*

$C > 0$, the gradient $\nabla p(\theta_*) \in \mathbb{R}^d$ is orthogonal to the null space of $I(\theta_*)$ and satisfies

$$\nabla p(\theta_*)^\top I(\theta_*)^\dagger \nabla p(\theta_*) \le C\sigma^{2k}$$

where $I(\theta_*)^\dagger$ is the Moore-Penrose pseudo-inverse.

(b) In the projected orbit recovery model satisfying condition (4.4), the same statements hold with $\mathcal{R}^{\mathsf{G}}_{\le k}$, K, and d_k replaced by $\widetilde{\mathcal{R}}^{\mathsf{G}}_{\le k}$, $\widetilde{K}$, and $\tilde{d}_k$, where $\widetilde{K}$ is defined by Proposition 4.2.4(b).

Theorem 4.2.5(a1) implies that $I(\theta_*)$ has eigenvalues on differing scales of σ^{-2} in high-noise settings, with d_k such eigenvalues scaling as σ^{-2k}, and $d_0 = \dim(\mathcal{O}_{\theta_*})$ eigenvalues of 0 representing the non-identifiable degrees-of-freedom tangent to $\mathcal{O}_{\theta_*}$. Thus there are d_k degrees-of-freedom in θ_* that are estimated with asymptotic variance $O(\sigma^{2k}/n)$ by the MLE. The largest such variance is $O(\sigma^{2K}/n)$, which is in accordance with results about list-recovery of generic signals in Bandeira et al. (2017).

Theorem 4.2.5(a2) describes also the associated spaces of eigenvectors. In the limit $\sigma \to \infty$, the eigenspace of $I(\theta_*)$ corresponding to its eigenvalues of scales $\sigma^{-2}, \dots, \sigma^{-2k}$ coincides with the linear span of the gradients $\{\nabla p(\theta_*) : p \in \mathcal{R}^{\mathsf{G}}_{\le k}\}$. Thus, for large σ, the functional $p(\theta_*)$ for any $p \in \mathcal{R}^{\mathsf{G}}_{\le k}$ is also estimated by the plug-in MLE $p(\hat{\theta}_n)$ with asymptotic variance $O(\sigma^{2k}/n)$. Similar statements hold for projected models by Theorem 4.2.5(b).

The following result connects the above sequences of transcendence degrees and gradients $\{\nabla p(\theta_*)$: $p \in \mathcal{R}^{\mathsf{G}}_{\le k}\}$ to the terms $s_k(\theta)$ and $\tilde{s}_k(\theta)$ in the series expansions of $R(\theta)$ in Theorem 4.2.1. We will use this to deduce the values of these transcendence degrees for the function estimation examples of Sections 4.3 and 4.4.

Lemma 4.2.6. *(a) In the unprojected orbit recovery model, let $s_k(\theta)$ be defined by (4.7). Then each matrix $\nabla^2 s_k(\theta)|_{\theta=\theta_*}$ is positive semidefinite. For any $k \ge 1$, at generic $\theta_* \in \mathbb{R}^d$,*

$$\operatorname{trdeg}(\mathcal{R}^{\mathsf{G}}_{\le k}) = \operatorname{rank}\Big(\nabla^2 s_1(\theta) + \ldots + \nabla^2 s_k(\theta)\Big|_{\theta=\theta_*}\Big),$$

and the linear span of $\{\nabla p(\theta_*) : p \in \mathcal{R}^{\mathsf{G}}_{\le k}\}$ is the column span of $\nabla^2 s_1(\theta) + \ldots + \nabla^2 s_k(\theta)|_{\theta=\theta_*}$.

(b) In the projected orbit recovery model, the same holds for $\widetilde{\mathcal{R}}^{\mathsf{G}}_{\le k}$ and $\tilde{s}_k(\theta)$ as defined by (4.10).

Remark 4.2.2. *We restrict attention to generic signals $\theta_* \in \mathbb{R}^d$ in this work. Different behavior may be observed for non-generic signals: For $\mathsf{G} = \{+\mathrm{Id}, -\mathrm{Id}\}$, which has been studied in Xu et al. (2016); Wu and Zhou (2019), the Fisher information $I(\theta_*)$ is singular at $\theta_* = 0$ (even though $d_0 = 0$,*

as the group is discrete). This leads to a $n^{-1/4}$ rate of estimation error near $\theta_* = 0$, instead of the $n^{-1/2}$ parametric rate. This $n^{-1/4}$ rate holds more generally for any discrete group G at signals θ_* whose orbit points are not pairwise distinct, which are precisely those signals where the Fisher information $I(\theta_*)$ is singular Brunel (2019).

A different distinction between generic and non-generic signals was highlighted in Perry et al. (2019) when G is the group of cyclic rotations of coordinates in $\mathbb{R}^d$. There, orbits of generic signals are uniquely identified by moments up to the order $K = 3$, but identification of non-generic signals having zero power in certain Fourier frequencies may require moments up to the order $d - 1$. For such non-generic signals, we expect $I(\theta_*)$ to be non-singular and the MLE to attain the parametric rate, but with asymptotic variance scaling as $\sigma^{2(d-1)}/n$ rather than $\sigma^{2K}/n = \sigma^6/n$. In the case of (unprojected) continuous MRA, this was shown in Bandeira et al. (2020).

4.2.4 Global likelihood landscape

Theorem 4.2.1 also sheds light on the optimization trajectories of descent algorithms and the global likelihood landscape in high noise. In this section, we describe the global and local minimizers of the (negative) population log-likelihood $R(\theta)$, extending similar results of (Fan et al., 2020, Section 4.5) for the unprojected model and discrete groups.

We recall the following structural property for smooth non-convex optimization landscapes, under which convergence to the global optimum from a random initialization is guaranteed for various descent-based optimization algorithms Ge et al. (2015); Lee et al. (2016); Jin et al. (2017).

Definition 4.2.7. *The problem of minimizing a twice-continuously differentiable function $f : \mathcal{V} \to \mathbb{R}$ over a smooth manifold $\mathcal{V}$ is* globally benign *if each point $x \in \mathcal{V}$ where $\nabla f(x)|_{\mathcal{V}} = 0$ is either a global minimizer of f over $\mathcal{V}$, or has a direction of strict negative curvature, $\lambda_{\min}(\nabla^2 f(x)|_{\mathcal{V}}) < 0$.*

Here $\nabla f(x)|_{\mathcal{V}}$ and $\nabla^2 f(x)|_{\mathcal{V}}$ denote the gradient and Hessian of f on $\mathcal{V}$, which may be taken in any choice of a smooth local chart around $x \in \mathcal{V}$.

Minimizing $R(\theta)$ in high noise may be viewed as successively solving a sequence of moment optimizations defined by the terms of its expansion in Theorem 4.2.1. To ease notation, let us collect the vectorized moment tensors up to order k as

$$M_k(\theta) = \operatorname{vec}\Big(T_1(\theta), \dots, T_k(\theta)\Big) \in \mathbb{R}^{d+d^2+\dots+d^k}, \tag{4.13}$$

$$\widetilde{M}_k(\theta) = \operatorname{vec}\Big(\widetilde{T}_1(\theta), \dots, \widetilde{T}_k(\theta)\Big) \in \mathbb{R}^{\tilde{d}+\tilde{d}^2+\dots+\tilde{d}^k}. \tag{4.14}$$

Fixing the true signal $\theta_* \in \mathbb{R}^d$, we define the moment varieties

$$\mathcal{V}_k(\theta_*) = \Big\{\theta \in \mathbb{R}^d : M_k(\theta) = M_k(\theta_*)\Big\}, \qquad \mathcal{V}_0(\theta_*) = \mathbb{R}^d,$$
$$\widetilde{\mathcal{V}}_k(\theta_*) = \Big\{\theta \in \mathbb{R}^d : \widetilde{M}_k(\theta) = \widetilde{M}_k(\theta_*)\Big\}, \qquad \widetilde{\mathcal{V}}_0(\theta_*) = \mathbb{R}^d.$$

These are the points $\theta \in \mathbb{R}^d$ for which the mixed moments of the Gaussian mixture model defined by θ match those of the true signal θ_* up to the order k.

We state a general result on the optimization landscape, assuming that the Jacobian matrices $\mathrm{d}M_k$ and $\mathrm{d}\widetilde{M}_k$ have constant rank over $\mathcal{V}_k(\theta_*)$ and $\widetilde{\mathcal{V}}_k(\theta_*)$, so that $\mathcal{V}_k(\theta_*)$ and $\widetilde{\mathcal{V}}_k(\theta_*)$ are smooth manifolds of constant dimension. Then, recalling $s_k(\theta)$ and $\tilde{s}_k(\theta)$ from (4.7) and (4.10), we consider the optimization problem

$$\text{minimize } s_k(\theta) \text{ over } \theta \in \mathcal{V}_{k-1}(\theta_*) \tag{4.15}$$

in the unprojected setting, and

$$\text{minimize } \tilde{s}_k(\theta) \text{ over } \theta \in \widetilde{\mathcal{V}}_{k-1}(\theta_*) \tag{4.16}$$

in the projected setting. These are polynomial optimization problems in θ that are defined independently of the noise level σ^2.

Theorem 4.2.8. *For any generic $\theta_* \in \mathbb{R}^d$:*

(a) In the unprojected model, define K by Proposition 4.2.4(a). Suppose that $\mathcal{V}_K(\theta_*) = \mathcal{O}_{\theta_*}$. Suppose also that for each $k = 1, \dots, K$, $\mathrm{d}M_k(\theta)$ has constant rank over $\mathcal{V}_k(\theta_*)$, and the minimization of $s_k(\theta)$ over $\mathcal{V}_{k-1}(\theta_*)$ is globally benign. Then for some $\sigma_0 \equiv \sigma_0(\theta_*, \mathsf{G}, \Pi)$ and any $\sigma > \sigma_0$, the minimization of $R(\theta)$ is also globally benign.

(b) In the projected model satisfying (4.4), define $\widetilde{K}$ by Proposition 4.2.4(b). Suppose that $\widetilde{\mathcal{V}}_{\widetilde{K}}(\theta_*) = \{\theta : \Pi(\mathcal{O}_\theta) \equiv \Pi(\mathcal{O}_{\theta_*})\}$. Suppose also that for each $k = 1, \dots, \widetilde{K}$, $\mathrm{d}\widetilde{M}_k(\theta)$ has constant rank over $\widetilde{\mathcal{V}}_k(\theta_*)$ and the minimization of $\tilde{s}_k(\theta)$ over $\widetilde{\mathcal{V}}_{k-1}(\theta_*)$ is globally benign. Then for any $B > 0$, some $\sigma_0 \equiv \sigma_0(\theta_*, \mathsf{G}, \Pi, B)$, and any $\sigma > \sigma_0$, the minimization of $R(\theta)$ is globally benign over the domain $\{\theta \in \mathbb{R}^d : \|\theta\| < B(\|\theta_*\| + \sigma)\}$.

We illustrate part (a) of this result using a simple example of orthogonal Procrustes alignment at the conclusion of this section.

In Theorem 4.2.8(b), we have restricted to $\{\theta \in \mathbb{R}^d : \|\theta\| < B(\|\theta_*\| + \sigma)\}$, as the landscape of $R(\theta)$ outside this ball may have a complicated dependence on the specific structures of (Π, G). In

practice, such a bound for $\|\theta\|$ may be known a priori, so that optimization may indeed be restricted to this ball. In the unprojected setting of $\Pi = \mathrm{Id}$, the landscape of $R(\theta)$ outside this ball is easy to understand, allowing us to remove such a restriction for part (a).

In applications where the conditions of the above theorem do not hold, and $R(\theta)$ in fact has spurious local minimizers in high noise, Theorem 4.2.1 can be used to further establish a correspondence between the local minimizers of $R(\theta)$ and those of the above moment optimizations. We formalize one such result—not fully general, but sufficient to study many examples of interest—as follows.

Definition 4.2.9. *Suppose $\mathcal{V}_{K-1}(\theta_*)$ is a smooth manifold with constant dimension $\dim(\mathcal{V}_{K-1}(\theta_*))$. A critical point θ of $s_K(\theta)|_{\mathcal{V}_{K-1}(\theta_*)}$ is* non-degenerate up to orbit *if $\mathcal{O}_\theta$ is a smooth manifold of dimension d_0 in a local neighborhood of θ, and*

$$\operatorname{rank}\left(\nabla^2 s_K(\theta)|_{\mathcal{V}_{K-1}(\theta_*)}\right) = \dim(\mathcal{V}_{K-1}(\theta_*)) - d_0.$$

Note that $\nabla^2 s_K(\theta)|_{\mathcal{V}_{K-1}(\theta_*)}$ is a symmetric matrix of dimension $\dim(\mathcal{V}_{K-1}(\theta_*))$. For any critical point θ of $s_K|_{\mathcal{V}_{K-1}(\theta_*)}$, the null space of this Hessian must contain the tangent space to $\mathcal{O}_\theta$, so the definition is a "Morseness condition" ensuring that this Hessian has no further rank degeneracy.

Theorem 4.2.10. *For any generic $\theta_* \in \mathbb{R}^d$, any $B > 0$, some $\sigma_0 \equiv \sigma_0(\theta_*, \mathsf{G}, \Pi, B)$ and $(\theta_*, \mathsf{G}, \Pi, B)$-dependent function $\varepsilon(\sigma)$ satisfying $\varepsilon(\sigma) \to 0$ as $\sigma \to \infty$, and all $\sigma > \sigma_0$:*

(a) In the unprojected model, suppose that for each $k = 1, \dots, K-1$, $\mathrm{d}M_k(\theta)$ has constant rank over $\mathcal{V}_k(\theta_*)$ and the minimization of $s_k(\theta)$ over $\mathcal{V}_{k-1}(\theta_*)$ is globally benign.

1. *Let θ be any* local *minimizer of $s_K(\theta)$ over $\mathcal{V}_{K-1}(\theta_*)$ that is non-degenerate up to orbit. Then there exists a local minimizer θ' of $R(\theta)$ where $\|\theta - \theta'\| < \varepsilon(\sigma)$.*
2. *Conversely, suppose that all critical points of $s_K(\theta)$ over $\mathcal{V}_{K-1}(\theta_*)$ are non-degenerate up to orbit. Let θ be any local minimizer of $R(\theta)$ satisfying $\|\theta\| < B(\|\theta_*\| + \sigma)$. Then there is a local minimizer θ' of $s_K(\theta)$ over $\mathcal{V}_{K-1}(\theta_*)$ where $\|\theta - \theta'\| < \varepsilon(\sigma)$.*

(b) In the projected model satisfying (4.4), the same statements hold with K, d_K, M_k, $\mathcal{V}_k$, and s_k replaced by $\widetilde{K}$, $\tilde{d}_{\widetilde{K}}$, $\widetilde{M}_k$, $\widetilde{\mathcal{V}}_k$, and $\tilde{s}_k$.

The guarantees of Theorems 4.2.8 and 4.2.10 may be translated to the sample log-likelihood $R_n(\theta)$ by establishing concentration of $\nabla R_n(\theta)$ and $\nabla^2 R_n(\theta)$ around $\nabla R(\theta)$ and $\nabla^2 R(\theta)$ Mei et al. (2018). We omit these finite-sample statements here, and refer readers to Fan et al. (2020) for details of establishing the requisite concentration bounds in these types of orbit recovery problems.

Example 4.2.11 (Landscape of orthogonal Procrustes alignment)**.** *We illustrate Theorems 4.2.8 and 4.2.10 using the simple example of* orthogonal Procrustes alignment *Gower (1975); Goodall (1991); Pumir et al. (2019).*

In this problem, samples of an object consisting of $m \geq 3$ atoms in $\mathbb{R}^3$ are observed under random orthogonal rotations and reflections. We represent the object as $\theta_* \in \mathbb{R}^{3\times m} \cong \mathbb{R}^d$ where $d = 3m$. The rotational group is $\mathsf{G} = \mathsf{O}(3) \otimes \mathrm{Id}_m \subset \mathsf{O}(d)$, where a common orthogonal matrix in 3-dimensions is applied to all m atoms. Assuming the generic condition $\mathrm{rank}(\theta_*) = 3$, i.e. these m atoms do not lie on a common 2-dimensional subspace, we study the likelihood landscape for estimating θ_* from many independently rotated samples.

In this model, we check in Appendix C.2 that $K = 2$, $(d_0, d_1, d_2) = (3, 0, d-3)$, $\mathcal{V}_1(\theta_*) = \mathbb{R}^d$, and $\mathcal{V}_2(\theta_*) = \{g \cdot \theta_* : g \in \mathsf{G}\} = \mathcal{O}_{\theta_*}$. The terms $s_1(\theta)$ and $s_2(\theta)$ in (4.6) are given by $s_1(\theta) = 0$ and

$$s_2(\theta) = \frac{1}{12}\|\theta^\top\theta - \theta_*^\top\theta_*\|_{\mathrm{HS}}^2,$$

where $\theta^\top\theta, \theta_*^\top\theta_* \in \mathbb{R}^{m\times m}$. The minimization of $s_1(\theta)$ over $\mathcal{V}_0(\theta_*) = \mathbb{R}^d$ is trivially globally benign. We show in Appendix C.2 that the minimization of $s_2(\theta)$ over $\mathcal{V}_1(\theta_*) = \mathbb{R}^d$ is also globally benign, with minimizers given exactly by $\mathcal{V}_2(\theta_*) = \mathcal{O}_{\theta_*}$. Thus, Theorem 4.2.8(a) implies that the landscape of $R(\theta)$ is also globally benign for sufficiently high noise: The only local minimizers of $R(\theta)$ are the orbit points $\mathcal{O}_{\theta_*}$, constituting the rotations and reflections of the true object.

A commonly-arising variation of this problem is the rotation-only variant, where we observe 3-dimensional rotations (but not reflections) of the object. Then the rotational group is instead $\mathsf{G} = \mathsf{SO}(3) \otimes \mathrm{Id}_m \subset \mathsf{O}(d)$. We show in Appendix C.2 that still $K = 2$, $(d_0, d_1, d_2) = (3, 0, d-3)$, and the forms of $\mathcal{V}_1(\theta_*), \mathcal{V}_2(\theta_*), s_1(\theta), s_2(\theta)$ are identical to the above (even though the full log-likelihood $R(\theta)$ is not). Thus the minimization of $s_2(\theta)$ over $\mathcal{V}_1(\theta_*) = \mathbb{R}^d$ is still globally benign, with minimizers $\mathcal{V}_2(\theta_*)$. However, this set of minimizers is now written as

$$\mathcal{V}_2(\theta_*) = \{g \cdot \theta_* : g \in \mathsf{G}\} \cup \{-g \cdot \theta_* : g \in \mathsf{G}\} = \mathcal{O}_{\theta_*} \cup \mathcal{O}_{-\theta_*}$$

constituting two distinct orbits under this more restrictive group action. The first orbit $\mathcal{O}_{\theta_*}$ are the global minimizers of $R(\theta)$. The second orbit corresponds to the mirror reflection $-\theta_*$, which does not globally minimize $R(\theta)$, but the difference between $R(\theta_*)$ and $R(-\theta_*)$ lies in the remainder term of the expansion (4.6). Theorem 4.2.10(a) shows that for high noise, $R(\theta)$ will have spurious local minimizers near (but not exactly equal to) this second orbit $\mathcal{O}_{-\theta_*}$.

4.3 Continuous multi-reference alignment

We now specialize the preceding general results to an example of estimating a periodic function on the circle, observed under $\mathsf{SO}(2)$ rotations of its domain. We will refer to this as the *continuous multi-reference alignment* (MRA) model. We study the unprojected model in Section 4.3.1, and a version with a two-fold projection in Section 4.3.2. These provide simpler 1-dimensional analogues of the 2-dimensional and 3-dimensional problems that we will discuss in Section 4.4.

Our main results are the following:

1. We show that 3$^{\text{rd}}$-order moments are sufficient to locally identify θ_* up to orbit by showing that $\operatorname{trdeg}(\mathcal{R}^{\mathsf{G}}_{\leq K}) = \operatorname{trdeg}(\mathcal{R}^{\mathsf{G}})$ and $\operatorname{trdeg}(\widetilde{\mathcal{R}}^{\mathsf{G}}_{\leq \widetilde{K}}) = \operatorname{trdeg}(\mathcal{R}^{\mathsf{G}})$ for $K = \widetilde{K} = 3$. We also characterize the spectral structure of the Fisher information in Theorem 4.2.5 by establishing the values of (d_0, d_1, d_2, d_3) and $(\tilde{d}_0, \tilde{d}_1, \tilde{d}_2, \tilde{d}_3)$.

2. We describe more explicitly the moment optimization problems (4.15) and (4.16), by expressing $s_k(\theta)$ and $\tilde{s}_k(\theta)$ in terms of the Fourier power spectrum and bispectrum of the underlying signal θ_*.

3. Using Theorem 4.2.10, we exhibit the possible existence of spurious local minimizers of the likelihood landscape, even for generic signals. For simplicity, we do this only in the unprojected setting.

4.3.1 Unprojected continuous MRA

Let $\mathcal{S}^1 \cong [0,1)$ be the unit circle, and $f : \mathcal{S}^1 \to \mathbb{R}$ a periodic function. We consider observations of f in white noise, observed under uniform random rotations of its domain. We represent such a rotation as $\mathfrak{g}^{-1} \cdot t := t + \mathfrak{g} \bmod 1$ where $\mathfrak{g} \sim \operatorname{Unif}([0,1))$, and denote f rotated by $\mathfrak{g}$ as $f_{\mathfrak{g}}(t) = f(t + \mathfrak{g} \bmod 1)$. Then each sample is an observation of the whole function

$$f_{\mathfrak{g}}(t)\mathrm{d}t + \sigma\, \mathrm{d}W(t) \text{ over } t \in \mathcal{S}^1$$

where $\mathrm{d}W(t)$ is standard white noise on the circle $\mathcal{S}^1$.

To write this in the form of our preceding orbit recovery model, we pass to a Gaussian sequence form using the real Fourier basis on $\mathcal{S}^1$, given by

$$h_0(t) = 1, \qquad h_{l1}(t) = \sqrt{2}\cos 2\pi l t, \qquad h_{l2}(t) = \sqrt{2}\sin 2\pi l t \qquad \text{for } l = 1, 2, 3, \ldots. \tag{4.17}$$

We assume that $f : \mathcal{S}^1 \to \mathbb{R}$ has a finite bandlimit $L \geq 1$ in this basis, i.e. f admits a representation

$$f(t) = \theta^{(0)} h_0(t) + \sum_{l=1}^{L} \theta_1^{(l)} h_{l1}(t) + \sum_{l=1}^{L} \theta_2^{(l)} h_{l2}(t). \tag{4.18}$$

Importantly, the space of such bandlimited functions is closed under rotations of $\mathcal{S}^1$. Writing

$$\theta = (\theta^{(0)}, \theta_1^{(1)}, \theta_2^{(1)}, \ldots, \theta_1^{(L)}, \theta_2^{(L)}) \in \mathbb{R}^d, \qquad d = 2L + 1$$

for the vector of Fourier coefficients, the rotation $f \mapsto f_{\mathfrak{g}}$ corresponds to $\theta \mapsto g \cdot \theta$, where g belongs to the block-diagonal representation

$$\mathsf{G} = \left\{ \operatorname{diag}\left(1, \begin{pmatrix} \cos 2\pi\mathfrak{g} & \sin 2\pi\mathfrak{g} \\ -\sin 2\pi\mathfrak{g} & \cos 2\pi\mathfrak{g} \end{pmatrix}, \ldots, \begin{pmatrix} \cos 2\pi L\mathfrak{g} & \sin 2\pi L\mathfrak{g} \\ -\sin 2\pi L\mathfrak{g} & \cos 2\pi L\mathfrak{g} \end{pmatrix}\right) : \mathfrak{g} \in [0,1) \right\} \subset \mathsf{O}(d). \tag{4.19}$$

Uniform sampling of rotations $\mathfrak{g} \sim \mathrm{Unif}([0,1))$ induces the Haar-uniform distribution Λ over G. The Fourier basis (4.18) is orthonormal over $\mathcal{S}^1$, so white noise $\mathrm{d}W(t)$ exhibits as Gaussian noise in the sequence domain. Thus our observation model in Fourier sequence space takes the form of (4.1). The Fourier map $f \mapsto \theta$ is an L_2-isometry, so the squared error for estimating $\theta \in \mathbb{R}^d$ equates with the squared error for estimating $f \in L_2(\mathcal{S}^1)$.

The following Theorem 4.3.1 characterizes, for this application, the decomposition of total dimension described in Theorem 4.2.5(a). In Corollary 4.3.2, we summarize its statistical consequences.

Theorem 4.3.1. *For any $L \geq 1$, we have*

$$\operatorname{trdeg}(\mathcal{R}^{\mathsf{G}}_{\leq 1}) = 1, \quad \operatorname{trdeg}(\mathcal{R}^{\mathsf{G}}_{\leq 2}) = L + 1, \quad \operatorname{trdeg}(\mathcal{R}^{\mathsf{G}}_{\leq 3}) = \operatorname{trdeg}(\mathcal{R}^{\mathsf{G}}) = 2L.$$

Corollary 4.3.2. *A generic signal $\theta_* \in \mathbb{R}^d$ in the unprojected continuous MRA model has the following properties:*

(a) θ_* may be identified up to a finite list of orbits by its first $K = 3$ moments if $L \geq 2$ and its first $K = 2$ moments if $L = 1$.

(b) For (θ_*, G)-dependent constants $C, c > 0$ independent of σ and $k = 1, 2, 3$, the Fisher information $I(\theta_*)$ has $d_0 = 1$ eigenvalue of 0 and d_k eigenvalues in $[c\sigma^{-2k}, C\sigma^{-2k}]$ for $(d_1, d_2, d_3) = (1, L, L-1)$.

Proof. For (a), Theorem 4.3.1 shows $\operatorname{trdeg}(\mathcal{R}^{\mathsf{G}}_{\leq K}) = \operatorname{trdeg}(\mathcal{R}^{\mathsf{G}})$ for $K = 3$ if $L \geq 2$, and $K = 2$ if

$L = 1$. The claim follows by direct application of (Bandeira et al., 2017, Theorem 4.9).

For (b), the claim is an application of Theorem 4.2.5(a), using the transcendence degrees computed in Theorem 4.3.1. □

To describe the forms of the moment optimizations (4.15), denote the true function by $f_* : \mathcal{S}^1 \to \mathbb{R}$ and its Fourier coefficients by $\theta_* \in \mathbb{R}^d$. Define the complex Fourier coefficients

$$u^{(0)}(\theta) = \theta^{(0)} \in \mathbb{R}, \qquad u^{(l)}(\theta) = \theta_1^{(l)} + \mathbf{i}\theta_2^{(l)} = r_l(\theta)e^{\mathbf{i}\lambda_l(\theta)} \in \mathbb{C},$$

where $(r_l(\theta), \lambda_l(\theta))$ for $l \geq 1$ are the magnitude and phase of $u^{(l)}(\theta)$. Write as shorthand

$$r_{l,l',l''}(\theta) = r_l(\theta)r_{l'}(\theta)r_{l''}(\theta), \qquad \lambda_{l,l',l''}(\theta) = \lambda_l(\theta) - \lambda_{l'}(\theta) - \lambda_{l''}(\theta).$$

Here $\lambda_{l,l',l''}(\theta)$ are the elements of the Fourier bispectrum of θ.

Theorem 4.3.3. *For any $L \geq 1$,*

$$\begin{aligned}
s_1(\theta) &= \frac{1}{2}\Big(\theta^{(0)} - \theta_*^{(0)}\Big)^2 \\
s_2(\theta) &= \frac{1}{4}\Big((\theta^{(0)})^2 - (\theta_*^{(0)})^2\Big)^2 + \frac{1}{8}\sum_{l=1}^{L}\Big(r_l(\theta)^2 - r_l(\theta_*)^2\Big)^2 \\
s_3(\theta) &= \frac{1}{48}\Big((u^{(0)}(\theta))^3 - (u^{(0)}(\theta_*))^3\Big)^2 + \frac{1}{16}\sum_{\substack{l,l',l''=0 \\ l=l'+l''}}^{L}\Big|u^{(l)}(\theta)\overline{u^{(l')}(\theta)u^{(l'')}(\theta)} - u^{(l)}(\theta_*)\overline{u^{(l')}(\theta_*)u^{(l'')}(\theta_*)}\Big|^2 \\
&= \frac{1}{12}\Big((\theta^{(0)})^3 - (\theta_*^{(0)})^3\Big)^2 + \frac{1}{8}\sum_{l=1}^{L}\Big(\theta^{(0)} \cdot r_l(\theta)^2 - \theta_*^{(0)} \cdot r_l(\theta_*)^2\Big)^2 \\
&\quad + \frac{1}{16}\sum_{\substack{l,l',l''=1 \\ l=l'+l''}}^{L}\Big(r_{l,l',l''}(\theta)^2 + r_{l,l',l''}(\theta_*)^2 - 2r_{l,l',l''}(\theta)r_{l,l',l''}(\theta_*)\cos\big(\lambda_{l,l',l''}(\theta_*) - \lambda_{l,l',l''}(\theta)\big)\Big).
\end{aligned}$$

The moment varieties of (4.15) for this example are

$$\mathcal{V}_0(\theta_*) = \mathbb{R}^d, \qquad \mathcal{V}_1(\theta_*) = \{\theta : \theta^{(0)} = \theta_*^{(0)}\},$$

$$\mathcal{V}_2(\theta_*) = \{\theta : \theta^{(0)} = \theta_*^{(0)} \text{ and } r_l(\theta) = r_l(\theta_*) \text{ for each } l = 1, \ldots, L\}.$$

Thus the minimization of $s_1(\theta)$ on $\mathcal{V}_0(\theta_*)$ is over the global function mean $\theta^{(0)}$, the minimization of $s_2(\theta)$ on $\mathcal{V}_1(\theta_*)$ is over the Fourier power spectrum $\{r_l(\theta) : l = 1, \ldots, L\}$, and the minimization of $s_3(\theta)$ on $\mathcal{V}_2(\theta_*)$ is over the Fourier bispectrum $\{\lambda_{l,l',l''}(\theta) : l = l' + l''\}$. The following result describes

the nature of these three optimization landscapes.

Theorem 4.3.4. *For any $L \geq 1$ and generic $\theta_* \in \mathbb{R}^d$, the minimizations of $s_1(\theta)$ over $\mathcal{V}_0(\theta_*)$ and of $s_2(\theta)$ over $\mathcal{V}_1(\theta_*)$ are globally benign. However, for any $L \geq 30$, there exists a non-empty open subset $U \subset \mathbb{R}^d$ such that for any $\theta_* \in U$, the minimization of $s_3(\theta)$ over $\mathcal{V}_2(\theta_*)$ has a local minimizer outside $\mathcal{O}_{\theta_*}$ that is non-degenerate up to orbit.*

For this class of signals $\theta_* \in U$, Theorem 4.2.10(a) then implies that the landscape of the population log-likelihood $R(\theta)$ also has spurious local minimizers. The particular local minimizers that we exhibit in the proof of Theorem 4.3.4 correspond to certain Fourier phase shifts of the true signal. This example is somewhat analogous to the spurious local minimizers discovered in dimensions $d \geq 53$ for the log-likelihood landscape of discrete MRA in (Fan et al., 2020, Section 4.6).

We conjecture that similar examples of spurious local minimizers may appear in the 2-dimensional and 3-dimensional applications to be discussed in Section 4.4, and we leave this as an open question.

4.3.2 Projected continuous MRA

We consider now a projected version of the preceding model. Again writing $\mathcal{S}^1 \cong [0,1)$ for the unit circle and $f_{\mathfrak{g}}(t)$ for the periodic function $f : \mathcal{S}^1 \to \mathbb{R}$ rotated by $\mathfrak{g} \in [0,1)$, we consider the observations

$$(\Pi \cdot f_{\mathfrak{g}})(t)\mathrm{d}t + \sigma \, \mathrm{d}W(t) \text{ over } t \in (0, 1/2),$$

where

$$(\Pi \cdot f_{\mathfrak{g}})(t) = f_{\mathfrak{g}}(t) + f_{\mathfrak{g}}(1-t)$$

and $\mathrm{d}W(t)$ is standard white noise on the observation domain $(0, 1/2)$. The map Π represents a two-fold projection of the circle $\mathcal{S}^1$ onto the interval $(0, 1/2)$.

To represent this projected model in a Gaussian sequence space, observe that for the Fourier basis (4.17), we have $\Pi \cdot h_{l2} = 0$ for all $l \geq 1$, while $(\Pi \cdot h_0)/\sqrt{2}$ and $(\Pi \cdot h_{l1})/\sqrt{2}$ form an orthonormal basis over $(0, 1/2)$. Thus, expressing $\Pi \cdot f$ in this projected basis, Π may be represented as a linear map $\Pi : \mathbb{R}^d \to \mathbb{R}^{\tilde{d}}$ for $\tilde{d} = L + 1$, where

$$\Pi(\theta) = \sqrt{2}(\theta^{(0)}, \theta_1^{(1)}, \ldots, \theta_1^{(L)}). \tag{4.20}$$

In this projected basis, the observations correspond to (4.2) where $g \in \mathsf{G}$ is a random rotation from

the same group G as in (4.19).

The following result shows that the decomposition of total dimension in Theorem 4.2.5 is the same as in the unprojected setting. In particular, $\operatorname{trdeg} \widetilde{\mathcal{R}}^{\mathsf{G}}_{\leq \widetilde{K}} = \operatorname{trdeg} \mathcal{R}^{\mathsf{G}}$ for $\widetilde{K} = 3$. This model is a continuous analogue of the projected discrete MRA model studied in (Bandeira et al., 2017, Section 5.3.1), where an analogous conclusion was described as (Bandeira et al., 2017, Conjecture 5.3).

Theorem 4.3.5. *For any $L \geq 1$, we have*

$$\operatorname{trdeg}(\widetilde{\mathcal{R}}^{\mathsf{G}}_{\leq 1}) = 1, \qquad \operatorname{trdeg}(\widetilde{\mathcal{R}}^{\mathsf{G}}_{\leq 2}) = L + 1, \qquad \operatorname{trdeg}(\widetilde{\mathcal{R}}^{\mathsf{G}}_{\leq 3}) = \operatorname{trdeg}(\mathcal{R}^{\mathsf{G}}) = 2L,$$

which match the values of $\operatorname{trdeg}(\mathcal{R}^{\mathsf{G}}_{\leq 1})$, $\operatorname{trdeg}(\mathcal{R}^{\mathsf{G}}_{\leq 2})$, *and* $\operatorname{trdeg}(\mathcal{R}^{\mathsf{G}}_{\leq 3})$ *in the unprojected setting of Theorem 4.3.1.*

Corollary 4.3.6. *A generic signal $\theta_* \in \mathbb{R}^d$ in this projected continuous MRA model has the following properties:*

(a) θ_* may be identified up to a finite list of orbits by its first $\widetilde{K} = 3$ moments if $L \geq 2$ and its first $\widetilde{K} = 2$ moments if $L = 1$.

(b) For (θ_*, G)-dependent constants $C, c > 0$ independent of σ and $k = 1, 2, 3$, the Fisher information $I(\theta_*)$ has $\tilde{d}_0 = 1$ eigenvalue of 0 and $\tilde{d}_k$ eigenvalues in $[c\sigma^{-2k}, C\sigma^{-2k}]$ for $(\tilde{d}_1, \tilde{d}_2, \tilde{d}_3) = (1, L, L-1)$.

Proof. This follows from Theorem 4.3.5 by applying (Bandeira et al., 2017, Theorem 4.9) and Theorem 4.2.5(b). □

The following result describes the forms of $\tilde{s}_k(\theta)$ for $k = 1, 2, 3$, which are similar to those in the unprojected setting. In particular, the minimizations of $\tilde{s}_1(\theta)$, $\tilde{s}_2(\theta)$, and $\tilde{s}_3(\theta)$ in (4.16) are also optimization problems over the signal mean, Fourier power spectrum, and Fourier bispectrum respectively, although the specific forms are different from the unprojected counterparts.

Theorem 4.3.7. *For any $L \geq 1$,*

$$\tilde{s}_1(\theta) = \left(\theta^{(0)} - \theta_*^{(0)}\right)^2$$

$$\tilde{s}_2(\theta) = \left((\theta^{(0)})^2 - (\theta_*^{(0)})^2\right)^2 + \frac{1}{4}\sum_{l=1}^{L}\left(r_l(\theta)^2 - r_l(\theta_*)^2\right)^2$$

$$\begin{aligned}\tilde{s}_3(\theta) = \frac{2}{3}\left((\theta^{(0)})^3 - (\theta_*^{(0)})^3\right)^2 + \frac{1}{2}\sum_{l=1}^{L}\left(\theta^{(0)} r_l(\theta)^2 - \theta_*^{(0)} r_l(\theta_*)^2\right)^2 \\ + \frac{1}{16}\sum_{\substack{l,l',l''=1 \\ l=l'+l''}}^{L}\Big(r_{l,l',l''}(\theta)^2 + r_{l,l',l''}(\theta_*)^2 - 2r_{l,l',l''}(\theta) r_{l,l',l''}(\theta_*)\cos\left(\lambda_{l,l',l''}(\theta_*) - \lambda_{l,l',l''}(\theta)\right) \\ + r_{l,l',l''}(\theta)^2\cos\left(2\lambda_{l,l',l''}(\theta)\right) + r_{l,l',l''}(\theta_*)^2\cos\left(2\lambda_{l,l',l''}(\theta_*)\right) \\ - 2r_{l,l',l''}(\theta) r_{l,l',l''}(\theta_*)\cos\left(\lambda_{l,l',l''}(\theta_*) + \lambda_{l,l',l''}(\theta_*)\right)\Big).\end{aligned}$$

4.4 Spherical registration and cryo-EM

We now describe examples of estimating a function in 2 or 3 dimensions, observed under $\mathsf{SO}(3)$ rotations of its domain. Section 4.4.1 studies estimation on the sphere, Section 4.4.2 studies estimation in $\mathbb{R}^3$, and Section 4.4.3 studies a simplified "cryo-EM model" of estimation in $\mathbb{R}^3$ with a tomographic projection onto a 2-dimensional plane. Related analyses of method-of-moments estimators were performed for these examples in Bandeira et al. (2017).

We show in all three examples that 3rd-order moments are sufficient to locally identify the signal once the bandlimits exceed small constants by showing that $\mathrm{trdeg}(\mathcal{R}^{\mathsf{G}}_{\leq K}) = \mathrm{trdeg}(\mathcal{R}^{\mathsf{G}})$ and $\mathrm{trdeg}(\widetilde{\mathcal{R}}^{\mathsf{G}}_{\leq \widetilde{K}}) = \mathrm{trdeg}(\mathcal{R}^{\mathsf{G}})$ for $K = \widetilde{K} = 3$. We further characterize the scales of eigenvalues of the Fisher information by computing (d_0, d_1, d_2, d_3) or $(\tilde{d}_0, \tilde{d}_1, \tilde{d}_2, \tilde{d}_3)$ corresponding to the decomposition of total dimension in Theorem 4.2.5. Finally, we provide the forms of $s_k(\theta)$ or $\tilde{s}_k(\theta)$ that describe the moment optimizations (4.15–4.16). These results resolve several conjectures of Bandeira et al. (2017).

4.4.1 Spherical registration

Let $\mathcal{S}^2 \subset \mathbb{R}^3$ be the unit sphere, and let $f : \mathcal{S}^2 \to \mathbb{R}$ be a function on this sphere. We parametrize $\mathcal{S}^2$ by the latitude $\phi_1 \in [0, \pi]$ and longitude $\phi_2 \in [0, 2\pi)$. Writing $f_{\mathfrak{g}}(\phi_1, \phi_2) = f(\mathfrak{g}^{-1} \cdot (\phi_1, \phi_2))$ for the rotation of the function f, we consider the observations

$$f_{\mathfrak{g}}(\phi_1, \phi_2)\,\mathrm{d}(\phi_1, \phi_2) + \sigma\,\mathrm{d}W(\phi_1, \phi_2) \text{ over } (\phi_1, \phi_2) \in \mathcal{S}^2,$$

where $\mathfrak{g} \in \mathsf{SO}(3)$ is a uniform random rotation for each sample, $\mathrm{d}(\phi_1, \phi_2) = \sin\phi_1 \, \mathrm{d}\phi_1 \, \mathrm{d}\phi_2$ denotes the surface area measure on $\mathcal{S}^2$, and $\mathrm{d}W(\phi_1, \phi_2)$ is standard white noise on $\mathcal{S}^2$.

As in (Bandeira et al., 2017, Section 5.4), we translate this model to a Gaussian sequence form using the basis of real spherical harmonics

$$h_{lm}(\phi_1, \phi_2) \quad \text{for } l = 0, 1, 2, \ldots \text{ and } m = -l, -l+1, \ldots, l-1, l.$$

This basis is reviewed in Appendix C.4.2. We assume that $f : \mathcal{S}^2 \to \mathbb{R}$ has a finite bandlimit $L \geq 1$ in this basis, i.e. it takes the form

$$f(\phi_1, \phi_2) = \sum_{l=0}^{L} \sum_{m=-l}^{l} \theta_m^{(l)} h_{lm}(\phi_1, \phi_2). \tag{4.21}$$

We may then represent f by its vector of real spherical harmonic coefficients

$$\theta = (\theta_m^{(l)} : l = 0, \ldots, L \text{ and } m = -l, \ldots, l) \in \mathbb{R}^d, \qquad d = (L+1)^2,$$

or equivalently, by its complex spherical harmonic coefficients $u \in \mathbb{C}^d$ defined as

$$u_m^{(l)} = \begin{cases} \frac{(-1)^m}{\sqrt{2}}(\theta_{|m|}^{(l)} - \mathbf{i}\theta_{-|m|}^{(l)}) & \text{if } m > 0 \\ \theta_0^{(l)} & \text{if } m = 0 \\ \frac{1}{\sqrt{2}}(\theta_{|m|}^{(l)} + \mathbf{i}\theta_{-|m|}^{(l)}) & \text{if } m < 0. \end{cases} \tag{4.22}$$

This relation (4.22) represents a linear map $u = V^*\theta$ for a unitary matrix $V \in \mathbb{C}^{d \times d}$. For vectors $\theta \in \mathbb{R}^d$ taking real values, we have the sign symmetry of the complex coefficients

$$u_m^{(l)} = (-1)^m \overline{u_{-m}^{(l)}}. \tag{4.23}$$

The space of bandlimited functions (4.21) is closed under the action of $\mathsf{SO}(3)$, and the rotation $f \mapsto f_{\mathfrak{g}}$ is represented by the following subgroup $\mathsf{G} \subset \mathsf{O}(d)$ acting on $\theta \in \mathbb{R}^d$.

Lemma 4.4.1. *The action of* $\mathsf{SO}(3)$ *on the real spherical harmonic coefficients* $\theta \in \mathbb{R}^d$ *admits the representation*

$$\mathsf{G} = \left\{ V \cdot D(\mathfrak{g}) \cdot V^* : \mathfrak{g} \in \mathsf{SO}(3) \right\} \subset \mathsf{O}(d),$$

where $V \in \mathbb{C}^{d \times d}$ *is the unitary transform describing the map* $u = V^*\theta$ *in (4.22), and* $D(\mathfrak{g})$ *is the*

block-diagonal matrix

$$D(\mathfrak{g}) = \bigoplus_{l=0}^{L} D^{(l)}(\mathfrak{g}) \in \mathbb{C}^{d\times d} \tag{4.24}$$

with diagonal blocks $D^{(l)}(\mathfrak{g}) \in \mathbb{C}^{(2l+1)\times(2l+1)}$ *given by the complex Wigner D-matrices at frequencies* $l = 0, \ldots, L$ *(defined in Appendix C.4.1).*

The uniform distribution for $\mathfrak{g} \in \mathsf{SO}(3)$ induces the Haar-uniform distribution Λ over G. Since the basis $\{h_{lm}\}$ is orthonormal on $\mathcal{S}^2$, white noise $\mathrm{d}W(\phi_1, \phi_2)$ exhibits as standard Gaussian noise in the sequence domain. Thus observations in this model take the form (4.1) in sequence space.

The following results describe the decomposition of total dimension in Theorem 4.2.5(a) for bandlimits $L \geq 10$ and summarize its statistical consequences.

Theorem 4.4.2. *For any* $L \geq 10$*, we have*

$$\mathrm{trdeg}(\mathcal{R}^{\mathsf{G}}_{\leq 1}) = 1, \quad \mathrm{trdeg}(\mathcal{R}^{\mathsf{G}}_{\leq 2}) = L+1, \quad \mathrm{trdeg}(\mathcal{R}^{\mathsf{G}}_{\leq 3}) = \mathrm{trdeg}(\mathcal{R}^{\mathsf{G}}) = d-3.$$

Corollary 4.4.3. *A generic signal* $\theta_* \in \mathbb{R}^d$ *in the spherical registration model for* $L \geq 10$ *has the following properties:*

(a) θ_* *may be identified up to a finite list of orbits by its first* $K = 3$ *moments.*

(b) For (θ_*, G)*-dependent constants* $C, c > 0$ *independent of* σ *and* $k = 1, 2, 3$*, the Fisher information* $I(\theta_*)$ *has* $d_0 = 3$ *eigenvalues of 0 and* d_k *eigenvalues in* $[c\sigma^{-2k}, C\sigma^{-2k}]$ *for*

$$(d_1, d_2, d_3) = (1, L, L(L+1) - 3).$$

Proof. This follows from Theorem 4.4.2 by applying (Bandeira et al., 2017, Theorem 4.9) and Theorem 4.2.5(a). □

Remark 4.4.1. *Theorem 4.4.2 was conjectured for all bandlimits* $L \geq 10$ *in (Bandeira et al., 2017, Conjecture 5.6) and verified numerically in exact-precision arithmetic for* $L \in \{10, \ldots, 16\}$ *in (Bandeira et al., 2017, Theorem 5.5). Our result resolves this conjecture for all* $L \geq 10$ *by an induction which uses* $L = 10$ *as a base case. Conversely, for* $L \leq 9$*, it was shown in (Bandeira et al., 2017, Section 5.4) that* $K > 3$ *strictly, meaning that moments up to* 3^{rd} *order are insufficient to locally identify* θ_* *up to its orbit for low bandlimits.*

Turning to the forms of $s_k(\theta)$ in (4.15), let us fix the true function $f_* : \mathcal{S}^2 \to \mathbb{R}$, and denote its

real spherical harmonic coefficients by $\theta_* \in \mathbb{R}^d$. We write as shorthand

$$u^{(l)}(\theta) = (u_m^{(l)}(\theta) : m = -l, \dots, l) \in \mathbb{C}^{2l+1}$$

for the complex spherical harmonic coefficients at frequency l, defined by (4.22). We denote

$$B_{l,l',l''}(\theta) = \sum_{m=-l}^{l} \sum_{\substack{m'=-l' \\ m''=m+m'}}^{l'} \sum_{m''=-l''}^{l''} \langle l, m; l', m' | l'', m'' \rangle \overline{u_m^{(l)}(\theta) u_{m'}^{(l')}(\theta)} u_{m''}^{(l'')}(\theta), \tag{4.25}$$

where $\langle l, m; l', m' | l'', m'' \rangle \in \mathbb{R}$ is the Clebsch-Gordan coefficient, reviewed in Appendix C.4.1. These quantities $B_{l,l',l''}(\theta)$ are analogous to the scaled components $r_{l,l',l''}(\theta)\lambda_{l,l',l''}(\theta)$ of the Fourier bispectrum that appeared in the 1-dimensional MRA example of Section 4.3. The minimizations of $s_1(\theta)$, $s_2(\theta)$, and $s_3(\theta)$ may be analogously understood as minimizations of the global function mean, the power in each spherical harmonic frequency, and certain "bispectrum" variables for each frequency.

Theorem 4.4.4. *For any $L \geq 1$,*

$$\begin{aligned}
s_1(\theta) &= \frac{1}{2}\Big(u^{(0)}(\theta) - u^{(0)}(\theta_*)\Big)^2 \\
s_2(\theta) &= \frac{1}{4}\sum_{l=0}^{L} \frac{1}{2l+1}\Big(\|u^{(l)}(\theta)\|^2 - \|u^{(l)}(\theta_*)\|^2\Big)^2 \\
s_3(\theta) &= \frac{1}{6} \sum_{\substack{l,l',l''=0 \\ |l-l'| \leq l'' \leq l+l'}}^{L} \frac{1}{2l''+1}\Big|B_{l,l',l''}(\theta) - B_{l,l',l''}(\theta_*)\Big|^2.
\end{aligned}$$

4.4.2 Unprojected cryo-EM

Consider now a function $f : \mathbb{R}^3 \to \mathbb{R}$, and the action of $\mathsf{SO}(3)$ on $\mathbb{R}^3$ given by rotation about the origin. Write $f_{\mathfrak{g}}(x) = f(\mathfrak{g}^{-1} \cdot x)$ for the rotated function. We observe samples

$$f_{\mathfrak{g}}(x)\,\mathrm{d}x + \sigma\,\mathrm{d}W(x) \text{ over } x \in \mathbb{R}^3,$$

where $\mathfrak{g} \in \mathsf{SO}(3)$ is uniformly random for each sample, and $\mathrm{d}W(x)$ is white noise on $\mathbb{R}^3$. This serves as a simplified unprojected model of the single-particle reconstruction problem in cryo-EM, to which we will add a tomographic projection in the next section. This model may be of independent interest for applications to cryo-ET, described in Appendix C.6.1.

We model f in a function basis over $\mathbb{R}^3$ by a construction that is similar to the approach of (Bandeira et al., 2017, Section 5.5 and Appendix A.1)—we describe this briefly here, and provide

more details in Appendix C.4.3. Let $\hat{f} : \mathbb{R}^3 \to \mathbb{C}$ be the Fourier transform of f. We parametrize the Fourier domain by spherical coordinates (ρ, ϕ_1, ϕ_2), and decompose $\hat{f}(\rho, \phi_1, \phi_2)$ in a basis $\{\hat{j}_{lsm}\}$ given by the product of the complex spherical harmonics $y_{lm}(\phi_1, \phi_2)$ with radial functions $z_s(\rho)$:

$$\hat{j}_{lsm}(\rho, \phi_1, \phi_2) = z_s(\rho) y_{lm}(\phi_1, \phi_2) \quad \text{for } s \geq 1, \quad l \geq 0, \quad m \in \{-l, \ldots, l\}. \tag{4.26}$$

Here $\{z_s : s \geq 1\}$ may be any system of radial basis functions $z_s : [0, \infty) \to \mathbb{R}$ satisfying the orthogonality relation

$$\int_0^\infty \rho^2 z_s(\rho) z_{s'}(\rho) d\rho = \mathbf{1}\{s = s'\}, \tag{4.27}$$

so that $\{\hat{j}_{lsm}\}$ are orthonormal. The inverse Fourier transforms $\{j_{lsm}\}$ of $\{\hat{j}_{lsm}\}$ then provide a complex orthonormal basis in the original signal domain of f.

Fixing integer bandlimits $L \geq 1$ and $S_0, \ldots, S_L \geq 1$, we define the index set

$$\mathcal{I} = \Big\{(l, s, m) : 0 \leq l \leq L,\ 1 \leq s \leq S_l,\ -l \leq m \leq l\Big\}, \qquad d = |\mathcal{I}| = \sum_{l=0}^{L} (2l+1) S_l \tag{4.28}$$

and assume that f is $(L, S_0, \ldots, S_L)$-*bandlimited* in the sense of admitting the finite basis representation

$$f = \sum_{(l,s,m) \in \mathcal{I}} u_m^{(ls)} \cdot j_{lsm}, \qquad u = \big(u_m^{(ls)} : (l, s, m) \in \mathcal{I}\big) \in \mathbb{C}^d. \tag{4.29}$$

This corresponds to modeling the Fourier transform $\hat{f}$ up to the spherical frequency L, and up to the radial frequency S_l for each spherical component $l = 0, 1, \ldots, L$.[5] For real-valued functions f, these coefficients $u_m^{(ls)} \in \mathbb{C}$ will satisfy a sign symmetry (154). Writing $u = \hat{V}^* \theta$ for a unitary transform $\hat{V} \in \mathbb{C}^{d \times d}$ defined explicitly in (156), we then obtain a real sequence representation

$$f = \sum_{(l,s,m) \in \mathcal{I}} \theta_m^{(ls)} \cdot h_{lsm}, \qquad \theta = \big(\theta_m^{(ls)} : (l, s, m) \in \mathcal{I}\big) \in \mathbb{R}^d \tag{4.30}$$

for certain basis functions $h_{lsm} : \mathbb{R}^3 \to \mathbb{R}$ that are real-valued and orthonormal.

This class of $(L, S_0, \ldots, S_L)$-bandlimited functions (4.30) is closed under rotations by $\mathsf{SO}(3)$. The rotations admit the following representation by a subgroup $\mathsf{G} \subset \mathsf{O}(d)$ acting on the basis coefficients $\theta \in \mathbb{R}^d$.

Lemma 4.4.5. *The action of* $\mathsf{SO}(3)$ *on the space of real-valued* $(L, S_0, \ldots, S_L)$*-bandlimited functions*

5. For example, one may wish to use larger radial bandlimits S_l for lower spherical frequencies l.

is given by

$$\mathsf{G} = \left\{ \hat{V} \cdot D(\mathfrak{g}) \cdot \hat{V}^* : \mathfrak{g} \in \mathsf{SO}(3) \right\} \subset \mathsf{O}(d) \tag{4.31}$$

where $\hat{V} \in \mathbb{C}^{d \times d}$ *is the unitary transform defined in (156) for which* $u = \hat{V}^* \theta$*, and* $D(\mathfrak{g})$ *is the block-diagonal matrix*

$$D(\mathfrak{g}) = \bigoplus_{l=0}^{L} \bigoplus_{s=1}^{S_l} D^{(l)}(\mathfrak{g}) \tag{4.32}$$

with diagonal blocks $D^{(l)}(\mathfrak{g}) \in \mathbb{C}^{(2l+1)\times(2l+1)}$ *given by the complex Wigner D-matrices.*

The following result describes the decomposition of total dimension in Theorem 4.2.5(a) under the mild assumption that the spherical bandlimit satisfies $L \geq 2$ and the radial bandlimits satisfy $S_l \geq 2$ for each $l = 0, \ldots, L$.[6] In particular, this verifies that $\operatorname{trdeg} \mathcal{R}^{\mathsf{G}}_{\leq K} = \operatorname{trdeg} \mathcal{R}^{\mathsf{G}}$ for $K = 3$; we then summarize the statistical consequences in Corollary 4.4.7.

Theorem 4.4.6. *For any* $L \geq 1$ *and* $S_0, \ldots, S_L \geq 2$*, we have*

$$\begin{aligned}
&\operatorname{trdeg}(\mathcal{R}^{\mathsf{G}}_{\leq 1}) = S_0 \\
&\operatorname{trdeg}(\mathcal{R}^{\mathsf{G}}_{\leq 2}) = \sum_{l=0}^{L} d(S_l), \qquad d(S_l) \equiv \begin{cases} \frac{S_l(S_l+1)}{2} & \text{for } S_l < 2l+1 \\ (2l+1)(S_l - l) & \text{for } S_l \geq 2l+1 \end{cases} \\
&\operatorname{trdeg}(\mathcal{R}^{\mathsf{G}}_{\leq 3}) = \operatorname{trdeg}(\mathcal{R}^{\mathsf{G}}) = d - 3.
\end{aligned}$$

Corollary 4.4.7. *A generic signal* $\theta_* \in \mathbb{R}^d$ *in this unprojected cryo-EM model for* $L \geq 1$ *and* $S_0, \ldots, S_L \geq 2$ *has the following properties:*

(a) θ_* *may be identified up to a finite list of orbits by its first* $K = 3$ *moments if* $L \geq 2$ *and its first* $K = 2$ *moments if* $L = 1$*.*

(b) For (θ_*, G)*-dependent constants* $C, c > 0$ *independent of* σ *and* $k = 1, 2, 3$*, the Fisher information* $I(\theta_*)$ *has* $d_0 = 3$ *eigenvalues of 0 and* d_k *eigenvalues in* $[c\sigma^{-2k}, C\sigma^{-2k}]$ *for*

$$(d_1, d_2, d_3) = \Big(S_0, \sum_{l=1}^{L} d(S_l), d - \sum_{l=0}^{L} d(S_l) - 3 \Big).$$

Proof. This follows from Theorem 4.4.6 by applying (Bandeira et al., 2017, Theorem 4.9) and Theorem 4.2.5(a). □

6. Note that the case of $S_0 = \ldots = S_L = 1$ would be similar to the spherical registration example of Section 4.4.1, and a lower bound of $L \geq 10$ would be needed in this case to ensure $K = 3$.

Remark 4.4.2. *In (Bandeira et al., 2017, Conjecture B.1), the authors conjectured that a generic signal $\theta_* \in \mathbb{R}^d$ may be identified by moments of degree at most 3 up to a* single *orbit for $L \geq 1$ and $S_0 = \cdots = S_L \geq 3$. They verified their conjecture using computer algebra and a "frequency-marching" technique for $L \in \{1, \ldots, 15\}$. Our Corollary 4.4.7(a) is complementary to this conjecture, showing that θ_* may be identified up to a finite list of orbits, but requiring only 2 rather than 3 shells.*

Turning to the forms of $s_k(\theta)$ that define the moment optimization (4.15), write $\theta_* \in \mathbb{R}^d$ for the true coefficients in the above real basis $\{h_{lsm}\}$. Let

$$u^{(ls)}(\theta) = (u_m^{(ls)}(\theta) : m = -l, \ldots, l) \in \mathbb{C}^{2l+1} \tag{4.33}$$

be the components of the *complex* coefficients $u = \hat{V}^*\theta$ for the frequency pair (l, s), and define analogously to (4.25)

$$B_{(l,s),(l',s'),(l'',s'')}(\theta) = \sum_{m=-l}^{l} \sum_{\substack{m'=-l' \\ m''=m+m'}}^{l'} \sum_{m''=-l''}^{l''} \langle l, m; l', m' | l'', m'' \rangle \overline{u_m^{(ls)}(\theta) u_{m'}^{(l's')}(\theta)} u_{m''}^{(l''s'')}(\theta). \tag{4.34}$$

When the original function $f : \mathbb{R}^3 \to \mathbb{R}$ is real-valued, we verify in the proof of Theorem 4.4.8 below that each $B_{(l,s),(l',s'),(l'',s'')}(\theta)$ is also real-valued.

Theorem 4.4.8. *For any $L \geq 1$ and $S_0, \ldots, S_L \geq 1$,*

$$\begin{aligned}
s_1(\theta) &= \frac{1}{2} \sum_{s=1}^{S_0} \left(u^{(0s)}(\theta) - u^{(0s)}(\theta_*) \right)^2 \\
s_2(\theta) &= \frac{1}{4} \sum_{l=0}^{L} \frac{1}{2l+1} \sum_{s,s'=1}^{S_l} \left(\langle u^{(ls)}(\theta), u^{(ls')}(\theta) \rangle - \langle u^{(ls)}(\theta_*), u^{(ls')}(\theta_*) \rangle \right)^2 \\
s_3(\theta) &= \frac{1}{12} \sum_{\substack{l,l',l''=0 \\ |l-l'| \leq l'' \leq l+l'}}^{L} \frac{1}{2l''+1} \sum_{s=1}^{S_l} \sum_{s'=1}^{S_{l'}} \sum_{s''=1}^{S_{l''}} \left(B_{(l,s),(l',s'),(l'',s'')}(\theta) - B_{(l,s),(l',s'),(l'',s'')}(\theta_*) \right)^2.
\end{aligned}$$

In this case, the optimization of $s_2(\theta)$ depends not just on the power $\|u^{(ls)}(\theta)\|^2$ within each frequency pair (l, s), but also on the cross-correlations between $u^{(ls)}$ and $u^{(ls')}$ for different radial frequencies s and s'.

4.4.3 Projected cryo-EM

We now add a tomographic projection to the previous example. Writing as before $f : \mathbb{R}^3 \to \mathbb{R}$ and $f_{\mathfrak{g}}$ for its rotation by $\mathfrak{g} \in \mathsf{SO}(3)$, we observe samples

$$(\Pi \cdot f_{\mathfrak{g}})(x)\mathrm{d}x + \sigma\, \mathrm{d}W(x) \text{ over } x \in \mathbb{R}^2,$$

where, for $x = (x_1, x_2) \in \mathbb{R}^2$,

$$(\Pi \cdot f_{\mathfrak{g}})(x_1, x_2) = \int_{-\infty}^{\infty} f_{\mathfrak{g}}(x_1, x_2, x_3)\mathrm{d}x_3 \tag{4.35}$$

and $\mathrm{d}W(x)$ is white noise on the projected signal domain $\mathbb{R}^2$.

We construct basis functions for both the signal domain $\mathbb{R}^3$ and projected signal domain $\mathbb{R}^2$ using an approach similar to that of the preceding section, and also similar to (Bandeira et al., 2017, Appendix A)—we defer details to Appendix C.4.4. In 3-D Fourier space parametrized by spherical coordinates (ρ, ϕ_1, ϕ_2), we again take a product basis

$$\hat{j}_{lsm}(\rho, \phi_1, \phi_2) = \tilde{z}_s(\rho) y_{lm}(\phi_1, \phi_2) \quad \text{for } s \geq 1, \quad l \geq 0 \quad m \in \{-l, \ldots, l\}. \tag{4.36}$$

In 2-D Fourier space parametrized by polar coordinates (ρ, ϕ_2), we introduce $b_m(\phi_2) = (2\pi)^{-1/2} e^{\mathbf{i}m\phi_2}$ and take a corresponding product basis

$$\hat{j}_{sm}(\rho, \phi_2) = \tilde{z}_s(\rho) b_m(\phi_2) \quad \text{for } s \geq 1, \quad m \in \mathbb{Z}. \tag{4.37}$$

This will be an orthonormal basis under the orthogonality relation for $\{\tilde{z}_s\}$ in (4.41) below. We write $\{j_{lsm}\}$ for the 3-D inverse Fourier transform of $\{\hat{j}_{lsm}\}$, and $\{j_{sm}\}$ for the 2-D inverse Fourier transform of $\{\hat{j}_{sm}\}$.

Recalling the index set (4.28), we again assume that f is $(L, S_0, \ldots, S_L)$-bandlimited, so it admits the representations

$$f = \sum_{(l,s,m) \in \mathcal{I}} u_m^{(ls)} \cdot j_{lsm} = \sum_{(l,s,m) \in \mathcal{I}} \theta_m^{(ls)} \cdot h_{lsm} \tag{4.38}$$

for complex coefficients $u \in \mathbb{C}^d$ satisfying a sign symmetry (154), or equivalently for real coefficients $\theta \in \mathbb{R}^d$ related to u via the unitary transform $u = \hat{V}^* \theta$ in (156). The action of the rotation $f \mapsto f_{\mathfrak{g}}$ on $\theta \in \mathbb{R}^d$ has been described in Lemma 4.4.5. Letting $S = \max(S_0, \ldots, S_L)$, by the Fourier slice theorem, any such $(L, S_0, \ldots, S_L)$-bandlimited function f has projection $\Pi \cdot f$ bandlimited to the

indices

$$\widetilde{\mathcal{I}} = \Big\{(s,m) : 1 \le s \le S,\ -L \le m \le L\Big\}, \qquad \tilde{d} = |\widetilde{\mathcal{I}}| = S(2L+1)$$

of the projected basis, i.e.

$$\Pi \cdot f = \sum_{(s,m)\in\widetilde{\mathcal{I}}} \tilde{u}_m^{(s)} j_{sm} = \sum_{(s,m)\in\widetilde{\mathcal{I}}} \tilde{\theta}_m^{(s)} h_{sm} \tag{4.39}$$

for some complex coefficients $\tilde{u} \in \mathbb{C}^{\tilde{d}}$ satisfying a sign symmetry (175), or real coefficients $\tilde{\theta} \in \mathbb{R}^{\tilde{d}}$ related to $\tilde{u}$ via a unitary transform $\tilde{u} = \widetilde{V}^* \tilde{\theta}$ defined in (174). The projection Π is then an explicit linear map of $\theta \in \mathbb{R}^d$ (representing f) to $\tilde{\theta} \in \mathbb{R}^{\tilde{d}}$ (representing $\Pi \cdot f$), given by

$$\Pi = \widetilde{V} \cdot \Pi^{\mathbb{C}} \cdot \hat{V}^* \in \mathbb{R}^{\tilde{d}\times d}, \qquad \Pi^{\mathbb{C}}_{(s',m'),(l,s,m)} = \mathbf{1}\{s = s'\} \cdot \mathbf{1}\{m = m'\} \cdot p_{lm} \tag{4.40}$$

for constants p_{lm} that are defined in (172).

Finally, we choose the radial basis functions $\{\tilde{z}_s : s \ge 1\}$ in (4.36) and (4.37) to satisfy a modified orthogonality relation

$$\int_0^\infty \rho\, \tilde{z}_s(\rho)\tilde{z}_{s'}(\rho)\mathrm{d}\rho = \mathbf{1}\{s = s'\} \tag{4.41}$$

with weight ρ instead of ρ^2, which ensures that the projected basis $\{h_{sm}\}$ is orthonormal over $\mathbb{R}^2$. Then white noise $\mathrm{d}W(x)$ on $\mathbb{R}^2$ exhibits as standard Gaussian noise in the projected sequence domain $\mathbb{R}^{\tilde{d}}$, and our observation model takes the form (4.2).

Remark 4.4.3. *Note that if $\{\tilde{z}_s : s = 1,\dots,S\}$ has the same linear span as $\{z_s : s = 1,\dots,S\}$ of the preceding section, then the two spaces of bandlimited functions (4.38) and (4.30) coincide. However, we caution that here under the orthogonality relation (4.41), the* unprojected *basis $\{h_{lsm}\}$ is not orthonormal for this function space, so $f \mapsto \theta$ is not an isometric parametrization of $f \in L_2(\mathbb{R}^3)$.*

The following Theorem 4.4.9 verifies that, under the mild assumption $L \ge 1$ and $S_l \ge 4$ for each $l = 0,\dots,L$, we have also $\operatorname{trdeg} \widetilde{\mathcal{R}}^{\mathsf{G}}_{\le \widetilde{K}} = \operatorname{trdeg} \mathcal{R}^{\mathsf{G}}$ for $\widetilde{K} = 3$. We summarize its statistical consequences in Corollary 4.4.10.

Theorem 4.4.9. *For any $L \geq 1$ and $S_0, \ldots, S_L \geq 4$, we have*

$$\begin{aligned}
&\mathrm{trdeg}(\widetilde{\mathcal{R}}^{\mathsf{G}}_{\leq 1}) = S_0 \\
&\mathrm{trdeg}(\widetilde{\mathcal{R}}^{\mathsf{G}}_{\leq 2}) = \sum_{l=0}^{L} d(S_l), \qquad d(S_l) \equiv \begin{cases} \frac{S_l(S_l+1)}{2} & \text{for } S_l < 2l+1 \\ (2l+1)(S_l - l) & \text{for } S_l \geq 2l+1 \end{cases} \\
&\mathrm{trdeg}(\widetilde{\mathcal{R}}^{\mathsf{G}}_{\leq 3}) = \mathrm{trdeg}(\mathcal{R}^{\mathsf{G}}) = d - 3,
\end{aligned}$$

which matches the values of $\mathrm{trdeg}(\mathcal{R}^{\mathsf{G}}_{\leq 1})$, $\mathrm{trdeg}(\mathcal{R}^{\mathsf{G}}_{\leq 2})$, *and* $\mathrm{trdeg}(\mathcal{R}^{\mathsf{G}}_{\leq 3})$ *in the unprojected setting of Theorem 4.4.6.*

Corollary 4.4.10. *A generic signal $\theta_* \in \mathbb{R}^d$ in this projected cryo-EM model for $L \geq 1$ and $S_0, \ldots, S_L \geq 4$ has the following properties:*

(a) θ_* may be identified up to a finite list of orbits by its first $\widetilde{K} = 3$ moments if $L \geq 2$ and its first $\widetilde{K} = 2$ moments if $L = 1$.

(b) For (θ_*, G)-dependent constants $C, c > 0$ independent of σ and $k = 1, 2, 3$, the Fisher information $I(\theta_*)$ has $\tilde{d}_0 = 3$ eigenvalues of 0 and $\tilde{d}_k$ eigenvalues in $[c\sigma^{-2k}, C\sigma^{-2k}]$ for

$$(\tilde{d}_1, \tilde{d}_2, \tilde{d}_3) = \Big(S_0, \sum_{l=1}^{L} d(S_l), d - \sum_{l=0}^{L} d(S_l) - 3\Big).$$

Proof. This follows from Theorem 4.4.9 by applying (Bandeira et al., 2017, Theorem 4.9) and Theorem 4.2.5(b). □

Remark 4.4.4. *Taking $S_0 = \ldots = S_L = S$ specializes our results to the case of (projected) cryo-EM with S spherical shells in (Bandeira et al., 2017, Section 5.5). In (Bandeira et al., 2017, Conjecture 5.11), the authors conjectured that a generic θ_* may be identified up to a finite list of orbits by moments up to degree 3 if $S \geq 2$. Corollary 4.4.10(a) thus resolves this conjecture positively when $S \geq 4$. The constraint $S \geq 4$ is technical, and we believe that the conjecture holds as stated for $S \in \{2, 3\}$ as well, but we do not pursue these cases in this work.*

The following provides the explicit forms for $\tilde{s}_k(\theta)$ in the optimization problem (4.16). Recalling

the entries p_{lm} of $\Pi^{\mathbb{C}}$ in (4.40), define

$$Q_{kl} = \frac{(-1)^{k+l}}{(2k+1)(2l+1)} \sum_{q=-(k\wedge l)}^{k\wedge l} p_{kq}^2 p_{lq}^2, \tag{4.42}$$

$$M_{k,k',k'',l,l',l''} = \frac{(-1)^{k''+l''}}{(2k''+1)(2l''+1)} \sum_{q=-(k\wedge l)}^{k\wedge l} \sum_{\substack{q'=-(k'\wedge l') \\ q''=q+q'}}^{k'\wedge l'} \sum_{q''=-(k''\wedge l'')}^{k''\wedge l''} \langle k, q; k', q' | k'', q'' \rangle \langle l, q; l', q' | l'', q'' \rangle p_{kq} p_{k'q'} p_{k''q''} p_{lq} p_{l'q'} p_{l''q''}. \tag{4.43}$$

Recall also $u^{(ls)}(\theta)$ and $B_{(l,s),(l',s'),(l'',s'')}(\theta)$ from (4.33) and (4.34).

Theorem 4.4.11. *For any $L \geq 1$ and $S_0, \ldots, S_L \geq 1$,*

$$\tilde{s}_1(\theta) = \frac{p_{00}^2}{2} \sum_{s=1}^{S_0} \left(u^{(0s)}(\theta) - u^{(0s)}(\theta_*) \right)^2$$

$$\tilde{s}_2(\theta) = \frac{1}{4} \sum_{k,l=0}^{L} Q_{kl} \sum_{s,s'=1}^{S_k \wedge S_l} \left(\langle u^{(ks)}(\theta), u^{(ks')}(\theta) \rangle - \langle u^{(ks)}(\theta_*), u^{(ks')}(\theta_*) \rangle \right) \times \left(\langle u^{(ls)}(\theta), u^{(ls')}(\theta) \rangle - \langle u^{(ls)}(\theta_*), u^{(ls')}(\theta_*) \rangle \right)$$

$$\tilde{s}_3(\theta) = \frac{1}{12} \sum_{\substack{k,k',k'',l,l',l''=0 \\ |k-k'| \leq k'' \leq k+k' \text{ and } |l-l'| \leq l'' \leq l+l'}}^{L} M_{k,k',k'',l,l',l''} \sum_{s=1}^{S_k \wedge S_l} \sum_{s'=1}^{S_{k'} \wedge S_{l'}} \sum_{s''=1}^{S_{k''} \wedge S_{l''}} \left(B_{(k,s),(k',s'),(k'',s'')}(\theta) - B_{(k,s),(k',s'),(k'',s'')}(\theta_*) \right) \left(B_{(l,s),(l',s'),(l'',s'')}(\theta) - B_{(l,s),(l',s'),(l'',s'')}(\theta_*) \right).$$

4.5 Numerical evaluations of the Fisher information

We conclude with an empirical investigation of the accuracy of this theory for describing the spectrum of the Fisher information matrix in two simulated examples of the unprojected $\mathsf{SO}(3)$-rotations model described in Section 4.4.2.

In each example, we begin with a near-atomic-resolution electric potential map estimated from a cryo-EM experiment. We obtain a lower-resolution finite-dimensional approximation to this map by applying a low-pass filter to its Fourier transform, followed by a basis approximation for the filtered map. We simulate noisy and rotated samples from the unprojected cryo-EM model of Section 4.4.2 using this finite-dimensional approximation as the underlying true signal, for various inverse-SNR parameters

$$\alpha \equiv \sigma^2 / \|\theta_*\|^2.$$

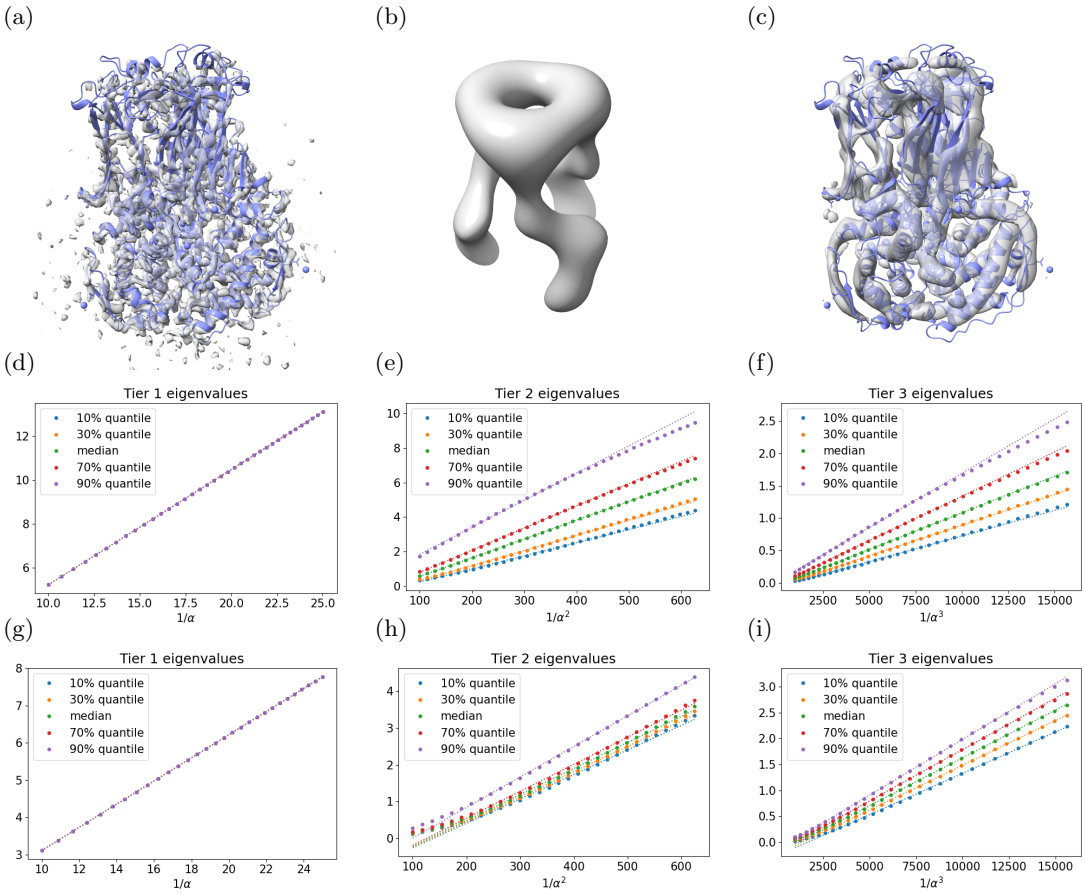

Figure 4.1: (a) 3.8Å-resolution cryo-EM map of the rotavirus VP6 trimer, overlaid with the atomic structure. (b) A finite-dimensional approximation using 405 basis functions at 24.6Å-resolution (displayed in a rotated orientation for clarity). (c) An approximation using 4410 basis functions at 8.2Å-resolution. (d–f) We stratify the eigenvalues of the 405-dimensional observed Fisher information corresponding to (b) into three "eigenvalue tiers" according to Theorem 4.4.6, and plot the scalings of the 10^{th}, 30^{th}, 50^{th}, 70^{th}, and 90^{th} percentiles of eigenvalues in each tier against $1/\alpha \propto \sigma^{-2}$, $1/\alpha^2 \propto \sigma^{-4}$, and $1/\alpha^3 \propto \sigma^{-6}$. (These quantiles nearly overlap for Tier 1.) Linear trends fitted using least squares are shown as dashed lines. (g–i) The same for the 4410-dimensional Fisher information matrix corresponding to (c).

We then study the dependence of eigenvalues of the observed Fisher information on α. Note that to simplify these experiments, we are simulating a setting without tomographic projection, and in an idealized model that ignores complications of real cryo-EM such as the contrast transfer function and deviations from uniform viewing angles.

Rotavirus VP6 trimer. We consider a map of the VP6 trimer in bovine rotavirus, reported in Zhang et al. (2008) (EMDB:1461). A contour plot of this map is overlaid with the atomic structure previously obtained by Mathieu et al. (2001) (PDB:1QHD), in Figure 4.1(a). We applied low-pass filters to this map in the Fourier domain at two different frequencies: a low-resolution filter with cutoff frequency $(24.6\text{Å})^{-1}$, and a medium-resolution filter with cutoff frequency $(8.2\text{Å})^{-1}$. The corresponding smoothed maps in the spatial domain are depicted in Figure C.1 of Appendix C.5.

We approximated each smoothed map using a function basis constructed as a product of radial functions $\{z_s : s = 1 \ldots, S\}$ with spherical harmonics $\{y_{lm} : 1 \leq l \leq L, -l \leq m \leq l\}$, as described in Section 4.4.2. To minimize the number of basis functions needed, we used an adaptive construction of the radial basis $\{z_s\}$ so as to maximize the power captured by each successive component. Details of this construction and of our numerical integration procedures are described in Appendix C.5.

Choosing bandlimits $(S, L) = (5, 8)$, yielding a basis of dimension $d = 5 \times (8 + 1)^2 = 405$, gave an accurate approximation to the 24.6Å-resolution map, as depicted in Figure 4.1(b). This approximation reveals the trimer composition of the VP6 complex and the shape of its hexagonal head, but loses more detailed information about the molecular structure. For the 8.2Å-resolution map, we chose a basis with bandlimits $(S, L) = (10, 20)$ and total dimension $d = 4410$, as shown in Figure 4.1(c). This approximation captures more interesting aspects of the tertiary and secondary structure, including the bundle of α-helices forming the base of the complex and the β-sheets forming the head. We denote the basis coefficients of these approximated maps as $\theta_* \in \mathbb{R}^d$.

We computed the empirical Hessians $\nabla^2 R_n(\theta_*)$ from $n = 500{,}000$ samples simulated according to the model of Section 4.4.2, with inverse-SNRs $\alpha = \sigma^2/\|\theta_*\|^2 \in [0.04, 0.10]$. To mitigate discretization effects of our numerical quadrature over $\mathsf{SO}(3)$, we simulated rotations also using this discretization, as detailed in Appendix C.5. For each tested α, we sorted the largest $d - 3$ eigenvalues of the Hessian $\nabla^2 R_n(\theta_*)$ and stratified these eigenvalues into three "tiers" of sizes (d_1, d_2, d_3), as described by Theorem 4.4.6. Figure 4.1(d–f) depicts representative eigenvalues in each tier, plotted against $1/\alpha \propto 1/\sigma^2$, $1/\alpha^2 \propto 1/\sigma^4$, and $1/\alpha^3 \propto 1/\sigma^6$ respectively. A linear trend is observed across the bulk of the tested range for α in all settings, in agreement with the prediction of Theorem 4.2.5. This

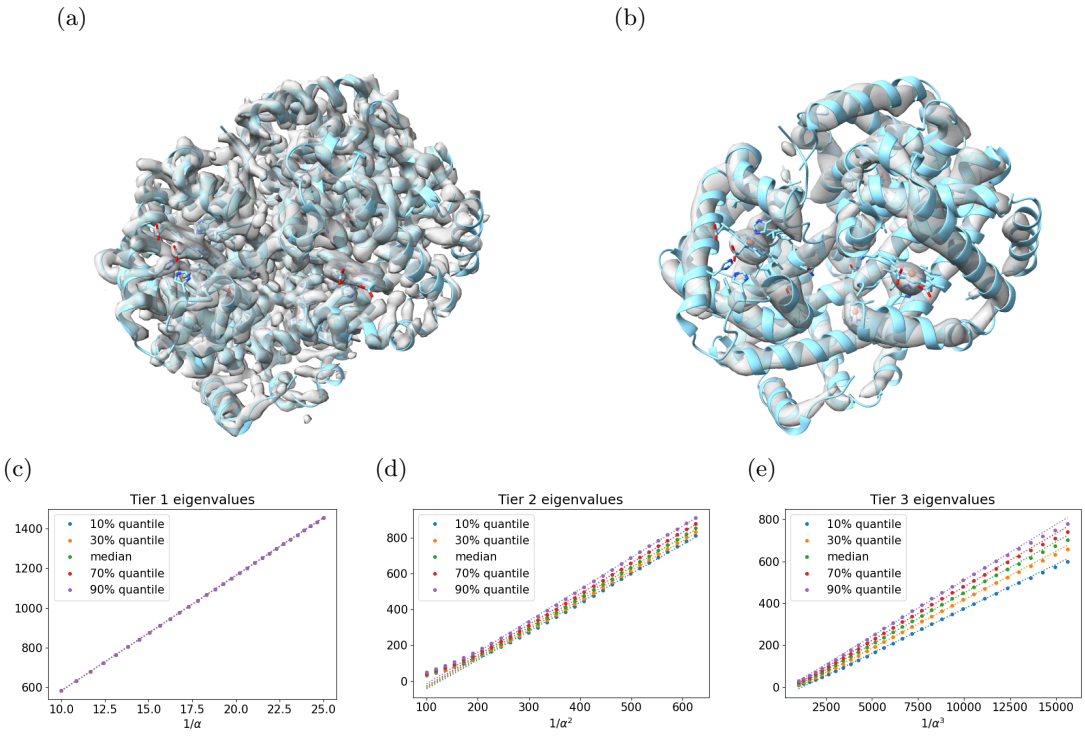

Figure 4.2: (a) 3.4Å-resolution cryo-EM map of hemoglobin, overlaid with the atomic structure. (b) A finite-dimensional approximation using 3528 basis functions at 7.0Å-resolution. (c–e) The 10^{th}, 30^{th}, 50^{th}, 70^{th}, and 90^{th} percentiles of eigenvalues within each "eigenvalue tier" of the 3528-dimensional observed Fisher information, plotted against $1/\alpha \propto \sigma^{-2}$, $1/\alpha^2 \propto \sigma^{-4}$, $1/\alpha^3 \propto \sigma^{-6}$ as in Figure 4.1.

may be contrasted with Figure C.2 in Appendix C.5, which instead plots eigenvalues in all three tiers against $1/\alpha \propto 1/\sigma^2$, and where non-linearity of the scaling is visually apparent for Tiers 2 and 3.

Hemoglobin. As a second example, we consider the more recent cryo-EM map of hemoglobin reported in Khoshouei et al. (2017) (EMDB:3650, PDB:5NI1). A contour plot overlaid with the atomic structure is presented in Figure 4.2(a). We applied a low-pass filter with cutoff frequency $(7.0\text{Å})^{-1}$ in the Fourier domain, depicted in Figure C.1. We then applied a basis approximation, again with an adaptively defined radial basis using the procedure of Appendix C.5, with bandlimits $(S, L) = (8, 20)$ and total basis dimension $d = 3528$. The approximated map is shown in Figure 4.2(b), and captures much of the α-helix structure and the locations of the embedded prosthetic heme groups that carry out the molecule's oxygen-binding function. We denote the basis coefficients of this approximation as θ_*.

Figure 4.2(c–e) again depicts the leading $d-3$ eigenvalues of $\nabla^2 R_n(\theta_*)$ from $n = 500{,}000$ samples

simulated according to the model of Section 4.4.2, stratified into the three tiers of sizes (d_1, d_2, d_3). Linear trends with $1/\alpha \propto 1/\sigma^2$, $1/\alpha^2 \propto 1/\sigma^4$, and $1/\alpha^3 \propto 1/\sigma^6$ are again observed across the bulk of the tested inverse-SNR range $\alpha \in [0.04, 0.10]$, in agreement with Theorem 4.2.5. This may be contrasted against the non-linear scalings of Tiers 2 and 3 with $1/\alpha$, as depicted in Figure C.2.

In the above two examples, we do see some deviations from the predicted linear trends at the higher and lower ends of tested SNR: For the higher dimensions $d = 4410$ and $d = 3528$, deviations occur in Tier 2 at larger noise $\alpha \approx 0.1$ (corresponding to $1/\alpha^2 \approx 100$), which are likely finite-sample effects due to high dimensionality. Concentration of $\nabla^2 R_n(\theta_*)$ around the (population) Fisher information $I(\theta_*)$ worsens with increasing σ^2 Fan et al. (2020), so these finite-sample effects will first be observed for larger noise. We observe also deviations from linearity near smaller noise $\alpha \approx 0.04$ in Tiers 2 and 3, in particular in the upper quantiles of eigenvalues in these tiers. This may reflect true behavior of the (population) Fisher information $I(\theta_*)$. We note that due to variation in the power captured by differing radial frequencies $s \in \{1, \ldots, S\}$, the eigenvalues span a large range within each of Tiers 2 and 3, and there is not a clear boundary between these tiers for any fixed inverse-SNR α.[7] In these examples, $\alpha = 0.04$ still represents a high level of noise compared to cryo-EM applications, as the spectral SNR (average power of signal / average power of noise at a fixed Fourier radius) reaches only 0.2–0.4 at the smallest Fourier radii. This is a limitation of the simplifying large-σ regime in which we have conducted our analysis.

4.6 Conclusion

In this work, we have provided a theoretical characterization of the Fisher information matrix and log-likelihood landscape for continuous group orbit estimation problems with a sufficiently high level of observational noise σ^2. This assumption of high noise facilitates a simplified analysis of the log-likelihood function, via a series expansion in $1/\sigma^2$. Such an analysis reveals a connection between properties of the Fisher information matrix and of the log-likelihood landscape with the graded structure of the invariant algebra of the underlying rotational group.

We studied several specific examples of group orbit estimation that correspond to function estimation in finite-dimensional function spaces, establishing the values of the relevant transcendence degrees that were previously conjectured for these examples. In particular, in a simplified model

7. We do observe clear gaps between these three tiers of eigenvalues in settings of sufficiently high noise and lower dimension $d \leq 100$.

of cryo-EM with tomographic projection, our results combine with the analyses of Bandeira et al. (2017) to show that 3^{rd}-order moments are sufficient to locally identify a generic signal up to its orbit.

In many interesting applications including single-particle cryo-EM, the target function at full spatial resolution may not admit an accurate low-dimensional approximation. In such settings, our theoretical results may have relevance to estimating lower-dimensional smoothed approximations of the function. We demonstrated in simulation that this theory can accurately predict the noise scalings of the Fisher information eigenvalues, for two small protein molecules, over a certain range of SNR. We highlight extensions of this theory to high-dimensional and infinite-dimensional settings and to a broader range of SNR as important directions for future work.

Acknowledgments

We would like to thank Fred Sigworth for helpful discussions about cryo-EM, and for suggesting to us the hemoglobin example. Zhou Fan was supported in part by NSF DMS-1916198. Roy R. Lederman was supported in part by NIH/NIGMS 1R01GM136780-01. Yi Sun was supported in part by NSF DMS-1701654, DMS-2039183, and DMS-2054838.

This work was accomplished by the joint effort of the authors with virtual meeting every other week over a year during the COVID-19 pandemic. My main contribution to this work is on the theoretical side, which includes the analyses of the general orbit recovery model and the following specific examples. I would thank Professors Zhou Fan, Roy R. Lederman, and Yi Sun for their excellent guidance and help discussions on this work. I would also thank my fellow student Tianhao Wang for his helpful discussions and substantial contribution from the empirical side.

Bibliography

Abbe, E., Bendory, T., Leeb, W., Pereira, J. M., Sharon, N. and Singer, A. (2019) Multireference alignment is easier with an aperiodic translation distribution. *IEEE Transactions on Information Theory*, **65**, 3565–3584.

Abbe, E., Pereira, J. M. and Singer, A. (2018) Estimation in the group action channel. In *2018 IEEE International Symposium on Information Theory (ISIT)*, 561–565. IEEE.

Arias-Castro, E., Candès, E. J. and Durand, A. (2011) Detection of an anomalous cluster in a network. *The Annals of Statistics*, **39**, 278–304.

Auger, I. E. and Lawrence, C. E. (1989) Algorithms for the optimal identification of segment neighborhoods. *Bulletin of mathematical biology*, **51**, 39–54.

Bandeira, A. S., Blum-Smith, B., Kileel, J., Perry, A., Weed, J. and Wein, A. S. (2017) Estimation under group actions: Recovering orbits from invariants. *arXiv preprint arXiv:1712.10163*.

Bandeira, A. S., Niles-Weed, J. and Rigollet, P. (2020) Optimal rates of estimation for multi-reference alignment. *Mathematical Statistics and Learning*, **2**, 25–75.

Baraniuk, R. G. (2007) Compressive sensing [lecture notes]. *IEEE signal processing magazine*, **24**, 118–121.

Barnett, A. H., Magland, J. and af Klinteberg, L. (2019) A parallel nonuniform fast fourier transform library based on an "exponential of semicircle" kernel. *SIAM Journal on Scientific Computing*, **41**, C479–C504.

Beck, A. and Teboulle, M. (2009) A fast iterative shrinkage-thresholding algorithm for linear inverse problems. *SIAM Journal on Imaging Sciences*, **2**, 183–202.

Bendory, T., Bartesaghi, A. and Singer, A. (2020a) Single-particle cryo-electron microscopy: Mathematical theory, computational challenges, and opportunities. *IEEE signal processing magazine*, **37**, 58–76.

Bendory, T., Jaffe, A., Leeb, W., Sharon, N. and Singer, A. (2020b) Super-resolution multi-reference alignment. *arXiv preprint arXiv:2006.15354*.

Bertsimas, D., King, A. and Mazumder, R. (2016) Best subset selection via a modern optimization lens. *The Annals of Statistics*, **44**, 813–852.

Blumensath, T. and Davies, M. E. (2009) Iterative hard thresholding for compressed sensing. *Applied and Computational Harmonic Analysis*, **27**, 265–274.

Böhm, A. (2013) *Quantum mechanics: foundations and applications*. Springer Science & Business Media.

Boykov, Y. and Kolmogorov, V. (2004) An experimental comparison of min-cut/max-flow algorithms for energy minimization in vision. *IEEE Transactions on Pattern Analysis & Machine Intelligence*, **9**, 1124–1137.

Boykov, Y., Veksler, O. and Zabih, R. (1999) Fast approximate energy minimization via graph cuts. In *Proceedings of the Seventh IEEE International Conference on Computer Vision*, vol. 1, 377–384. IEEE.

Boysen, L., Kempe, A., Liebscher, V., Munk, A. and Wittich, O. (2009) Consistencies and rates of convergence of jump-penalized least squares estimators. *The Annals of Statistics*, **37**, 157–183.

Brunel, V.-E. (2019) Learning rates for Gaussian mixtures under group action. In *Conference on Learning Theory*, 471–491.

Bühlmann, P., Rütimann, P., van de Geer, S. and Zhang, C.-H. (2013) Correlated variables in regression: clustering and sparse estimation. *Journal of Statistical Planning and Inference*, **143**, 1835–1858.

Cai, J.-F. and Xu, W. (2015) Guarantees of total variation minimization for signal recovery. *Information and Inference: A Journal of the IMA*, **4**, 328–353.

Cai, T. T., Ma, Z. and Wu, Y. (2013) Sparse pca: Optimal rates and adaptive estimation. *The Annals of Statistics*, **41**, 3074–3110.

Candès, E. J. (1998) *Ridgelets: Theory and applications*. Ph.D. thesis, Stanford University Stanford.

Candès, E. J. and Donoho, D. L. (2000) Curvelets: A surprisingly effective nonadaptive representation for objects with edges. *Tech. rep.*, Stanford University Dept of Statistics.

— (2004) New tight frames of curvelets and optimal representations of objects with piecewise C^2 singularities. *Communications on Pure and Applied Mathematics*, **57**, 219–266.

Candès, E. J., Eldar, Y. C., Needell, D. and Randall, P. (2011) Compressed sensing with coherent and redundant dictionaries. *Applied and Computational Harmonic Analysis*, **31**, 59–73.

Candès, E. J., Li, X. and Soltanolkotabi, M. (2015) Phase retrieval via wirtinger flow: Theory and algorithms. *IEEE Transactions on Information Theory*, **61**, 1985–2007.

Candès, E. J. and Recht, B. (2009) Exact matrix completion via convex optimization. *Foundations of Computational mathematics*, **9**, 717–772.

Candès, E. J., Romberg, J. and Tao, T. (2006a) Robust uncertainty principles: Exact signal reconstruction from highly incomplete frequency information. *IEEE Transactions on Information Theory*, **52**, 489.

Candès, E. J., Romberg, J. K. and Tao, T. (2006b) Stable signal recovery from incomplete and inaccurate measurements. *Communications on Pure and Applied Mathematics*, **59**, 1207–1223.

Candès, E. J. and Tao, T. (2010) The power of convex relaxation: Near-optimal matrix completion. *IEEE Transactions on Information Theory*, **56**, 2053–2080.

Candès, E. J. and Wakin, M. B. (2008) An introduction to compressive sampling. *IEEE signal processing magazine*, **25**, 21–30.

Chen, Y. and Candès, E. (2015) Solving random quadratic systems of equations is nearly as easy as solving linear systems. *Advances in Neural Information Processing Systems*, **28**.

Cheraghchi, M., Guruswami, V. and Velingker, A. (2013) Restricted isometry of fourier matrices and list decodability of random linear codes. *SIAM Journal on Computing*, **42**, 1888–1914.

Chi, Y., Lu, Y. M. and Chen, Y. (2019) Nonconvex optimization meets low-rank matrix factorization: An overview. *IEEE Transactions on Signal Processing*, **67**, 5239–5269.

Dalalyan, A. S., Hebiri, M. and Lederer, J. (2017) On the prediction performance of the Lasso. *Bernoulli*, **23**, 552–581.

Dasgupta, S. (1999) Learning mixtures of gaussians. In *40th Annual Symposium on Foundations of Computer Science (Cat. No. 99CB37039)*, 634–644. IEEE.

d'Aspremont, A., Ghaoui, L., Jordan, M. and Lanckriet, G. (2004) A direct formulation for sparse pca using semidefinite programming. *Advances in neural information processing systems*, **17**.

Daubechies, I. (1988) Orthonormal bases of compactly supported wavelets. *Communications on pure and applied mathematics*, **41**, 909–996.

Dauphin, Y. N., Pascanu, R., Gulcehre, C., Cho, K., Ganguli, S. and Bengio, Y. (2014) Identifying and attacking the saddle point problem in high-dimensional non-convex optimization. *Advances in neural information processing systems*, **27**.

Davenport, M. A. and Romberg, J. (2016) An overview of low-rank matrix recovery from incomplete observations. *IEEE Journal of Selected Topics in Signal Processing*, **10**, 608–622.

Donoho, D. L. (2006) Compressed sensing. *IEEE Transactions on Information Theory*, **52**, 1289–1306.

Donoho, D. L. and Johnstone, I. M. (1994) Ideal spatial adaptation by wavelet shrinkage. *Biometrika*, **81**, 425–455.

— (1995) Adapting to unknown smoothness via wavelet shrinkage. *Journal of the American Statistical Association*, **90**, 1200–1224.

Donoho, D. L. and Tanner, J. (2006) Thresholds for the recovery of sparse solutions via l1 minimization. In *2006 40th Annual Conference on Information Sciences and Systems*, 202–206. IEEE.

Du, S., Lee, J., Li, H., Wang, L. and Zhai, X. (2019) Gradient descent finds global minima of deep neural networks. In *International conference on machine learning*, 1675–1685. PMLR.

Dubochet, J., Adrian, M., Chang, J.-J., Homo, J.-C., Lepault, J., McDowall, A. W. and Schultz, P. (1988) Cryo-electron microscopy of vitrified specimens. *Quarterly reviews of biophysics*, **21**, 129–228.

Eisenstein, F., Danev, R. and Pilhofer, M. (2019) Improved applicability and robustness of fast cryo-electron tomography data acquisition. *Journal of structural biology*, **208**, 107–114.

Elad, M., Milanfar, P. and Rubinstein, R. (2007) Analysis versus synthesis in signal priors. *Inverse Problems*, **23**, 947.

Elenberg, E. R., Khanna, R., Dimakis, A. G. and Negahban, S. (2018) Restricted strong convexity implies weak submodularity. *The Annals of Statistics*, **46**, 3539–3568.

Fan, J. and Li, R. (2001) Variable selection via nonconcave penalized likelihood and its oracle properties. *Journal of the American statistical Association*, **96**, 1348–1360.

Fan, Z. and Guan, L. (2018) Approximate ℓ_0-penalized estimation of piecewise-constant signals on graphs. *The Annals of Statistics*, **46**, 3217–3245.

Fan, Z., Sun, Y., Wang, T. and Wu, Y. (2020) Likelihood landscape and maximum likelihood estimation for the discrete orbit recovery model. *arXiv preprint arXiv:2004.00041*.

Fessler, J. A. and Hero, A. O. (1994) Space-alternating generalized EM algorithms for penalized maximum-likelihood image reconstruction. *Tech. rep.*, Technical Report 286, Comm. and Sign. Proc. Lab., Dept. of EECS, Univ. of ....

Foucart, S. (2011) Hard thresholding pursuit: an algorithm for compressive sensing. *SIAM Journal on Numerical Analysis*, **49**, 2543–2563.

Frank, J. (2006) *Three-dimensional electron microscopy of macromolecular assemblies: visualization of biological molecules in their native state*. Oxford University Press.

Fryzlewicz, P. (2014) Wild binary segmentation for multiple change-point detection. *The Annals of Statistics*, **42**, 2243–2281.

Gavish, M., Nadler, B. and Coifman, R. R. (2010) Multiscale wavelets on trees, graphs and high dimensional data: Theory and applications to semi supervised learning. In *ICML*, 367–374.

Ge, R., Huang, F., Jin, C. and Yuan, Y. (2015) Escaping from saddle points—online stochastic gradient for tensor decomposition. In *Conference on Learning Theory*, 797–842.

Gibbs, P. and Hiroshi, S. (1996) What is Occam's Razor? Archived at `https://math.ucr.edu/home/baez/physics/General/occam.html`.

Glaeser, R. M., Nogales, E. and Chiu, W. (eds.) (2021) *Single-particle Cryo-EM of Biological Macromolecules*. 2053-2563. IOP Publishing. URL: `http://dx.doi.org/10.1088/978-0-7503-3039-8`.

Gong, C., Han, C., Gan, G., Deng, Z., Zhou, Y., Yi, J., Zheng, X., Xie, C. and Jin, X. (2017) Low-dose dynamic myocardial perfusion CT image reconstruction using pre-contrast normal-dose CT scan induced structure tensor total variation regularization. *Physics in Medicine & Biology*, **62**, 2612.

Goodall, C. (1991) Procrustes methods in the statistical analysis of shape. *Journal of the Royal Statistical Society: Series B (Methodological)*, **53**, 285–321.

Gower, J. C. (1975) Generalized procrustes analysis. *Psychometrika*, **40**, 33–51.

Guntuboyina, A., Lieu, D., Chatterjee, S. and Sen, B. (2017) Adaptive risk bounds in univariate total variation denoising and trend filtering. *arXiv preprint arXiv:1702.05113*.

Harchaoui, Z. and Lévy-Leduc, C. (2010) Multiple change-point estimation with a total variation penalty. *Journal of the American Statistical Association*, **105**, 1480–1493.

Hastie, T., Tibshirani, R. and Tibshirani, R. J. (2017) Extended comparisons of best subset selection, forward stepwise selection, and the lasso. *arXiv preprint arXiv:1707.08692*.

Henderson, R., Baldwin, J. M., Ceska, T. A., Zemlin, F., Beckmann, E. A. and Downing, K. H. (1990) Model for the structure of bacteriorhodopsin based on high-resolution electron cryo-microscopy. *Journal of molecular biology*, **213**, 899–929.

Huang, J., Ma, S. and Zhang, C.-H. (2008) Adaptive lasso for sparse high-dimensional regression models. *Statistica Sinica*, **18**, 1603–1618.

Hütter, J.-C. and Rigollet, P. (2016) Optimal rates for total variation denoising. In *Conference on Learning Theory*, 1115–1146.

Ibragimov, I. and Has'minskii, R. (1981) *Statistical estimation: Asymptotic theory*. Springer.

Jain, P., Tewari, A. and Kar, P. (2014) On iterative hard thresholding methods for high-dimensional M-estimation. In *Advances in Neural Information Processing Systems*, 685–693.

Jin, C., Ge, R., Netrapalli, P., Kakade, S. M. and Jordan, M. I. (2017) How to escape saddle points efficiently. In *Proceedings of the 34th International Conference on Machine Learning-Volume 70*, 1724–1732. JMLR. org.

Johnstone, I. M. (2017) *Gaussian estimation: Sequence and wavelet models*. unpublished draft.

Katsevich, A. and Bandeira, A. (2020) Likelihood maximization and moment matching in low SNR Gaussian mixture models. *arXiv preprint arXiv:2006.15202*.

Khoshouei, M., Radjainia, M., Baumeister, W. and Danev, R. (2017) Cryo-EM structure of haemoglobin at 3.2 Å determined with the Volta phase plate. *Nature communications*, **8**, 1–6.

Killick, R., Fearnhead, P. and Eckley, I. A. (2012) Optimal detection of changepoints with a linear computational cost. *Journal of the American Statistical Association*, **107**, 1590–1598.

Kim, S.-J., Koh, K., Boyd, S. and Gorinevsky, D. (2009) ℓ_1 trend filtering. *SIAM review*, **51**, 339–360.

Kim, Y. and Gao, C. (2019) Bayesian model selection with graph structured sparsity. *arXiv preprint arXiv:1902.03316*.

Kleinberg, J. and Tardos, E. (2002) Approximation algorithms for classification problems with pairwise relationships: Metric labeling and markov random fields. *Journal of the ACM (JACM)*, **49**, 616–639.

Kolda, T. G. and Bader, B. W. (2009) Tensor decompositions and applications. *SIAM review*, **51**, 455–500.

Krahmer, F. and Ward, R. (2014) Stable and robust sampling strategies for compressive imaging. *IEEE Transactions on Image Processing*, **23**, 612–622.

Krishnamuthy, A., Sharpnack, J. and Singh, A. (2013) Recovering graph-structured activations using adaptive compressive measurements. In *2013 Asilomar Conference on Signals, Systems and Computers*, 765–769. IEEE.

Lang, S. (2002) *Algebra*. Springer, 3rd edn.

LeCun, Y., Bengio, Y. and Hinton, G. (2015) Deep learning. *nature*, **521**, 436–444.

Lee, J. D., Simchowitz, M., Jordan, M. I. and Recht, B. (2016) Gradient descent only converges to minimizers. In *Conference on learning theory*, 1246–1257.

Li, Y., Mark, B., Raskutti, G. and Willett, R. (2018) Graph-based regularization for regression problems with highly-correlated designs. In *2018 IEEE Global Conference on Signal and Information Processing (GlobalSIP)*, 740–742. IEEE.

Lin, K., Sharpnack, J. L., Rinaldo, A. and Tibshirani, R. J. (2017) A sharp error analysis for the fused lasso, with application to approximate changepoint screening. In *Advances in Neural Information Processing Systems*, 6884–6893.

Lustig, M., Donoho, D. and Pauly, J. M. (2007) Sparse MRI: The application of compressed sensing for rapid MR imaging. *Magnetic Resonance in Medicine: An Official Journal of the International Society for Magnetic Resonance in Medicine*, **58**, 1182–1195.

Ma, C., Wang, K., Chi, Y. and Chen, Y. (2018) Implicit regularization in nonconvex statistical estimation: Gradient descent converges linearly for phase retrieval and matrix completion. In *International Conference on Machine Learning*, 3345–3354. PMLR.

Mammen, E. and van de Geer, S. (1997) Locally adaptive regression splines. *The Annals of Statistics*, **25**, 387–413.

Mathieu, M., Petitpas, I., Navaza, J., Lepault, J., Kohli, E., Pothier, P., Prasad, B. V., Cohen, J. and Rey, F. A. (2001) Atomic structure of the major capsid protein of rotavirus: Implications for the architecture of the virion. *The EMBO Journal*, **20**, 1485–1497.

Mazumder, R., Radchenko, P. and Dedieu, A. (2017) Subset selection with shrinkage: Sparse linear modeling when the SNR is low. *arXiv preprint arXiv:1708.03288*.

Mei, S., Bai, Y. and Montanari, A. (2018) The landscape of empirical risk for nonconvex losses. *Annals of Statistics*, **46**, 2747–2774.

Meinshausen, N. and Bühlmann, P. (2006) High-dimensional graphs and variable selection with the lasso. *The annals of statistics*, **34**, 1436–1462.

Mityagin, B. S. (2020) The zero set of a real analytic function. *Matematicheskie Zametki*, **107**, 473–475.

Mumford, D. and Shah, J. (1989) Optimal approximations by piecewise smooth functions and associated variational problems. *Communications on pure and applied mathematics*, **42**, 577–685.

Nam, S., Davies, M. E., Elad, M. and Gribonval, R. (2013) The cosparse analysis model and algorithms. *Applied and Computational Harmonic Analysis*, **34**, 30–56.

Needell, D. and Tropp, J. A. (2009) CoSaMP: Iterative signal recovery from incomplete and inaccurate samples. *Applied and Computational Harmonic Analysis*, **26**, 301–321.

Needell, D. and Ward, R. (2013a) Near-optimal compressed sensing guarantees for total variation minimization. *IEEE Transactions on Image Processing*, **22**, 3941–3949.

— (2013b) Stable image reconstruction using total variation minimization. *SIAM Journal on Imaging Sciences*, **6**, 1035–1058.

Negahban, S. N., Ravikumar, P., Wainwright, M. J. and Yu, B. (2012) A unified framework for high-dimensional analysis of m-estimators with decomposable regularizers. *Statistical Science*, **27**, 538–557.

Nesterov, Y. (2013) *Introductory lectures on convex optimization: A basic course*, vol. 87. Springer Science & Business Media.

Ortelli, F. and van de Geer, S. (2018) On the total variation regularized estimator over a class of tree graphs. *Electronic Journal of Statistics*, **12**, 4517–4570.

Padilla, O. H. M., Sharpnack, J. and Scott, J. G. (2017) The dfs fused lasso: Linear-time denoising over general graphs. *The Journal of Machine Learning Research*, **18**, 6410–6445.

Parikh, N. and Boyd, S. (2014) Proximal algorithms. *Foundations and Trends® in Optimization*, **1**, 127–239.

Perry, A., Weed, J., Bandeira, A. S., Rigollet, P. and Singer, A. (2019) The sample complexity of multireference alignment. *SIAM Journal on Mathematics of Data Science*, **1**, 497–517.

Pettersen, E. F., Goddard, T. D., Huang, C. C., Meng, E. C., Couch, G. S., Croll, T. I., Morris, J. H. and Ferrin, T. E. (2021) Ucsf ChimeraX: Structure visualization for researchers, educators, and developers. *Protein Science*, **30**, 70–82.

Pumir, T., Singer, A. and Boumal, N. (2019) The generalized orthogonal Procrustes problem in the high noise regime. *arXiv preprint arXiv:1907.01145*.

Punjani, A., Rubinstein, J. L., Fleet, D. J. and Brubaker, M. A. (2017) cryoSPARC: algorithms for rapid unsupervised cryo-EM structure determination. *Nature methods*, **14**, 290–296.

Rinaldo, A. (2009) Properties and refinements of the fused lasso. *The Annals of Statistics*, **37**, 2922–2952.

Romanov, E., Bendory, T. and Ordentlich, O. (2021) Multi-reference alignment in high dimensions: sample complexity and phase transition. *SIAM Journal on Mathematics of Data Science*, **3**, 494–523.

Rose, M. E. (1995) *Elementary theory of angular momentum*. Courier Corporation.

Rudelson, M. and Vershynin, R. (2008) On sparse reconstruction from Fourier and Gaussian measurements. *Communications on Pure and Applied Mathematics*, **61**, 1025–1045.

Rudin, L. I., Osher, S. and Fatemi, E. (1992) Nonlinear total variation based noise removal algorithms. *Physica D: Nonlinear Phenomena*, **60**, 259–268.

Sadhanala, V., Wang, Y.-X., Sharpnack, J. L. and Tibshirani, R. J. (2017) Higher-order total variation classes on grids: Minimax theory and trend filtering methods. In *Advances in Neural Information Processing Systems*, 5800–5810.

Sadhanala, V., Wang, Y.-X. and Tibshirani, R. J. (2016) Total variation classes beyond 1d: Minimax rates, and the limitations of linear smoothers. In *Advances in Neural Information Processing Systems*, 3513–3521.

Scheres, S. H. (2012) RELION: implementation of a Bayesian approach to cryo-EM structure determination. *Journal of structural biology*, **180**, 519–530.

Scheres, S. H., Gao, H., Valle, M., Herman, G. T., Eggermont, P. P., Frank, J. and Carazo, J.-M. (2007) Disentangling conformational states of macromolecules in 3D-EM through likelihood optimization. *Nature methods*, **4**, 27–29.

Schmidhuber, J. (2015) Deep learning in neural networks: An overview. *Neural networks*, **61**, 85–117.

Segars, W., Sturgeon, G., Mendonca, S., Grimes, J. and Tsui, B. M. (2010) 4D XCAT phantom for multimodality imaging research. *Medical Physics*, **37**, 4902–4915.

Sharon, N., Kileel, J., Khoo, Y., Landa, B. and Singer, A. (2020) Method of moments for 3D single particle ab initio modeling with non-uniform distribution of viewing angles. *Inverse Problems*, **36**, 044003.

Sharpnack, J., Singh, A. and Krishnamurthy, A. (2013) Detecting activations over graphs using spanning tree wavelet bases. In *Artificial Intelligence and Statistics*, 536–544.

Sharpnack, J., Singh, A. and Rinaldo, A. (2012) Sparsistency of the edge lasso over graphs. In *Artificial Intelligence and Statistics*, 1028–1036.

Sidiropoulos, N. D., De Lathauwer, L., Fu, X., Huang, K., Papalexakis, E. E. and Faloutsos, C. (2017) Tensor decomposition for signal processing and machine learning. *IEEE Transactions on Signal Processing*, **65**, 3551–3582.

Sigworth, F. J. (1998) A maximum-likelihood approach to single-particle image refinement. *Journal of structural biology*, **122**, 328–339.

Singer, A. and Sigworth, F. J. (2020) Computational methods for single-particle electron cryomicroscopy. *Annual Review of Biomedical Data Science*, **3**.

Tibshirani, R., Saunders, M., Rosset, S., Zhu, J. and Knight, K. (2005) Sparsity and smoothness via the fused lasso. *Journal of the Royal Statistical Society: Series B (Statistical Methodology)*, **67**, 91–108.

Tibshirani, R. J. (2011) *The solution path of the generalized lasso*. PhD thesis, Stanford University.

Tropp, J. A. and Gilbert, A. C. (2007) Signal recovery from random measurements via orthogonal matching pursuit. *IEEE Transactions on Information Theory*, **53**, 4655–4666.

Tsybakov, A. B. (2008) *Introduction to nonparametric estimation*. Springer Science & Business Media.

Turk, M. and Baumeister, W. (2020) The promise and the challenges of cryo-electron tomography. *FEBS letters*, **594**, 3243–3261.

Vershynin, R. (2010) Introduction to the non-asymptotic analysis of random matrices. *arXiv preprint arXiv:1011.3027*.

Wang, Y.-X., Sharpnack, J., Smola, A. J. and Tibshirani, R. J. (2016) Trend filtering on graphs. *The Journal of Machine Learning Research*, **17**, 3651–3691.

Wu, Y. and Zhou, H. H. (2019) Randomly initialized EM algorithm for two-component Gaussian mixture achieves near optimality in $o(\sqrt{n})$ iterations. *arXiv preprint arXiv:1908.10935*.

Xiao, L. and Zhang, T. (2013) A proximal-gradient homotopy method for the sparse least-squares problem. *SIAM Journal on Optimization*, **23**, 1062–1091.

Xu, J., Hsu, D. and Maleki, A. (2016) Global analysis of expectation maximization for mixtures of two Gaussians. In *Proceedings of the 30th International Conference on Neural Information Processing Systems*, 2684–2692.

Xu, L., Lu, C., Xu, Y. and Jia, J. (2011) Image smoothing via l_0 gradient minimization. *ACM Transactions on Graphics (TOG)*, **30**, 174.

Xu, S. and Fan, Z. (2021) Iterative alpha expansion for estimating gradient-sparse signals from linear measurements. *Journal of the Royal Statistical Society: Series B (Statistical Methodology)*, **83**, 271–292.

Xu, S., Fan, Z. and Negahban, S. (2020) Tree-projected gradient descent for estimating gradient-sparse parameters on graphs. In *Conference on Learning Theory*, 3683–3708. PMLR.

Zhang, C.-H. (2010) Nearly unbiased variable selection under minimax concave penalty. *The Annals of statistics*, **38**, 894–942.

Zhang, T. (2011) Sparse recovery with orthogonal matching pursuit under RIP. *IEEE Transactions on Information Theory*, **57**, 6215–6221.

Zhang, X., Settembre, E., Xu, C., Dormitzer, P. R., Bellamy, R., Harrison, S. C. and Grigorieff, N. (2008) Near-atomic resolution using electron cryomicroscopy and single-particle reconstruction. *Proceedings of the National Academy of Sciences*, **105**, 1867–1872.

Zhang, Y., Wainwright, M. J. and Jordan, M. I. (2014) Lower bounds on the performance of polynomial-time algorithms for sparse linear regression. In *Conference on Learning Theory*, 921–948.

Zhao, P. and Yu, B. (2006) On model selection consistency of lasso. *The Journal of Machine Learning Research*, **7**, 2541–2563.

Zou, H., Hastie, T. and Tibshirani, R. (2006) Sparse principal component analysis. *Journal of computational and graphical statistics*, **15**, 265–286.

A Appendix for Chapter 2

A.1 Proof of robust recovery guarantee

In this appendix, we prove Theorem 2.3.5 providing the estimation guarantee under approximate gradient-sparsity and discretization and measurement error.

Lemma A.1.1. *Suppose G has maximum vertex degree D, and $\mathbf{A} \in \mathbb{R}^{n\times p}$ satisfies (κ, ρ)-cRIP. Then for any $\mathbf{u} \in \mathbb{R}^p$ and $s \geq 1$,*

$$\|\mathbf{A}\mathbf{u}\|_2 \leq \left(1 + \kappa + \sqrt{D\rho(s)}\right) \cdot \left(\|\mathbf{u}\|_2 + \frac{\|\mathbf{u}\|_1}{\sqrt{s}}\right).$$

Proof. Let $T_1 \subseteq \{1, \ldots, p\}$ be the s indices corresponding to the s entries of $\mathbf{u}$ with largest magnitude (breaking ties arbitrarily). Let $T_2 \subseteq \{1, \ldots, p\} \setminus T_1$ be the s indices corresponding to the next s entries of $\mathbf{u}$ with largest magnitude, and define sequentially $T_3, T_4, \ldots, T_m$ for $m = \lceil p/s \rceil$ in this way. Denote by $\mathbf{u}_{T_i} \in \mathbb{R}^p$ the vector with j^{th} entry equal to u_j if $j \in T_i$, or 0 otherwise. Then $\|\nabla \mathbf{u}_{T_i}\|_0 \leq Ds$ for each i. Applying the triangle inequality and cRIP condition for $\mathbf{A}$,

$$\|\mathbf{A}\mathbf{u}\|_2 \leq \sum_{i=1}^{m} \|\mathbf{A}\mathbf{u}_{T_i}\|_2 \leq \left(1 + \kappa + \sqrt{\rho(Ds)}\right) \cdot \sum_{i=1}^{m} \|\mathbf{u}_{T_i}\|_2.$$

For $i \geq 2$, we have $\|\mathbf{u}_{T_{i+1}}\|_\infty \leq \|\mathbf{u}_{T_i}\|_1/s$ by construction, so

$$\|\mathbf{u}_{T_{i+1}}\|_2 \leq \sqrt{s} \cdot \frac{\|\mathbf{u}_{T_i}\|_1}{s} = \frac{\|\mathbf{u}_{T_i}\|_1}{\sqrt{s}}.$$

Applying this for $i \geq 2$, and the bound $\|\mathbf{u}_{T_1}\|_2 \leq \|\mathbf{u}\|_2$ for $i = 1$,

$$\|\mathbf{A}\mathbf{u}\|_2 \leq \left(1 + \kappa + \sqrt{\rho(Ds)}\right) \cdot \left(\|\mathbf{u}\|_2 + \frac{\sum_{i=1}^{m-1} \|\mathbf{u}_{T_i}\|_1}{\sqrt{s}}\right) \leq \left(1 + \kappa + \sqrt{\rho(Ds)}\right) \left(\|\mathbf{u}\|_2 + \frac{\|\mathbf{u}\|_1}{\sqrt{s}}\right).$$

Finally, we have $(\rho(Ds) - \rho(0))/Ds \leq (\rho(s) - \rho(0))/s$ by the concavity of ρ, and hence $\rho(Ds) \leq D\rho(s)$

since $\rho(0) \geq 0$. $\square$

Proof of Theorem 2.3.5. Write $\mathbf{y} = \mathbf{A}\mathbf{x} + \tilde{\mathbf{e}}$ where $\tilde{\mathbf{e}} = \mathbf{A}(\mathbf{x}_* - \mathbf{x}) + \mathbf{e}$. Denote

$$s = \max(\|\nabla \mathbf{x}\|_0, 1), \qquad s_k = \|\nabla \mathbf{x}_k\|_0, \qquad \mathbf{r}_k = \mathbf{x}_k - \mathbf{x}.$$

As in the proof of Theorem 2.3.4, consider the partitions of $\{1, \ldots, p\}$ induced by the piecewise-constant structures of $\mathbf{x}_k$, $\mathbf{x}_{k+1}$, and $\mathbf{x}$, let $\mathcal{S}$ be their common refinement, and let $\mathbf{P}$ be the orthogonal projection onto the subspace of signals taking constant value over each set in $\mathcal{S}$. Applying

$$\mathbf{a}_{k+1} = \mathbf{x}_k - \eta \mathbf{A}^\mathsf{T}(\mathbf{A}\mathbf{x}_k - \mathbf{y}) = \mathbf{x}_k - \eta \mathbf{A}^\mathsf{T}\mathbf{A}\mathbf{r}_k + \eta \mathbf{A}^\mathsf{T}\tilde{\mathbf{e}},$$

the same arguments as leading to (2.15) yield

$$\big(\|\mathbf{r}_{k+1}\|_2 - \|\mathbf{r}_k - \eta \mathbf{P}\mathbf{A}^\mathsf{T}\mathbf{A}\mathbf{r}_k + \eta \mathbf{P}\mathbf{A}^\mathsf{T}\tilde{\mathbf{e}}\|_2\big)_+^2 \leq \|\mathbf{r}_k - \eta \mathbf{P}\mathbf{A}^\mathsf{T}\mathbf{A}\mathbf{r}_k + \eta \mathbf{P}\mathbf{A}^\mathsf{T}\tilde{\mathbf{e}}\|_2^2 + \lambda_k(4s - 2s_{k+1}). \quad (44)$$

Set $S_k = s + s_k + s_{k+1}$, $T_k = s + s_k$, and

$$\tau_k = \kappa + \sqrt{\rho(S_k)}, \quad \zeta_k = \kappa + \sqrt{\rho(T_k)}, \quad d_k = 2(1+\kappa)\sqrt{\rho(T_k)} + \rho(T_k).$$

Then we obtain analogously to (2.16) and (2.19) that

$$\lambda_k s_{k+1} \leq \|\mathbf{r}_k\|_2^2 + 2\|\sqrt{\eta}\mathbf{A}\mathbf{P}\|_{\mathrm{op}}^2 \cdot \|\sqrt{\eta}\mathbf{A}\mathbf{r}_k\|_2^2 + 2\|\eta \mathbf{P}\mathbf{A}^\mathsf{T}\tilde{\mathbf{e}}\|_2^2 + 2\lambda_k s,$$

and hence

$$\big(\lambda_k - 2(1+\zeta_k)^2 d_k \|\mathbf{r}_k\|_2^2/s\big) \cdot s_{k+1} \leq (1 + 2(1+\zeta_k)^4) \cdot \|\mathbf{r}_k\|_2^2 + 2\|\eta \mathbf{P}\mathbf{A}^\mathsf{T}\tilde{\mathbf{e}}\|_2^2 + 2\lambda_k s. \quad (45)$$

Similarly, taking the square-root in (44), we obtain analogously to (2.20) that

$$\|\mathbf{r}_{k+1}\|_2 \leq \Big[1 - t(\kappa) + 4\sqrt{\rho(S_k)} + 2\rho(S_k)\Big] \cdot \|\mathbf{r}_k\|_2 + 2\|\eta \mathbf{P}\mathbf{A}^\mathsf{T}\tilde{\mathbf{e}}\|_2 + \sqrt{4\lambda_k s}. \quad (46)$$

Recalling the bound $\|\sqrt{\eta}\mathbf{A}\mathbf{P}\|_{\mathrm{op}} \leq 1 + \tau_k$ from (2.17), we have

$$\|\eta \mathbf{P}\mathbf{A}^\mathsf{T}\tilde{\mathbf{e}}\|_2 \leq (1+\tau_k)(\|\sqrt{\eta}\mathbf{A}(\mathbf{x}_* - \mathbf{x})\|_2 + \|\sqrt{\eta} \cdot \mathbf{e}\|_2).$$

Bounding $\|\sqrt{\eta}\mathbf{A}(\mathbf{x}_* - \mathbf{x})\|_2$ using the given cRIP condition and Lemma A.1.1 with the choice $s = \max(\|\nabla\mathbf{x}\|_0, 1)$ as above, we get for a constant $c_1 > 0$ that

$$\|\eta\mathbf{P}\mathbf{A}^\mathsf{T}\tilde{\mathbf{e}}\|_2 \leq (1+\tau_k)c_1 E(\mathbf{x}).$$

Applying this and the bound $(1+\tau_k)^2 \leq (1+\zeta_k)^2 + d_k s_{k+1}/s$ from (2.18) to (45), we get

$$(\lambda_k - 2e_k d_k/s)\cdot s_{k+1} \leq \|\mathbf{r}_k\|_2^2 + 2e_k(1+\zeta_k)^2 + 2\lambda_k s \tag{47}$$

for the quantity

$$e_k = (1+\zeta_k)^2\|\mathbf{r}_k\|_2^2 + c_1^2 E(\mathbf{x})^2.$$

Also, applying this to (46), we get

$$\|\mathbf{r}_{k+1}\|_2 \leq \left[1 - t(\kappa) + 4\sqrt{\rho(S_k)} + 2\rho(S_k)\right]\cdot\|\mathbf{r}_k\|_2 + 2(1+\tau_k)c_1 E(\mathbf{x}) + \sqrt{4\lambda_k s}. \tag{48}$$

We now claim by induction on k that if $\rho(s) \leq c_0$ and $\lambda_k \geq C_0 E(\mathbf{x})^2/s$ for every $k \leq k_*$, where $C_0 > 0$ is sufficiently large and $c_0 > 0$ is sufficiently small, then for every $k \leq k_*$ we have

$$s_k \leq \frac{200}{t(\kappa)^2}s, \qquad \|\mathbf{r}_k\|_2 \leq \frac{4\sqrt{\lambda_k s}}{t(\kappa)}. \tag{49}$$

For $k = 0$, these are satisfied as $s_0 = 0$ and $\lambda_0 = \lambda_{\max} \geq \|\mathbf{r}_0\|_2^2$. Assume inductively that these hold for k, where $k \leq k_* - 1$. Then for small enough c_0, we have $(1+\zeta_k)^2 < 2$ and hence

$$e_k \leq \frac{32\lambda_k s}{t(\kappa)^2} + c_1^2 E(\mathbf{x})^2.$$

Also, $d_k \leq C\sqrt{c_0}$ for a constant $C \equiv C(\kappa) > 0$ independent of c_0. Then for C_0 large enough and c_0 small enough, we obtain from (47) and the condition $\lambda_k \geq C_0 E(\mathbf{x})^2/s$ that

$$\frac{3}{4}\lambda_k s_{k+1} \leq \|\mathbf{r}_k\|_2^2 + 4e_k + 2\lambda_k s \leq \frac{146\lambda_k s}{t(\kappa)^2} + 4c_1^2 E(\mathbf{x})^2 < \frac{150\lambda_k s}{t(\kappa)^2}.$$

This gives the bound

$$s_{k+1} \leq \frac{200}{t(\kappa)^2}s.$$

Then applying (49) and this bound to (48), again for $\rho(s) \leq c_0$ and $\lambda_k s \geq C_0 E(\mathbf{x})^2$ with C_0

sufficiently large and c_0 sufficiently small, we get

$$\|\mathbf{r}_{k+1}\|_2 \le \left(1 - \frac{4}{5}t(\kappa)\right)\|\mathbf{r}_k\|_2 + 6c_1 E(\mathbf{x}) + \sqrt{4\lambda_k s} < \left(\frac{4}{t(\kappa)} - 1\right)\sqrt{\lambda_k s}.$$

Applying $\sqrt{\lambda_k} = \sqrt{\lambda_{k+1}/\gamma} \le \sqrt{\lambda_{k+1}}(1 - t(\kappa)/4)^{-1}$, we obtain

$$\|\mathbf{r}_{k+1}\|_2 \le \frac{4\sqrt{\lambda_{k+1} s}}{t(\kappa)},$$

completing the induction. This establishes (49) for every $k \le k_*$, provided $\lambda_{k_*} \ge C_0 E(\mathbf{x})^2/s$. In particular, at the iterate k_*, we have $\lambda_{k_*} s \asymp E(\mathbf{x})^2$ and hence $\|\mathbf{r}_{k_*}\|_2 \lesssim E(\mathbf{x})$. □

A.2 Proofs of cut-restricted isometry property

In this appendix, we prove Propositions 2.3.2 and 2.3.3 establishing cRIP for the sub-Gaussian and weighted 2D-Fourier designs.

Proof of Proposition 2.3.2. First fix $s \in \{1, \dots, |E|\}$. For each partition $\mathcal{S}$ of $V = \{1, \dots, p\}$ with $|\partial\mathcal{S}| = s$, let $\mathbf{P}_{\mathcal{S}} : \mathbb{R}^p \to K_{\mathcal{S}}$ be the associated orthogonal projection onto the subspace $K_{\mathcal{S}}$ of signals which are constant on each set in $\mathcal{S}$. Note that the dimension of $K_{\mathcal{S}}$ is the number of sets in $\mathcal{S}$, which is at most $s + 1$ because G is a connected graph. Write $\mathbf{P}_{\mathcal{S}} = \mathbf{Q}_{\mathcal{S}}\mathbf{Q}_{\mathcal{S}}^\mathsf{T}$, where $\mathbf{Q}_{\mathcal{S}}$ has orthonormal columns spanning $K_{\mathcal{S}}$. Then $\mathbf{A}\mathbf{Q}_{\mathcal{S}}$ still has independent rows $\mathbf{a}_i^\mathsf{T}\mathbf{Q}_{\mathcal{S}}/\sqrt{n}$, where $\|\mathbf{a}_i^\mathsf{T}\mathbf{Q}_{\mathcal{S}}\|_{\psi_2} \le K$ and $\mathrm{Cov}[\mathbf{a}_i^\mathsf{T}\mathbf{Q}_{\mathcal{S}}] = \mathbf{Q}_{\mathcal{S}}^\mathsf{T}\mathbf{\Sigma}\mathbf{Q}_{\mathcal{S}}$. Applying (Vershynin, 2010, Eq. (5.25)) to $\mathbf{A}\mathbf{Q}_{\mathcal{S}}$, for any $t > 0$ and some constants $C, c > 0$ depending only on K,

$$\mathbb{P}\left[\|\mathbf{Q}_{\mathcal{S}}^\mathsf{T}\mathbf{A}^\mathsf{T}\mathbf{A}\mathbf{Q}_{\mathcal{S}} - \mathbf{Q}_{\mathcal{S}}^\mathsf{T}\mathbf{\Sigma}\mathbf{Q}_{\mathcal{S}}\|_{\mathrm{op}} \ge \max(\delta, \delta^2)\right] \le 2e^{-ct^2}, \qquad \delta \equiv \frac{C\sqrt{s} + t}{\sqrt{n}}.$$

Let $g(s) = s\log(1 + |E|/s)$, and note that there are at most $\binom{|E|}{s} \le e^{g(s)}$ partitions $\mathcal{S}$ where $|\partial\mathcal{S}| = s$. Taking a union bound over $\mathcal{S}$, and noting that any $\mathbf{u}$ with $\|\nabla\mathbf{u}\|_0 = s$ may be represented as $\mathbf{u} = \mathbf{Q}_{\mathcal{S}}\mathbf{v}$ for some such $\mathcal{S}$, this yields

$$\mathbb{P}\left[\sup_{\mathbf{u}\in\mathbb{R}^p : \|\mathbf{u}\|_2 = 1, \|\nabla\mathbf{u}\|_0 = s} |\mathbf{u}^\mathsf{T}\mathbf{A}^\mathsf{T}\mathbf{A}\mathbf{u} - \mathbf{u}^\mathsf{T}\mathbf{\Sigma}\mathbf{u}| \ge \max(\delta, \delta^2)\right] \le 2e^{g(s) - ct^2}.$$

When $\|\mathbf{u}\|_2 = 1$ and $|\mathbf{u}^\mathsf{T}\mathbf{A}^\mathsf{T}\mathbf{A}\mathbf{u} - \mathbf{u}^\mathsf{T}\mathbf{\Sigma}\mathbf{u}| \le \max(\delta, \delta^2)$, we have

$$\|\mathbf{A}\mathbf{u}\|_2 \le \sqrt{\mathbf{u}^\mathsf{T}\mathbf{\Sigma}\mathbf{u} + \max(\delta, \delta^2)} \le \sqrt{(1 + \kappa)^2 + \max(\delta, \delta^2)} \le 1 + \kappa + \delta.$$

We also have

$$\|\mathbf{A}\mathbf{u}\|_2 \geq \sqrt{(\mathbf{u}^\mathsf{T}\boldsymbol{\Sigma}\mathbf{u} - \max(\delta, \delta^2))_+} \geq \sqrt{((1-\kappa)^2 - \max(\delta, \delta^2))_+} \geq 1 - \kappa - \frac{\delta}{1-\kappa},$$

where the last inequality is trivial for $\delta \geq (1-\kappa)^2$ and may be checked for $\delta \leq (1-\kappa)^2$ by squaring both sides and applying $\max(\delta, \delta^2) = \delta$ in this case. Then, for any k and some constants $C_0, C_1 > 0$ depending on k, setting $t = \sqrt{C_0 g(s)}$ and applying $g(s) \geq g(1) = \log(1 + |E|)$, we get

$$\mathbb{P}\left[\sup_{\mathbf{u}\in\mathbb{R}^p : \|\mathbf{u}\|_2 = 1, \|\nabla\mathbf{u}\|_0 = s} \Big| \|\mathbf{A}\mathbf{u}\|_2 - 1 \Big| \leq \kappa + \sqrt{\frac{C_1 g(s)}{n}}\right] \leq |E|^{-k-1}.$$

Taking a union bound over $s = 1, \ldots, |E|$ and applying scale invariance of the cRIP condition to $\|\mathbf{u}\|_2$ concludes the proof. □

Next, we establish Proposition 2.3.3 on the weighted Fourier design. Its proof follows closely that of (Rudelson and Vershynin, 2008, Theorem 3.3): For each sparsity level $s \geq 1$, we define $\kappa_s = \sup_{\mathbf{x}\in K_s} |\mathbf{x}^*(\mathbf{A}^*\mathbf{A} - \mathbf{I})\mathbf{x}|$ where K_s is the set of complex unit vectors with gradient-sparsity at most s. It suffices to show with high probability that $\kappa_s \leq 2\sqrt{\rho(s)} + \rho(s)$ for all $s = 1, \ldots, |E|$. We first control $\mathbb{E}[\kappa_s]$ using a metric entropy argument, and then establish concentration of κ_s around $\mathbb{E}[\kappa_s]$ following the same proof as (Rudelson and Vershynin, 2008, Theorem 3.9).

The main additional steps in our proof lie in bounding the covering number of K_s in the pseudo-norm $\|\mathbf{x}\|_\mathbf{A} = \sqrt{2}\|\mathbf{A}\mathbf{x}\|_\infty$, which is used to control $\mathbb{E}[\kappa_s]$. In the argument of Rudelson and Vershynin (2008), the analogue of K_s is the set of unit vectors which are s-sparse. This set is contained in the ℓ_1-ball $\{\mathbf{x} : \|\mathbf{x}\|_1 \leq \sqrt{s}\}$, and Rudelson and Vershynin (2008) uses Maurey's probabilistic method and a bound on $\|\mathbf{A}\mathbf{v}\|_\infty$ for standard basis vectors $\mathbf{v}$ to control the covering number of this ℓ_1 ball. In our setting, the condition $\|\nabla\mathbf{x}\|_0 \leq s$ gives only a bound on $\|\nabla\mathbf{x}\|_1$, and not on $\|\mathbf{x}\|_1$. We instead use a decay of the coefficients of $\mathbf{x}$ in the Haar wavelet basis, proven in Needell and Ward (2013b) and restated as Lemma A.2.2 below, to bound the ℓ_1-norm of $\mathbf{x}$ in the Haar basis. We then bound $\|\mathbf{A}\mathbf{v}\|_\infty$ for Haar basis vectors $\mathbf{v}$ using Lemma A.2.1 below, and finally apply this together with Maurey's argument as in Rudelson and Vershynin (2008) to control the covering number of K_s. The additional logarithmic factor in Proposition 2.3.3 over the results of Rudelson and Vershynin (2008) and Cheraghchi et al. (2013) are due to this approach: The ℓ_1-norm of $\mathbf{x}$ in the Haar basis is inflated by a factor of $\log p$, and the bound for $\|\mathbf{A}\mathbf{v}\|_\infty$ is also inflated by $\log p$ because of our reweighting for the Fourier matrix. (We only use the connection to the Haar basis here, and do not incur this logarithmic inflation in our analysis of the sub-Gaussian design in Proposition 2.3.2.)

In the remainder of this section, we provide the details of this argument.

Lemma A.2.1. *Let $p = N_1 N_2$, let $S \times T \subset \{1, \dots, N_1\} \times \{1, \dots, N_2\}$ be any connected rectangle, and let $\mathcal{F} \in \mathbb{C}^{p \times p}$ be the 2-D discrete Fourier matrix defined in Section 2.3.1. Then for any $(i, j) \in \{1, \dots, N_1\} \times \{1, \dots, N_2\}$,*

$$\left| \sum_{(i',j') \in S \times T} \mathcal{F}_{(i,j),(i',j')} \right| \leq \sqrt{\frac{|S|}{1 + \min(i-1, N_1 - i + 1)} \cdot \frac{|T|}{1 + \min(j-1, N_2 - j + 1)}}.$$

Proof. Since

$$\left| \sum_{(i',j') \in S \times T} \mathcal{F}_{(i,j),(i',j')} \right| = \left| \sum_{i' \in S} \mathcal{F}^1_{i,i'} \cdot \sum_{j' \in T} \mathcal{F}^2_{j,j'} \right|$$

for the 1-D Fourier matrices $\mathcal{F}^1 \in \mathbb{C}^{N_1 \times N_1}$ and $\mathcal{F}^2 \in \mathbb{C}^{N_2 \times N_2}$, it suffices to show

$$\left| \sum_{k \in S} \mathcal{F}^1_{ik} \right| \leq \sqrt{\frac{|S|}{1 + \min(i-1, N_1 - i + 1)}}.$$

For this, denote the elements of S as $\{k_1 + 1, \dots, k_1 + |S|\}$, and write

$$\left| \sum_{k \in S} \mathcal{F}^1_{ik} \right| = \left| \frac{1}{\sqrt{N_1}} \sum_{t=0}^{|S|-1} e^{2\pi \mathbf{i} \cdot \frac{(i-1)k_1}{N_1}} \cdot e^{2\pi \mathbf{i} \cdot \frac{(i-1)t}{N_1}} \right| = \frac{1}{\sqrt{N_1}} \left| \sum_{t=0}^{|S|-1} e^{2\pi \mathbf{i} \cdot \frac{(i-1)t}{N_1}} \right|.$$

This is at most $|S|/\sqrt{N_1}$, which implies the bound for $i = 1$. For $i \geq 2$, apply further

$$|1 - e^{2\pi \mathbf{i} t}| \geq 4 \min(t, 1 - t)$$

for $t \in [0, 1]$. Then summing the geometric series, we also have

$$\begin{aligned} \left| \sum_{k \in S} \mathcal{F}^1_{ik} \right| &= \frac{1}{\sqrt{N_1}} \left| 1 - e^{2\pi \mathbf{i} \frac{(i-1)|S|}{N_1}} \right| \cdot \left| 1 - e^{2\pi \mathbf{i} \frac{(i-1)}{N_1}} \right|^{-1} \\ &\leq \frac{\sqrt{N_1}}{2 \min(i-1, N_1 - i + 1)} \leq \frac{\sqrt{N_1}}{1 + \min(i-1, N_1 - i + 1)}. \end{aligned}$$

The result follows from combining this with the previous upper bound bound $|S|/\sqrt{N_1}$, using $\min(a, b) \leq \sqrt{ab}$. □

Lemma A.2.2. *Let $p = N_1 N_2$, where N_1, N_2 are powers of 2 and $1/K \leq N_1/N_2 \leq K$ for a constant $K > 0$. Let G be the 2-D lattice graph of size $N_1 \times N_2$. For $\mathbf{x} \in \mathbb{C}^p$, let $|c_{(1)}(\mathbf{x})| \geq \ldots \geq |c_{(p)}(\mathbf{x})|$ be the ordered magnitudes of the coefficients of $\mathbf{x}$ in the bivariate Haar wavelet basis. If $\mathbf{x}$ is centered*

to have mean entry 0, then for a constant $C \equiv C(K) > 0$ and each $k = 1, \ldots, p$,

$$|c_{(k)}(\mathbf{x})| \leq C \cdot \frac{\|\nabla \mathbf{x}\|_1}{k}$$

where ∇ is the discrete gradient operator on G.

Proof. See (Needell and Ward, 2013b, Proposition 8) for the case $N_1 = N_2$. For $N_1 < N_2$, we may apply this result to the "stretched" image where each original vertex value is copied to N_2/N_1 consecutive values in a vertical strip. This stretching changes $\|\nabla \mathbf{x}\|_1$ and each original bivariate Haar wavelet coefficient by at most a constant factor, and introduces $N_2^2 - N_1 N_2$ new Haar wavelet coefficients which are identically 0. Thus the result still holds in this case, and similarly for $N_1 > N_2$. □

Proof of Proposition 2.3.3. For each partition $\mathcal{S} = (S_1, \ldots, S_k)$ of G into k connected pieces, let $K_{\mathcal{S}} \subset \mathbb{C}^p$ be the k-dimensional subspace of vectors which take a constant value over each set of $\mathcal{S}$. For each sparsity level $s \geq 1$, define

$$K_s = \bigcup_{\mathcal{S}:|\partial \mathcal{S}| \leq s} \{\mathbf{x} \in K_{\mathcal{S}} : \|\mathbf{x}\|_2 \leq 1\}, \qquad \kappa_s = \sup_{\mathbf{x} \in K_s} |\mathbf{x}^*(\mathbf{A}^*\mathbf{A} - \mathbf{I})\mathbf{x}|.$$

It suffices to show, with the stated probability and form of ρ, that

$$\kappa_s \leq 2\sqrt{\rho(s)} + \rho(s)$$

holds simultaneously for all $s = 1, \ldots, |E|$.

We first control $\mathbb{E}[\kappa_s]$ using a metric entropy argument: Letting $\mathbf{A}_r^*$ be row r of $\mathbf{A}$,

$$n \cdot \mathbb{E}[\mathbf{A}_r \mathbf{A}_r^*] = \mathbb{E}\left[\frac{\mathcal{F}_{(i_r,j_r)}\mathcal{F}^*_{(i_r,j_r)}}{\nu(i_r, j_r)}\right] = \sum_{(i,j)} \mathcal{F}_{(i,j)}\mathcal{F}^*_{(i,j)} = \mathbf{I}.$$

So

$$\kappa_s = \sup_{\mathbf{x} \in K_s} \cdot \left| \sum_{r=1}^{n} \left(|\mathbf{A}_r^*\mathbf{x}|^2 - \mathbb{E}|\mathbf{A}_r^*\mathbf{x}|^2 \right) \right|.$$

Applying Gaussian symmetrization,

$$\mathbb{E}[\kappa_s] \leq C\, \mathbb{E} \sup_{\mathbf{x} \in K_s} \left| \sum_{r=1}^{n} g_r |\mathbf{A}_r^*\mathbf{x}|^2 \right|$$

for a constant $C > 0$ and $g_1, \ldots, g_n \overset{iid}{\sim} \mathcal{N}(0,1)$ independent of $\mathbf{A}$.

Condition on $\mathbf{A}$, and define by $E(\mathbf{A})$ the right side above with the expectation taken only over $g_1, \ldots, g_n$. Introducing the pseudo-metric

$$d(\mathbf{x}, \mathbf{y}) = \sqrt{\sum_{r=1}^{n} (|\mathbf{A}_r^* \mathbf{x}|^2 - |\mathbf{A}_r^* \mathbf{y}|^2)^2},$$

Dudley's inequality yields

$$E(\mathbf{A}) \leq C \int_0^\infty \sqrt{\log N(K_s, d, u)}\, du$$

where $N(K_s, d, u)$ is the covering number of K_s by balls of radius u in the metric d. For $\mathbf{x}, \mathbf{y} \in K_s$,

$$\begin{aligned} d(\mathbf{x}, \mathbf{y}) &\leq \sqrt{\sum_{r=1}^{n} |\mathbf{A}_r^* \mathbf{x} + \mathbf{A}_r^* \mathbf{y}|^2 |\mathbf{A}_r^* \mathbf{x} - \mathbf{A}_r^* \mathbf{y}|^2} \\ &\leq \sqrt{2 \sup_{\mathbf{z} \in K_s} \sum_{r=1}^{n} |\mathbf{A}_r^* \mathbf{z}|^2} \cdot \max_{r=1}^{n} |\mathbf{A}_r^* \mathbf{x} - \mathbf{A}_r^* \mathbf{y}| = R(\mathbf{A}) \cdot \|\mathbf{x} - \mathbf{y}\|_{\mathbf{A}}, \end{aligned}$$

where

$$R(\mathbf{A})^2 = \sup_{\mathbf{z} \in K_s} \mathbf{z}^* \mathbf{A}^* \mathbf{A} \mathbf{z}, \qquad \|\mathbf{x}\|_{\mathbf{A}} = \sqrt{2} \cdot \max_{r=1}^{n} |\mathbf{A}_r^* \mathbf{x}|.$$

Applying this bound and a change-of-variables $v = u/R(\mathbf{A})$,

$$E(\mathbf{A}) \leq C R(\mathbf{A}) \int_0^\infty \sqrt{\log N(K_s, \|\cdot\|_{\mathbf{A}}, v)}\, dv. \tag{50}$$

The pseudo-norm $\|\cdot\|_{\mathbf{A}}$ has the following property: For any $\mathbf{x} \in K_s$,

$$\|\nabla \mathbf{x}\|_1 \leq \sqrt{s} \|\nabla \mathbf{x}\|_2 \leq \sqrt{8s} \|\mathbf{x}\|_2 \leq \sqrt{8s} \tag{51}$$

where the middle inequality applies $(x-y)^2 \leq 2x^2 + 2y^2$ and the fact that the maximal vertex degree in G is 4. Let $\mathbf{v}_1, \ldots, \mathbf{v}_p$ be the bivariate Haar wavelet basis, and write the orthogonal decomposition $\mathbf{x} = \sum_k c_k \mathbf{v}_k$. Then, as $\|\mathbf{x}\|_2 \leq 1$, $\|\nabla \mathbf{x}\|_1 \leq \sqrt{8s}$, and $\sum_{k=1}^{p} 1/k \leq C \log p$, Lemma A.2.2 implies

$$\sum_{k=1}^{p} |c_k| \leq C \sqrt{s} \log p. \tag{52}$$

Each Haar vector $\mathbf{v}_k$ is supported on a number $\alpha \in \{1, 2, 4\}$ of rectangular pieces of some size

$|S| \times |T|$, with a constant value $\pm 1/\sqrt{\alpha |ST|}$ on each piece. Then Lemma A.2.1 implies for each (i,j)

$$|\mathcal{F}^*_{(i,j)} \mathbf{v}_k| \leq C \sqrt{\frac{1}{1+\min(i-1, N_1 - i + 1)} \cdot \frac{1}{1+\min(j-1, N_2 - j + 1)}}.$$

From the definition of ν and the bound $\sum_{k=1}^{p} 1/k \leq C \log p$,

$$\nu(j) \geq \frac{c}{(\log p)^2} \cdot \frac{1}{C_0 + \min(i-1, N_1 - i + 1)} \cdot \frac{1}{C_0 + \min(j-1, N_2 - j + 1)}$$

for a constant $c > 0$. Then from the definitions of $\mathbf{A}$ and $\|\cdot\|_{\mathbf{A}}$, the bound (52), and the condition $1/K < N_1/N_2 < K$, we obtain

$$\|\mathbf{v}_k\|_{\mathbf{A}} \leq C(\log p)/\sqrt{n}, \qquad \|\mathbf{x}\|_{\mathbf{A}} \leq B \equiv C(\log p)^2 \sqrt{s/n}. \tag{53}$$

As in (Rudelson and Vershynin, 2008, Theorem 3.3), we bound the covering number $N(K_s, \|\cdot\|_{\mathbf{A}}, v)$ in two ways: First, fix any $\mathbf{x} \in K_s$ and write now its Haar decomposition as

$$\mathbf{x} = \sum_{k=1}^{p} (a_k + \mathbf{i} b_k) \mathbf{v}_k$$

where $a_k, b_k \in \mathbb{R}$. Then for some universal constant $L > 0$, we obtain from (52)

$$\sum_{k=1}^{p} |a_k| + |b_k| \leq L\sqrt{s} \log p.$$

Applying Maurey's argument, define a discrete distribution over a random vector $\mathbf{z} \in \mathbb{C}^p$ by

$$\begin{aligned}
\mathbb{P}\Big[\mathbf{z} = L\sqrt{s} \log p \cdot \operatorname{sign}(a_k) \mathbf{v}_k\Big] &= \frac{|a_k|}{L\sqrt{s} \log p}, \\
\mathbb{P}\Big[\mathbf{z} = L\sqrt{s} \log p \cdot \operatorname{sign}(b_k) \mathbf{i} \mathbf{v}_k\Big] &= \frac{|b_k|}{L\sqrt{s} \log p}, \\
\mathbb{P}\Big[\mathbf{z} = 0\Big] &= 1 - \sum_{k=1}^{p} \frac{|a_k| + |b_k|}{L\sqrt{s} \log p}.
\end{aligned}$$

Then by construction, $\mathbb{E}[\mathbf{z}] = \mathbf{x}$. Letting $\mathbf{z}_1, \ldots, \mathbf{z}_m$ be independent copies of $\mathbf{z}$, for a value m to be chosen later, Gaussian symmetrization yields (with all expectations conditional on $\mathbf{A}$)

$$\mathbb{E} \left\| \mathbf{x} - \frac{1}{m} \sum_{j=1}^{m} \mathbf{z}_j \right\|_{\mathbf{A}} = \mathbb{E} \max_{r=1}^{n} \left| \frac{1}{m} \sum_{j=1}^{m} \mathbf{A}^*_r \mathbf{z}_j - \mathbb{E} \mathbf{A}^*_r \mathbf{z}_j \right| \leq \frac{C}{m} \mathbb{E} \max_{r=1}^{n} \left| \sum_{j=1}^{m} g_j \mathbf{A}^*_r \mathbf{z}_j \right| \tag{54}$$

for $g_1, \ldots, g_m \overset{iid}{\sim} \mathcal{N}(0,1)$. The bound (53) yields for every r

$$\sum_{j=1}^{m} |\mathbf{A}_r^* \mathbf{z}_j|^2 \leq \frac{Csm(\log p)^4}{n}.$$

Applying this to (54) with a Gaussian tail bound and union bound,

$$\mathbb{E} \left\| \mathbf{x} - \frac{1}{m} \sum_{j=1}^{m} \mathbf{z}_j \right\|_{\mathbf{A}} \leq C\sqrt{\log n} \cdot (\log p)^2 \sqrt{\frac{s}{mn}}.$$

For any $v > 0$, choosing $m = C(\log n)(\log p)^4 s/(nv^2)$ ensures this bound is at most v. Then by the probabilistic method, $\mathbf{x}$ belongs to the $\|\cdot\|_{\mathbf{A}}$-ball of radius v around some vector of the form $m^{-1}\sum_{j=1}^{m} \mathbf{z}_j$. The support of the distribution of $\mathbf{z}_j$ has cardinality at most $2p+1$, and this support is the same for all $\mathbf{x} \in K_s$. Then there are at most $(2p+1)^m$ such vectors, so we obtain

$$\sqrt{\log N(K_s, \|\cdot\|_{\mathbf{A}}, v)} \leq \sqrt{m \log(2p+1)} \leq C\sqrt{s(\log n)(\log p)^5/n} \cdot 1/v. \tag{55}$$

We obtain a second covering bound by a union bound over $\mathcal{S}$: For any $\mathcal{S} = (S_1, \ldots, S_k)$ with $|\partial\mathcal{S}| \leq s$, note that $k \leq s+1$. Define $\mathbf{U}_{\mathcal{S}} \in \mathbb{R}^{p \times k}$ such that its ith column is $\mathbf{e}_{S_i}/\sqrt{|S_i|}$ where $\mathbf{e}_{S_i} \in \{0,1\}^p$ is the indicator of S_i. Then $\mathbf{U}_{\mathcal{S}}\mathbf{U}_{\mathcal{S}}^*$ is the projection onto $K_{\mathcal{S}}$, and

$$K_{\mathcal{S}} = \{\mathbf{U}_{\mathcal{S}}\mathbf{y} : \|\mathbf{y}\|_2 \leq 1\}.$$

As $\max\{\|\mathbf{U}_{\mathcal{S}}\mathbf{y}\|_{\mathbf{A}} : \mathbf{y} \in \mathbb{C}^k, \|\mathbf{y}\|_2 \leq 1\} \leq B$ by (53), a standard volume argument yields for $v \leq B$

$$N(K_{\mathcal{S}}, \|\cdot\|_{\mathbf{A}}, v) \leq (CB/v)^k.$$

The number of partitions $\mathcal{S}$ with $|\partial\mathcal{S}| \leq s$ is at most $\sum_{j=0}^{s} \binom{|E|}{j} \leq (Cp)^{s+1}$. Applying $k \leq s+1$ and summing over $\mathcal{S}$,

$$\sqrt{\log N(K_s, \|\cdot\|_{\mathbf{A}}, v)} \leq C\sqrt{s \log(CBp/v)}. \tag{56}$$

Returning to the entropy integral in (50), note that (53) implies $N(K_s, \|\cdot\|_{\mathbf{A}}, v) = 1$ for $v > B$, so the integral may be restricted to $v \in [0, B]$. Setting $t = 1/\sqrt{n}$, applying (56) for $v \in [0, t]$, and

also applying Cauchy-Schwarz and $\log(B/t) \le C \log p$, we get

$$\int_0^t \sqrt{\log N(K_s, \|\cdot\|_{\mathbf{A}}, v)}\, dv \le \sqrt{t} \cdot \sqrt{\int_0^t \log N(K_s, \|\cdot\|_{\mathbf{A}}, v) dv}$$
$$\le Ct\sqrt{s\left(1 + \log \frac{CBp}{t}\right)} \le C\sqrt{\frac{s \log p}{n}}.$$

Applying (55) for $v \in [t, B]$, we get

$$\int_t^B \sqrt{\log N(K_s, \|\cdot\|_{\mathbf{A}}, v)}\, dv \le C\sqrt{s(\log n)(\log p)^7/n}.$$

Applying these bounds to (50) gives

$$E(\mathbf{A}) \le C\sqrt{s(\log n)(\log p)^7/n} \cdot R(\mathbf{A}).$$

Taking now the expectation over $\mathbf{A}$ and applying Cauchy-Schwarz and the triangle inequality,

$$\mathbb{E}[\kappa_s] \le \mathbb{E}[E(\mathbf{A})] \le C\sqrt{s(\log n)(\log p)^7/n}\sqrt{\mathbb{E}[R(\mathbf{A})^2]}$$
$$\le C\sqrt{s(\log n)(\log p)^7/n}\sqrt{\mathbb{E}[\kappa_s] + 1}.$$

This yields

$$\mathbb{E}[\kappa_s] \le E(p, n, s) \equiv C \max\left(\sqrt{s(\log n)(\log p)^7/n},\ s(\log n)(\log p)^7/n\right).$$

We now show concentration of each quantity κ_s around its mean. The argument is similar to (Rudelson and Vershynin, 2008, Theorem 3.9), and we omit some details. Write

$$\kappa_s = \left\| \sum_{r=1}^n \mathbf{A}_r \mathbf{A}_r^* - \mathbf{I} \right\|_{K_s}$$

where $\|\mathbf{M}\|_{K_s} = \sup_{\mathbf{x} \in K_s} |\mathbf{x}^* \mathbf{M} \mathbf{x}|$. Let $\mathbf{A}'$ be an independent copy of $\mathbf{A}$ and define

$$\gamma_s = \left\| \sum_{r=1}^n \mathbf{A}_r \mathbf{A}_r^* - (\mathbf{A}_r')(\mathbf{A}_r')^* \right\|_{K_s}.$$

Then by the same arguments as (Rudelson and Vershynin, 2008, Theorem 3.9), for any $t > 0$,

$$\mathbb{P}[\kappa_s \ge 2\mathbb{E}[\kappa_s] + t] \le 2\mathbb{P}[\gamma_s \ge t], \quad \mathbb{E}[\gamma_s] \le 2\mathbb{E}[\kappa_s] \le 2E(p, n, s). \tag{57}$$

From (53), we have

$$\|\mathbf{A}_r\mathbf{A}_r^*\|_{K_s} \leq B^2$$

for every r. Then applying (Rudelson and Vershynin, 2008, Theorem 3.8), for any integers $l \geq q$, any $r > 0$, and some constants $C_1, C_2 > 0$,

$$\mathbb{P}[\gamma_s \geq 8q\mathbb{E}[\gamma_s] + 2B^2 l + r] \leq (C_1/q)^l + 2\exp\left(-\frac{r^2}{C_2 q\mathbb{E}[\gamma_s]^2}\right).$$

Let us assume without loss of generality $C_1 \geq 1/e$ and set $l = [2eC_1(\log n)(\log p)^3]$, $q = [eC_1]$, and $r = 2\sqrt{C_2 q} \cdot 2E(p,n,s) \cdot t\sqrt{\log p}$, where $[\cdot]$ denotes the integer part. Then combining this with (57), we get for some constants $C, t_0 > 0$ and all $t > t_0$ that

$$\mathbb{P}[\kappa_s \geq C\sqrt{t} \cdot E(p,n,s)\sqrt{\log p}] \leq e^{-2(\log n)(\log p)^3} + 2e^{-4t(\log p)}.$$

Setting $\rho(s) = Cst(\log p)^8(\log n)/n$ for a sufficiently large constant $C > 0$, this yields

$$\mathbb{P}[\kappa_s \geq 2\sqrt{\rho(s)} + \rho(s)] \leq e^{-2(\log n)(\log p)^3} + 2e^{-4t(\log p)}.$$

The result follows from taking a union bound over $s = 1, \ldots, |E|$, and noting $|E| \leq 2p$ and

$$2p\left(e^{-2(\log n)(\log p)^3} + 2e^{-4t(\log p)}\right) \leq e^{-(\log n)(\log p)^3} + p^{-t}$$

for all $t > t_0$ and sufficiently large $t_0 > 0$. □

A.3 RMSE for optimal parameter tuning

We report here the best-achieved RMSE, rather than RMSE for cross-validated selection of tuning parameters, corresponding to Tables 2.1, 2.2, 2.3, 2.4, and 2.5. We repeated each experiment 20 times with different random noise vectors, and we report also the standard deviations across these 20 simulations.

Table A.1: Mean and standard deviation of best-achieved RMSE for the 1-D spike signal across 20 simulations.

n/p		$\sigma = 0$	$\sigma = 1$	$\sigma = 2$	$\sigma = 3$	$\sigma = 4$	$\sigma = 5$	$\sigma = 6$	$\sigma = 7$
10%	ITALE	**0.000**	**0.011**	**0.050**	**0.081**	**0.115**	**0.138**	**0.177**	**0.198**
		(0.000)	(0.004)	(0.024)	(0.023)	(0.033)	(0.034)	(0.031)	(0.025)
	TV	**0.000**	0.045	0.086	0.122	0.152	0.176	0.193	0.206
		(0.000)	(0.011)	(0.017)	(0.018)	(0.017)	(0.016)	(0.017)	(0.015)
15%	ITALE	**0.000**	**0.008**	**0.019**	**0.042**	**0.069**	**0.091**	**0.114**	**0.133**
		(0.000)	(0.002)	(0.007)	(0.016)	(0.023)	(0.029)	(0.028)	(0.029)
	TV	**0.000**	0.029	0.057	0.085	0.109	0.130	0.149	0.165
		(0.000)	(0.006)	(0.011)	(0.016)	(0.020)	(0.020)	(0.020)	(0.020)
20%	ITALE	**0.000**	**0.007**	**0.013**	**0.028**	**0.049**	**0.070**	**0.090**	**0.102**
		(0.000)	(0.002)	(0.003)	(0.012)	(0.019)	(0.019)	(0.017)	(0.020)
	TV	**0.000**	0.022	0.044	0.066	0.087	0.107	0.126	0.143
		(0.000)	(0.002)	(0.004)	(0.006)	(0.008)	(0.009)	(0.010)	(0.010)
30%	ITALE	**0.000**	**0.006**	**0.012**	**0.019**	**0.029**	**0.045**	**0.061**	**0.075**
		(0.000)	(0.001)	(0.003)	(0.006)	(0.009)	(0.014)	(0.011)	(0.013)
	TV	**0.000**	0.017	0.034	0.051	0.068	0.085	0.101	0.116
		(0.000)	(0.001)	(0.003)	(0.004)	(0.006)	(0.007)	(0.008)	(0.009)
40%	ITALE	**0.000**	**0.005**	**0.010**	**0.015**	**0.024**	**0.038**	**0.048**	**0.062**
		(0.000)	(0.001)	(0.002)	(0.003)	(0.007)	(0.012)	(0.015)	(0.016)
	TV	**0.000**	0.014	0.028	0.042	0.056	0.070	0.084	0.097
		(0.000)	(0.001)	(0.003)	(0.004)	(0.006)	(0.007)	(0.008)	(0.010)
50%	ITALE	**0.000**	**0.005**	**0.009**	**0.014**	**0.021**	**0.029**	**0.036**	**0.047**
		(0.000)	(0.001)	(0.002)	(0.003)	(0.006)	(0.011)	(0.013)	(0.013)
	TV	**0.000**	0.013	0.025	0.038	0.050	0.063	0.074	0.086
		(0.000)	(0.002)	(0.003)	(0.005)	(0.006)	(0.008)	(0.008)	(0.009)

Table A.2: Mean and standard deviation of best-achieved RMSE for the 1-D wave signal across 20 simulations.

n/p		$\sigma = 0$	$\sigma = 1$	$\sigma = 2$	$\sigma = 3$	$\sigma = 4$	$\sigma = 5$	$\sigma = 6$	$\sigma = 7$
10%	ITALE	0.019	**0.030**	0.075	0.126	0.155	0.203	0.233	0.256
		(0.081)	(0.066)	(0.055)	(0.057)	(0.064)	(0.059)	(0.070)	(0.068)
	TV	**0.000**	0.031	**0.062**	**0.090**	**0.114**	**0.137**	**0.157**	**0.176**
		(0.000)	(0.005)	(0.011)	(0.016)	(0.018)	(0.021)	(0.022)	(0.024)
15%	ITALE	**0.000**	**0.008**	**0.022**	**0.052**	**0.083**	**0.105**	0.134	0.154
		(0.000)	(0.002)	(0.011)	(0.023)	(0.027)	(0.030)	(0.027)	(0.035)
	TV	**0.000**	0.022	0.044	0.066	0.087	0.106	**0.124**	**0.141**
		(0.000)	(0.003)	(0.006)	(0.009)	(0.011)	(0.013)	(0.014)	(0.016)
20%	ITALE	**0.000**	**0.006**	**0.015**	**0.032**	**0.050**	**0.072**	**0.093**	**0.109**
		(0.000)	(0.001)	(0.006)	(0.011)	(0.016)	(0.023)	(0.027)	(0.027)
	TV	**0.000**	0.018	0.036	0.054	0.071	0.088	0.104	0.118
		(0.000)	(0.002)	(0.004)	(0.007)	(0.009)	(0.011)	(0.012)	(0.013)
30%	ITALE	**0.000**	**0.006**	**0.011**	**0.017**	**0.032**	**0.046**	**0.062**	**0.077**
		(0.000)	(0.001)	(0.002)	(0.004)	(0.010)	(0.012)	(0.015)	(0.015)
	TV	**0.000**	0.014	0.027	0.041	0.055	0.068	0.082	0.095
		(0.000)	(0.001)	(0.003)	(0.004)	(0.005)	(0.007)	(0.008)	(0.010)
40%	ITALE	**0.000**	**0.005**	**0.010**	**0.016**	**0.024**	**0.033**	**0.046**	**0.057**
		(0.000)	(0.001)	(0.002)	(0.004)	(0.009)	(0.012)	(0.014)	(0.017)
	TV	**0.000**	0.012	0.024	0.036	0.048	0.060	0.072	0.083
		(0.000)	(0.001)	(0.002)	(0.003)	(0.005)	(0.006)	(0.007)	(0.008)
50%	ITALE	**0.000**	**0.004**	**0.009**	**0.015**	**0.022**	**0.030**	**0.038**	**0.049**
		(0.000)	(0.001)	(0.002)	(0.005)	(0.009)	(0.011)	(0.012)	(0.018)
	TV	**0.000**	0.011	0.021	0.032	0.042	0.053	0.063	0.073
		(0.000)	(0.001)	(0.003)	(0.004)	(0.005)	(0.007)	(0.008)	(0.009)

Table A.3: Mean and standard deviation of best-achieved RMSE for the Shepp-Logan phantom across 20 simulations.

n/p		$\sigma = 0$	$\sigma = 4$	$\sigma = 8$	$\sigma = 12$	$\sigma = 16$	$\sigma = 20$	$\sigma = 24$	$\sigma = 28$
10%	ITALE	**0.000**	**0.005**	**0.011**	**0.016**	**0.027**	**0.035**	**0.047**	**0.062**
		(0.000)	(0.000)	(0.000)	(0.001)	(0.001)	(0.002)	(0.002)	(0.003)
	TV	0.002	0.011	0.021	0.030	0.039	0.048	0.056	0.064
		(0.000)	(0.000)	(0.000)	(0.000)	(0.001)	(0.001)	(0.001)	(0.001)
15%	ITALE	**0.000**	**0.003**	**0.010**	**0.013**	**0.017**	**0.026**	**0.033**	**0.041**
		(0.000)	(0.000)	(0.000)	(0.000)	(0.001)	(0.002)	(0.001)	(0.002)
	TV	0.001	0.008	0.016	0.024	0.031	0.038	0.044	0.052
		(0.000)	(0.000)	(0.000)	(0.000)	(0.001)	(0.001)	(0.001)	(0.001)
20%	ITALE	**0.000**	**0.002**	**0.008**	**0.012**	**0.014**	**0.020**	**0.028**	**0.034**
		(0.000)	(0.000)	(0.000)	(0.000)	(0.001)	(0.001)	(0.001)	(0.002)
	TV	0.001	0.007	0.014	0.020	0.027	0.033	0.039	0.045
		(0.000)	(0.000)	(0.000)	(0.000)	(0.000)	(0.001)	(0.001)	(0.001)
30%	ITALE	**0.000**	**0.002**	**0.006**	**0.010**	**0.012**	**0.015**	**0.018**	**0.026**
		(0.000)	(0.000)	(0.000)	(0.000)	(0.000)	(0.001)	(0.001)	(0.001)
	TV	0.002	0.006	0.011	0.017	0.022	0.027	0.032	0.036
		(0.000)	(0.000)	(0.000)	(0.000)	(0.000)	(0.000)	(0.000)	(0.001)
40%	ITALE	**0.000**	**0.001**	**0.005**	**0.009**	**0.011**	**0.013**	**0.015**	**0.018**
		(0.000)	(0.000)	(0.000)	(0.000)	(0.000)	(0.001)	(0.001)	(0.001)
	TV	0.001	0.005	0.010	0.014	0.019	0.023	0.027	0.031
		(0.000)	(0.000)	(0.000)	(0.000)	(0.000)	(0.000)	(0.000)	(0.001)
50%	ITALE	**0.000**	**0.001**	**0.004**	**0.008**	**0.011**	**0.012**	**0.014**	**0.016**
		(0.000)	(0.000)	(0.000)	(0.000)	(0.000)	(0.000)	(0.001)	(0.001)
	TV	0.001	0.004	0.009	0.013	0.017	0.021	0.025	0.028
		(0.000)	(0.000)	(0.000)	(0.000)	(0.000)	(0.000)	(0.001)	(0.001)

Table A.4: Mean and standard deviation of best-achieved RMSE for the brain phantom across 20 simulations.

n/p		$\sigma = 0$	$\sigma = 8$	$\sigma = 16$	$\sigma = 24$	$\sigma = 32$	$\sigma = 40$	$\sigma = 48$	$\sigma = 56$
10%	ITALE	**0.000**	**0.002**	**0.010**	**0.026**	**0.042**	**0.060**	0.079	0.095
		(0.000)	(0.000)	(0.001)	(0.001)	(0.001)	(0.001)	(0.002)	(0.002)
	TV	0.002	0.014	0.028	0.041	0.053	0.065	**0.077**	**0.087**
		(0.000)	(0.000)	(0.000)	(0.000)	(0.001)	(0.001)	(0.001)	(0.001)
15%	ITALE	**0.000**	**0.001**	**0.006**	**0.016**	**0.030**	**0.043**	**0.057**	**0.071**
		(0.000)	(0.000)	(0.001)	(0.001)	(0.001)	(0.001)	(0.001)	(0.002)
	TV	0.001	0.011	0.022	0.032	0.043	0.053	0.062	0.072
		(0.000)	(0.000)	(0.000)	(0.000)	(0.000)	(0.001)	(0.001)	(0.001)
20%	ITALE	**0.000**	**0.001**	**0.004**	**0.011**	**0.024**	**0.034**	**0.046**	**0.057**
		(0.000)	(0.000)	(0.000)	(0.001)	(0.001)	(0.001)	(0.002)	(0.002)
	TV	0.001	0.009	0.019	0.028	0.037	0.045	0.054	0.062
		(0.000)	(0.000)	(0.000)	(0.000)	(0.000)	(0.001)	(0.001)	(0.001)
30%	ITALE	**0.000**	**0.001**	**0.003**	**0.007**	**0.014**	**0.025**	**0.032**	**0.042**
		(0.000)	(0.000)	(0.000)	(0.001)	(0.001)	(0.001)	(0.001)	(0.001)
	TV	0.001	0.008	0.015	0.023	0.030	0.037	0.044	0.052
		(0.000)	(0.000)	(0.000)	(0.000)	(0.000)	(0.000)	(0.001)	(0.001)
40%	ITALE	**0.000**	**0.001**	**0.002**	**0.005**	**0.010**	**0.018**	**0.025**	**0.033**
		(0.000)	(0.000)	(0.000)	(0.000)	(0.001)	(0.001)	(0.001)	(0.001)
	TV	0.001	0.006	0.013	0.020	0.026	0.032	0.038	0.044
		(0.000)	(0.000)	(0.000)	(0.000)	(0.000)	(0.000)	(0.000)	(0.001)
50%	ITALE	**0.000**	**0.000**	**0.002**	**0.004**	**0.008**	**0.013**	**0.020**	**0.027**
		(0.000)	(0.000)	(0.000)	(0.000)	(0.001)	(0.001)	(0.001)	(0.001)
	TV	0.001	0.006	0.012	0.017	0.023	0.029	0.034	0.040
		(0.000)	(0.000)	(0.000)	(0.000)	(0.000)	(0.000)	(0.000)	(0.001)

Table A.5: Mean and standard deviation of best-achieved RMSE for the XCAT chest slice phantom across 20 simulations.

n/p		$\sigma = 0$	$\sigma = 4$	$\sigma = 8$	$\sigma = 12$	$\sigma = 16$	$\sigma = 20$	$\sigma = 24$	$\sigma = 28$
10%	ITALE	**0.002**	0.029	0.050	0.063	0.077	0.086	0.095	0.104
		(0.000)	(0.007)	(0.006)	(0.005)	(0.001)	(0.002)	(0.001)	(0.002)
	TV	0.006	**0.019**	**0.032**	**0.043**	**0.053**	**0.061**	**0.067**	**0.073**
		(0.000)	(0.000)	(0.000)	(0.000)	(0.000)	(0.000)	(0.001)	(0.001)
15%	ITALE	**0.002**	**0.007**	**0.017**	**0.029**	0.043	0.061	0.076	0.085
		(0.000)	(0.000)	(0.000)	(0.001)	(0.002)	(0.003)	(0.001)	(0.001)
	TV	0.003	0.014	0.024	0.034	**0.042**	**0.050**	**0.057**	**0.063**
		(0.000)	(0.000)	(0.000)	(0.000)	(0.000)	(0.000)	(0.000)	(0.001)
20%	ITALE	**0.002**	**0.005**	**0.014**	**0.022**	**0.031**	**0.042**	0.054	0.069
		(0.000)	(0.000)	(0.000)	(0.001)	(0.001)	(0.001)	(0.002)	(0.003)
	TV	**0.002**	0.011	0.020	0.028	0.036	0.043	**0.049**	**0.055**
		(0.000)	(0.000)	(0.000)	(0.000)	(0.000)	(0.000)	(0.001)	(0.000)
30%	ITALE	**0.002**	**0.004**	**0.010**	**0.017**	**0.024**	**0.031**	**0.039**	0.048
		(0.000)	(0.000)	(0.000)	(0.000)	(0.000)	(0.001)	(0.001)	(0.001)
	TV	**0.002**	0.008	0.016	0.023	0.029	0.035	0.041	**0.047**
		(0.000)	(0.000)	(0.000)	(0.000)	(0.000)	(0.000)	(0.000)	(0.000)
40%	ITALE	0.002	**0.003**	**0.008**	**0.015**	**0.020**	**0.026**	**0.032**	**0.039**
		(0.000)	(0.000)	(0.000)	(0.000)	(0.000)	(0.001)	(0.001)	(0.001)
	TV	**0.001**	0.007	0.014	0.020	0.026	0.031	0.036	0.041
		(0.000)	(0.000)	(0.000)	(0.000)	(0.000)	(0.000)	(0.000)	(0.000)
50%	ITALE	**0.001**	**0.003**	**0.007**	**0.013**	**0.018**	**0.022**	**0.027**	**0.033**
		(0.000)	(0.000)	(0.000)	(0.000)	(0.000)	(0.000)	(0.001)	(0.001)
	TV	**0.001**	0.006	0.012	0.018	0.023	0.028	0.032	0.037
		(0.000)	(0.000)	(0.000)	(0.000)	(0.000)	(0.000)	(0.000)	(0.000)

B Appendix for Chapter 3

B.1 Correctness and complexity of algorithm

We prove Lemmas 3.2.1 and 3.2.2 on basic guarantees for the two steps of the tree-PGD algorithm.

Proof of Lemma 3.2.1. For the first statement, since $d_{\max} \geq 2$, the vertex w corresponding to each deleted edge (v, w) must be a child of v which is not its first child in the ordering $\mathcal{O}_{DFS}$. Then its preceding vertex w' must be a leaf vertex of $\tilde{T}$. Each such w corresponds to a different such leaf w', so deleting these edges (v, w) and adding (w', w) preserves the connectedness and tree structure. By construction, each non-leaf vertex of $\tilde{T}$ has degree at most $d_{\max}$ in T. Each leaf vertex of $\tilde{T}$ has degree at most $2 \leq d_{\max}$ in T, so T has maximum degree $\leq d_{\max}$.

For the second statement, since the edges of $\tilde{T}$ are a subset of those of G,

$$\|\nabla_{\tilde{T}} \boldsymbol{\theta}\|_0 \leq \|\nabla_G \boldsymbol{\theta}\|_0.$$

Let the root vertex of T be 1. For each other vertex $i \geq 2$, denote its parent in T by $p(i)$. Then

$$\|\nabla_T \boldsymbol{\theta}\|_0 = \sum_{i=2}^{p} \mathbf{1}\{\theta_i \neq \theta_{p(i)}\}. \tag{58}$$

Now consider two cases: If the edge $(i, p(i))$ exists in $\tilde{T}$, then it is a forward edge in the DFS of $\tilde{T}$, and $\mathbf{1}\{\theta_i \neq \theta_{p(i)}\}$ contributes to $\|\nabla_{\tilde{T}} \boldsymbol{\theta}\|_0$. If $(i, p(i))$ is not an edge of $\tilde{T}$, then $p(i)$ is a leaf node in $\tilde{T}$, and there is path of backward edges $(p_1, p_2, \ldots, p_r)$ in the DFS of $\tilde{T}$ where $p_1 = p(i)$ and $p_r = i$. The triangle inequality then implies

$$\mathbf{1}\{\theta_i \neq \theta_{p(i)}\} \leq \sum_{j=1}^{r-1} \mathbf{1}\{\theta_{p_j} \neq \theta_{p_{j+1}}\},$$

where each term on the right contributes to $\|\nabla_{\tilde{T}} \boldsymbol{\theta}\|_0$. Applying this to each term on the right of

(58), and invoking the fundamental property that DFS visits each edge of $\tilde{T}$ exactly twice, we get

$$\|\nabla_T \boldsymbol{\theta}\|_0 \leq 2\|\nabla_{\tilde{T}} \boldsymbol{\theta}\|_0 \leq 2\|\nabla_G \boldsymbol{\theta}\|_0.$$

□

Proof of Lemma 3.2.2. It is clear that Step 1 computes (3.8) at the leaf vertices v. For Step 2, assume inductively that $f_w(c,s)$ is the value (3.8) for all children w of v. The value $g_w(c,s)$ represents the minimum value of $\|\boldsymbol{\theta} - \mathbf{u}_{T_w}\|_2^2$, if $\theta_v = c$ and the gradient-sparsity of $\boldsymbol{\theta}$ on T_w *and* the additional edge (v,w) is at most s—we have either $\theta_w = c$ and $g_w(c,s) = f_w(c,s)$, or $\theta_w \neq c$, in which case $\theta_w = \operatorname{argmin}_{c\in\Delta} f_w(c,s-1)$ and $g_w(c,s) = m_w(s-1)$. Then (3.9) computes (3.8) at v by partitioning the gradient-sparsity s across its k children, and summing the costs $g_{w_i}(c,s_i)$ and the additional cost $(c-u_v)^2$ for the best such partition. Thus Step 2 correctly computes (3.8) for each vertex v. In particular, the minimum value for (3.7) is given by $\min_{c\in\Delta} f_o(c,S)$. The minimizer $\boldsymbol{\theta}$ is obtained by examining the minimizing choices in Steps 1 and 2, which is carried out in Steps 3 and 4: Each θ_v is the value of $\boldsymbol{\theta}$ at v, and each S_v is (an upper-bound for) the value of $\|\nabla_{T_v}\boldsymbol{\theta}\|_0$ at the minimizer $\boldsymbol{\theta}$.

For each vertex v, Step 1 has complexity $(S+1)|\Delta|$, Steps 2(a) and 2(b) both have complexity $(S+1)k|\Delta|$, and Step 2(c) has complexity $(S+1)|\Delta|k\binom{S+k-1}{k-1}$, as there are $\binom{s+k-1}{k-1} \leq \binom{S+k-1}{k-1}$ partitions of s into $s_1,\ldots,s_k$. Note that $k \leq d_{\max}-1$, where this holds also for the root vertex o because we chose it to have degree 1 in T. Then $\binom{S+k-1}{k-1} = O((S+d_{\max})^{d_{\max}-2})$. Storing the relevant minimizers in Steps 1 and 2, the complexity of Steps 3 and 4 is $O(1)$ per vertex. So the total complexity is $O(d_{\max}p|\Delta|(S+d_{\max})^{d_{\max}-1})$. □

B.2 Proof of Lemma 3.3.6

Proof. Let $\mathcal{P}^S$ be the partition of $\{1,\ldots,p\}$ induced by $\mathbf{u}^S$ over T. We have $|\partial_T \mathcal{P}^S| \leq S$. If $|\partial_T \mathcal{P}^S| < S$, then let us arbitrarily split some vertex sets in $\mathcal{P}^S$ along edges of T, until $|\partial_T \mathcal{P}^S| = S$. Thus, we may assume henceforth that $|\partial_T \mathcal{P}^S| = S$.

We construct another partition $\mathcal{P}'$ of $\{1,\ldots,p\}$ into the (disjoint) vertex sets $(V_1,\ldots,V_B,R)$, such that each set of $\mathcal{P}'$ is connected over T, and $\mathcal{P}'$ satisfies the following properties:

1. For each $b = 1,\ldots,B$, the number of edges (i,j) in T where both $i,j \in V_b$, but i and j do not belong to the same set of $\mathcal{P}^S$, is greater than or equal to $s^* + \sqrt{\kappa s^*}$.

2. B has the upper and lower bounds

$$\frac{S - s^* - \sqrt{S}}{(d_{\max} - 1)(s^* + \sqrt{S} + 1) + 1} \leq B \leq \sqrt{S} \tag{59}$$

We construct this partition $\mathcal{P}'$ in the following way: Initialize $\tilde{T} = T$ and pick any degree-1 vertex of T as its root. Assign to each edge (i, j) of $\tilde{T}$ a "score" of 1 if i and j belong to the same set of $\mathcal{P}^S$, and 0 otherwise. Repeat the following steps for all vertices i of T, in reverse-breadth-first-search order (starting from a vertex i farthest from the root):

- Let $\tilde{T}_i$ be the sub-tree of $\tilde{T}$ rooted at i and consisting of the descendants of i in $\tilde{T}$.
- If the total score of edges in $\tilde{T}_i$ is at least $s^* + \sqrt{\kappa s^*}$, then add the vertices of $\tilde{T}_i$ as a set V_b to the partition $\mathcal{P}'$, and remove $\tilde{T}_i$ (including the edge from i to its parent) from $\tilde{T}$.

This terminates when the remaining tree $\tilde{T}$ has total score less than $s^* + \sqrt{\kappa s^*}$. Take the last set R of $\mathcal{P}'$ to be the vertices of this remaining tree.

By construction, each set $V_1, \ldots, V_B, R$ is connected on T, and property 1 above holds. To verify the bounds in property 2, note that the total score of the starting tree $\tilde{T} = T$ is S, and the total score of the final tree belongs to the range $[0, s^* + \sqrt{\kappa s^*})$. Each time we remove a sub-tree $\tilde{T}_i$, the score of $\tilde{T}$ decreases by at least $s^* + \sqrt{\kappa s^*}$. We claim that the score also decreases by at most $(d_{\max} - 1)(s^* + \sqrt{\kappa s^*} + 1) + 1$: This is because i has at most $d_{\max} - 1$ children, and if $\tilde{T}_i$ has total score $\geq (d_{\max} - 1)(s^* + \sqrt{\kappa s^*} + 1)$, then some sub-tree rooted at one of its children j would have total score $\geq s^* + \sqrt{\kappa s^*}$. (The additional +1 accounts for a possible +1 score on the edge (i, j).) This sub-tree $\tilde{T}_j$ would have been removed under the above reverse-breadth-first-search ordering, so this is not possible. Thus, $\tilde{T}_i$ has total score $< (d_{\max} - 1)(s^* + \sqrt{\kappa s^*} + 1)$, verifying our claim. Then the total number B of sub-trees removed must satisfy

$$\frac{S - (s_* + \sqrt{\kappa s^*})}{(d_{\max} - 1)(s^* + \sqrt{\kappa s^*} + 1) + 1} \leq B \leq \frac{S}{s^* + \sqrt{\kappa s^*}}.$$

Recalling $S = \kappa s^*$, this implies (59) as desired.

Now let $\mathcal{P}^*$ be the partition of $\{1, \ldots, p\}$ induced by $\mathbf{u}^*$ over T, and let $\mathcal{P}$ be the common refinement of $\mathcal{P}^S$, $\mathcal{P}^*$, and $\mathcal{P}'$ constructed above: Each edge of T which connects two different sets of $\mathcal{P}$ must connect two different sets of at least one of $\mathcal{P}^S$, $\mathcal{P}^*$, and $\mathcal{P}'$. Then the subspace K

associated to $\mathcal{P}$ contains K^S and K^*, and furthermore

$$|\partial_T \mathcal{P}| \le |\partial_T \mathcal{P}^S| + |\partial_T \mathcal{P}^*| + |\partial_T \mathcal{P}'| \le S + s^* + B \le S + s^* + \sqrt{S}.$$

Here, we have used $|\partial_T \mathcal{P}'| = B$ because $\mathcal{P}'$ consists of $B+1$ connected sets over T.

For each $b = 1, \dots, B$, recall the set V_b of $\mathcal{P}'$, and construct a vector $\mathbf{v}^b \in \mathbb{R}^p$ whose coordinates are

$$(\mathbf{v}^b)_i = \begin{cases} (\mathbf{u}^*)_i & \text{if } i \in V_b \\ (\mathbf{P}_K \mathbf{u})_i & \text{if } i \notin V_b. \end{cases}$$

That is, $\mathbf{v}^b$ is equal to $\mathbf{u}^*$ on V_b and equal to $\mathbf{P}_K \mathbf{u}$ outside V_b. Then

$$\|\mathbf{P}_K \mathbf{u} - \mathbf{u}^*\|_2^2 \ge \sum_{b=1}^{B} \sum_{i \in V_b} |(\mathbf{P}_K \mathbf{u})_i - (\mathbf{u}^*)_i|^2 = \sum_{b=1}^{B} \|\mathbf{P}_K \mathbf{u} - \mathbf{v}^b\|_2^2. \tag{60}$$

We claim that $\|\nabla_T \mathbf{v}^b\|_0 \le S$: Indeed, the edges (i,j) of T where $(\mathbf{v}^b)_i \ne (\mathbf{v}^b)_j$ are contained in the union of $\partial_T \mathcal{P}^*$, $\partial_T \mathcal{P}'$, and the edges of $\partial_T \mathcal{P}^S$ whose endpoints both belong to the complement of V_b. Since $|\partial_T \mathcal{P}^S| = S$, and of these S edges, at least $s^* + \sqrt{\kappa s^*}$ have both endpoints in V_b by property 1 of our construction of $\mathcal{P}'$, this implies $\|\nabla_T \mathbf{v}^b\|_0 \le s^* + B + (S - s^* - \sqrt{\kappa s^*}) \le S$.

Finally, we use this to lower-bound the right side of (60): Observe that by construction, $\mathbf{u}^S$ and all of the vectors $\mathbf{v}^b$ for $b = 1, \dots, B$ belong to the subspace K associated to $\mathcal{P}$. Note that

$$\|\mathbf{u} - \mathbf{v}^b\|_2^2 \ge \|\mathbf{u} - \mathbf{u}^S\|_2^2 \tag{61}$$

by optimality of $\mathbf{u}^S$ and the condition $\|\nabla_T \mathbf{v}^b\|_0 \le S$ shown above. So, applying the Pythagorean identity for the projection $\mathbf{P}_K$ and its orthogonal projection $\mathbf{P}_K^\perp$,

$$\|\mathbf{P}_K \mathbf{u} - \mathbf{v}^b\|_2^2 = \|\mathbf{u} - \mathbf{v}^b\|_2^2 - \|\mathbf{P}_K^\perp \mathbf{u}\|_2^2 \ge \|\mathbf{u} - \mathbf{u}^S\|_2^2 - \|\mathbf{P}_K^\perp \mathbf{u}\|_2^2 = \|\mathbf{P}_K \mathbf{u} - \mathbf{u}^S\|_2^2.$$

Applying this to (60), we get

$$\|\mathbf{P}_K \mathbf{u} - \mathbf{u}^*\|_2^2 \ge B \cdot \|\mathbf{P}_K \mathbf{u} - \mathbf{u}^S\|_2^2.$$

Combining this with the lower-bound on B in (59) yields the lemma. □

B.3 Proof of Theorem 3.3.5

We first extend the result of Lemma 3.3.6 to address the discretization error in our approximate projection step (3.6).

Lemma B.3.1. *In the setting of Lemma 3.3.6, suppose that* $\mathbf{u}$ *and* $\mathbf{u}^*$ *are as defined in Lemma 3.3.6, but*

$$\mathbf{u}^S = \underset{\boldsymbol{\theta}\in\Delta^p:\|\nabla_T\boldsymbol{\theta}\|_0\le S}{\operatorname{argmin}} \|\mathbf{u}-\boldsymbol{\theta}\|_2 \tag{62}$$

where the minimization is over the discrete lattice $\Delta = (\Delta_{\min}, \Delta_{\min}+\delta, \ldots, \Delta_{\max}-\delta, \Delta_{\max})$. *If* $[-\|\mathbf{u}\|_\infty, \|\mathbf{u}\|_\infty] \subseteq [\Delta_{\min}, \Delta_{\max}]$, *then the result of Lemma 3.3.6 still holds, with (3.15) replaced by*

$$\|\mathbf{P}_K\mathbf{u}-\mathbf{u}^S\|_2^2 \le \frac{(d_{\max}-1)(s^*+\sqrt{S}+1)+1}{S-s^*-\sqrt{S}}\,\|\mathbf{P}_K\mathbf{u}-\mathbf{u}^*\|_2^2 + p\delta^2. \tag{63}$$

Proof. The proof is the same as Lemma 3.3.6, up until (61) where we used optimality of $\mathbf{u}^S$: We define $\mathcal{P}^S$ and construct $\mathcal{P}$ as in Lemma 3.3.6, using this discrete vector $\mathbf{u}^S$. Now let us denote by $\check{\mathbf{u}}^S$ the minimizer of (62) over $\mathbb{R}^p$ rather than over Δ^p. Note that we do not necessarily have $\check{\mathbf{u}}^S \in K^S$, i.e. $\check{\mathbf{u}}^S$ may have a different gradient-sparsity pattern from $\mathbf{u}^S$. However, since $\|\nabla_T\mathbf{v}^b\|_0 \le S$, we still have the bound $\|\mathbf{u}-\mathbf{v}^b\|_2^2 \ge \|\mathbf{u}-\check{\mathbf{u}}^S\|_2^2$ in place of (61), by optimality of $\check{\mathbf{u}}^S$.

Let $\check{\mathbf{u}}^S_\Delta$ be the vector $\check{\mathbf{u}}^S$ with each entry rounded to the closest value in Δ. Note that the value of $\check{\mathbf{u}}^S$ on each set of its induced partition over T is the average of the entries of $\mathbf{u}$ over this set: This implies that $\|\check{\mathbf{u}}^S\|_\infty \le \|\mathbf{u}\|_\infty$, and also that the residual $\mathbf{u}-\check{\mathbf{u}}^S$ is orthogonal to $\check{\mathbf{u}}^S - \check{\mathbf{u}}^S_\Delta$. By the given condition on $\Delta_{\min}$ and $\Delta_{\max}$, we have the entrywise bound $\|\check{\mathbf{u}}^S_\Delta - \check{\mathbf{u}}^S\|_\infty \le \delta$ from the rounding. Then

$$\|\mathbf{u}-\mathbf{v}^b\|_2^2 \ge \|\mathbf{u}-\check{\mathbf{u}}^S\|_2^2 = \|\mathbf{u}-\check{\mathbf{u}}^S_\Delta\|_2^2 - \|\check{\mathbf{u}}^S_\Delta - \check{\mathbf{u}}^S\|_2^2 \ge \|\mathbf{u}-\check{\mathbf{u}}^S_\Delta\|_2^2 - p\delta^2.$$

Since $\check{\mathbf{u}}^S_\Delta \in \Delta^p$ also satisfies $\|\nabla_T\check{\mathbf{u}}^S_\Delta\|_0 \le S$, optimality of $\mathbf{u}^S$ implies $\|\mathbf{u}-\check{\mathbf{u}}^S_\Delta\|_2^2 \ge \|\mathbf{u}-\mathbf{u}^S\|_2^2$. Substituting above and continuing the proof as in Lemma 3.3.6, we get the bound

$$\|\mathbf{P}_K\mathbf{u}-\mathbf{u}^*\|_2^2 \ge B\cdot(\|\mathbf{P}_K\mathbf{u}-\mathbf{u}^S\|_2^2 - p\delta^2),$$

and rearranging and applying the lower-bound for B concludes the proof as before. □

The second step of the proof is carried out by the following lemma, establishing a key property of the gradient mapping following ideas of Theorem 2.2.7 in (Nesterov, 2013).

Lemma B.3.2. *Let (T_1, T_2) be two trees on $\{1, \ldots, p\}$. Let $(\mathcal{P}_1, \mathcal{P}_2)$ be two partitions of $\{1, \ldots, p\}$, with associated subspaces (K_1, K_2), such that $|\partial_{T_1}\mathcal{P}_1| \leq s$ and $|\partial_{T_2}\mathcal{P}_2| \leq s$ for some sparsity level $s > 0$. Let $K = K_1 + K_2$, and let $\mathbf{P}_K$ be the orthogonal projection onto K.*

Let $\mathcal{L}$ be a loss function satisfying cRSC and cRSS with respect to (T_1, T_2), at sparsity level s and with convexity and smoothness constants $\alpha, L > 0$. Fix $\boldsymbol{\theta}_1 \in K_1$ and define

$$\mathbf{u} = \mathbf{P}_K(\boldsymbol{\theta}_1 - \nabla\mathcal{L}(\boldsymbol{\theta}_1)/L), \qquad \mathbf{v} = \operatorname*{argmin}_{\boldsymbol{\theta} \in K} \mathcal{L}(\boldsymbol{\theta}).$$

Then

(a) $\|\mathbf{u} - \mathbf{v}\|_2 \leq \sqrt{1 - \alpha/L} \cdot \|\boldsymbol{\theta}_1 - \mathbf{v}\|_2$, *and*

(b) $\|\boldsymbol{\theta}_1 - \mathbf{v}\|_2 \leq (2/\alpha) \cdot \|\mathbf{P}_K \nabla\mathcal{L}(\boldsymbol{\theta}_1)\|_2$.

Proof. Denote

$$\mathbf{g} = \mathbf{P}_K \nabla\mathcal{L}(\boldsymbol{\theta}_1).$$

Since $\boldsymbol{\theta}_1 \in K$, we have $\mathbf{u} = \boldsymbol{\theta}_1 - \mathbf{g}/L$. Then

$$\|\mathbf{u} - \mathbf{v}\|_2^2 = \|\boldsymbol{\theta}_1 - \mathbf{v} - \mathbf{g}/L\|_2^2 = \|\boldsymbol{\theta}_1 - \mathbf{v}\|_2^2 + \frac{1}{L^2}\|\mathbf{g}\|_2^2 - \frac{2}{L}\langle \mathbf{g}, \boldsymbol{\theta}_1 - \mathbf{v}\rangle.$$

So part (a) will follow from

$$\langle \mathbf{g}, \boldsymbol{\theta}_1 - \mathbf{v}\rangle \geq \frac{1}{2L}\|\mathbf{g}\|_2^2 + \frac{\alpha}{2}\|\boldsymbol{\theta}_1 - \mathbf{v}\|_2^2. \tag{64}$$

To show (64), observe that $\mathbf{v} \in K = K_1 + K_2$, so we may apply the cRSC condition to $\boldsymbol{\theta}_1$ and $\mathbf{v}$. This gives

$$\mathcal{L}(\mathbf{v}) \geq \mathcal{L}(\boldsymbol{\theta}_1) + \langle \nabla\mathcal{L}(\boldsymbol{\theta}_1), \mathbf{v} - \boldsymbol{\theta}_1\rangle + \frac{\alpha}{2}\|\mathbf{v} - \boldsymbol{\theta}_1\|_2^2. \tag{65}$$

Then, introducing

$$Q(\boldsymbol{\theta}) = \mathcal{L}(\boldsymbol{\theta}_1) + \langle \nabla\mathcal{L}(\boldsymbol{\theta}_1), \boldsymbol{\theta} - \boldsymbol{\theta}_1\rangle + \frac{L}{2}\|\boldsymbol{\theta} - \boldsymbol{\theta}_1\|_2^2,$$

we get

$$\mathcal{L}(\mathbf{v}) \geq Q(\mathbf{u}) - \frac{L}{2}\|\mathbf{u} - \boldsymbol{\theta}_1\|_2^2 + \langle \nabla\mathcal{L}(\boldsymbol{\theta}_1), \mathbf{v} - \mathbf{u}\rangle + \frac{\alpha}{2}\|\mathbf{v} - \boldsymbol{\theta}_1\|_2^2.$$

Applying $\mathbf{u} - \boldsymbol{\theta}_1 = -\mathbf{g}/L$ and $\mathbf{v} - \mathbf{u} \in K$, this gives

$$\begin{aligned}\mathcal{L}(\mathbf{v}) &\geq Q(\mathbf{u}) - \frac{1}{2L}\|\mathbf{g}\|_2^2 + \langle \mathbf{g}, \mathbf{v} - \mathbf{u}\rangle + \frac{\alpha}{2}\|\mathbf{v} - \boldsymbol{\theta}_1\|_2^2 \\ &= Q(\mathbf{u}) + \frac{1}{2L}\|\mathbf{g}\|_2^2 + \langle \mathbf{g}, \mathbf{v} - \boldsymbol{\theta}_1\rangle + \frac{\alpha}{2}\|\mathbf{v} - \boldsymbol{\theta}_1\|_2^2.\end{aligned}$$

Next, observe that $\mathbf{u} \in K = K_1 + K_2$, so we may apply the cRSS condition to $\boldsymbol{\theta}_1$ and $\mathbf{u}$. This yields $\mathcal{L}(\mathbf{u}) \leq Q(\mathbf{u})$. Since $\mathcal{L}(\mathbf{v}) \leq \mathcal{L}(\mathbf{u})$ by optimality of $\mathbf{v}$, combining these observations gives

$$0 \geq \frac{1}{2L}\|\mathbf{g}\|_2^2 + \langle \mathbf{g}, \mathbf{v} - \boldsymbol{\theta}_1\rangle + \frac{\alpha}{2}\|\mathbf{v} - \boldsymbol{\theta}_1\|_2^2.$$

Rearranging yields (64), which establishes part (a).

For part (b), let us again apply (65) and the optimality condition $\mathcal{L}(\mathbf{v}) \leq \mathcal{L}(\boldsymbol{\theta}_1)$ to get

$$\begin{aligned}0 &\geq \langle \nabla\mathcal{L}(\boldsymbol{\theta}_1), \mathbf{v} - \boldsymbol{\theta}_1\rangle + \frac{\alpha}{2}\|\mathbf{v} - \boldsymbol{\theta}_1\|_2^2 \\ &= \langle \mathbf{g}, \mathbf{v} - \boldsymbol{\theta}_1\rangle + \frac{\alpha}{2}\|\mathbf{v} - \boldsymbol{\theta}_1\|_2^2 \\ &\geq -\|\mathbf{g}\|_2 \cdot \|\mathbf{v} - \boldsymbol{\theta}_1\|_2 + \frac{\alpha}{2}\|\mathbf{v} - \boldsymbol{\theta}_1\|_2^2.\end{aligned}$$

Rearranging yields part (b). □

Proof of Theorem 3.3.5. Let $\mathbf{u}_t = \boldsymbol{\theta}_{t-1} - \frac{1}{L}\nabla\mathcal{L}(\boldsymbol{\theta}_{t-1}; Z_1^n)$. We claim by induction that

$$[-\|\mathbf{u}_t\|_\infty, \|\mathbf{u}_t\|_\infty] \subseteq [\Delta_{\min}, \Delta_{\max}] \tag{66}$$

and

$$\|\boldsymbol{\theta}_t - \boldsymbol{\theta}^*\|_2 \leq \Gamma \cdot \|\boldsymbol{\theta}_{t-1} - \boldsymbol{\theta}^*\|_2 + \frac{4(1+\gamma)}{\alpha} \cdot \Phi(S') + \delta\sqrt{p} \tag{67}$$

for each $t = 1, \ldots, \tau$.

To start the induction, first observe that for every $t \in \{1, \ldots, \tau\}$, the following holds: Fix any $i \in \{1, \ldots, p\}$ and let $K = K_{t-1} + K^* + \text{span}(\mathbf{e}_i)$ where (K_{t-1}, K^*) are the subspaces associated to the partitions induced by $(\boldsymbol{\theta}_{t-1}, \boldsymbol{\theta}^*)$ over T_{t-1}, and $\text{span}(\mathbf{e}_i)$ is the 1-dimensional span of the i^{th} standard basis vector $\mathbf{e}_i$. If $\mathcal{P}$ is the partition associated to K, then $|\partial_{T_{t-1}}\mathcal{P}| \leq S + 2s^* + d_{\max} \leq S'$ because $\|\nabla_{T_{t-1}}\boldsymbol{\theta}_{t-1}\|_0 \leq S$, $\|\nabla_{T_{t-1}}\boldsymbol{\theta}^*\|_0 \leq 2s^*$ by Lemma 3.2.1, and $\|\nabla_{T_{t-1}}\mathbf{e}_i\|_0 \leq d_{\max}$. Applying the cRSS property for $\mathcal{L}$ with respect to (T_{t-1}, T_t), we get that the loss $\mathcal{L}(\cdot\,; Z_1^n)$ is L-strongly-smooth

restricted to K, meaning for all $\mathbf{u}, \mathbf{v} \in K$,

$$\mathcal{L}(\mathbf{u}; Z_1^n) \leq \mathcal{L}(\mathbf{v}; Z_1^n) + \langle \nabla \mathcal{L}(\mathbf{v}), \mathbf{u} - \mathbf{v} \rangle + \frac{L}{2} \|\mathbf{u} - \mathbf{v}\|_2^2.$$

Then applying Eq. (2.1.8) of (Nesterov, 2013) to the loss $\mathcal{L}(\cdot\,; Z_1^n)$ restricted to K, we have for all $\mathbf{u}, \mathbf{v} \in K$ that

$$\|\mathbf{P}_K \nabla \mathcal{L}(\mathbf{u}; Z_1^n) - \mathbf{P}_K \nabla \mathcal{L}(\mathbf{v}; Z_1^n)\|_2 \leq L \|\mathbf{u} - \mathbf{v}\|_2,$$

where $\mathbf{P}_K$ is the orthogonal projection onto K. In particular,

$$\left| \langle \mathbf{e}_i, \nabla \mathcal{L}(\boldsymbol{\theta}_{t-1}; Z_1^n) - \nabla \mathcal{L}(\boldsymbol{\theta}^*; Z_1^n) \rangle \right| \leq L \|\boldsymbol{\theta}_{t-1} - \boldsymbol{\theta}^*\|_2.$$

This holds for each standard basis vector $\mathbf{e}_i$, so

$$\frac{1}{L} \|\nabla \mathcal{L}(\boldsymbol{\theta}_{t-1}; Z_1^n)\|_\infty \leq \frac{1}{L} \|\nabla \mathcal{L}(\boldsymbol{\theta}^*; Z_1^n)\|_\infty + \|\boldsymbol{\theta}_{t-1} - \boldsymbol{\theta}^*\|_2. \tag{68}$$

Then (66) holds for $t = 1$ by the initialization $\boldsymbol{\theta}_0 = 0$ and the given conditions for $\Delta_{\min}, \Delta_{\max}$.

Suppose by induction that (66) holds for t. We apply Lemma B.3.1 to $T = T_t$, $\mathbf{u}^* = \boldsymbol{\theta}^*$, and $\mathbf{u} = \mathbf{u}_t$. Note that by Lemma 3.2.1, $\|\nabla_T \boldsymbol{\theta}^*\|_0 \leq 2s^*$. Then by the definition of the update (3.6), we have $\mathbf{u}^S = \boldsymbol{\theta}_t$ in Lemma B.3.1. Denote by $\mathcal{P}_2$ the partition guaranteed by Lemma B.3.1, with associated subspace K_2. Then the lemma guarantees that

$$|\partial_{T_t} \mathcal{P}_2| \leq S + 2s^* + \sqrt{S} \leq S',$$

and furthermore

$$\|\mathbf{P}_{K_2} \mathbf{u}_t - \boldsymbol{\theta}_t\|_2 \leq \gamma \cdot \|\mathbf{P}_{K_2} \mathbf{u}_t - \boldsymbol{\theta}^*\|_2 + \delta\sqrt{p}.$$

This bound implies

$$\|\boldsymbol{\theta}_t - \boldsymbol{\theta}^*\|_2 \leq \|\boldsymbol{\theta}_t - \mathbf{P}_{K_2} \mathbf{u}_t\|_2 + \|\mathbf{P}_{K_2} \mathbf{u}_t - \boldsymbol{\theta}^*\|_2 \leq (1 + \gamma) \|\mathbf{P}_{K_2} \mathbf{u}_t - \boldsymbol{\theta}^*\|_2 + \delta\sqrt{p}. \tag{69}$$

Next, let us apply Lemma B.3.2: Take (T_1, T_2) in Lemma B.3.2 to be (T_{t-1}, T_t). Take $\mathcal{P}_1$ to be the common refinement of the partitions induced by $\boldsymbol{\theta}_{t-1}$ and $\boldsymbol{\theta}^*$ over T_{t-1}, and let $\mathcal{P}_2$ be as above. Then $|\partial_{T_{t-1}} \mathcal{P}_1| \leq S + 2s^* < S'$ and $|\partial_{T_t} \mathcal{P}_2| \leq S'$, so the cRSC and cRSS conditions required in

Lemma B.3.2 are satisfied. Let K_1, K_2 be the associated subspaces, and set $K = K_1 + K_2$ and

$$\mathbf{v} = \operatorname*{argmin}_{\boldsymbol{\theta} \in K} \mathcal{L}(\boldsymbol{\theta}; Z_1^n).$$

First, we take $\boldsymbol{\theta}_1$ to be $\boldsymbol{\theta}_{t-1}$, and apply Lemma B.3.2(a) with $\mathbf{u} = \mathbf{P}_K \mathbf{u}_t$. This gives

$$\|\mathbf{P}_K \mathbf{u}_t - \mathbf{v}\|_2 \leq \sqrt{1 - \frac{\alpha}{L}} \cdot \|\boldsymbol{\theta}_{t-1} - \mathbf{v}\|_2. \tag{70}$$

Note that $\|\mathbf{P}_{K_2} \mathbf{u}_t - \boldsymbol{\theta}^*\|_2 \leq \|\mathbf{P}_K \mathbf{u}_t - \boldsymbol{\theta}^*\|_2$ because $\boldsymbol{\theta}^* \in K_2 \subseteq K$. Applying this and (70) to (69),

$$\begin{aligned}
\|\boldsymbol{\theta}_t - \boldsymbol{\theta}^*\|_2 &\leq (1+\gamma)\|\mathbf{P}_K \mathbf{u}_t - \boldsymbol{\theta}^*\|_2 + \delta\sqrt{p} \\
&\leq (1+\gamma)\left(\sqrt{1 - \frac{\alpha}{L}} \cdot \|\boldsymbol{\theta}_{t-1} - \mathbf{v}\|_2 + \|\mathbf{v} - \boldsymbol{\theta}^*\|_2\right) + \delta\sqrt{p} \\
&\leq (1+\gamma)\left(\sqrt{1 - \frac{\alpha}{L}} \cdot \|\boldsymbol{\theta}_{t-1} - \boldsymbol{\theta}_*\|_2 + 2\|\mathbf{v} - \boldsymbol{\theta}_*\|_2\right) + \delta\sqrt{p}.
\end{aligned} \tag{71}$$

Now, let us apply Lemma B.3.2(b) with $\boldsymbol{\theta}_1$ being $\boldsymbol{\theta}^*$. This gives

$$\|\mathbf{v} - \boldsymbol{\theta}_*\|_2 \leq (2/\alpha)\|\mathbf{P}_K \nabla \mathcal{L}(\boldsymbol{\theta}^*; Z_1^n)\|_2 \leq (2/\alpha)\Phi(S'),$$

the second bound holding by the cPGB assumption. Applying this to (71) establishes (67) at the iterate t.

We may apply (67) recursively for $1, \ldots, t$, using $\boldsymbol{\theta}_0 = 0$ and $1 + \Gamma + \Gamma^2 + \ldots = 1/(1-\Gamma)$, to get

$$\|\boldsymbol{\theta}_t - \boldsymbol{\theta}^*\|_2 \leq \Gamma^t \cdot \|\boldsymbol{\theta}^*\|_2 + \frac{1}{1-\Gamma}\left(\frac{4(1+\gamma)}{\alpha} \cdot \Phi(S') + \delta\sqrt{p}\right) = \Gamma^t \cdot \|\boldsymbol{\theta}^*\|_2 + \Lambda. \tag{72}$$

In particular,

$$\|\boldsymbol{\theta}_t\|_2 \leq 2\|\boldsymbol{\theta}^*\|_2 + \Lambda.$$

Then, applying also (68),

$$\begin{aligned}
\|\mathbf{u}_{t+1}\|_\infty &\leq \|\boldsymbol{\theta}_t\|_\infty + \frac{1}{L}\|\nabla \mathcal{L}(\boldsymbol{\theta}^*; Z_1^n)\|_\infty + \|\boldsymbol{\theta}_t - \boldsymbol{\theta}^*\|_\infty \\
&\leq \frac{1}{L}\|\nabla \mathcal{L}(\boldsymbol{\theta}^*; Z_1^n)\|_\infty + 3\|\boldsymbol{\theta}^*\|_2 + 2\Lambda.
\end{aligned}$$

Then the given condition for $\Delta_{\min}, \Delta_{\max}$ implies that (66) holds for iteration $t+1$, completing the induction. Finally, the theorem follows by applying (72) at $t = \tau$. □

B.4 Proofs for cRSC, cRSS, and cPGB

Proof of Lemma 3.3.4. Note that there are $\binom{p-1}{S}$ different partitions $\mathcal{P}_1$ of $V = \{1, \ldots, p\}$ with $|\partial_{T_1}\mathcal{P}_1| = S$, and similarly for $\mathcal{P}_2$, because each such partition corresponds to cutting S of the $p-1$ edges of T_1. Let $g(S) = S\log(1 + p/S)$. Then there are at most $\binom{p-1}{S} \cdot \binom{p-1}{S} \leq e^{2g(S)}$ different combinations of (K_1, K_2), and hence at most this many subspaces K. Taking a union bound over all such K gives, for any $\zeta > 0$,

$$\mathbb{P}(\max_K \|\mathbf{P}_K \nabla\mathcal{L}(\boldsymbol{\theta}^*; Z_1^n)\|_2 \geq \zeta) \leq e^{2g(S)} \cdot \max_K \mathbb{P}(\|\mathbf{P}_K \nabla\mathcal{L}(\boldsymbol{\theta}^*; Z_1^n)\|_2 \geq \zeta).$$

Note that the dimension of K is less than the sum of dimensions of K_1 and K_2, which is at most $2(S+1)$. Applying a covering net argument, we may find a $1/2$-net $\mathcal{N}_{1/2}$ for the set $\{\mathbf{v} \in K : \|\mathbf{v}\|_2 = 1\}$ of cardinality at most 5^{2S+2}. Thus,

$$\begin{aligned}\mathbb{P}(\|\mathbf{P}_K \nabla\mathcal{L}(\boldsymbol{\theta}^*; Z_1^n)\|_2 \geq \zeta) &\leq \mathbb{P}(2 \max_{\mathbf{v}\in\mathcal{N}_{1/2}} |\mathbf{v}^\top \nabla\mathcal{L}(\boldsymbol{\theta}^*; Z_1^n)| \geq \zeta) \\ &\leq 5^{2S+2} \cdot \max_{\mathbf{v}\in\mathcal{N}_{1/2}} \mathbb{P}(2|\mathbf{v}^\top \nabla\mathcal{L}(\boldsymbol{\theta}^*; Z_1^n)| \geq \zeta).\end{aligned}$$

Applying the subgaussian assumption on $\mathbf{v}^\top \nabla\mathcal{L}(\boldsymbol{\theta}^*; Z_1^n)$, we get

$$\mathbb{P}(\max_K \|\mathbf{P}_K \nabla\mathcal{L}(\boldsymbol{\theta}^*; Z_1^n)\|_2 \geq \zeta) \leq e^{2g(S)} \cdot 5^{2S+2} \cdot 2e^{-n\zeta^2/8\sigma^2}.$$

Then for any $k > 0$ and some constant $C_k > 0$ depending only on k, setting $\zeta = \sqrt{C_k\sigma^2 g(S)/n}$ and applying $g(S) \geq \log(1+p)$, we get

$$\mathbb{P}(\max_K \|\mathbf{P}_K \nabla\mathcal{L}(\boldsymbol{\theta}^*; Z_1^n)\|_2 \geq \sqrt{C_k\sigma^2 g(S)/n}) \leq p^{-k}.$$

□

Proof of Proposition 3.4.1. We will consider a fixed t, and then apply a union bound over $1 \leq t \leq \tau$.

For cRSC and cRSS, note that $\mathcal{L}(\boldsymbol{\theta}; Z_1^n) = \frac{1}{2n}\|\mathbf{y} - \mathbf{X}\boldsymbol{\theta}\|_2^2$ for the linear model, which gives $\mathcal{L}(\boldsymbol{\theta}_2; Z_1^n) - \mathcal{L}(\boldsymbol{\theta}_1; Z_1^n) - \langle \boldsymbol{\theta}_2 - \boldsymbol{\theta}_1, \nabla\mathcal{L}(\boldsymbol{\theta}_1; Z_1^n)\rangle = \frac{1}{2n}\|\mathbf{X}(\boldsymbol{\theta}_1 - \boldsymbol{\theta}_2)\|_2^2$. Then the cRSC and cRSS bounds will hold as long as

$$\sup_K \sup_{\mathbf{u}\in K:\|\mathbf{u}\|_2=1} \frac{1}{n}\|\mathbf{X}\mathbf{u}\|_2^2 \leq 3\lambda_1/2 \quad \text{and} \quad \inf_K \inf_{\mathbf{u}\in K:\|\mathbf{u}\|_2=1} \frac{1}{n}\|\mathbf{X}\mathbf{u}\|_2^2 \geq \lambda_p/2, \tag{73}$$

where the supremum and infimum are over all subspaces $K = K_1 + K_2$ as in Definition 3.3.2. This property (73) is invariant under a common rescaling of $\mathbf{X}^\top\mathbf{X}$, λ_1, and λ_p, so we may assume that $\lambda_p = 1$.

Fixing any such subspace K, note that the dimension of K is upper bounded by $2S' + 2$. Let $\mathbf{P}_K$ be the orthogonal projection onto K, and write $\mathbf{P}_K = \mathbf{Q}_K\mathbf{Q}_K^\top$, where $\mathbf{Q}_K$ has orthonormal columns spanning K. Then $\mathbf{X}\mathbf{Q}_K$ also has independent rows $\mathbf{x}_i^\top\mathbf{Q}_K$, where $\|\mathbf{Q}_K^\top\mathbf{x}_i\|_{\psi_2}^2 \le D$ and $\mathrm{Cov}[\mathbf{Q}_K^\top\mathbf{x}_i] = \mathbf{Q}_K^\mathsf{T}\mathbf{\Sigma}\mathbf{Q}_K$. Applying Eq. (5.25) of (Vershynin, 2010) to $\mathbf{X}\mathbf{Q}_K$, for any $\zeta > 0$ and some constants $C_3, C_4 > 0$ depending only on D,

$$\mathbb{P}\left[\left\|\frac{1}{n}\mathbf{Q}_K^\top\mathbf{X}^\top\mathbf{X}\mathbf{Q}_K - \mathbf{Q}_K^\top\mathbf{\Sigma}\mathbf{Q}_K\right\|_{\mathrm{op}} \ge \max(\omega, \omega^2)\right] \le 2e^{-C_3\zeta^2}, \qquad \omega \equiv \frac{C_4\sqrt{S'} + \zeta}{\sqrt{n}}.$$

Recall $g(S') = S'\log(1 + \frac{p}{S'})$. Note that there are at most $\binom{p-1}{S'} \cdot \binom{p-1}{S'} \le e^{2g(S')}$ different subspaces K. Taking a union bound over K, and noting that any $\mathbf{u} \in K$ may be represented as $\mathbf{u} = \mathbf{Q}_K\mathbf{v}$ for such K, this yields

$$\mathbb{P}\left[\sup_K \sup_{\mathbf{u}\in K:\|\mathbf{u}\|_2=1} \left|\frac{1}{n}\mathbf{u}^\mathsf{T}\mathbf{X}^\mathsf{T}\mathbf{X}\mathbf{u} - \mathbf{u}^\mathsf{T}\mathbf{\Sigma}\mathbf{u}\right| \ge \max(\omega, \omega^2)\right] \le 2e^{2g(S')-C_3\zeta^2}$$

When $\|\mathbf{u}\|_2 = 1$, $\mathbf{u}^\mathsf{T}\mathbf{\Sigma}\mathbf{u} \in [\lambda_p, \lambda_1]$. It follows, with probability at least $1 - 2e^{2g(S')-C_3\zeta^2}$ and under our scaling $\lambda_p = 1$, that

$$\sup_K \sup_{\mathbf{u}\in K:\|\mathbf{u}\|_2=1} \frac{1}{n}\|\mathbf{X}\mathbf{u}\|_2^2 \le \lambda_1 + \max(\omega, \omega^2),$$

and

$$\inf_K \inf_{\mathbf{u}\in K:\|\mathbf{u}\|_2=1} \frac{1}{n}\|\mathbf{X}\mathbf{u}\|_2^2 \ge (1 - \max(\omega, \omega^2))_+.$$

Then, for any $k > 0$ and some constants $C_1, C_5 > 0$ depending only on k, D, assuming $n \ge C_1 g(S')$ and setting $\zeta = \sqrt{C_5 g(S')}$, (73) holds with probability at least $1 - 2e^{-kg(S')}$. Applying $g(S') \ge \log p$, this probability is at least $1 - 2p^{-k}$.

For cPGB, it follows from the first part of the proof that with probability at least $1 - 2p^{-k}$, $\|\mathbf{X}\mathbf{u}\|_2^2/n^2 \le 3\lambda_1/2n$ for every such subspace K and every $\mathbf{u} \in K$. Applying Lemma 5.9 of (Vershynin, 2010) and the assumption $\|e_i\|_{\psi_2}^2 \le \sigma^2$, conditional on $\mathbf{X}$ and this event, $\mathbf{u}^\mathsf{T}\mathbf{X}^\top\mathbf{e}/n$ is a subgaussian random variable with subgaussian parameter $C_6\lambda_1\sigma^2/n$, where $C_6 > 0$ is some absolute constant. Noting that $\nabla\mathcal{L}(\boldsymbol{\theta}^*; Z_1^n) = -\mathbf{X}^\top\mathbf{e}/n$ and applying Lemma 3.3.4, $\mathcal{L}$ has the cPGB

$\Phi(S') = C_2\sigma\sqrt{\lambda_1 g(S')/n}$ with probability at least $1 - 3p^{-k}$.

The bound for $\|\nabla\mathcal{L}(\boldsymbol{\theta}^*; Z_1^n)\|_\infty = \|\mathbf{X}^\top \mathbf{e}/n\|_\infty$ follows from similarly noting that with probability at least $1 - 2p^{-k}$, $\|\mathbf{X}\mathbf{u}\|_2^2/n^2 \leq 3\lambda_1/2n$ for each standard basis vector $\mathbf{u} \in \mathbb{R}^p$. Conditional on $\mathbf{X}$ and this event, $\mathbf{u}^\mathsf{T}\mathbf{X}^\top\mathbf{e}/n$ is subgaussian with parameter $C_6\lambda_1\sigma^2/n$ for every standard basis vector $\mathbf{u}$. Then the bound for $\|\mathbf{X}^\top\mathbf{e}/n\|_\infty$ follows from the subgaussian tail bound and a union bound over all such $\mathbf{u}$. Finally, applying a union bound over $1 \leq t \leq \tau$ completes the proof. □

Proof of Proposition 3.4.3. Similar to the proof of Proposition 3.4.1, we consider fixed t and then apply a union bound over $1 \leq t \leq \tau$.

For cRSC and cRSS, note that $\mathcal{L}(\boldsymbol{\theta}; Z_1^n) = \frac{1}{n}\sum_{i=1}^n (b(\mathbf{x}_i^\top\boldsymbol{\theta}) - y_i\mathbf{x}_i^\top\boldsymbol{\theta})$, which gives

$$\begin{aligned}
&\mathcal{L}(\boldsymbol{\theta}_2; Z_1^n) - \mathcal{L}(\boldsymbol{\theta}_1; Z_1^n) - \langle\boldsymbol{\theta}_2 - \boldsymbol{\theta}_1, \nabla\mathcal{L}(\boldsymbol{\theta}_1; Z_1^n)\rangle \\
&= \frac{1}{n}\sum_{i=1}^n (b(\mathbf{x}_i^\mathsf{T}\boldsymbol{\theta}_2) - b(\mathbf{x}_i^\mathsf{T}\boldsymbol{\theta}_1) - b'(\mathbf{x}_i^\mathsf{T}\boldsymbol{\theta}_1)x_i^\mathsf{T}(\boldsymbol{\theta}_2 - \boldsymbol{\theta}_1)).
\end{aligned}$$

Applying the assumption on b,

$$\frac{\alpha_b}{2n}\|\mathbf{X}(\boldsymbol{\theta}_2 - \boldsymbol{\theta}_1)\|_2^2 \leq \mathcal{L}(\boldsymbol{\theta}_2; Z_1^n) - \mathcal{L}(\boldsymbol{\theta}_1; Z_1^n) - \langle\boldsymbol{\theta}_2 - \boldsymbol{\theta}_1, \nabla\mathcal{L}(\boldsymbol{\theta}_1; Z_1^n)\rangle \leq \frac{L_b}{2n}\|\mathbf{X}(\boldsymbol{\theta}_2 - \boldsymbol{\theta}_1)\|_2^2.$$

Then cRSC and cRSS hold for (T_{t-1}, T_t) with probability $1 - 2p^{-k}$, by (73) and the same argument as Proposition 3.4.1.

For cPGB, note that $\nabla\mathcal{L}(\boldsymbol{\theta}^*; Z_1^n) = -\frac{1}{n}\sum_{i=1}^n \mathbf{x}_i e_i = -\mathbf{X}^\mathsf{T}\mathbf{e}/n$ where $\mathbf{e} = (e_1, \ldots, e_n)$. Similar to the proof of Proposition 3.4.1, we condition on $\mathbf{X}$ and the probability $1 - 2e^{-kg(S')}$ event $\mathcal{E}$ that $\frac{1}{n}\|\mathbf{X}\mathbf{u}\|_2^2 \leq 3\lambda_1/2$ for every $K = K_1 + K_2$ and every $\mathbf{u} \in K$. Then similar to the proof of Lemma 3.3.4, we get for any $\zeta > 0$

$$\begin{aligned}
&\mathbb{P}(\sup_K \|\mathbf{P}_K\mathbf{X}^\mathsf{T}\mathbf{e}\|_2/\sqrt{n} > \zeta) \\
&\leq e^{2g(S')} \cdot 5^{2S'+2} \cdot \Big(\sup_{\mathbf{w}:\|\mathbf{w}\|_2=1} \mathbb{P}(\{2|\mathbf{w}^\mathsf{T}\mathbf{X}^\mathsf{T}\mathbf{e}|/\sqrt{n} \geq \zeta\} \cap \mathcal{E}) + 2e^{-kg(S')}\Big).
\end{aligned}$$

Note that (3.21) implies $\mathrm{Var}(e_i) \leq C_3$ where $C_3 > 0$ is some constant depending only on D_1, D_2, β. If $1 < \beta \leq 2$, applying Lemma B.5.1,

$$\mathbb{P}(\sup_K \|\mathbf{P}_K\mathbf{X}^\mathsf{T}\mathbf{e}\|_2/\sqrt{n} > \zeta) \leq e^{2g(S')} \cdot 5^{2S'+2} \cdot \Big(2e^{-\zeta^\beta/(C_4\sqrt{\lambda_1})^\beta} + 2e^{-kg(S')}\Big),$$

where $C_4 > 0$ is some constant depending only on D_1, D_2, β. Then for any $k > 0$ and some constant

$C_2 > 0$ depending only on k, D, D_1, D_2, β, setting $\zeta = C_2\sqrt{\lambda_1} \cdot g(S')^{1/\beta}$ and applying $g(S') \geq \log p$, we have

$$\mathbb{P}(\sup_K \|\mathbf{P}_K \mathbf{X}^\mathsf{T}\mathbf{e}\|_2/n > C_2\sqrt{\lambda_1/n} \cdot g(S')^{1/\beta}) \leq p^{-k}.$$

If $\beta = 1$, applying Lemma B.5.1, we get

$$\mathbb{P}(\sup_K \|\mathbf{P}_K \mathbf{X}^\mathsf{T}\mathbf{e}\|_2/n > C_2\sqrt{\lambda_1/n} \log n \cdot g(S')) \leq p^{-k}.$$

The bound for $\|\nabla\mathcal{L}(\boldsymbol{\theta}^*; Z_1^n)\|_\infty = \|\mathbf{X}^\top\mathbf{e}/n\|_\infty$ is similar to the proof of Proposition 3.4.1. Note that with probability at least $1 - 2p^{-k}$, $\|\mathbf{X}\mathbf{u}_i\|_2^2/n \leq 3\lambda_1/2$ for each standard basis vector $\mathbf{u}_i \in \mathbb{R}^p$ with $1 \leq i \leq p$. We condition on $\mathbf{X}$ and this event $\mathcal{E}'$ and get for any $\zeta > 0$

$$\mathbb{P}(\max_{1\leq i\leq p} |\mathbf{u}_i\mathbf{X}^\mathsf{T}\mathbf{e}|/\sqrt{n} > \zeta) \leq p \cdot \Big(\max_{1\leq i\leq p} \mathbb{P}(\{|\mathbf{u}_i\mathbf{X}^\mathsf{T}\mathbf{e}|/\sqrt{n} > \zeta\} \cap \mathcal{E}') + 2p^{-k}\Big).$$

Similarly, if $1 < \beta \leq 2$, applying Lemma B.5.1, for any $k > 0$ and some constant C_3 depending only on k, D, D_1, D_2, β, we get

$$\mathbb{P}(\max_{1\leq i\leq p} |\mathbf{u}_i\mathbf{X}^\mathsf{T}\mathbf{e}|/n > C_3(\log p)^{1/\beta}\sqrt{\lambda_1/n}) \leq p^{-k}.$$

If $\beta = 1$, applying Lemma B.5.1, we get

$$\mathbb{P}(\max_{1\leq i\leq p} |\mathbf{u}_i\mathbf{X}^\mathsf{T}\mathbf{e}|/n > C_3(\log n)(\log p)\sqrt{\lambda_1/n}) \leq p^{-k}.$$

Finally, applying the union bound over $1 \leq t \leq \tau$ completes the proof. □

B.5 Auxilliary lemmas

The following lemma comes from (Huang et al., 2008, Lemma 1).

Lemma B.5.1. *Suppose $X_1, \ldots, X_n$ are i.i.d. random variables with $\mathbb{E}X_i = 0$ and $\mathrm{Var}(X_i) = \sigma^2$. Further suppose, for $1 \leq d \leq 2$ and certain constants $C_1, C_2 > 0$, their tail probabilities satisfy*

$$\mathbb{P}(|X_i| \geq \zeta) \leq C_1 \exp(-C_2\zeta^d),$$

for all $\zeta > 0$. Let $c_1, \ldots, c_n$ be constants satisfying $\sum_{i=1}^n c_i \leq M^2$ and $W = \sum_{i=1}^n c_i X_i$. Then we

have

$$\|W\|_{\psi_d} \leq \begin{cases} K_d M\{\sigma + C_3\}, & 1 < d \leq 2 \\ K_1 M\{\sigma + C_4 \log n\}, & d = 1 \end{cases}$$

where K_d *is a positive constant depending only on* d, C_3 *is some positive constant depending only on* C_1, C_2, d *and* C_4 *is some positive constant depending only on* C_1, C_2. *Consequently,*

$$\mathbb{P}(|W| > \zeta) \leq \begin{cases} 2\exp\{-(\zeta/(K_d M(\sigma + C_3)))^d\}, & 1 < d \leq 2, \\ 2\exp\{-\zeta/(K_1 M(\sigma + C_4 \log n))\}, & d = 1. \end{cases}$$

C Appendix for Chapter 4

C.1 Proofs for general results on the orbit recovery model

C.1.1 High-noise expansion

We first provide a form for $s_k(\theta)$ and $\tilde{s}_k(\theta)$ that will be more convenient for later computations. We then prove Theorem 4.2.1.

Lemma C.1.1. *The expressions $s_k(\theta)$ and $\tilde{s}_k(\theta)$ from (4.7) and (4.10) have the equivalent forms*

$$s_k(\theta) = \frac{1}{2(k!)}\mathbb{E}_g[\langle\theta, g\cdot\theta\rangle^k - 2\langle\theta, g\cdot\theta_*\rangle^k + \langle\theta_*, g\cdot\theta_*\rangle^k]$$
$$\tilde{s}_k(\theta) = \frac{1}{2(k!)}\mathbb{E}_{g,h}[\langle\Pi\cdot g\cdot\theta, \Pi\cdot h\cdot\theta\rangle^k - 2\langle\Pi\cdot g\cdot\theta, \Pi\cdot h\cdot\theta_*\rangle^k + \langle\Pi\cdot g\cdot\theta_*, \Pi\cdot h\cdot\theta_*\rangle^k].$$

Proof. For the first statement, expanding the square in the definition of s_k from (4.7), we have

$$\begin{aligned}
s_k(\theta) &= \frac{1}{2(k!)}\|T_k(\theta) - T_k(\theta_*)\|_{\mathrm{HS}}^2 \\
&= \frac{1}{2(k!)}\left\|\mathbb{E}_g[(g\cdot\theta)^{\otimes k}] - \mathbb{E}_g[(g\cdot\theta_*)^{\otimes k}]\right\|_{\mathrm{HS}}^2 \\
&= \frac{1}{2(k!)}\mathbb{E}_{g,h}\left[\left\langle(g\cdot\theta)^{\otimes k}, (h\cdot\theta)^{\otimes k}\right\rangle - 2\left\langle(g\cdot\theta)^{\otimes k}, (h\cdot\theta_*)^{\otimes k}\right\rangle + \left\langle(g\cdot\theta_*)^{\otimes k}, (h\cdot\theta_*)^{\otimes k}\right\rangle\right] \\
&= \frac{1}{2(k!)}\mathbb{E}_{g,h}\left[\langle g\cdot\theta, h\cdot\theta\rangle^k - 2\langle g\cdot\theta, h\cdot\theta_*\rangle^k + \langle g\cdot\theta_*, h\cdot\theta_*\rangle^k\right] \\
&= \frac{1}{2(k!)}\mathbb{E}_g\left[\langle\theta, g\cdot\theta\rangle^k - 2\langle\theta, g\cdot\theta_*\rangle^k + \langle\theta_*, g\cdot\theta_*\rangle^k\right].
\end{aligned}$$

The last step above applies $\langle g\cdot u, h\cdot v\rangle = \langle u, (g^\top h)\cdot v\rangle$ and the equality in law $g^\top h \overset{L}{=} g$. The second statement follows similarly from (4.10), omitting this last step. □

Proof of Theorem 4.2.1. Part (a) follows from specializing part (b) to $\tilde{d} = d$ and $\Pi = \mathrm{Id}$, and observing that in this case, the term $\langle\tilde{T}_k(\theta), P_k(\theta)\rangle$ in (4.9) also belongs to $\mathcal{R}^{\mathsf{G}}_{\le k-1}$ and hence may

be absorbed into $q_k(\theta)$—see (Katsevich and Bandeira, 2020, Proposition 2.3) or (Fan et al., 2020, Lemma 4.8).

Most of the claims in part (b) follow directly from (Katsevich and Bandeira, 2020, Lemma 2.2): Specializing to our setting (where ρ and ρ_* in Katsevich and Bandeira (2020) are the distributions of $\Pi \cdot g \cdot \theta$ and $\Pi \cdot h \cdot \theta_*$ for $g, h \sim \Lambda$, and where δ in (Katsevich and Bandeira, 2020, Eqs. (2.12–2.13)) is bounded as $\delta \leq C(1 \vee \|\theta\|)$ for all $\theta \in \mathbb{R}^d$), this result guarantees that the expansion (4.9) holds for $\tilde{s}_k$, $\tilde{T}_k$, P_k, and q_k having all of the stated properties, and for a remainder $q(\theta)$ that satisfies

$$|q(\theta)| \leq \frac{C_K(1 \vee \|\theta\|)^{2K+2}}{\sigma^{2K+2}} \tag{74}$$

when $\|\theta\| \leq \sigma$. This remainder $q(\theta)$ must also be G-invariant, as all of the other terms in (4.9) are G-invariant.

It remains to verify the bounds for $\|\nabla q(\theta)\|$ and $\|\nabla^2 q(\theta)\|$ in (4.8). These types of bounds were shown in the unprojected setting of $\Pi = \mathrm{Id}$ in (Fan et al., 2020, Lemma 4.7). They were not stated explicitly in Katsevich and Bandeira (2020), but may be deduced from a small extension of the analysis: Denote by $\mathbb{E}_g, \mathbb{E}_h$ the expectations over $g, h \sim \Lambda$, and by $\mathbb{E}_\varepsilon, \mathbb{E}_{\varepsilon'}$ those over $\varepsilon, \varepsilon' \sim \mathcal{N}(0, \mathrm{Id})$. Write

$$t = 1/\sigma, \qquad Y = \Pi \cdot h \cdot \theta_* + t^{-1}\varepsilon, \qquad w = \Pi \cdot g \cdot \theta - \Pi \cdot h \cdot \theta_* \in \mathbb{R}^{\tilde{d}},$$

and define

$$f(t) = -\log M(t), \qquad M(t) = \mathbb{E}_g \left[\exp\left(-\frac{t^2 \|w\|^2}{2} + t w^\top \varepsilon \right) \right]$$

Comparing with (4.3), this function $f(t)$ is the negative log-likelihood for the single sample Y, up to a θ-independent constant and viewed as a function of $t = 1/\sigma$. Applying a Taylor expansion of $f(t)$ around $t = 0$, and then taking expectations over (h, ε) that define Y, we have

$$R(\theta) = \text{constant} + \sum_{p=1}^{2K+1} \frac{t^p}{p!} \mathbb{E}_{h,\varepsilon}[f^{(p)}(0)] + \frac{t^{2K+2}}{(2K+2)!} \mathbb{E}_{h,\varepsilon}[f^{(2K+2)}(\xi(h,\varepsilon))] \tag{75}$$

for a random point $\xi(h, \varepsilon)$ between 0 and $t = 1/\sigma$. This is a rewriting of the Taylor expansion in (Katsevich and Bandeira, 2020, Eq. (5.7)). It is shown in Katsevich and Bandeira (2020) that the leading terms in (75) of orders $t^1, \ldots, t^{2K+1}$ give exactly the leading terms of (4.9), and the last term of (75) is the remainder $q(\theta)$ in (4.9). The bound (74) for $q(\theta)$ follows from (Katsevich and Bandeira, 2020, Eq. (5.22)).

To bound $\partial_{\theta_a} q(\theta)$ for any index $a \in \{1, \ldots, d\}$, we may apply a similar Taylor expansion for

$\partial_{\theta_a} R(\theta)$, and write

$$\partial_{\theta_a} R(\theta) = \sum_{p=1}^{2K+1} \frac{t^p}{p!} \mathbb{E}_{h,\varepsilon}[\partial_t^p \partial_{\theta_a} f(0)] + \frac{t^{2K+2}}{(2K+2)!} \mathbb{E}_{h,\varepsilon}[\partial_t^{2K+2} \partial_{\theta_a} f(\xi(h,\varepsilon))]$$

for a possibly different point $\xi(h,\varepsilon) \in (0,t)$ depending on the index a. Then

$$\partial_{\theta_a} q(\theta) = \frac{t^{2K+2}}{(2K+2)!} \mathbb{E}_{h,\varepsilon}[\partial_t^{2K+2} \partial_{\theta_a} f(\xi(h,\varepsilon))] \tag{76}$$

and we wish to bound this term for each $a \in \{1, \dots, d\}$. The function $\partial_{\theta_a} f(t)$ is the θ_a-derivative of f, given by

$$\partial_{\theta_a} f(t) = -\frac{\partial_{\theta_a} M(t)}{M(t)}.$$

Then differentiating $2K+2$ times in t, we see that $\partial_t^{2K+2} \partial_{\theta_a} f(t)$ is a sum of at most C_K terms of the form

$$C_{\ell_0,\dots,\ell_j} \cdot \frac{\partial_t^{\ell_0} \partial_{\theta_a} M(t)}{M(t)} \cdot \frac{\partial_t^{\ell_1} M(t)}{M(t)} \cdot \dots \cdot \frac{\partial_t^{\ell_j} M(t)}{M(t)}$$

for some integers $j \geq 0$ and $\ell_0, \dots, \ell_j \geq 0$ such that $\ell_0 + \ldots + \ell_j = 2K+2$, and for some universal constants $C_{\ell_0,\dots,\ell_j}$ depending only on $\ell_0, \dots, \ell_j$.

From (Katsevich and Bandeira, 2020, Eq. (5.20)), we have

$$\left| \frac{\partial_t^\ell M(\xi)}{M(\xi)} \right| \leq \delta^\ell \mathbb{E}_{\varepsilon'} \Big[(\|W\| + |\xi|\delta)^\ell \Big], \qquad W = \varepsilon + \mathbf{i}\varepsilon', \qquad \delta = \sup_{g,h \in \mathsf{G}} \|\Pi \cdot g \cdot \theta - \Pi \cdot h \cdot \theta_*\|$$

where $\varepsilon' \sim \mathcal{N}(0, \mathrm{Id}_{\tilde{d} \times \tilde{d}})$ is an independent copy of ε. Applying this to any $\xi \in (0,t)$, and applying $\delta \leq C(1 \vee \|\theta\|) \leq C\sigma = Ct^{-1}$, we obtain

$$\left| \frac{\partial_t^\ell M(\xi)}{M(\xi)} \right| \leq C_\ell \delta^\ell (1 + \|\varepsilon\|)^\ell. \tag{77}$$

We may bound the t-derivatives of $\partial_{\theta_a} M(t)$ using a similar argument: Introducing the a^{th} standard basis vector $e_a \in \mathbb{R}^d$, observe that

$$\begin{aligned} \partial_{\theta_a} M(t) &= \mathbb{E}_g \left[e_a^\top g^\top \Pi^\top (t\varepsilon - t^2 w) \cdot \exp\left(-\frac{t^2 \|w\|^2}{2} + t w^\top \varepsilon \right) \right] \\ &= \mathbb{E}_g \left[e_a^\top g^\top \Pi^\top (t\varepsilon - t^2 w) \cdot \mathbb{E}_{\varepsilon'}[e^{t w^\top W}] \right], \qquad \text{where } W = \varepsilon + \mathbf{i}\varepsilon'. \end{aligned}$$

Then applying Leibniz' rule and the same argument as (Katsevich and Bandeira, 2020, Eqs. (5.18–

5.19)) to differentiate in t, we obtain

$$\begin{aligned}\partial_t^\ell \partial_{\theta_a} M(t) = \mathbb{E}_g\left[e_a^\top g^\top \Pi^\top (t\varepsilon - t^2 w)\cdot \mathbb{E}_{\varepsilon'}[e^{tw^\top W}]\cdot \mathbb{E}_{\varepsilon'}[(w^\top(W-tw))^\ell]\right] \\ + \ell\cdot \mathbb{E}_g\left[e_a^\top g^\top \Pi^\top (\varepsilon - 2tw)\cdot \mathbb{E}_{\varepsilon'}[e^{tw^\top W}]\cdot \mathbb{E}_{\varepsilon'}[(w^\top(W-tw))^{\ell-1}]\right] \\ + \binom{\ell}{2}\cdot \mathbb{E}_g\left[e_a^\top g^\top \Pi^\top (-2w)\cdot \mathbb{E}_{\varepsilon'}[e^{tw^\top W}]\cdot \mathbb{E}_{\varepsilon'}[(w^\top(W-tw))^{\ell-2}]\right].\end{aligned}$$

Applying also $M(t) = \mathbb{E}_g[\mathbb{E}_{\varepsilon'}[e^{tw^\top W}]]$, so that $\mathbb{E}_g[(\cdot)\mathbb{E}_{\varepsilon'}[e^{tw^\top W}]]/M(t)$ is a reweighted average over $g \in \mathsf{G}$, this yields analogously to (Katsevich and Bandeira, 2020, Eq. (5.20)) that

$$\begin{aligned}\left|\frac{\partial_t^\ell \partial_{\theta_a} M(\xi)}{M(\xi)}\right| \le C_\ell\Big[(|\xi|\|\varepsilon\| + \xi^2\delta)\cdot \delta^\ell \mathbb{E}_{\varepsilon'}[(\|W\| + |\xi|\delta)^\ell] \\ + (\|\varepsilon\| + |\xi|\delta)\cdot \delta^{\ell-1}\mathbb{E}_{\varepsilon'}[(\|W\| + |\xi|\delta)^{\ell-1}] + \delta\cdot\delta^{\ell-2}\mathbb{E}_{\varepsilon'}[(\|W\| + |\xi|\delta)^{\ell-2}]\Big]\end{aligned}$$

where we have absorbed $\|e_a^\top g^\top \Pi\|$ into the constant C_ℓ. Applying this with $\xi \in (0,t)$ and $\delta \le C(1\vee\|\theta\|) \le Ct^{-1}$, we get

$$\left|\frac{\partial_t^\ell \partial_{\theta_a} M(\xi)}{M(\xi)}\right| \le C_\ell \delta^{\ell-1}(1+\|\varepsilon\|)^{\ell+1}. \tag{78}$$

Then combining with (77) and applying to the previously stated form of $\partial_t^{2K+2}\partial_{\theta_a} f$,

$$|\partial_t^{2K+2}\partial_{\theta_a} f(\xi)| \le C_K \sum_{\substack{\ell_0,\dots,\ell_j \ge 0 \\ \ell_0+\dots+\ell_j = 2K+2}} \delta^{\ell_0+\dots+\ell_j-1}(1+\|\varepsilon\|)^{\ell_0+\dots+\ell_j+1} \le C_K'(1\vee\|\theta\|)^{2K+1}(1+\|\varepsilon\|)^{2K+3}.$$

Finally, taking the expectation over ε and applying this to (76) for each $a \in \{1,\dots,d\}$, we obtain the desired bound

$$\|\nabla q(\theta)\| \le \frac{C_K(1\vee\|\theta\|)^{2K+1}}{\sigma^{2K+2}}.$$

The argument to bound $\|\nabla^2 q(\theta)\|$ is similar: For any $a, b \in \{1,\dots,d\}$, applying a Taylor expansion of $\partial^2_{\theta_a,\theta_b} R(\theta)$, we wish to bound

$$\partial^2_{\theta_a,\theta_b} q(\theta) = \frac{t^{2K+2}}{(2K+2)!}\mathbb{E}_{h,\varepsilon}[\partial_t^{2K+2}\partial^2_{\theta_a,\theta_b} f(\xi(h,\varepsilon))]$$

for some $\xi(h,\varepsilon) \in (0,t)$ depending on a, b. We may compute

$$\partial^2_{\theta_a,\theta_b} f(t) = -\frac{\partial^2_{\theta_a,\theta_b} M(t)}{M(t)} + \frac{\partial_{\theta_a} M(t)}{M(t)}\frac{\partial_{\theta_b} M(t)}{M(t)},$$

differentiate this $2K+2$ times in t, and apply (77), (78), and the analogous bound

$$\left|\frac{\partial_t^\ell \partial_{\theta_a,\theta_b}^2 M(\xi)}{M(\xi)}\right| \le C_\ell \delta^{\ell-2}(1+\|\varepsilon\|)^{\ell+2}$$

which is derived similarly. This yields $|\partial_t^{2K+2}\partial_{\theta_a} f(\xi)| \le C_K(1 \vee \|\theta\|)^{2K}(1+\|\varepsilon\|)^{2K+4}$, and taking the expectation over ε gives the desired bound for $\|\nabla^2 q(\theta)\|$. □

C.1.2 Identifiability and transcendence degree

Proof of Proposition 4.2.4. Since $\operatorname{trdeg}\mathcal{R}^{\mathsf{G}} < \infty$ (see (Bandeira et al., 2017, Proposition 4.11)), we may take any transcendence basis φ of $\mathcal{R}^{\mathsf{G}}$, and let k be the maximum degree of the polynomials constituting φ. Then $\operatorname{trdeg}\mathcal{R}^{\mathsf{G}}_{\le k} = |\varphi| = \operatorname{trdeg}\mathcal{R}^{\mathsf{G}}$, and (a) follows.

Part (b) is similar to the statement of (Bandeira et al., 2017, Theorem 4.9): $\Pi(\mathcal{O}_\theta)$ is a continuous image of the compact group G, and hence is also compact. Then the distribution of $\Pi\cdot g\cdot\theta$ is uniquely determined by its sequence of mixed moments. Thus

$$\Big\{\theta : \Pi(\mathcal{O}_\theta) \equiv \Pi(\mathcal{O}_{\theta_*})\Big\} = \Big\{\theta : \widetilde{T}_k(\theta) = \widetilde{T}_k(\theta_*) \text{ for all } k \ge 1\Big\}. \tag{79}$$

Suppose that $\operatorname{trdeg}\widetilde{\mathcal{R}}^{\mathsf{G}}_{\le k} = \operatorname{trdeg}\mathcal{R}^{\mathsf{G}}$ for some integer k. Let U_k be the linear subspace of $\mathcal{R}^{\mathsf{G}}$ spanned by 1 and all entries of $\widetilde{T}_1,\dots,\widetilde{T}_k$. Since U_k generates $\widetilde{\mathcal{R}}^{\mathsf{G}}_{\le k}$, we have $\operatorname{trdeg}U_k = \operatorname{trdeg}\widetilde{\mathcal{R}}^{\mathsf{G}}_{\le k}$, where $\operatorname{trdeg}U_k$ is the maximum number of algebraically independent elements in U_k (Lang, 2002, Chapter 8, Theorem 1.1). Then (Bandeira et al., 2017, Theorem 4.9) shows that for generic $\theta_* \in \mathbb{R}^d$, there are only finitely many orbits $\mathcal{O}_\theta$ such that $P(\theta) = P(\theta_*)$ for all $P \in U_k$. This condition must hold for all θ belonging to (79), so (79) also consists of finitely many orbits.

Conversely, suppose $\operatorname{trdeg}\widetilde{\mathcal{R}}^{\mathsf{G}}_{\le k} < \operatorname{trdeg}\mathcal{R}^{\mathsf{G}}$ for all $k \ge 1$. Consider $\widetilde{\mathcal{R}}^{\mathsf{G}} = \bigcup_{k\ge1}\widetilde{\mathcal{R}}^{\mathsf{G}}_{\le k}$ (the subalgebra generated by entries of $\widetilde{T}_k$ for all $k \ge 1$). By the argument of (a), $\operatorname{trdeg}\widetilde{\mathcal{R}}^{\mathsf{G}} = \operatorname{trdeg}\widetilde{\mathcal{R}}^{\mathsf{G}}_{\le k}$ for some integer k, so also $\operatorname{trdeg}\widetilde{\mathcal{R}}^{\mathsf{G}} < \operatorname{trdeg}\mathcal{R}^{\mathsf{G}}$. We now apply an extension of the argument in (Bandeira et al., 2017, Section 8.3): Fix any transcendence basis φ^0 of $\widetilde{\mathcal{R}}^{\mathsf{G}}$. Then the gradient vectors of φ^0 are linearly independent at generic $\theta_* \in \mathbb{R}^d$ (see (Bandeira et al., 2017, Corollary 4.19)). Fix any such θ_*. In a sufficiently small open neighborhood O of θ_*, we claim that

$$\Big\{\theta \in O : \widetilde{T}_k(\theta) = \widetilde{T}_k(\theta_*) \text{ for all } k \ge 1\Big\} = \Big\{\theta \in O : \varphi^0(\theta) = \varphi^0(\theta_*)\Big\}. \tag{80}$$

To see this, choose any $d - |\varphi^0|$ additional functions $\bar\varphi$ for which $\varphi = (\varphi^0, \bar\varphi)$ has non-singular

derivative at θ_*, and hence forms an invertible local reparametrization over a sufficiently small such neighborhood O, by the inverse function theorem. Let $p(\theta)$ be any entry of $\widetilde{T}_k$ for any $k \geq 1$, and write $q(\varphi) = p(\theta(\varphi))$ for its reparametrization by the local coordinates φ on O. By the chain rule,

$$\nabla p(\theta) = \mathrm{d}_\theta \varphi(\theta)^\top \nabla_\varphi q(\varphi(\theta)).$$

Since $p \in \widetilde{\mathcal{R}}^{\mathsf{G}}$, and φ^0 is a transcendence basis for $\widetilde{\mathcal{R}}^{\mathsf{G}}$, we have that (p, φ^0) is algebraically dependent. Then the gradients of p and of φ^0 are linearly dependent at every $\theta \in O$ (see (Bandeira et al., 2017, Corollary 4.19)), so $\nabla p(\theta)$ belongs to the span of columns of $\mathrm{d}_\theta \varphi(\theta)^\top$ corresponding to only the coordinates of φ^0. Then $\nabla_\varphi q(\varphi(\theta))$ must be 0 in the remaining coordinates $\bar{\varphi}$. This holds for all $\theta \in O$, so $q(\varphi)$ is a function only of φ^0 in this local parametrization over O. This shows our claim (80). The set (80) forms a manifold of dimension $d - |\varphi^0| = d - \operatorname{trdeg} \widetilde{\mathcal{R}}^{\mathsf{G}}$. On the other hand, (Bandeira et al., 2017, Section 8.3) shows that for generic θ_*, each orbit $\mathcal{O}_\theta \cap O$ is a manifold of dimension $d - \operatorname{trdeg} \mathcal{R}^{\mathsf{G}}$, which is strictly smaller when $\operatorname{trdeg} \widetilde{\mathcal{R}}^{\mathsf{G}} < \operatorname{trdeg} \mathcal{R}^{\mathsf{G}}$. Thus (79) must contain infinitely many orbits corresponding to $\theta \in O$. □

C.1.3 Fisher information and transcendence degree

We prove Theorem 4.2.5 and Lemma 4.2.6, following ideas similar to (Fan et al., 2020, Section 4). Throughout, we assume that (4.4) holds in the projected setting, and we denote by K and $\widetilde{K}$ the (smallest) integers satisfying Proposition 4.2.4. Recall d_k and $\tilde{d}_k$ from (4.11–4.12), and the combined moment functions $M_k(\theta)$ and $\widetilde{M}_k(\theta)$ from (4.13–4.14).

Lemma C.1.2. *In the unprojected model, for generic $\theta \in \mathbb{R}^d$ and every $k = 1, \ldots, K$, the rank of $\mathrm{d}M_k(\theta)$ equals $d_1 + \ldots + d_k$.*

Furthermore, for any $k \in \{1, \ldots, K\}$ and any $\theta \in \mathbb{R}^d$ where $\operatorname{rank} \mathrm{d}M_k(\theta) = d_1 + \ldots + d_k$, there exist functions $\varphi^j : \mathbb{R}^d \to \mathbb{R}^{d_j}$ for each $j = 1, \ldots, k$ and $\bar{\varphi} : \mathbb{R}^d \to \mathbb{R}^{d - d_1 - \ldots - d_k}$, such that:

(a) For each $j = 1, \ldots, k$, the d_j coordinates of φ^j are entries of the moment tensor T_j.

(b) The combined map $\varphi = (\varphi^1, \ldots, \varphi^k, \bar{\varphi}) : \mathbb{R}^d \to \mathbb{R}^d$ has non-singular derivative $\mathrm{d}\varphi(\theta) \in \mathbb{R}^{d \times d}$ at this point θ, and hence an analytic inverse function $\theta(\varphi)$ over a neighborhood U of θ.

(c) For any $j = 1, \ldots, k$, any polynomial $p \in \mathcal{R}^{\mathsf{G}}_{\leq j}$, and sufficiently small such neighborhood U, $\varphi \mapsto p(\theta(\varphi))$ is a function only of the $d_1 + \ldots + d_j$ coordinates $\varphi^1, \ldots, \varphi^j$, over $\varphi(U)$.

(d) Suppose $k = K$. Then for any G-invariant continuous function $f : \mathbb{R}^d \to \mathbb{R}$ and sufficiently

small such neighborhood U, $\varphi \mapsto f(\theta(\varphi))$ is a function only of the $d_1 + \ldots + d_K$ coordinates $\varphi^1, \ldots, \varphi^K$, over $\varphi(U)$. Also,

$$\left\{\theta' \in U : (\varphi^1(\theta'), \ldots, \varphi^K(\theta')) = (\varphi^1(\theta), \ldots, \varphi^K(\theta))\right\} = U \cap \mathcal{O}_\theta. \tag{81}$$

In the projected model, the same statements hold with $\widetilde{K}$, $\widetilde{M}_j$, $\widetilde{T}_j$, $\tilde{d}_j$, and $\widetilde{\mathcal{R}}^{\mathsf{G}}_{\leq j}$ in place of K, M_j, T_j, d_j, and $\mathcal{R}^{\mathsf{G}}_{\leq j}$.

Proof. In the unprojected model, $\mathcal{R}^{\mathsf{G}}_{\leq k}$ is generated by the entries of $T_1, \ldots, T_k$, and $\operatorname{trdeg} \mathcal{R}^{\mathsf{G}}_{\leq k} = d_1 + \ldots + d_k$. Thus there are exactly $d_1 + \ldots + d_k$ algebraically independent entries of $T_1, \ldots, T_k$ (Lang, 2002, Chapter 8, Theorem 1.1). Then $\mathrm{d}M_k(\theta)$ has rank $d_1 + \ldots + d_k$ at generic $\theta \in \mathbb{R}^d$, and rank at most $d_1 + \ldots + d_k$ at *every* $\theta \in \mathbb{R}^d$, see e.g. (Bandeira et al., 2017, Corollary 4.19).

If $\theta \in \mathbb{R}^d$ has $\operatorname{rank} \mathrm{d}M_k(\theta) = d_1 + \ldots + d_k$, then this implies that also $\operatorname{rank} \mathrm{d}M_j(\theta) = d_1 + \ldots + d_j$ for each $j = 1, \ldots, k$. Then for each $j = 1, \ldots, k$, we may pick d_j entries of T_j to be φ^j, such that $(\varphi^1, \ldots, \varphi^k)$ have linearly independent gradients at θ. We may arbitrarily pick $d - d_1 - \ldots - d_k$ additional analytic functions to be $\bar{\varphi}$, so that $\varphi = (\varphi^1, \ldots, \varphi^k, \bar{\varphi})$ has non-singular derivative $\mathrm{d}\varphi(\theta)$. This shows properties (a) and (b), where the existence of an analytic inverse $\theta(\varphi)$ on U follows from the inverse function theorem.

Part (c) follows from the same argument as (80): Denote $q(\varphi) = p(\theta(\varphi))$. Applying the chain rule, for any $x \in U$,

$$\nabla p(x) = \mathrm{d}_x \varphi(x)^\top \nabla_\varphi q(\varphi(x)).$$

Since p is a function of $T_1, \ldots, T_j$, its gradient is a linear combination of the gradients of the entries of $T_1, \ldots, T_j$, and hence linearly dependent with the gradients of $\varphi^1, \ldots, \varphi^j$. Thus $\nabla p(x)$ belongs to the span of the columns of $\mathrm{d}_x \varphi(x)^\top$ corresponding to $\varphi^1, \ldots, \varphi^j$, implying that $\nabla_\varphi q(\varphi(x))$ is 0 in the remaining coordinates $\varphi^{j+1}, \ldots, \varphi^k, \bar{\varphi}$. This holds at every $x \in U$, so q is a function only of $\varphi^1, \ldots, \varphi^j$.

For (d), denote $h(\varphi) = f(\theta(\varphi))$. Suppose first that $f \in \mathcal{R}^{\mathsf{G}}$ is a G-invariant polynomial. Since $d_1 + \ldots + d_K = \operatorname{trdeg} \mathcal{R}^{\mathsf{G}}$, we must have that $(\varphi^1, \ldots, \varphi^K, f)$ are algebraically dependent. Then their gradients are linearly dependent at every $x \in U$. Then the same argument as in (c) shows that $h(\varphi)$ depends only on $\varphi^1, \ldots, \varphi^K$. For a general G-invariant continuous function f, let $r > 0$ be large enough such that $U \subset \overline{B_r} = \{x \in \mathbb{R}^d : \|x\| \leq r\}$. For any $\varepsilon > 0$, by the Stone-Weierstrass theorem, there is a polynomial p such that $|p(x) - f(x)| < \varepsilon$ for all $x \in \overline{B_r}$. Applying the Reynolds

operator $\bar{p}(x) = \int p(g \cdot x) \mathrm{d}\Lambda(g)$, we then have $\bar{p} \in \mathcal{R}^{\mathsf{G}}$, and also

$$|\bar{p}(x) - f(x)| = \left| \int \Big(p(g \cdot x) - f(g \cdot x) \Big) \mathrm{d}\Lambda(g) \right| < \varepsilon \quad \text{for all } x \in \overline{B_r}$$

because $g \cdot x \in \overline{B_r}$ for any orthogonal matrix g. Writing $\bar{q}(\varphi) = \bar{p}(\theta(\varphi))$, we have shown that $\bar{q}$ depends only on $\varphi^1, \ldots, \varphi^K$. So for any $\varphi, \varphi' \in \mathbb{R}^d$ differing in only the coordinates of $\bar{\varphi}$, $|h(\varphi) - h(\varphi')| \leq |h(\varphi) - \bar{q}(\varphi)| + |h(\varphi') - \bar{q}(\varphi')| < 2\varepsilon$. Here $\varepsilon > 0$ is arbitrary, so in fact $h(\varphi) = h(\varphi')$. Thus h depends only on $\varphi^1, \ldots, \varphi^K$.

To show (81), clearly if $\mathcal{O}_{\theta'} = \mathcal{O}_\theta$, then $(\varphi^1(\theta'), \ldots, \varphi^K(\theta')) = (\varphi^1(\theta), \ldots, \varphi^K(\theta))$. For the converse direction, if $\mathcal{O}_{\theta'}$ and $\mathcal{O}_\theta$ are distinct, then they are disjoint compact subsets of $\mathbb{R}^d$. Then there is a continuous function $f : \mathbb{R}^d \to \mathbb{R}$ taking value 1 on $\mathcal{O}_{\theta'}$ and 0 on $\mathcal{O}_\theta$. Then $\bar{f}(x) = \int f(g \cdot x) \mathrm{d}\Lambda(g)$ is a G-invariant continuous function with the same property. Thus $\bar{f}$ depends only on $\varphi^1, \ldots, \varphi^K$, implying that $(\varphi^1(\theta'), \ldots, \varphi^K(\theta')) \neq (\varphi^1(\theta), \ldots, \varphi^K(\theta))$. This shows (81), and concludes the proof in the unprojected setting.

The proof in the projected setting is the same, where the condition (4.4) and Proposition 4.2.4 are needed in part (d) to argue that $(\varphi^1, \ldots, \varphi^{\widetilde{K}}, f)$ are algebraically dependent for any $f \in \mathcal{R}^{\mathsf{G}}$. $\square$

Lemma C.1.3. *In the unprojected model, fix any $\theta_* \in \mathbb{R}^d$ and any $k \in \{1, \ldots, K\}$. Let $\tilde{\theta} \in \mathcal{V}_k(\theta_*)$ be such that $\operatorname{rank} \mathrm{d}M_k(\tilde{\theta}) = d_1 + \ldots + d_k$, and let $\varphi = (\varphi^1, \ldots, \varphi^k, \bar{\varphi})$ be the map defined by Lemma C.1.2 with inverse $\theta(\varphi)$ in a neighborhood of $\tilde{\theta}$. Let $s_k(\theta)$ be as defined in (4.7). Then in the parametrization by φ,*

$$\nabla^2_{\varphi^k} s_k(\theta(\varphi))\Big|_{\varphi = \varphi(\tilde{\theta})} \text{ has full rank } d_k \text{ and is positive definite.}$$

In the projected model, the same statements hold for $\widetilde{\mathcal{V}}_k$, $\widetilde{M}_k$, $\tilde{d}_k$, and $\tilde{s}_k$ in place of $\mathcal{V}_k$, M_k, d_k, and s_k.

Proof. We focus on the unprojected model, as the proof in the projected model is the same.

Since s_k is globally minimized at all points of $\mathcal{V}_k(\theta_*)$, we must have $\nabla^2_{\varphi^k} s_k(\theta(\varphi))|_{\varphi = \varphi(\tilde{\theta})} \succeq 0$. To show this has full rank d_k, observe that φ^k consists of a subset of entries of T_k. Thus the corresponding $d_k \times d_k$ submatrix of $\mathrm{d}_{\varphi^k} T_k$ is the identity, so $\mathrm{d}_{\varphi^k} T_k$ has full column rank d_k. Applying the chain rule and the observation $T_k(\tilde{\theta}) - T_k(\theta_*) = 0$, we may differentiate $s_k(\theta(\varphi))$ twice in φ^k to obtain

$$\nabla^2_{\varphi^k} s_k(\theta(\varphi))\Big|_{\varphi = \varphi(\tilde{\theta})} = \frac{1}{k!} \cdot \mathrm{d}_{\varphi^k} T_k(\theta(\varphi))^\top \mathrm{d}_{\varphi^k} T_k(\theta(\varphi))\Big|_{\varphi = \varphi(\tilde{\theta})}.$$

Thus this matrix has full rank d_k. □

Proof of Theorem 4.2.5. Consider the unprojected setting of part (a). For generic $\theta_* \in \mathbb{R}^d$, we have $\operatorname{rank} \mathrm{d}M_K(\theta_*) = d_1 + \ldots + d_K$. Let $\varphi = (\varphi^1, \ldots, \varphi^K, \bar{\varphi})$ be the map defined by Lemma C.1.2, with inverse $\theta(\varphi)$ in a neighborhood U of θ_*. We denote $\varphi_* = \varphi(\theta_*)$. With slight abuse of notation, we write as shorthand $f(\varphi)$ for $f(\theta(\varphi))$. In particular, recalling the expansion (4.6), we denote by $q_k(\varphi), s_k(\varphi), q(\varphi)$ the terms of this expansion parametrized by $\varphi \in \varphi(U)$.

For (a1), observe that by Lemma C.1.2(c–d) and the characterizations of s_k, q_k, q in Theorem 4.2.1, $s_k(\varphi)$ depends only on $\varphi^1, \ldots, \varphi^k$, $q_k(\varphi)$ depends only on $\varphi^1, \ldots, \varphi^{k-1}$, and $q(\varphi)$ depends only on $\varphi^1, \ldots, \varphi^K$. Let us decompose $\nabla^2_\varphi R(\varphi_*)$ into $(K+1) \times (K+1)$ blocks according to the partition $(\varphi^1, \ldots, \varphi^K, \bar{\varphi})$, of sizes $(d_1, \ldots, d_K, d_0)$. Differentiating the expansion (4.6) term-by-term, it then follows that the entries of $\nabla^2_\varphi R(\varphi_*)$ are non-zero only in the upper-left $K \times K$ blocks, and that these blocks have a "graded block structure" as defined in (Fan et al., 2020, Definition 4.14): There is a constant $C > 0$ (independent of σ) for which

$$\|\nabla^2_{\varphi^j, \varphi^k} R(\varphi_*)\| \le C\sigma^{-2\max(j,k)} \text{ for all } j, k = 1, \ldots, K, \tag{82}$$

where $\nabla^2_{\varphi^j, \varphi^k}$ denotes the (φ^j, φ^k) block of the Hessian in φ. Furthermore, as $\nabla^2_{\varphi^k} q_k(\varphi) = 0$ and $\nabla^2_{\varphi^k} s_k(\varphi_*)$ is strictly positive definite by Lemma C.1.3 (applied with $\tilde{\theta} = \theta_*$), there are constants $c, \sigma_0 > 0$ such that for all $\sigma > \sigma_0$,

$$\lambda_{\min}\Big(\nabla^2_{\varphi^k} R(\varphi_*)\Big) \ge c\sigma^{-2k} > 0 \text{ for all } k = 1, \ldots, K. \tag{83}$$

For the Hessian in θ rather than in φ, since $\nabla_\theta R(\theta_*) = 0$, we have by the chain rule

$$I(\theta_*) = \nabla^2_\theta R(\theta_*) = A^\top \cdot \nabla^2_\varphi R(\varphi_*) \cdot A, \qquad A = \mathrm{d}\varphi(\theta_*). \tag{84}$$

By the QR decomposition, there is a non-singular lower-triangular matrix L for which $Q = A^{-1}L$ is orthogonal. Direct calculation shows that for any L which is lower-triangular, $L^\top \cdot \nabla^2_\varphi R(\varphi_*) \cdot L$ also has a graded block structure as characterized by (82–83) in its upper-left $K \times K$ blocks, and equals zero elsewhere, where the constants $C, c > 0$ in (82–83) depend on L but remain independent of σ. Then, by the linear-algebraic result of (Fan et al., 2020, Lemma 4.17), $Q^\top I(\theta_*) Q = L^\mathsf{T} \cdot \nabla^2_\varphi R(\varphi_*) \cdot L$ has d_0 zero eigenvalues and d_k eigenvalues in $[c\sigma^{-2k}, C\sigma^{-2K}]$ for each $k = 1, \ldots, K$. Since Q is orthogonal, these are the same as the eigenvalues of $I(\theta_*)$. This shows (a1).

For (a2), observe that $\nabla_\theta p(\theta_*) = A^\top \nabla_\varphi p(\varphi_*)$ by the chain rule. Combining with (84),

$$\nabla_\theta p(\theta_*)^\top I(\theta_*)^\dagger \nabla_\theta p(\theta_*) = \nabla_\varphi p(\varphi_*)^\top \nabla_\varphi^2 R(\varphi_*)^\dagger \nabla_\varphi p(\varphi_*)$$

Lemma C.1.2(d) shows that p depends only on $\varphi^1, \ldots, \varphi^k$ in the parametrization by φ, so $\nabla_\varphi p(\varphi_*)$ is non-zero only in its first k blocks with respect to the partition $(\varphi^1, \ldots, \varphi^K, \bar{\varphi})$. Then

$$\nabla_\theta p(\theta_*)^\top I(\theta_*)^\dagger \nabla_\theta p(\theta_*) \leq C\sigma^{2k}$$

by the characterization of the maximum eigenvalue of the upper-left $k \times k$ blocks of $\nabla_\varphi^2 R(\varphi_*)^\dagger$ established also in (Fan et al., 2020, Lemma 4.17). If w is in the null space of $I(\theta_*)$, then Aw is in the null space of $\nabla_\varphi^2 R(\varphi_*)$, i.e. Aw is non-zero only in the last block corresponding to $\bar{\varphi}$. Then $\nabla_\theta p(\theta_*)^\top w = \nabla_\varphi p(\varphi_*)^\top Aw = 0$, so $\nabla_\theta p(\theta_*)$ is orthogonal to the null space of $I(\theta_*)$. This shows (a2).

The proof of part (b) in the projected setting is similar: When computing the Hessian of (4.9) in the parametrization by φ term-by-term, there is an additional contribution from the term $\langle \widetilde{T}_k(\varphi), P_k(\varphi) \rangle$. This depends only on $\varphi^1, \ldots, \varphi^k$. Furthermore, its Hessian is the sum of three terms, corresponding to differentiating twice $\widetilde{T}_k(\varphi)$, twice $P_k(\varphi)$, or once each $\widetilde{T}_k(\varphi)$ and $P_k(\varphi)$. The first term vanishes upon evaluating at $\varphi = \varphi_*$, because $P_k(\varphi_*) = 0$ by its characterization in Theorem 4.2.1. The remaining two terms are 0 on the (k, k) block, because $P_k(\varphi)$ depends only on $\varphi^1, \ldots, \varphi^{k-1}$. Thus, $\nabla_\varphi^2 R(\varphi_*)$ still has the graded block structure described by (82–83), and the remainder of the proof is the same as in the unprojected setting of part (a). □

Proof of Lemma 4.2.6. We focus on the unprojected setting, as the proof in the projected setting is the same.

Note that θ_* is a global minimizer of $s_k(\theta)$, so $\nabla_\theta s_k(\theta_*) = 0$ and $\nabla_\theta^2 s_k(\theta_*) \succeq 0$. For generic θ_*, we have $\operatorname{rank} \mathrm{d}M_K(\theta_*) = d_1 + \ldots + d_K$. Let $\varphi = (\varphi^1, \ldots, \varphi^K, \bar{\varphi})$ be the map defined by Lemma C.1.2, with inverse $\theta(\varphi)$ in a neighborhood U of θ_*. Let $\varphi_* = \varphi(\theta_*)$. Then by the chain rule,

$$\nabla_\varphi^2 s_k(\theta(\varphi))\big|_{\varphi=\varphi_*} = \mathrm{d}_\varphi \theta(\varphi_*)^\top \cdot \nabla_\theta^2 s_k(\theta_*) \cdot \mathrm{d}_\varphi \theta(\varphi_*). \tag{85}$$

Since $\mathrm{d}_\varphi \theta(\varphi_*)$ is non-singular, this yields

$$\operatorname{rank}\Big(\nabla_\theta^2 s_1(\theta_*) + \ldots + \nabla_\theta^2 s_k(\theta_*)\Big) = \operatorname{rank}\Big(\nabla_\varphi^2 s_1(\theta(\varphi)) + \ldots + \nabla_\varphi^2 s_k(\theta(\varphi))\Big|_{\varphi=\varphi_*}\Big).$$

Lemma C.1.2(c) ensures that $s_1(\theta(\varphi)), \ldots, s_k(\theta(\varphi))$ depend only on $\varphi^1, \ldots, \varphi^k$, so

$$\operatorname{rank}\left(\nabla^2_\varphi s_1(\theta(\varphi)) + \ldots + \nabla^2_\varphi s_k(\theta(\varphi))\Big|_{\varphi=\varphi_*}\right) \le d_1 + \ldots + d_k = \operatorname{trdeg}(\mathcal{R}^{\mathsf{G}}_{\le k}).$$

Lemma C.1.3 applied with $\tilde\theta = \theta_*$ shows that $\nabla^2_{\varphi_j} s_j(\theta(\varphi))|_{\varphi=\varphi_*} \succ 0$ for each $j = 1, \ldots, k$. Then, since each matrix $\nabla^2_\varphi s_j(\theta(\varphi))$ is also positive semidefinite, this implies $v^\top[\nabla^2_\varphi s_1(\theta(\varphi)) + \ldots + \nabla^2_\varphi s_k(\theta(\varphi))|_{\varphi=\varphi_*}]v > 0$ strictly, for any v supported on the coordinates of $\varphi^1, \ldots, \varphi^k$. So in fact

$$\operatorname{rank}\left(\nabla^2_\varphi s_1(\theta(\varphi)) + \ldots + \nabla^2_\varphi s_k(\theta(\varphi))\Big|_{\varphi=\varphi_*}\right) = d_1 + \ldots + d_k = \operatorname{trdeg}(\mathcal{R}^{\mathsf{G}}_{\le k}).$$

This shows also that the column span of $\nabla^2_\varphi s_1(\theta(\varphi)) + \ldots + \nabla^2_\varphi s_k(\theta(\varphi))|_{\varphi=\varphi_*}$ is exactly the space of vectors v supported on the coordinates of $\varphi^1, \ldots, \varphi^k$. Then by (85), the column span of $\nabla^2_\theta s_1(\theta_*) + \ldots + \nabla^2_\theta s_k(\theta_*)$ is the span of the first $d_1 + \ldots + d_K$ rows of $\mathrm{d}_\varphi\theta(\varphi_*)^{-1} = \mathrm{d}_\theta\varphi(\theta_*)$, which are the gradients $\nabla\varphi^1(\theta_*), \ldots, \nabla\varphi^k(\theta_*)$. By Lemma C.1.2, the span of these gradients is exactly the span of $\{\nabla p(\theta_*) : p \in \mathcal{R}^{\mathsf{G}}_{\le k}\}$, concluding the proof. □

C.1.4 Global landscape

We prove Theorems 4.2.8 and 4.2.10 using ideas similar to (Fan et al., 2020, Sections 4.5–4.6).

Lemma C.1.4. *In the unprojected model, for some constants $M, c, \sigma_0 > 0$ depending on θ_*, G and for all $\sigma > \sigma_0$,*

$$\|\nabla R(\theta)\| \ge c\sigma^{-4} \quad \text{for all } \theta \text{ satisfying } \|\theta\| > M.$$

In the projected model with projection Π, for any $B > 0$, some constants $M, c, \sigma_0 > 0$ depending on $\theta_*, \mathsf{G}, \Pi, B$, and all $\sigma > \sigma_0$,

$$\|\nabla R(\theta)\| \ge c\sigma^{-4} \quad \text{for all } \theta \text{ satisfying } B(\|\theta_*\| + \sigma) > \|\theta\| > M.$$

Proof. The argument is an extension of (Fan et al., 2020, Lemmas 2.10 and 4.19).

Step 1: Forms of $\nabla R(\theta)$. We first consider the projected model, which will reduce to the unprojected model when $\Pi = \mathrm{Id}$. Write $\mathbb{E}_g$ and $\mathbb{E}_{g,g'}$ for expectations over independent group elements $g, g' \sim \Lambda$, and $\mathbb{E}_Y$ for that over the sample $Y \sim p_{\theta_*}$. Introduce the weight

$$p(g, Y) = \frac{\exp\left(-\frac{1}{2\sigma^2}\|Y - \Pi g\theta\|^2\right)}{\mathbb{E}_{g'}\left[\exp\left(-\frac{1}{2\sigma^2}\|Y - \Pi g'\theta\|^2\right)\right]} = \frac{\exp\left(\frac{1}{\sigma^2}Y^\top\Pi g\theta - \frac{1}{2\sigma^2}\|\Pi g\theta\|^2\right)}{\mathbb{E}_{g'}\left[\exp\left(\frac{1}{\sigma^2}Y^\top\Pi g'\theta - \frac{1}{2\sigma^2}\|\Pi g'\theta\|^2\right)\right]}.$$

Then

$$\sigma^2 \nabla R(\theta) = \sigma^2 \nabla_\theta \mathbb{E}_Y[-\log p_\theta(Y)] = -\mathbb{E}_Y\left[\mathbb{E}_g\left[p(g,Y) g^\top \Pi^\top (Y - \Pi g\theta)\right]\right]. \tag{86}$$

We derive a second alternative form for $\sigma^2 \nabla R(\theta)$ using Gaussian integration by parts. Let us represent $Y = \Pi h\theta_* + \sigma\varepsilon$, where $h \sim \Lambda$ and $\varepsilon \sim \mathcal{N}(0, \mathrm{Id})$, and write $\mathbb{E}_Y = \mathbb{E}_{h,\varepsilon}$. Applying the integration by parts identity $\mathbb{E}_{\xi\sim\mathcal{N}(0,1)}[\xi f(\xi)] = \mathbb{E}_{\xi\sim\mathcal{N}(0,1)}[f'(\xi)]$ to each coordinate of ε, we have

$$\begin{aligned}\mathbb{E}_\varepsilon\left[\mathbb{E}_g\left[p(g,Y) g^\top \Pi^\top (\sigma\varepsilon)\right]\right] &= \sigma\, \mathbb{E}_\varepsilon\left[\mathbb{E}_g\left[g^\top \Pi^\top \nabla_\varepsilon p(g,Y)\right]\right] \\ &= \mathbb{E}_\varepsilon\left[\mathbb{E}_g\left[p(g,Y) g^\top \Pi^\top \Pi g\theta\right] - \mathbb{E}_{g,g'}\left[p(g,Y) p(g',Y) g^\top \Pi^\top \Pi g'\theta\right]\right]\end{aligned}$$

where the second line explicitly differentiates $p(g,Y) = p(g, \Pi h\theta_* + \sigma\varepsilon)$ in ε. Then, substituting this for the $g^\top \Pi^\top (\sigma\varepsilon)$ component of $g^\top \Pi^\top Y$ in (86),

$$\sigma^2 \nabla R(\theta) = \mathbb{E}_{h,\varepsilon}\left[\mathbb{E}_{g,g'}\left[p(g,Y) p(g',Y) g^\top \Pi^\top \Pi g'\theta\right] - \mathbb{E}_g\left[p(g,Y) g^\top \Pi^\top \Pi h\theta_*\right]\right]. \tag{87}$$

The expressions (86) and (87) hold also in the unprojected model upon substituting $\Pi = \mathrm{Id}$.

Step 2: Gradient bound for $\|\theta\| \geq B(\|\theta_*\| + \sigma)$. In the unprojected model, fixing a sufficiently large constant $B > 0$, let us first derive a bound $\|\nabla R(\theta)\| \geq c\sigma^{-1}$ for $\|\theta\| \geq B(\|\theta_*\| + \sigma)$. Restricting to $\Pi = \mathrm{Id}$ and taking the inner-product of (86) with θ,

$$\sigma^2 \|\theta\| \cdot \|\nabla R(\theta)\| \geq \sigma^2 \theta^\top \nabla R(\theta) = \|\theta\|^2 - \mathbb{E}_Y\Big[\mathbb{E}_g\Big[p(g,Y)\theta^\top g^\top Y\Big]\Big] \geq \|\theta\|^2 - C(\|\theta_*\| + \sigma)\|\theta\|$$

for a constant $C = C(\theta_*, \mathsf{G}) > 0$. Then for sufficiently large $B > 0$ and large σ, this shows $\|\nabla R(\theta)\| \geq c\sigma^{-1}$ as claimed.

Step 3: Gradient bound for $\|\theta\| \geq C_0\sigma^{2/3}$. We now show, in both the projected and unprojected models, the lower bound $\|\nabla R(\theta)\| \geq c\sigma^{-2}$ when $B(\|\theta_*\| + \sigma) \geq \|\theta\| \geq C_0\sigma^{2/3}$, for a large enough constant $C_0 > 0$ and $\sigma > \sigma_0(\theta_*, \mathsf{G}, \Pi, B)$. The result for the unprojected model follows from specializing the below to $\Pi = \mathrm{Id}$.

Define unit vectors $\bar{\theta} = \theta/\|\theta\|$ and $\bar{Y} = Y/\|Y\|$. Now taking the inner-product of (87) with $\bar{\theta}$,

$$\begin{aligned}\sigma^2\|\nabla R(\theta)\| &\geq \sigma^2 \cdot \bar{\theta}^\top \nabla R(\theta) \\ &= \|\theta\| \cdot \mathbb{E}_{h,\varepsilon}\left[\left\|\mathbb{E}_g\left[p(g,Y)\Pi g\bar{\theta}\right]\right\|^2\right] - \bar{\theta}^\top \mathbb{E}_{h,\varepsilon}\left[\mathbb{E}_g\left[p(g,Y)g^\top \Pi^\top \Pi h\right]\right] \cdot \theta_* \\ &\geq \|\theta\| \cdot \mathbb{E}_{h,\varepsilon}\left[\left(\bar{Y}^\top \mathbb{E}_g\left[p(g,Y)\Pi g\bar{\theta}\right]\right)^2\right] - \|\Pi\|^2 \cdot \|\theta_*\|.\end{aligned}$$

For fixed θ and Y, define

$$K(t) = \log \mathbb{E}_g\left[\exp\left(t\bar{Y}^\top \Pi g\bar{\theta} - \frac{1}{2\sigma^2}\|\Pi g\theta\|^2\right)\right], \qquad t(Y,\theta) = \frac{\|Y\| \cdot \|\theta\|}{\sigma^2}.$$

Then $\bar{Y}^\top \mathbb{E}_g[p(g,Y)\Pi g\bar{\theta}] = \mathbb{E}_g[p(g,Y)\bar{Y}^\top \Pi g\bar{\theta}] = K'(t(Y,\theta))$, so

$$\sigma^2\|\nabla R(\theta)\| \geq \|\theta\| \cdot \mathbb{E}_{h,\varepsilon}\left[K'(t(Y,\theta))^2\right] - \|\Pi\|^2 \cdot \|\theta_*\|. \tag{88}$$

Define a tilted probability distribution $\bar{\Lambda}$ for $g \in \mathsf{G}$, having density $\mathrm{d}\bar{\Lambda}(g) \propto \exp(-\frac{\|\Pi g\theta\|^2}{2\sigma^2})\mathrm{d}\Lambda(g)$ with respect to the Haar measure Λ. Note that for $\|\theta\| < B(\|\theta_*\| + \sigma)$, this tilting satisfies

$$\frac{\mathrm{d}\bar{\Lambda}}{\mathrm{d}\Lambda}(g) \in [c, C] \tag{89}$$

for some $(\theta_*, \mathsf{G}, \Pi, B)$-dependent constants $C, c > 0$. Observe that $K(t) - K(0)$ is the cumulant generating function for the law of $\bar{Y}^\top \Pi g\bar{\theta}$ (fixing $\bar{Y}$) that is induced by $g \sim \bar{\Lambda}$. This random variable $\bar{Y}^\top \Pi g\bar{\theta}$ is bounded as $|\bar{Y}^\top \Pi g\bar{\theta}| \leq \|\Pi\|$, so for $|t| < 1/(\|\Pi\|e)$, $K(t) - K(0)$ is defined equivalently by the convergent cumulant series

$$K(t) - K(0) = \sum_{\ell \geq 1} \kappa_\ell(\bar{Y}^\top \Pi g\bar{\theta})\frac{t^\ell}{\ell!}$$

where $\kappa_\ell = \kappa_\ell(\bar{Y}^\top \Pi g\bar{\theta})$ is the ℓ^{th} cumulant of $\bar{Y}^\top \Pi g\bar{\theta}$ under this law—see (Fan et al., 2020, Lemma A.1). Then for any $0 < t < 1/(\|\Pi\|e)$, applying $|\kappa_\ell| \leq (\|\Pi\|\ell)^\ell$ from (Fan et al., 2020, Lemma A.1), $\ell! \geq (\ell/e)^\ell$, and convexity of the cumulant generating function $K(t)$,

$$K'(t) \geq \frac{K(t) - K(0)}{t} = \sum_{\ell \geq 1} \kappa_\ell \frac{t^{\ell-1}}{\ell!} \geq \kappa_1 + \frac{t}{2}\kappa_2 - \sum_{\ell \geq 3}(\|\Pi\|e)^\ell t^{\ell-1}. \tag{90}$$

We now lower-bound the mean and variance κ_1, κ_2 when $\bar{Y}$ belongs to some "good" subset U of the unit sphere: First note that for any non-zero $\theta \in \mathbb{R}^d$, $\Pi g\theta$ cannot be identically 0 over all

$g \in \mathsf{G}$. This is because otherwise, $\Pi(\mathcal{O}_{\theta_*}) \equiv \Pi(\mathcal{O}_{\theta_*+c\theta})$ for any $\theta_* \in \mathbb{R}^d$ and any $c \in \mathbb{R}$, where $\{\mathcal{O}_{\theta_*+c\theta} : c \in \mathbb{R}\}$ is an infinite family of distinct orbits, violating (4.4). Thus,

$$\sup_{\bar{y}:\|\bar{y}\|=1} \sup_{g\in\mathsf{G}} \bar{y}^\top \Pi g\bar{\theta} > 0 \text{ for all unit vectors } \bar{\theta}$$

By continuity of the left side as a function of $\bar{\theta}$ and by compactness of the unit sphere, there is then a constant $c = c(\Pi, \mathsf{G}) > 0$ such that

$$\sup_{\bar{y}:\|\bar{y}\|=1} \sup_{g\in\mathsf{G}} \bar{y}^\top \Pi g\bar{\theta} > c \text{ for all unit vectors } \bar{\theta}.$$

Let Γ denote the uniform probability measure on the unit sphere. Then the above implies

$$\Gamma \times \Lambda\Big((\bar{y}, g) : \bar{y}^\top \Pi g\bar{\theta} > c\Big) > 0 \text{ for all unit vectors } \bar{\theta}.$$

Again by continuity of the left side as a function of $\bar{\theta}$ and by compactness of the unit sphere, there is a constant $\delta = \delta(\Pi, \mathsf{G}) > 0$ such that

$$\Gamma \times \Lambda\Big((\bar{y}, g) : \bar{y}^\top \Pi g\bar{\theta} > c\Big) > \delta \text{ for all unit vectors } \bar{\theta}.$$

Then by (89), for a constant $\delta' = \delta'(\theta_*, \Pi, \mathsf{G}, B)$, we get $\Gamma \times \bar{\Lambda}((\bar{y}, g) : \bar{y}^\top \Pi g\bar{\theta} > c) > \delta'$. Define the $\bar{\theta}$-dependent subset of the unit sphere

$$U' = \Big\{\bar{y} : \bar{\Lambda}(g \in \mathsf{G} : \bar{y}^\top \Pi g\bar{\theta} > c) > \delta'/2\Big\}.$$

Then the above implies $\Gamma(U') + (\delta'/2)(1 - \Gamma(U')) > \delta'$, so $\Gamma(U') > \delta'/2$. If any random variable $X \in \mathbb{R}$ satisfies $\mathbb{P}[X > c] > \delta'/2$, then $\max(\mathbb{E}[X], \mathrm{Var}[X]) > c'$ for a constant $c' = c'(c, \delta') > 0$, and furthermore either $\mathbb{E}[X] \geq 0$ or $\mathbb{E}[-X] \geq 0$. Thus, defining U from U' by multiplying each element $\bar{y} \in U'$ by an appropriate choice of $\pm$ sign, we obtain $\Gamma(U) > \delta'/4$ and

$$\max\Big(\kappa_1(\bar{Y}^\top \Pi g\bar{\theta}), \kappa_2(\bar{Y}^\top \Pi g\bar{\theta})\Big) > c' \text{ and } \kappa_1(\bar{Y}^\top \Pi g\bar{\theta}), \kappa_2(\bar{Y}^\top \Pi g\bar{\theta}) \geq 0 \text{ whenever } \bar{Y} \in U. \quad (91)$$

Recalling that $Y = \Pi h\theta_* + \sigma\varepsilon$ and $\bar{Y} = Y/\|Y\|$, the law of $\bar{Y}$ converges to the uniform measure Γ on the sphere as $\sigma \to \infty$. Thus, for $\sigma > \sigma_0(\Pi, \mathsf{G}, \theta_*, B)$, we have $\mathbb{P}[\bar{Y} \in U] \geq \Gamma(U)/2 > \delta'/8$. For $C_0 = C_0(\Pi, \mathsf{G}, \theta_*, B) > 0$ large enough, if $\|\theta\| \geq C_0\sigma^{2/3}$, then $t(Y, \theta) \geq \sigma^{-1/3}$ with probability at least $1 - \delta'/16$. Then, on an event of probability at least $\delta'/16$ where $\bar{Y} \in U$ and $t(Y, \theta) \geq \sigma^{-1/3}$,

and for $\sigma > \sigma_0(\Pi, \mathsf{G}, \theta_*, B)$, we have

$$K'(t(Y,\theta)) \geq K'(\sigma^{-1/3}) \geq (c'/3)\sigma^{-1/3},$$

the first inequality applying convexity of $K(t)$ and the second applying (90) with the bound (91). Then, applying this to (88),

$$\sigma^2 \|\nabla R(\theta)\|^2 \geq C_0 \sigma^{2/3} \cdot (\delta'/16) \cdot (c'/3)^2 \sigma^{-2/3} - \|\Pi\|^2 \cdot \|\theta_*\|.$$

Here, the constants $c', \delta' > 0$ are as defined in the argument leading to (91), and do not depend on C_0. Thus, for $C_0 = C_0(\Pi, \mathsf{G}, \theta_*, B)$ large enough, we have $\|\nabla R(\theta)\|^2 \geq c\sigma^{-2}$ as desired.

Step 4: Gradient bound for $\|\theta\| > M$. Finally, we show $\|\nabla R(\theta)\| \geq c\sigma^{-4}$ for $C_0\sigma^{2/3} \geq \|\theta\| > M$ and a sufficiently large constant $M > 0$. Define $v = (\theta - \theta_*)/\|\theta - \theta_*\|$, and suppose first that $\|\mathbb{E}_g[\Pi g v]\| \geq c_0$ for a constant $c_0 > 0$ to be determined. We apply Theorem 4.2.1(b) with $K = 1$. Noting that $P_1(\theta) = 0$ (because it is a constant that is 0 at $\theta = \theta_*$) and $q_1(\theta)$ is a constant,

$$\nabla R(\theta) = \frac{1}{\sigma^2} \nabla \tilde{s}_1(\theta) + \nabla q(\theta), \qquad \|\nabla q(\theta)\| \leq \frac{C\|\theta\|^3}{\sigma^4}.$$

Applying the form of $\tilde{s}_1(\theta)$ in Lemma C.1.1,

$$\nabla R(\theta) = \frac{1}{\sigma^2} \mathbb{E}_{g,h}[g^\top \Pi^\top \Pi h](\theta - \theta_*) + \nabla q(\theta).$$

Then

$$\sigma^2 \|\nabla R(\theta)\| \geq \sigma^2 \, v^\top \nabla R(\theta) \geq \|\theta - \theta_*\| \cdot \|\mathbb{E}_g[\Pi g v]\|^2 - C\|\theta\|^3/\sigma^2.$$

When $C_0\sigma^{2/3} \geq \|\theta\| > M$ and $M = M(C_0, c_0, \Pi, \theta_*)$ is large enough, this is lower-bounded by a positive constant, so $\|\nabla R(\theta)\| \geq c\sigma^{-2}$.

Now suppose $\|\mathbb{E}_g[\Pi g \bar{\theta}]\| < c_0$. We apply Theorem 4.2.1(b) with $K = 2$. Then similarly,

$$\sigma^4 \|\nabla R(\theta)\| \geq \sigma^4 \, v^\top \nabla R(\theta) \geq v^\top \nabla \tilde{s}_2(\theta) + v^\top \nabla [\langle \widetilde{T}_2(\theta), P_2(\theta) \rangle] + v^\top \nabla q_2(\theta) - C\|\theta\|^5/\sigma^2,$$

where we have applied $v^\top \nabla \tilde{s}_1(\theta) \geq 0$ as shown above to drop the contribution from the $k = 1$ term.

We bound each expression on the right side: First, applying the form of $\tilde{s}_2(\theta)$ in Lemma C.1.1,

$$\begin{aligned} v^\top \nabla \tilde{s}_2(\theta) &= v^\top \mathbb{E}_{g,h}\Big[g^\top \Pi^\top \Pi h\theta \cdot \theta^\top g^\top \Pi^\top \Pi h\theta - g^\top \Pi^\top \Pi h\theta_* \cdot \theta^\top g^\top \Pi^\top \Pi h\theta_*\Big] \\ &\geq \|\theta - \theta_*\|^3 \cdot \mathbb{E}_{g,h}[(v^\top g^\top \Pi^\top \Pi h v)^2] - C\|\theta\|^2, \end{aligned}$$

where the second line is obtained by writing each θ as $(\theta - \theta_*) + \theta_*$ and absorbing all but the term with cubic dependence on $(\theta - \theta_*)$ into the $C\|\theta\|^2$ remainder. As noted in Step 2 above, $\Pi g v$ is not identically 0 over $g \in \mathsf{G}$, for any unit vector v. Then $(v^\top g^\top \Pi^\top \Pi h v)^2$ is the squared-inner product between two i.i.d. non-zero vectors, and hence is strictly positive with positive probability. So $\mathbb{E}_{g,h}[(v^\top g^\top \Pi^\top \Pi h v)^2] > 0$. Then by compactness of the unit sphere, $\mathbb{E}_{g,h}[(v^\top g^\top \Pi^\top \Pi h v)^2] > c > 0$ for every unit vector v and some constant $c = c(\Pi, \mathsf{G}) > 0$. So for $\|\theta\| > M$ and large enough $M = M(\Pi, G, \theta_*)$, this shows

$$v^\top \nabla \tilde{s}_2(\theta) \geq (c/2)\|\theta\|^3.$$

Next, consider $v^\top \nabla q_2(\theta)$. Since $q_2 \in \widetilde{\mathcal{R}}^{\mathsf{G}}_{\leq 1}$ which is generated by $\widetilde{T}_1(\theta) = \mathbb{E}_g[\Pi g\theta]$, $q_2(\theta)$ is a quartic polynomial of the entries of $\mathbb{E}_g[\Pi g\theta]$, whose specific form depends only on $\Pi, \mathsf{G}, \theta_*$. Then by the chain rule,

$$\big|v^\top \nabla q_2(\theta)\big| \leq \|\nabla q_2(\theta)\| \leq C(\|\mathbb{E}_g[\Pi g\theta]\|^3 + 1) \leq C((c_0\|\theta - \theta_*\| + \|\Pi\|\|\theta_*\|)^3 + 1) \leq C'(c_0^3\|\theta\|^3 + 1)$$

for constants $C = C(\Pi, \mathsf{G}, \theta_*)$ and $C' = C'(\Pi, \mathsf{G}, \theta_*)$. Similarly, consider $v^\top \nabla[\langle \widetilde{T}_2(\theta), P_2(\theta)\rangle]$. Each entry of $P_2(\theta)$ is a quadratic polynomial of $\mathbb{E}_g[\Pi g\theta]$. Noting that $\widetilde{T}_2(\theta)$ is also quadratic in θ, again by the chain rule,

$$\big|v^\top \nabla[\langle \widetilde{T}_2(\theta), P_2(\theta)\rangle]\big| \leq C(\|\mathbb{E}_g[\Pi g\theta]\| \cdot \|\theta\|^2 + \|\mathbb{E}_g[\Pi g\theta]\|^2 \cdot \|\theta\| + \|\theta\|^2) \leq C'(c_0\|\theta\|^3 + \|\theta\|^2).$$

Finally, we may bound $\|\theta\|^5/\sigma^2 \leq \|\theta\|^3 \cdot C_0^2\sigma^{-2/3}$. Combining all of the above, for sufficiently small $c_0 > 0$, sufficiently large $M = M(\Pi, G, \theta_*) > 0$, and sufficiently large $\sigma > \sigma_0$, we obtain that $\sigma^4\|\nabla R(\theta)\|$ is lower-bounded by a constant, so $\|\nabla R(\theta)\| \geq c\sigma^{-4}$ as desired. □

Proof of Theorem 4.2.8. Consider the unprojected setting of part (a). Fixing a generic point $\theta_* \in \mathbb{R}^d$, Lemma C.1.2 shows that for any $k = 1, \ldots, K$, the rank of $\mathrm{d}M_k(\theta_*)$ is $d_1 + \ldots + d_k$. Then by the assumption that $\mathrm{d}M_k(\theta)$ has constant rank over $\mathcal{V}_k(\theta_*)$, since $\theta_* \in \mathcal{V}_k(\theta_*)$, this constant rank must be $d_1 + \ldots + d_k$.

We now consider two cases for a (possibly non-generic) point $\tilde{\theta} \in \mathbb{R}^d$:

- $\tilde{\theta} \in \mathcal{V}_{k-1}(\theta_*) \subseteq \ldots \subseteq \mathcal{V}_0(\theta_*) = \mathbb{R}^d$, but $\tilde{\theta} \notin \mathcal{V}_k(\theta_*)$, for some $k \in \{1, \ldots, K\}$. By the constant rank assumption, $\mathrm{d}M_{k-1}(\tilde{\theta})$ has rank $d_1 + \ldots + d_{k-1}$. Let $\varphi = (\varphi^1, \ldots, \varphi^{k-1}, \bar{\varphi})$ be the map of Lemma C.1.2, with inverse $\theta(\varphi)$ in a neighborhood $U_{\tilde{\theta}}$ of $\tilde{\theta}$. (If $k = 1$, we take $\varphi = \bar{\varphi} : \mathbb{R}^d \to \mathbb{R}^d$ to be an arbitrary invertible map, say the identity map.) We write $f(\varphi)$ as shorthand for $f(\theta(\varphi))$.

  In the parametrization by φ, each entry of $T_1, \ldots, T_{k-1}$ depends only on the coordinates $\varphi^1, \ldots, \varphi^{k-1}$, by Lemma C.1.2(c). Thus

$$\mathcal{V}_{k-1}(\theta_*) \cap U_{\tilde{\theta}} = \Big\{\theta \in U_{\tilde{\theta}} : \varphi^1(\theta) = \varphi^1(\theta_*), \ldots, \varphi^{k-1}(\theta) = \varphi^{k-1}(\theta_*)\Big\},$$

  and the remaining coordinates $\bar{\varphi}$ form a local chart for the manifold $\mathcal{V}_{k-1}(\theta_*)$ over $U_{\tilde{\theta}}$. This holds trivially also for $k = 1$.

  Consider now the minimization of s_k over $\mathcal{V}_{k-1}(\theta_*)$. By the form of s_k in (4.7), its global minimizers over $\mathcal{V}_{k-1}(\theta_*)$ are exactly the points of $\mathcal{V}_k(\theta_*)$. Since $\tilde{\theta} \notin \mathcal{V}_k(\theta_*)$, and the minimization of s_k over $\mathcal{V}_{k-1}(\theta_*)$ is globally benign by assumption, this implies that

$$\text{either} \qquad \nabla_{\bar{\varphi}} s_k(\varphi(\tilde{\theta})) \neq 0 \qquad \text{or} \qquad \lambda_{\min}\Big(\nabla^2_{\bar{\varphi}} s_k(\varphi(\tilde{\theta}))\Big) < 0.$$

  Applying continuity of s_k and its derivatives, and reducing the size of $U_{\tilde{\theta}}$ as necessary, we may then ensure

$$\text{either} \quad \|\nabla_{\bar{\varphi}} s_k(\varphi)\| > c \quad \text{or} \quad \lambda_{\min}\Big(\nabla^2_{\bar{\varphi}} s_k(\varphi)\Big) < -c \quad \text{for all } \varphi \in \varphi(U_{\tilde{\theta}}).$$

  Here, the size of the neighborhood $U_{\tilde{\theta}}$ and the constant $c > 0$ are independent of σ, as s_k does not depend on σ. Now differentiating (4.6) term-by-term in $\varphi = (\varphi^1, \ldots, \varphi^{k-1}, \bar{\varphi})$, and observing that $\{s_j : j \leq k-1\}$ and $\{q_j : j \leq k\}$ depend only on $(\varphi^1, \ldots, \varphi^{k-1})$ and not on $\bar{\varphi}$, we obtain that for some constant $\sigma_0 = \sigma_0(\tilde{\theta}) > 0$, all $\sigma > \sigma_0$, and all $\varphi \in \varphi(U_{\tilde{\theta}})$,

$$\text{either} \quad \|\nabla_{\varphi} R(\varphi)\| > (c/2)\sigma^{-2k} \quad \text{or} \quad \lambda_{\min}\Big(\nabla^2_{\varphi} R(\varphi)\Big) < -(c/2)\sigma^{-2k}. \tag{92}$$

Finally, changing variables back to θ by the chain rule, this implies

$$\text{either} \quad \nabla_\theta R(\theta) \neq 0 \quad \text{or} \quad \lambda_{\min}\Big(\nabla^2_\theta R(\theta)\Big) < 0 \qquad \text{for all } \theta \in U_{\tilde\theta}. \tag{93}$$

- $\tilde\theta \in \mathcal{V}_K(\theta_*)$. By the constant rank assumption, $\mathrm{d}M_K(\tilde\theta) = d_1 + \ldots + d_K$. Let $\varphi = (\varphi^1, \ldots, \varphi^K, \bar\varphi)$ be the map of Lemma C.1.2 in a neighborhood $U_{\tilde\theta}$ of $\tilde\theta$, with inverse $\theta(\varphi)$. We again write as shorthand $f(\varphi) = f(\theta(\varphi))$.

  Let us write $\nabla^2_\varphi R(\varphi)$ in the $(K+1) \times (K+1)$ block decomposition corresponding to $(\varphi^1, \ldots, \varphi^K, \bar\varphi)$. In (4.6), each $s_k(\varphi)$ depends only on $\varphi^1, \ldots, \varphi^k$, each $q_k(\varphi)$ depends only on $\varphi^1, \ldots, \varphi^{k-1}$, and $q(\varphi)$ and $R(\varphi)$ depend only on $\varphi^1, \ldots, \varphi^K$. Furthermore, Lemma C.1.3 shows $\nabla^2_{\varphi^k} s_k(\varphi(\tilde\theta)) \succ 0$ strictly for each $k = 1, \ldots, K$, so $\nabla^2_{\varphi^k} s_k(\varphi) \succ c\,\mathrm{Id}$ for all $\varphi \in \varphi(U_{\tilde\theta})$ by continuity, for a sufficiently small neighborhood $U_{\tilde\theta}$ and constant $c > 0$. Then differentiating (4.6) term-by-term, $\nabla^2_\varphi R(\varphi)$ is zero outside the upper-left $K \times K$ blocks, and these $K \times K$ blocks have the graded block structure

$$\|\nabla^2_{\varphi_j, \varphi_k} R(\varphi)\| \leq C\sigma^{-2\max(j,k)} \text{ for all } j, k = 1, \ldots, K,$$

$$\lambda_{\min}\Big(\nabla^2_{\varphi_k} R(\varphi)\Big) \geq c\sigma^{-2k} > 0 \text{ for all } k = 1, \ldots, K \tag{94}$$

  at every point $\varphi \in \varphi(U_{\tilde\theta})$ and for some constants $C, c > 0$ and all $\sigma > \sigma_0 = \sigma_0(\tilde\theta)$. Then, applying (Fan et al., 2020, Lemma 4.17), the upper-left $K \times K$ blocks of $\nabla^2_\varphi R(\varphi)$ form a strictly positive-definite matrix. Recalling that $R(\varphi)$ depends only on $\varphi^1, \ldots, \varphi^K$ and not on $\bar\varphi$, let us write $\bar R(\varphi^1, \ldots, \varphi^K) = R(\varphi)$, and also reduce to a smaller neighborhood $U_{\tilde\theta}$ such that $\varphi(U_{\tilde\theta})$ has a product form $V \times W$, where $V \subset \mathbb{R}^{d_1 + \ldots + d_K}$ and $W \subset \mathbb{R}^{d_0}$. Then this shows that

$$\bar R(\varphi^1, \ldots, \varphi^K) \text{ is strictly convex on } V. \tag{95}$$

  Now applying the assumption that $\mathcal{V}_K(\theta_*) = \mathcal{O}_{\theta_*}$, we have that $\tilde\theta \in \mathcal{O}_{\theta_*}$ is a global minimizer of $R(\theta)$. Thus $(\varphi^1(\tilde\theta), \ldots, \varphi^K(\tilde\theta))$ is the global minimizer and unique critical point of $\bar R$ on V. Changing coordinates back to θ by the chain rule, the critical points of $R(\theta)$ on $U_{\tilde\theta}$ are then given exactly by

$$\Big\{\theta \in U_{\tilde\theta} : (\varphi^1(\theta), \ldots, \varphi^K(\theta)) = (\varphi^1(\tilde\theta), \ldots, \varphi^K(\tilde\theta))\Big\}.$$

Applying (81), this shows

$$\Big\{\theta \in U_{\tilde\theta} : \nabla R(\theta) = 0\Big\} = U_{\tilde\theta} \cap \mathcal{O}_{\tilde\theta} = U_{\tilde\theta} \cap \mathcal{O}_{\theta_*} \tag{96}$$

Finally, we combine these two cases using a compactness argument: By Lemma C.1.4, there are no critical points of $R(\theta)$ outside a sufficiently large ball $\overline{B_M} = \{\theta : \|\theta\| \le M\}$. For each point $\tilde\theta \in \overline{B_M}$, construct the neighborhood $U_{\tilde\theta}$ as above, and take a finite set S of such points $\tilde\theta$ for which $\bigcup_{\tilde\theta\in S} U_{\tilde\theta}$ covers $\overline{B_M}$. Set $\sigma_0 = \max_{\tilde\theta\in S}\sigma_0(\tilde\theta)$, where $\sigma_0(\tilde\theta)$ is as defined in the two cases above. Then for any $\sigma > \sigma_0$, the conditions (93) and (96) combine to show that any critical point of $R(\theta)$ inside $\overline{B_M}$ either belongs to the locus $\mathcal{O}_{\theta_*}$ of global minimizers, or has $\lambda_{\min}(\nabla^2 R(\theta)) < 0$. Thus the minimization of $R(\theta)$ is globally benign, concluding the proof of part (a).

The proof in the projected model in part (b) is similar, with the following minor modifications: For the first case where $\tilde\theta \in \widetilde{\mathcal{V}}_{k-1}(\theta_*) \subseteq \ldots \subseteq \widetilde{\mathcal{V}}_0(\theta_*) = \mathbb{R}^d$ but $\tilde\theta \notin \widetilde{\mathcal{V}}_k(\theta_*)$, Lemma C.1.2 still yields a local parametrization $\varphi = (\varphi^1, \ldots, \varphi^{k-1}, \bar\varphi)$ where $\bar\varphi$ forms a local chart for $\widetilde{V}_{k-1}(\theta_*)$. Differentiating (4.9) instead of (4.6) term-by-term in $\varphi = (\varphi^1, \ldots, \varphi^{k-1}, \bar\varphi)$, the gradient and Hessian of $R(\varphi)$ in $\bar\varphi$ have an additional $O(\sigma^{-2k})$ contribution from $\langle \widetilde{T}_k(\varphi), P_k(\varphi)\rangle$. Since P_k depends only on $\varphi^1, \ldots, \varphi^{k-1}$ and not on $\bar\varphi$, the gradient and Hessian in $\bar\varphi$ are obtained by differentiating only $\widetilde{T}_k$. Then both $\nabla_{\bar\varphi}[\langle \widetilde{T}_k(\varphi), P_k(\varphi)\rangle]|_{\varphi=\varphi(\tilde\theta)} = 0$ and $\nabla^2_{\bar\varphi}[\langle \widetilde{T}_k(\varphi), P_k(\varphi)\rangle]|_{\varphi=\varphi(\tilde\theta)} = 0$, because $P_k(\tilde\theta) = P_k(\theta_*) = 0$ for any $\tilde\theta \in \mathcal{V}_{k-1}(\theta_*)$. Then by continuity, for a sufficiently small neighborhood $U_{\tilde\theta}$, we still obtain (92) for all $\varphi \in \varphi(U_{\tilde\theta})$, and hence (93) still holds.

For the second case where $\tilde\theta \in \widetilde{\mathcal{V}}_{\widetilde{K}}(\theta_*)$, similarly when computing the Hessian of (4.9) in $\varphi = (\varphi^1, \ldots, \varphi^{\widetilde{K}}, \bar\varphi)$ term-by-term, each k^{th} row block and column block of the Hessian, corresponding to the variables φ^k, has an additional $O(\sigma^{-2k})$ contribution from differentiating $\langle \widetilde{T}_k(\varphi), P_k(\varphi)\rangle$. For the (k,k) block corresponding to $\nabla^2_{\varphi^k} R(\varphi)$, we again have $\nabla^2_{\varphi^k}[\langle \widetilde{T}_k(\varphi), P_k(\varphi)\rangle]|_{\varphi=\varphi(\tilde\theta)} = 0$, because only $\widetilde{T}_k$ depends on φ^k whereas $P_k(\tilde\theta) = P_k(\theta_*) = 0$. Then again by continuity, we still obtain (94) and hence (95) over a sufficiently small neighborhood $U_{\tilde\theta}$ of $\tilde\theta$. Now by the assumption given in part (b) of the theorem, we have $\Pi(\mathcal{O}_{\tilde\theta}) \equiv \Pi(\mathcal{O}_{\theta_*})$ for $\tilde\theta \in \widetilde{\mathcal{V}}_{\widetilde{K}}(\theta_*)$. Then $\tilde\theta$ is a global minimizer of $R(\theta)$. As in the analysis of the unprojected case, the convexity of (95) then implies $\{\theta \in U_{\tilde\theta} : \nabla R(\theta) = 0\} = U_{\tilde\theta} \cap \mathcal{O}_{\tilde\theta}$. Over the given domain $\{\theta : \|\theta\| < B(\|\theta_*\| + \sigma)\}$, Lemma C.1.4 ensures that there are no critical points of $R(\theta)$ outside the smaller ball $\{\theta : \|\theta\| \le M\}$, which is independent of σ. We conclude the proof by applying the same compactness argument over $\{\theta : \|\theta\| \le M\}$ as in the unprojected case. $\square$

Proof of Theorem 4.2.10. Consider the unprojected setting of part (a). Fix a generic point $\theta_* \in \mathbb{R}^d$. Lemma C.1.2 shows that $\operatorname{rank} \mathrm{d}M_k(\theta_*) = d_1 + \ldots + d_k$ for each $k = 1, \ldots, K$. Then the given constant rank assumption ensures that $\operatorname{rank} \mathrm{d}M_k(\theta) = d_1 + \ldots + d_k$ for all $\theta \in \mathcal{V}_k(\theta_*)$ and $k = 1, \ldots, K-1$.

Statement (a2) is established by a small extension of the argument in Theorem 4.2.8: Lemma C.1.4 ensures that all critical points of $R(\theta)$ in the given domain $\{\theta : \|\theta\| < B(\|\theta_*\| + \sigma)\}$ belong to the ball $\overline{B_M} = \{\theta : \|\theta\| \le M\}$. Fix any constant $\varepsilon > 0$, and let $N_{\varepsilon,M}$ be the points in $\overline{B_M}$ at distance $\ge \varepsilon$ from all critical points of $s_K(\theta)|_{\mathcal{V}_{K-1}(\theta_*)}$. We consider two cases for a point $\tilde{\theta} \in N_{\varepsilon,M}$:

- $\tilde{\theta} \in \mathcal{V}_{k-1}(\theta_*) \subseteq \ldots \subseteq \mathcal{V}_0(\theta_*)$, but $\tilde{\theta} \notin \mathcal{V}_k(\theta_*)$, for some $k \in \{1, \ldots, K-1\}$. Then we have

$$\text{either} \quad \nabla_\theta R(\theta) \neq 0 \quad \text{or} \quad \lambda_{\min}\Big(\nabla^2_\theta R(\theta)\Big) < 0 \qquad \text{for all } \theta \in U_{\tilde{\theta}}$$

  by the same argument as leading to (93) in Theorem 4.2.8.

- $\tilde{\theta} \in \mathcal{V}_{K-1}(\theta_*)$. Then Lemma C.1.2 provides a local reparametrization $\varphi = (\varphi^1, \ldots, \varphi^{K-1}, \bar{\varphi})$ on a neighborhood $U_{\tilde{\theta}}$ of $\tilde{\theta}$, where $\varphi^j : \mathbb{R}^d \to \mathbb{R}^{d_j}$ and T_j depends only on $(\varphi^1, \ldots, \varphi^j)$ for each $j = 1, \ldots, K-1$. Then $\bar{\varphi}$ forms a local chart for $\mathcal{V}_{K-1}(\theta_*)$ at $\tilde{\theta}$. Let $\tilde{\varphi} = \varphi(\tilde{\theta})$.

  If $\nabla_{\bar{\varphi}} s_K(\tilde{\varphi}) = 0$, then $\tilde{\theta}$ is a critical point of $s_K|_{\mathcal{V}_{K-1}(\theta_*)}$, which by the given assumption must be non-degenerate up to orbit. Hence $\mathcal{O}_{\tilde{\theta}}$ is locally a manifold of dimension d_0 at $\tilde{\theta}$, so we may choose the parametrization $\bar{\varphi}$ above to have a decomposition $\bar{\varphi} = (\varphi^K, \varphi^0)$, where φ^0 has d_0 coordinates forming a local chart for $\mathcal{O}_{\tilde{\theta}}$, and φ^K has d_K remaining coordinates. Since s_K is constant over $\mathcal{O}_{\tilde{\theta}}$, we must have $\nabla_{\varphi^0} s_K = 0$, so s_K depends only on φ^K and not on φ^0 in this chart $\bar{\varphi} = (\varphi^K, \varphi^0)$ for $\mathcal{V}_{K-1}(\theta_*)$. Then non-degeneracy of $\tilde{\theta}$ up to orbit further implies that $\nabla^2_{\varphi^K} s_K(\tilde{\varphi})$ is a $d_K \times d_K$ matrix of full rank d_K. If this were positive definite, then $\tilde{\theta}$ would be a local minimizer of s_K on $\mathcal{V}_{K-1}(\theta_*)$, but we have assumed $\tilde{\theta} \in N_{\varepsilon,M}$ which does not include such local minimizers. Therefore $\nabla^2_{\varphi^K} s_K(\tilde{\varphi})$ must have a negative eigenvalue. This shows that

$$\text{either} \quad \nabla_{\bar{\varphi}} s_K(\tilde{\varphi}) \neq 0 \quad \text{or} \quad \lambda_{\min}\Big(\nabla^2_{\bar{\varphi}} s_K(\tilde{\varphi})\Big) < 0.$$

  Thus, differentiating (4.6) term-by-term in $\varphi = (\varphi^1, \ldots, \varphi^{K-1}, \bar{\varphi})$, also in this case

$$\text{either} \quad \nabla_\theta R(\theta) \neq 0 \quad \text{or} \quad \lambda_{\min}\Big(\nabla^2_\theta R(\theta)\Big) < 0 \qquad \text{for all } \theta \in U_{\tilde{\theta}}.$$

Taking a finite cover of $N_{\varepsilon,M}$ by such neighborhoods $U_{\tilde{\theta}}$, this shows that for any $\varepsilon > 0$ and all $\sigma > \sigma_0(\varepsilon)$, all local minimizers of $R(\theta)$ must be ε-close to some local minimizer of $s_K(\theta)$ on $\mathcal{V}_{K-1}(\theta_*)$.

Then there exists a slowly decreasing sequence $\varepsilon(\sigma) \to 0$ as $\sigma \to \infty$, for which all local minimizers of $R(\theta)$ are $\varepsilon(\sigma)$-close to a local minimizer of $s_K(\theta)$, for all σ. This establishes (a2). The proof of (b2) in the projected setting is the same, with the modifications as described at the end of the proof of Theorem 4.2.8.

We now show the converse direction (a1). Let $\tilde{\theta}$ be a local minimizer of $s_K|_{\mathcal{V}_{K-1}(\theta_*)}$ that is non-degenerate up to orbit. By Lemma C.1.2 and the same argument as above, there is a local reparametrization $\varphi = (\varphi^1, \ldots, \varphi^{K-1}, \varphi^K, \varphi^0)$ on a neighborhood $U_{\tilde{\theta}}$ of $\tilde{\theta}$ such that $T_k(\varphi)$ depends only on $\varphi^1, \ldots, \varphi^k$ for each $k = 1, \ldots, K-1$, and $s_K(\varphi)$ and $R(\varphi)$ depend only on $\varphi^1, \ldots, \varphi^K$. Let $\tilde{\varphi} = \varphi(\tilde{\theta})$. For $k = 1, \ldots, K-1$, some constant $c > 0$, and all $\varphi \in \varphi(U_{\tilde{\theta}})$,

$$\lambda_{\min}\Big(\nabla^2_{\varphi^k} s_k(\varphi)\Big) > c \tag{97}$$

by Lemma C.1.3 and continuity of this Hessian. This holds also for $k = K$, by the non-degeneracy of $\tilde{\theta}$ up to orbit. Then, writing the Hessian $\nabla^2_{\varphi} R(\varphi)$ in the $(K+1) \times (K+1)$ block structure corresponding to $(\varphi^1, \ldots, \varphi^K, \varphi^0)$, we obtain as in Theorem 4.2.8 that the upper-left $K \times K$ blocks have a graded block structure, in a sufficiently small neighborhood $U_{\tilde{\theta}}$ where $\varphi(U_{\tilde{\theta}}) = V \times W$ has a product form. So, defining $\bar{R}(\varphi^1, \ldots, \varphi^K) = R(\varphi)$, $\bar{R}$ is strictly convex over V.

However, in contrast to Theorem 4.2.8, $\tilde{\theta}$ is not necessarily a global (or local) minimizer of $R(\theta)$, so the existence of a local minimizer of $\bar{R}(\varphi^1, \ldots, \varphi^K)$ in V is less immediate. This existence is guaranteed by the argument of (Fan et al., 2020, Lemma 4.15), which for readers' convenience we reproduce here: By further reducing $U_{\tilde{\theta}}$, we may assume V takes a product form $V = V_1 \times \ldots \times V_K$ where V_k corresponds to the coordinates of φ^k. Let $\bar{V}, \bar{V}_k$ be the closures of V, V_k, which are compact. Let $\hat{\varphi} = (\hat{\varphi}^1, \ldots, \hat{\varphi}^K)$ be a point which minimizes $\bar{R}$ over $\bar{V}$. We aim to show that $\hat{\varphi}$ in fact belongs to the interior of $\bar{V}$, and hence is a critical point and local minimizer of $\bar{R}$.

Let us write $s_k(\varphi^1, \ldots, \varphi^k) = s_k(\varphi)$, as this does not depend on the remaining coordinates of φ. Because $\tilde{\theta} \in \mathcal{V}_1(\theta_*)$, $\tilde{\theta}$ is a global minimizer of s_1 over $\bar{V}_1$. Then, applying (97) for $k = 1$, we get

$$s_1(\hat{\varphi}^1) - s_1(\tilde{\varphi}^1) \geq c\|\hat{\varphi}^1 - \tilde{\varphi}^1\|^2.$$

Applying this to the series expansion (4.6), and noting that $q_1 \in \mathcal{R}^{\mathsf{G}}_{\leq 0}$ must be a constant, we obtain

$$\bar{R}(\hat{\varphi}^1, \ldots, \hat{\varphi}^K) - \bar{R}(\tilde{\varphi}^1, \ldots, \tilde{\varphi}^K) \geq c\sigma^{-2}\|\hat{\varphi}^1 - \tilde{\varphi}^1\|^2 - C\sigma^{-4}, \tag{98}$$

for all $\sigma > \sigma_0$ and large enough σ_0. Since $\hat{\varphi}$ minimizes $\bar{R}(\varphi)$ over $\bar{V}$, the left side is non-positive, so

we obtain $c\sigma^{-2}\|\hat{\varphi}^1 - \tilde{\varphi}^1\|^2 - C\sigma^{-4} \leq 0$. This shows

$$\|\hat{\varphi}^1 - \tilde{\varphi}^1\| \leq \sigma^{-\eta} \tag{99}$$

for, say, $\eta = 0.1$.

Now consider the functions $\tilde{h}(\varphi^2) = s_2(\tilde{\varphi}^1, \varphi^2)$ and $\hat{h}(\varphi^2) = s_2(\hat{\varphi}^1, \varphi^2)$ on $\bar{V}_2$. Since s_2 is a polynomial function of its arguments, applying (99), we have

$$\sup_{\varphi^2 \in \bar{V}_2} |\tilde{h}(\varphi^2) - \hat{h}(\varphi^2)| < C\sigma^{-\eta}, \qquad \sup_{\varphi^2 \in \bar{V}_2} \|\nabla^2 \tilde{h}(\varphi^2) - \nabla^2 \hat{h}(\varphi^2)\| < C\sigma^{-\eta} \tag{100}$$

for a constant $C > 0$ depending on the neighborhood $\bar{V}$ and the function s_2, but not on σ. Both $\tilde{h}$ and $\hat{h}$ are strongly convex over $\bar{V}_2$, by (97). Since $\tilde{\theta} \in \mathcal{V}_2(\theta_*)$, we know that $\tilde{\varphi}^2$ is a global minimizer of $\tilde{h}$. Then (100) guarantees that the global minimizer $\bar{\varphi}^2$ of $\hat{h}$ over $\bar{V}_2$ satisfies

$$\|\bar{\varphi}^2 - \tilde{\varphi}^2\| < C'\sigma^{-\eta} \tag{101}$$

for a different constant $C' > 0$, see e.g. (Fan et al., 2020, Lemma 2.8). In particular, $\bar{\varphi}^2$ must be in the interior of $\bar{V}_2$ and is a critical point of $\hat{h}$, for sufficiently large σ_0. So (97) implies

$$s_2(\hat{\varphi}^1, \hat{\varphi}^2) - s_2(\hat{\varphi}^1, \bar{\varphi}^2) \geq c\|\hat{\varphi}^2 - \bar{\varphi}^2\|^2.$$

Applying this to the series expansion (4.6), and recalling that q_2 depends only on φ^1, we get

$$\bar{R}(\hat{\varphi}^1, \ldots, \hat{\varphi}^K) - \bar{R}(\hat{\varphi}^1, \bar{\varphi}^2, \tilde{\varphi}^3, \ldots, \tilde{\varphi}^K) \geq c\sigma^{-4}\|\hat{\varphi}^2 - \bar{\varphi}^2\|^2 - C\sigma^{-6}. \tag{102}$$

This is again non-positive because $\hat{\varphi}$ minimizes $\bar{R}$ over $\bar{V}$. So $\|\hat{\varphi}^2 - \bar{\varphi}^2\| \leq \sigma^{-\eta}$. Combining with (101) we obtain

$$\|\hat{\varphi}^2 - \tilde{\varphi}^2\| \leq C\sigma^{-\eta}. \tag{103}$$

Now define $\tilde{h}(\varphi^3) = s_3(\tilde{\varphi}^1, \tilde{\varphi}^2, \varphi^3)$ and $\hat{h}(\varphi^3) = s_3(\hat{\varphi}^1, \hat{\varphi}^2, \varphi^3)$ on $\bar{V}_3$. We may repeat this argument to show $\|\hat{\varphi}^3 - \tilde{\varphi}^3\| \leq C\sigma^{-\eta}$, etc., until we arrive at $\|\hat{\varphi}^K - \tilde{\varphi}^K\| \leq C\sigma^{-\eta}$. (In the last step for $k = K$, $\tilde{\varphi}^K$ is the minimizer of $\tilde{h}$ over $\bar{V}_K$ not because $\tilde{\theta} \in \mathcal{V}_K(\theta_*)$, but instead because $\tilde{\theta}$ is assumed to be a local minimizer of s_K over $\mathcal{V}_{K-1}(\theta_*)$.) Finally, for a large enough constant $\sigma_0 > 0$ and any $\sigma > \sigma_0$, this ensures that $\hat{\varphi}$ belongs to the interior of $\bar{V}$, and hence is a critical point and local minimizer of $\bar{R}$. Then the point $\theta(\hat{\varphi}^1, \ldots, \hat{\varphi}^K, \tilde{\varphi}^0)$ is a local minimizer of $R(\theta)$ on $\mathbb{R}^d$, which is

$\varepsilon(\sigma)$-close to $\tilde{\theta}$ for $\varepsilon(\sigma) = C'\sigma^{-\eta}$. This shows (a1).

The proof of (b1) in the projected setting is similar, applying (4.9) in place of (4.6). In the first step for $k = 1$ we observe, in addition to $q_1 \in \mathcal{R}^{\mathsf{G}}_{\le 0}$ being constant, that $P_1 = 0$ because it is also constant and equals 0 at θ_*. Thus we obtain (98) and (99) without modification. In the second step for $k = 2$, in place of (102), we have

$$\begin{aligned}&\bar{R}(\hat{\varphi}^1, \dots, \hat{\varphi}^K) - \bar{R}(\hat{\varphi}^1, \bar{\varphi}^2, \tilde{\varphi}^3, \dots, \tilde{\varphi}^K)\\ &\ge \sigma^{-4}\Big(c\|\hat{\varphi}^2 - \bar{\varphi}^2\|^2 + \Big\langle \widetilde{T}_2(\hat{\varphi}^1, \hat{\varphi}^2) - \widetilde{T}_2(\hat{\varphi}^1, \bar{\varphi}^2), P_2(\hat{\varphi}^1)\Big\rangle\Big) - C\sigma^{-6}.\end{aligned}$$

We may bound

$$\|\widetilde{T}_2(\hat{\varphi}^1, \hat{\varphi}^2) - \widetilde{T}_2(\hat{\varphi}^1, \bar{\varphi}^2)\|_{\mathrm{HS}} \le C\|\hat{\varphi}^2 - \bar{\varphi}^2\|$$

and

$$\|P_2(\hat{\varphi}^1)\|_{\mathrm{HS}} = \|P_2(\hat{\varphi}^1) - P_2(\tilde{\varphi}^1)\|_{\mathrm{HS}} \le C\|\hat{\varphi}^1 - \tilde{\varphi}^1\| \le C'\sigma^{-\eta},$$

because $\tilde{\theta} \in \mathcal{V}_1(\theta_*)$ so $P_2(\tilde{\varphi}^1) = P_2(\varphi^1_*) = 0$. This yields

$$0 \ge \bar{R}(\hat{\varphi}^1, \dots, \hat{\varphi}^K) - \bar{R}(\hat{\varphi}^1, \bar{\varphi}^2, \tilde{\varphi}^3, \dots, \tilde{\varphi}^K) \ge \sigma^{-4}\Big(c\|\hat{\varphi}^2 - \bar{\varphi}^2\|^2 - C\sigma^{-\eta}\|\hat{\varphi}^2 - \bar{\varphi}^2\|\Big) - C\sigma^{-6}.$$

Viewing the right side as a quadratic function in $\|\hat{\varphi}^2 - \bar{\varphi}^2\|$, this implies that $\|\hat{\varphi}^2 - \bar{\varphi}^2\|$ is at most the larger of the two roots of this quadratic function, which still gives (103). Applying this modification to each step $k = 1, \dots, K$, we obtain $\|\hat{\varphi}^k - \tilde{\varphi}^k\| \le C\sigma^{-\eta}$ for each $k = 1, \dots, K$, and the proof is concluded as in the unprojected setting of (a1). □

C.2 Analysis of orthogonal procrustes alignment

We provide the details for Example 4.2.11 on the Procrustes alignment model, either with or without reflections. Recall that the group is either $\mathsf{G} = \mathsf{O}(3) \otimes \mathrm{Id}_m$ or $\mathsf{G} = \mathsf{SO}(3) \otimes \mathrm{Id}_m$, acting on $\mathbb{R}^{3\times m} \cong \mathbb{R}^d$. We represent an element of this group as $g \otimes \mathrm{Id}_m$, where $g \in \mathsf{O}(3)$ or $g \in \mathsf{SO}(3)$ is a 3×3 matrix. For the Haar-uniform law on both $\mathsf{O}(3)$ and $\mathsf{SO}(3)$, we have the moment identities

$$\mathbb{E}_g[g_{ij}] = 0, \qquad \mathbb{E}_g[g_{ij}g_{i'j'}] = \frac{1}{3} \cdot \mathbf{1}\{(i,j) = (i',j')\}. \tag{104}$$

The first identity and the second for $(i,j) \ne (i',j')$ follow from the fact that g is invariant in law under negation of any two rows or two columns. The second identity for $(i,j) = (i',j')$ follows from

$\operatorname{Tr} g^\top g = \sum_{i,j=1}^3 g_{ij}^2 = 3$, and the equality in law of the entries g_{ij}. The action of this element $g \otimes \mathrm{Id}_m$ on $\theta \in \mathbb{R}^{3\times m}$ is given by the matrix product

$$\theta \mapsto g\theta,$$

and the Euclidean inner-product may be written as $\langle \theta, \theta' \rangle = \operatorname{Tr} \theta^\top \theta' = \operatorname{Tr} \theta' \theta^\top$.

Let us first compute $d_0 = \max_\theta \dim(\mathcal{O}_\theta) = \dim(\mathsf{G}) - \min_\theta \dim(\mathsf{G}_\theta)$, where $\mathsf{G}_\theta = \{g \in \mathsf{G} : g\theta = \theta\}$ is the stabilizer of θ. For both $\mathsf{G} = \mathsf{O}(3) \otimes \mathrm{Id}_m$ and $\mathsf{G} = \mathsf{SO}(3) \otimes \mathrm{Id}_m$, we have $\dim(\mathsf{G}) = 3$. For any $\theta \in \mathbb{R}^{3\times m}$ having full rank 3, there is a right inverse $\theta^\dagger \in \mathbb{R}^{m\times 3}$ for which $\theta\theta^\dagger = \mathrm{Id}$. Thus $g\theta = \theta$ requires $g = \mathrm{Id}$, so that $\dim(\mathsf{G}_\theta) = 0$. Thus, we obtain

$$d_0 = 3, \qquad \operatorname{trdeg} \mathcal{R}^{\mathsf{G}} = d - d_0 = d - 3.$$

We now verify the values of d_1, d_2 and the forms of $\mathcal{V}_1(\theta_*)$, $\mathcal{V}_2(\theta_*)$, $s_1(\theta)$, and $s_2(\theta)$ as stated in Example 4.2.11. For $s_1(\theta)$, by the first identity of (104), $T_1(\theta) = \mathbb{E}_g[g\theta] = 0$. So by the definitions of $s_1(\theta)$ and $\mathcal{V}_1(\theta_*)$ and Lemma 4.2.6,

$$s_1(\theta) = 0, \qquad d_1 = 0, \qquad \mathcal{V}_1(\theta_*) = \mathbb{R}^d.$$

For $s_2(\theta)$, applying Lemma C.1.1, we have

$$\begin{aligned} s_2(\theta) &= \frac{1}{4}\mathbb{E}_g\Big[\langle \theta, g\theta\rangle^2 - 2\langle \theta, g\theta_*\rangle^2 + \langle \theta_*, g\theta_*\rangle^2\Big] \\ &= \frac{1}{4}\mathbb{E}_g\Big[(\operatorname{Tr} g\theta\theta^\top)^2 - 2(\operatorname{Tr} g\theta_*\theta^\top)^2 + (\operatorname{Tr} g\theta_*\theta_*^\top)^2\Big]. \end{aligned}$$

For any $A \in \mathbb{R}^{3\times 3}$, we may apply the second identity of (104) to get

$$\mathbb{E}_g[(\operatorname{Tr} gA^\top)^2] = \sum_{i,j,i',j'=1}^3 \mathbb{E}_g[g_{ij}g_{i'j'}]A_{ij}A_{i'j'} = \frac{1}{3}\operatorname{Tr} A^\top A.$$

So

$$s_2(\theta) = \frac{1}{12}\operatorname{Tr}\left(\theta\theta^\top\theta\theta^\top - 2\theta_*\theta^\top\theta\theta_*^\top + \theta_*\theta_*^\top\theta_*\theta_*^\top\right) = \frac{1}{12}\|\theta^\top\theta - \theta_*^\top\theta_*\|_{\mathrm{HS}}^2.$$

We have $\mathcal{V}_2(\theta_*) = \{\theta : s_2(\theta) = 0\} = \{\theta : \theta^\top\theta = \theta_*^\top\theta_*\}$. For such θ, the row span of θ coincides with that of θ_*. Assuming $\operatorname{rank}(\theta_*) = 3$, this implies $\theta = A\theta_*$ for some invertible matrix $A \in \mathbb{R}^{3\times 3}$. Then $\theta^\top\theta = \theta_*^\top\theta_*$ requires $0 = \theta_*^\top(A^\top A - \mathrm{Id})\theta_*$, so $A^\top A - \mathrm{Id} = 0$. Then A is orthogonal, and we obtain

that $\theta \in \{g\theta_* : g \in \mathsf{O}(3)\}$. This verifies

$$\mathcal{V}_2(\theta_*) = \{g\theta_* : g \in \mathsf{O}(3)\},$$

which is exactly $\mathcal{O}_{\theta_*}$ if $\mathsf{G} = \mathsf{O}(3) \otimes \mathrm{Id}_m$, and $\mathcal{O}_{\theta_*} \cup \mathcal{O}_{-\theta_*}$ if $\mathsf{G} = \mathsf{SO}(3) \otimes \mathrm{Id}_m$.

To compute d_2, we apply Lemma 4.2.6. Differentiating twice at $\theta = \theta_*$ by the chain rule,

$$\nabla^2 s_2(\theta_*) = \frac{1}{6} \mathrm{d}_\theta[\theta^\top\theta]^\top \cdot \mathrm{d}_\theta[\theta^\top\theta]\Big|_{\theta=\theta_*}$$

where $\mathrm{d}_\theta[\theta^\top\theta]$ denotes the Jacobian of the vectorization of $\theta^\top\theta$ as a function of θ. For generic $\theta_* \in \mathbb{R}^{3\times m}$, specializing Lemma C.4.4 to follow with $l = 1$ and $S = m \geq 3$, we then get $\mathrm{rank}[\nabla^2 s_2(\theta_*)] = \mathrm{rank}(\mathrm{d}_\theta[\theta^\top\theta]|_{\theta=\theta_*}) = 3(m-1) = d-3$. Thus, recalling $d_1 = 0$, Lemma 4.2.6 shows

$$d_2 = \mathrm{trdeg}\, \mathcal{R}^{\mathsf{G}}_{\leq 2} = d - 3.$$

This coincides with $\mathrm{trdeg}\, \mathcal{R}^{\mathsf{G}}$, so also $K = 2$ is the smallest integer satisfying Proposition 4.2.4.

Finally, we analyze the optimization landscape of $s_2(\theta)$ over $\mathcal{V}_1(\theta_*) = \mathbb{R}^d$, and show that its only critical points are strict saddles or the global minimizers $\mathcal{V}_2(\theta_*)$. Computing the gradient, we have

$$\nabla s_2(\theta) = \frac{1}{3}\theta\Big(\theta^\top\theta - \theta_*^\top\theta_*\Big) \in \mathbb{R}^{3\times m}.$$

The row span of $\theta\theta^\top\theta$ is the same as that of θ (regardless of the rank of θ), while the row span of $\theta\theta_*^\top\theta_*$ is contained in the row span of θ_*. Thus, at any critical point θ satisfying $\nabla s_2(\theta) = 0$, the row span of θ is contained in that of θ_*, i.e. we have

$$\theta = A\theta_*$$

for some (possibly singular) matrix $A \in \mathbb{R}^{3\times 3}$. Then $0 = \nabla s_2(\theta)$ implies

$$0 = A\theta_*\theta_*^\top A^\top A\theta_* - A\theta_*\theta_*^\top\theta_* = A\theta_*\theta_*^\top(A^\top A - \mathrm{Id})\theta_*.$$

When $\mathrm{rank}(\theta_*) = 3$, the rows of θ_* are linearly independent, so this implies

$$0 = A\theta_*\theta_*^\top(A^\top A - \mathrm{Id}).$$

We now consider two cases for a critical point θ of $s_2(\theta)$:

Case 1: θ has full rank 3. Then A must be nonsingular. Multiplying by $(\theta_*\theta_*^\top)^{-1}A^{-1}$, we get $0 = A^\top A - \mathrm{Id}$, so $A^\top A = \mathrm{Id}$. Thus, A is an orthogonal matrix, so $\theta \in \mathcal{V}_2(\theta_*)$, and this is a global minimizer of $s_2(\theta)$.

Case 2: θ has some rank $k \le 2$. Then also $\mathrm{rank}(A) = \mathrm{rank}(A^\top A) = k$. Then $P = \mathrm{Id} - A^\top A$ has $3-k$ eigenvalues equal to 1, and in particular, $\mathrm{rank}\, P \ge 3-k$. On the other hand, since $\mathrm{rank}(A\theta_*\theta_*^\top) = k$ and $0 = A\theta_*\theta_*^\top P$, the kernel of P has dimension at least k. Then also $\mathrm{rank}\, P \le 3-k$, so $\mathrm{rank}\, P = 3-k$ exactly. Then P has $3-k$ eigenvalues 1 and k eigenvalues 0, so it is an orthogonal projection onto a subspace of dimension $3-k$ in $\mathbb{R}^3$.

Using this observation, we now exhibit a direction of negative curvature in $\nabla^2 s_2(\theta)$: Let $\Delta = uv^\top \in \mathbb{R}^{3\times m}$ be any rank-one non-zero matrix where $A^\top u = 0$ and $P\theta_* v \neq 0$. Such vectors u and v exist because $\mathrm{rank}\, A < 3$ and $\mathrm{rank}\, P > 0$. Consider

$$\theta_t = \theta + t\Delta = A\theta_* + t\Delta,$$

and the Hessian $\nabla^2 s_2(\theta)$ in the direction of Δ, given by $\partial_t^2 s_2(\theta_t)|_{t=0}$. Applying $A^\top\Delta = A^\top uv^\top = 0$ by the condition $A^\top u = 0$, observe that $\theta_t^\top\theta_t = \theta_*^\top A^\top A\theta_* + t^2\Delta^\top\Delta$, so

$$s_2(\theta_t) = \frac{1}{12}\left\|\theta_t^\top\theta_t - \theta_*^\top\theta_*\right\|_{\mathrm{HS}}^2 = \frac{1}{12}\left\|t^2\Delta^\top\Delta - \theta_*^\top P\theta_*\right\|_{\mathrm{HS}}^2.$$

This is a polynomial in t, whose quadratic term is

$$[t^2]s_2(\theta_t) = -\frac{1}{6}\,\mathrm{Tr}\,\theta_*^\top P\theta_*\Delta^\top\Delta.$$

So

$$\partial_t^2 s_2(\theta_t)\Big|_{t=0} = -\frac{1}{3}\,\mathrm{Tr}\,\theta_*^\top P\theta_*\Delta^\top\Delta = -\frac{1}{3}\|P\theta_*\Delta^\top\|_{\mathrm{HS}}^2.$$

Finally, note that $P\theta_*\Delta^\top = (P\theta_* v)u^\top \neq 0$ because $P\theta_* v \neq 0$ and $u \neq 0$. Then this is strictly negative, so $\lambda_{\min}(\nabla^2 s_2(\theta)) < 0$.

Combining these two cases, this verifies the claim in Example 4.2.11 that for generic θ_*, the minimization of $s_2(\theta)$ over $\mathcal{V}_1(\theta_*) = \mathbb{R}^d$ is globally benign. For the claims about the landscape of $R(\theta)$, observe that for any $\theta = g\theta_*$ where $g \in \mathsf{O}(3)$, we have $s_2(\theta) = 0$, so $T_2(\theta) = T_2(\theta_*)$.

Then applying the chain rule to differentiate twice $s_2(\theta) = \|T_2(\theta) - T_2(\theta_*)\|_{\mathrm{HS}}^2/4$, and applying also $s_1(\theta) = 0$, we obtain $\operatorname{rank} \nabla^2 s_2(\theta) = \operatorname{rank} \mathrm{d}T_2(\theta) = \operatorname{rank} \mathrm{d}M_2(\theta)$. On the other hand, for any such θ, the preceding computation shows also $\operatorname{rank} \nabla^2 s_2(\theta) = \operatorname{rank} \mathrm{d}_\theta[\theta^\top \theta] = d - 3$, as this rank is the same at $\theta = g\theta_*$ as at θ_*. Therefore $\operatorname{rank} \mathrm{d}M_2(\theta) = d - 3$. Thus $\mathrm{d}M_2(\theta)$ has constant rank on $\mathcal{V}_2(\theta_*)$, and the minimizers $\mathcal{V}_2(\theta_*) = \{g\theta_* : g \in \mathsf{O}(3)\}$ of $s_2(\theta_*)$ are non-degenerate up to orbit. Then the claims about the landscape of $R(\theta)$ for large σ follow from Theorems 4.2.8 and 4.2.10.

C.3 Analysis of continuous multi-reference alignment

C.3.1 Unprojected continuous MRA

In this section we prove Theorems 4.3.1 and 4.3.3.

Proof of Theorem 4.3.3. Recall by Lemma C.1.1 that

$$s_k(\theta) = \frac{1}{2(k!)} \mathbb{E}_g \left[\langle \theta, g \cdot \theta \rangle^k - 2 \langle \theta, g \cdot \theta_* \rangle^k + \langle \theta_*, g \cdot \theta_* \rangle^k \right]. \tag{105}$$

Let $\theta, \vartheta \in \mathbb{R}^d$. Computing the form of $\mathbb{E}_g[\langle \theta, g \cdot \vartheta \rangle^k]$ will give the form of $s_k(\theta)$.

Case $k = 1$: By (4.19), $\mathbb{E}_g[g] = \operatorname{diag}(1, 0, \ldots, 0)$. It follows from (105) that

$$s_1(\theta) = \frac{1}{2} \left((\theta^{(0)})^2 - 2\theta^{(0)}\theta_*^{(0)} + (\theta_*^{(0)})^2 \right) = \frac{1}{2} \left(\theta^{(0)} - \theta_*^{(0)} \right)^2.$$

Case $k = 2$: Recall $u^{(0)}(\theta) = \theta^{(0)}$ and $u^{(l)}(\theta) = \theta_1^{(l)} + \mathbf{i}\theta_2^{(l)}$ for $l = 1, \ldots, L$. From (4.19), we may check that

$$u^{(l)}(g \cdot \theta) = e^{-\mathbf{i}2\pi l \mathfrak{g}} u^{(l)}(\theta). \tag{106}$$

Then, applying the identity $\operatorname{Re} a = (a + \bar{a})/2$,

$$\langle \theta, g \cdot \vartheta \rangle = \sum_{l=0}^{L} \operatorname{Re} \left[u^{(l)}(\theta) \cdot \overline{u^{(l)}(g \cdot \vartheta)} \right] = \frac{1}{2} \sum_{l=0}^{L} \left[u^{(l)}(\theta) \overline{u^{(l)}(\vartheta)} e^{\mathbf{i}2\pi l \mathfrak{g}} + \overline{u^{(l)}(\theta)} u^{(l)}(\vartheta) e^{-\mathbf{i}2\pi l \mathfrak{g}} \right]. \tag{107}$$

Taking the expected square on both sides gives

$$\begin{aligned}\mathbb{E}_g[\langle\theta, g\cdot\vartheta\rangle^2] =& \frac{1}{4}\mathbb{E}_{\mathfrak{g}}\left[\sum_{l_1,l_2=0}^{L} u^{(l_1)}(\theta)u^{(l_2)}(\theta)\overline{u^{(l_1)}(\vartheta)u^{(l_2)}(\vartheta)}e^{\mathbf{i}2\pi(l_1+l_2)\mathfrak{g}}\right] \\ &+ \frac{1}{4}\mathbb{E}_{\mathfrak{g}}\left[\sum_{l_1,l_2=0}^{L} \overline{u^{(l_1)}(\theta)u^{(l_2)}(\theta)}u^{(l_1)}(\vartheta)u^{(l_2)}(\vartheta)e^{-\mathbf{i}2\pi(l_1+l_2)\mathfrak{g}}\right] \\ &+ \frac{1}{4}\mathbb{E}_{\mathfrak{g}}\left[\sum_{l_1,l_2=0}^{L} u^{(l_1)}(\theta)\overline{u^{(l_2)}(\theta)u^{(l_1)}(\vartheta)}u^{(l_2)}(\vartheta)e^{\mathbf{i}2\pi(l_1-l_2)\mathfrak{g}}\right] \\ &+ \frac{1}{4}\mathbb{E}_{\mathfrak{g}}\left[\sum_{l_1,l_2=0}^{L} \overline{u^{(l_1)}(\theta)}u^{(l_2)}(\theta)u^{(l_1)}(\vartheta)\overline{u^{(l_2)}(\vartheta)}e^{-\mathbf{i}2\pi(l_1-l_2)\mathfrak{g}}\right],\end{aligned}$$

where $\mathfrak{g}$ is uniformly distributed over $[0,1)$. Applying the property

$$\mathbb{E}_{\mathfrak{g}}[e^{\mathbf{i}2\pi l\mathfrak{g}}] = \begin{cases} 1 & \text{for} \quad l=0, \\ 0 & \text{for} \quad l\neq 0, \end{cases} \tag{108}$$

gives

$$\begin{aligned}\mathbb{E}_g[\langle\theta, g\cdot\vartheta\rangle^2] &= (u^{(0)}(\theta))^2(u^{(0)}(\vartheta))^2 + \frac{1}{4}\sum_{l=1}^{L}\left[u^{(l)}(\theta)\overline{u^{(l)}(\theta)u^{(l)}(\vartheta)}u^{(l)}(\vartheta) + \overline{u^{(l)}(\theta)}u^{(l)}(\theta)u^{(l)}(\vartheta)\overline{u^{(l)}(\vartheta)}\right] \\ &= (\theta^{(0)})^2(\vartheta^{(0)})^2 + \frac{1}{2}\sum_{l=1}^{L} r_l(\theta)^2 r_l(\vartheta)^2.\end{aligned}$$

Then from (105),

$$s_2(\theta) = \frac{1}{4}\left((\theta^{(0)})^2 - (\theta_*^{(0)})^2\right)^2 + \frac{1}{8}\sum_{l=1}^{L}\left(r_l(\theta)^2 - r_l(\theta_*)^2\right)^2.$$

Case $k=3$: We now take the expected cube on both sides of (107). Applying (108),

$$\begin{aligned}\mathbb{E}_g[\langle\theta, g\cdot\vartheta\rangle^3] &= \frac{1}{4}(u^{(0)}(\theta))^3(u^{(0)}(\vartheta))^3 + \frac{3}{8}\sum_{\substack{l,l',l''=0 \\ l=l'+l''}}^{L} u^{(l)}(\theta)\overline{u^{(l')}(\theta)u^{(l'')}(\theta)u^{(l)}(\vartheta)}u^{(l')}(\vartheta)u^{(l'')}(\vartheta) \\ &\quad + \frac{3}{8}\sum_{\substack{l,l',l''=0 \\ l=l'+l''}}^{L} \overline{u^{(l)}(\theta)}u^{(l')}(\theta)u^{(l'')}(\theta)u^{(l)}(\vartheta)\overline{u^{(l')}(\vartheta)u^{(l'')}(\vartheta)}.\end{aligned}$$

Let us write as shorthand $u^{(l)} = u^{(l)}(\theta)$, $u_*^{(l)} = u^{(l)}(\theta_*)$, and similarly for $r_l, \lambda_l, r_{l,l',l''}, \lambda_{l,l',l''}$ and

$r_{*,l}, \lambda_{*,l}, r_{*,l,l',l''}, \lambda_{*,l,l',l''}$. Then from (105),

$$\begin{aligned}
s_3(\theta) &= \frac{1}{12}\mathbb{E}_g\left[\langle\theta, g\cdot\theta\rangle^3 - 2\langle\theta, g\cdot\theta_*\rangle^3 + \langle\theta_*, g\cdot\theta_*\rangle^3\right] \\
&= \frac{1}{48}\Big((u^{(0)})^3 - (u_*^{(0)})^3\Big)^2 + \frac{1}{16}\sum_{\substack{l,l',l''=0\\ l=l'+l''}}^{L}\Big|u^{(l)}u^{(l')}u^{(l'')}\Big|^2 + \Big|u_*^{(l)}u_*^{(l')}u_*^{(l'')}\Big|^2 \\
&\qquad - \frac{1}{16}\sum_{\substack{l,l',l''=0\\ l=l'+l''}}^{L} u^{(l)}\overline{u^{(l')}u^{(l'')}u_*^{(l)}}u_*^{(l')}u_*^{(l'')} + \overline{u^{(l)}}u^{(l')}u^{(l'')}u_*^{(l)}\overline{u_*^{(l')}u_*^{(l'')}} \\
&= \frac{1}{48}\Big((u^{(0)})^3 - (u_*^{(0)})^3\Big)^2 + \frac{1}{16}\sum_{\substack{l,l',l''=0\\ l=l'+l''}}^{L}\Big|u^{(l)}\overline{u^{(l')}u^{(l'')}} - u_*^{(l)}\overline{u_*^{(l')}u_*^{(l'')}}\Big|^2. \qquad (109)
\end{aligned}$$

This verifies the first expression for $s_3(\theta)$. For the second expression, we split the second sum of (109) into the cases $l = l' = l'' = 0$, only $l' = 0$ and $l = l'' \geq 1$, only $l'' = 0$ and $l = l' \geq 1$, and all $l, l', l'' \geq 1$. The first three cases are easily rewritten in terms of $u^{(0)}, r_l, u_*^{(0)}, r_{*,l}$. Each term of the last case $l, l', l'' \geq 1$ may be written as

$$\Big|u^{(l)}\overline{u^{(l')}u^{(l'')}} - u_*^{(l)}\overline{u_*^{(l')}u_*^{(l'')}}\Big|^2 = r_{l,l',l''}^2 + r_{*,l,l',l''}^2 - 2r_{l,l',l''}r_{*,l,l',l''}\cos\left(\lambda_{*,l,l',l''} - \lambda_{l,l',l''}\right),$$

and this yields the second expression for $s_3(\theta)$. □

Proof of Theorem 4.3.1. Note that for generic $\theta \in \mathbb{R}^d$, for example having $(\theta_1^{(1)}, \theta_2^{(1)}) \neq (0,0)$, its stabilizer $\mathsf{G}_\theta = \{g \in \mathsf{G} : g\cdot\theta = \theta\} = \{\mathrm{Id}\}$ is trivial. Thus $\dim \mathcal{O}_\theta = \dim \mathsf{G} = 1$, so $\operatorname{trdeg} \mathcal{R}^{\mathsf{G}} = d - 1 = 2L$.

We compute $\operatorname{trdeg}(\mathcal{R}^{\mathsf{G}}_{\leq k})$ for $k = 1, 2, 3$ by applying Lemma 4.2.6 at any generic point $\theta_* \in \mathbb{R}^d$ where $r_l(\theta_*) > 0$ for each $l = 1, \ldots, L$. Write as shorthand $u^{(l)}(\theta) = r_l e^{\mathbf{i}\lambda_l}$, $u^{(l)}(\theta_*) = r_{*,l}e^{\mathbf{i}\lambda_{*,l}}$, and define $t_l = \lambda_l - \lambda_{*,l} \in [-\pi, \pi)$ for each $l = 1, \ldots, L$. Setting

$$\zeta(\theta) = (\theta_0, r_1, \ldots, r_L, t_1, \ldots, t_L),$$

this map $\zeta(\theta)$ has non-singular derivative at θ_*. Then by the inverse function theorem, the coordinates $\zeta \in \mathbb{R}^{2L+1}$ provide an invertible reparametrization of θ in a local neighborhood of θ_*, with some inverse function $\theta(\zeta)$. Let $\zeta_* = \zeta(\theta_*)$. Note that θ_* is a global minimizer and hence critical point of $s_k(\theta)$ for each $k \geq 1$. Then by the chain rule,

$$\nabla_\zeta^2 s_k(\theta(\zeta))\big|_{\zeta=\zeta_*} = \mathrm{d}_\zeta\theta(\zeta_*)^\top \cdot \nabla_\theta^2 s_k(\theta_*) \cdot \mathrm{d}_\zeta\theta(\zeta_*).$$

Applying Lemma 4.2.6 and the fact that $\mathrm{d}_\zeta\theta(\zeta_*)$ is non-singular, this gives

$$\operatorname{rank}\Big(\nabla^2_\theta s_1(\theta_*)+\ldots+\nabla^2_\theta s_k(\theta_*)\Big)=\operatorname{rank}\Big(\nabla^2_\zeta s_1(\theta(\zeta))+\ldots+\nabla^2_\zeta s_k(\theta(\zeta))\Big|_{\zeta=\zeta_*}\Big).$$

For $k=1$ and $k=2$, by Theorem 4.3.3,

$$s_1(\theta(\zeta))=\frac{1}{2}(\theta_0-\theta_{*,0})^2,\qquad s_2(\theta(\zeta))=\frac{1}{4}(\theta_0^2-\theta_{*,0}^2)^2+\frac{1}{8}\sum_{l=1}^{L}(r_l^2-r_{*,l}^2)^2.$$

Then taking the Hessians yields

$$\operatorname{trdeg}(\mathcal{R}^{\mathsf{G}}_{\leq 1})=\operatorname{rank}\Big(\nabla^2_\zeta s_1(\theta(\zeta))\Big|_{\zeta=\zeta_*}\Big)=\operatorname{rank}\Big(\operatorname{diag}(1,0,\ldots,0)\Big)=1,$$

and

$$\begin{aligned}\operatorname{trdeg}(\mathcal{R}^{\mathsf{G}}_{\leq 2})&=\operatorname{rank}\Big(\nabla^2_\zeta s_1(\theta(\zeta))+\nabla^2_\zeta s_2(\theta(\zeta))\Big|_{\zeta=\zeta_*}\Big)\\&=\operatorname{rank}\Big(\operatorname{diag}(1,0,\ldots,0)+\operatorname{diag}(2\theta^2_{*,0},r^2_{*,1},\ldots,r^2_{*,L})\Big)=L+1.\end{aligned}$$

For $k=3$, noting that $\operatorname{trdeg}(\mathcal{R}^{\mathsf{G}}_{\leq 3})\leq\operatorname{trdeg}(\mathcal{R}^{\mathsf{G}})=2L$, it remains to show $\operatorname{trdeg}(\mathcal{R}^{\mathsf{G}}_{\leq 3})\geq 2L$. Denote

$$H(\zeta_*)=\nabla^2_\zeta s_1(\theta(\zeta))+\nabla^2_\zeta s_2(\theta(\zeta))+\nabla^2_\zeta s_3(\theta(\zeta))\Big|_{\zeta=\zeta_*},$$

so that $\operatorname{trdeg}(\mathcal{R}^{\mathsf{G}}_{\leq 3})=\operatorname{rank}(H(\zeta_*))$. Group the coordinates of ζ as $r=(\theta_0,r_1,\ldots,r_L)\in\mathbb{R}^{L+1}$ and $t=(t_1,\ldots,t_L)\in\mathbb{R}^L$, and define the corresponding block decomposition

$$H(\zeta_*)=\begin{pmatrix}H_{rr}(\zeta_*) & H_{rt}(\zeta_*)\\ H_{tr}(\zeta_*) & H_{tt}(\zeta_*)\end{pmatrix}.$$

Since $s_1(\theta(\zeta))$ and $s_2(\theta(\zeta))$ are functions only of r and not of t, we have

$$\begin{aligned}
H_{rr}(\zeta_*) &= \nabla_r^2 s_1(\theta(\zeta)) + \nabla_r^2 s_2(\theta(\zeta)) + \nabla_r^2 s_3(\theta(\zeta))\Big|_{\zeta=\zeta_*}, \\
H_{rt}(\zeta_*) &= \nabla_{rt}^2 s_3(\theta(\zeta))\Big|_{\zeta=\zeta_*}, \\
H_{tr}(\zeta_*) &= \nabla_{tr}^2 s_3(\theta(\zeta))\Big|_{\zeta=\zeta_*}, \\
H_{tt}(\zeta_*) &= \nabla_t^2 s_3(\theta(\zeta))\Big|_{\zeta=\zeta_*}.
\end{aligned}$$

For the upper-left block $H_{rr}(\zeta_*)$ of size $(L+1)\times(L+1)$, Lemma 4.2.6 ensures that each matrix $\nabla_\zeta^2 s_k(\theta(\zeta))$ is positive semidefinite, and hence so is each submatrix $\nabla_r^2 s_k(\theta(\zeta))$. Then from the analysis for $\mathrm{trdeg}(\mathcal{R}_{\le 2}^{\mathsf{G}})$,

$$\mathrm{rank}(H_{rr}(\zeta_*)) = \mathrm{rank}\left(\nabla_r^2 s_1(\theta(\zeta)) + \nabla_r^2 s_2(\theta(\zeta))\Big|_{\zeta=\zeta_*}\right) = L+1. \tag{110}$$

For the blocks $H_{rt}(\zeta_*)$ and $H_{tr}(\zeta_*)$, recall from the form of $s_3(\theta)$ in Theorem 4.3.3 that

$$s_3(\theta(\zeta)) = f(r) - \frac{1}{8}\sum_{\substack{l,l',l''=1\\ l=l'+l''}}^{L} r_{l,l',l''} r_{*,l,l',l''} \cos(t_l - t_{l'} - t_{l''}),$$

where $f(r)$ is a function depending only on r and not on t. Then, noting that $t_l = 0$ for all $l = 1,\dots,L$ at $\zeta = \zeta_*$, we get

$$\nabla_{r\lambda}^2 s_3(\theta(\zeta))\Big|_{\zeta=\zeta_*} = 0 \qquad \text{and} \qquad \nabla_{\lambda r}^2 s_3(\theta(\zeta))\Big|_{\zeta=\zeta_*} = 0,$$

which further implies

$$H_{rt}(\zeta_*) = 0 \qquad \text{and} \qquad H_{tr}(\zeta_*) = 0. \tag{111}$$

Finally, the lower-right block $H_{tt}(\zeta_*)$ of size $L\times L$ is given explicitly by

$$H_{tt}(\zeta_*) = -\frac{1}{8}\sum_{\substack{l,l',l''=1\\ l=l'+l''}}^{L} r_{*,l,l',l''}^2 \cdot \nabla_t^2\Big[\cos(t_l - t_{l'} - t_{l''})\Big]\Big|_{t=0}.$$

To show that its rank is at least $L-1$ for generic $\theta_* \in \mathbb{R}^d$, it suffices to exhibit a single such point θ_*. For simplicity, we pick θ_* such that $\theta_*^{(0)} = 1$ and $r_{*,l} = 1$ for all $l = 1,\dots,L$. Let e_l be the l^{th}

standard basis vector, and define the vector

$$w_{l,l',l''} = \nabla_t[t_l - t_{l'} - t_{l''}] = e_l - e_{l'} - e_{l''} \in \mathbb{R}^L. \tag{112}$$

By the chain rule,

$$\nabla_t^2\Big[\cos(t_l - t_{l'} - t_{l''})\Big]\Big|_{t=0} = -\cos(t_l - t_{l'} - t_{l''})\Big|_{t=0} \cdot w_{l,l',l''}w_{l,l',l''}^\top = -w_{l,l',l''}w_{l,l',l''}^\top.$$

Define the index set $\mathcal{L} = \{l, l', l'' \in \{1, \dots, L\} : l = l' + l''\}$, and let $W \in \mathbb{R}^{L \times |\mathcal{L}|}$ be the matrix with the vectors $w_{l,l',l''}$ as columns. Then

$$H_{tt}(\zeta_*) = \frac{1}{8}WW^\top.$$

Note that, in particular, W has a subset of $L-1$ columns corresponding to $l' = 1$, $l'' \in \{1, \dots, L-1\}$, and $l = 1 + l''$. These columns (in $\mathbb{R}^L$) are given by

$$\begin{pmatrix} 2 \\ -1 \\ 0 \\ 0 \\ \vdots \\ 0 \\ 0 \end{pmatrix}, \quad \begin{pmatrix} 1 \\ 1 \\ -1 \\ 0 \\ \vdots \\ 0 \\ 0 \end{pmatrix}, \quad \begin{pmatrix} 1 \\ 0 \\ 1 \\ -1 \\ \vdots \\ 0 \\ 0 \end{pmatrix}, \dots, \quad \begin{pmatrix} 1 \\ 0 \\ 0 \\ 0 \\ \vdots \\ 1 \\ -1 \end{pmatrix}.$$

The bottom $L - 1$ rows of these columns form an upper-triangular matrix with non-zero diagonal, and hence these columns are linearly independent. Thus $\operatorname{rank}(W) \geq L - 1$, so also

$$\operatorname{rank}(H_{tt}(\zeta_*)) \geq L - 1. \tag{113}$$

Combining (110), (111), and (113), we obtain $\operatorname{trdeg} \mathcal{R}^{\mathsf{G}}_{\leq 3} = \operatorname{rank}(H(\zeta_*)) \geq 2L$. Hence $\operatorname{trdeg} \mathcal{R}^{\mathsf{G}}_{\leq 3} = 2L$, as desired.

The statement $(d_0, d_1, d_2, d_3) = (1, 1, L, L - 1)$ now follows from these transcendence degrees. The smallest K for which $\operatorname{trdeg} \mathcal{R}^{\mathsf{G}}_{\leq K} = \operatorname{trdeg} \mathcal{R}^{\mathsf{G}} = 2L$ is $K = 3$, except in the case $L = 1$ where it is instead $K = 2$. □

C.3.2 Projected continuous MRA

In this section we prove Theorems 4.3.5 and 4.3.7.

Proof of Theorem 4.3.7. Recall by Lemma C.1.1 that

$$\tilde{s}_k(\theta) = \frac{1}{2(k!)}\mathbb{E}_{g,h}[\langle \Pi \cdot g \cdot \theta, \Pi \cdot h \cdot \theta\rangle^k - 2\langle \Pi \cdot g \cdot \theta, \Pi \cdot h \cdot \theta_*\rangle^k + \langle \Pi \cdot g \cdot \theta_*, \Pi \cdot h \cdot \theta_*\rangle^k]. \tag{114}$$

We compute $\mathbb{E}_{g,h}[\langle \Pi \cdot g \cdot \theta, \Pi \cdot h \cdot \vartheta\rangle^k]$ for $\theta, \vartheta \in \mathbb{R}^d$.

Case $k = 1$: Recall $u^{(0)}(\theta) = \theta^{(0)}$ and $u^{(l)}(\theta) = \theta_1^{(l)} + \mathbf{i}\theta_2^{(l)}$ for $l = 1, \ldots, L$. Write $g, h \in \mathsf{G}$ corresponding to the rotations $\mathfrak{g}, \mathfrak{h} \in [0, 1)$. Then, applying (106) and the identity $\operatorname{Re} a \cdot \operatorname{Re} b = (ab + \bar{a}\bar{b} + a\bar{b} + \bar{a}b)/4$, we have

$$\langle \Pi \cdot g \cdot \theta, \Pi \cdot h \cdot \vartheta\rangle = 2\sum_{l=0}^{L} \operatorname{Re} u^{(l)}(g \cdot \theta) \cdot \operatorname{Re} u^{(l)}(h \cdot \vartheta) = \frac{1}{2}M_1 + \frac{1}{2}M_2 \tag{115}$$

where

$$\begin{aligned} M_1 &:= \sum_{l=0}^{L} u^{(l)}(\theta)u^{(l)}(\vartheta)e^{-2\mathbf{i}\pi l(\mathfrak{g}+\mathfrak{h})} + \overline{u^{(l)}(\theta)u^{(l)}(\vartheta)}e^{2\mathbf{i}\pi l(\mathfrak{g}+\mathfrak{h})}, \\ M_2 &:= \sum_{l=0}^{L} u^{(l)}(\theta)\overline{u^{(l)}(\vartheta)}e^{-2\mathbf{i}\pi l(\mathfrak{g}-\mathfrak{h})} + \overline{u^{(l)}(\theta)}u^{(l)}(\vartheta)e^{2\mathbf{i}\pi l(\mathfrak{g}-\mathfrak{h})}. \end{aligned}$$

For independent and uniformly random $\mathfrak{g}, \mathfrak{h} \in [0, 1)$, taking the expected value on both sides using (108) gives $\mathbb{E}_{g,h}[\langle \Pi \cdot g \cdot \theta, \Pi \cdot h \cdot \vartheta\rangle] = 2u^{(0)}(\theta)u^{(0)}(\vartheta)$. Then from (114), we obtain

$$\tilde{s}_1(\theta) = \left(u^{(0)}(\theta) - u^{(0)}(\theta_*)\right)^2 = \left(\theta^{(0)} - \theta_*^{(0)}\right)^2. \tag{116}$$

Case $k = 2$: Taking the expected square on both sides of (115), we have

$$\mathbb{E}_{g,h}[\langle \Pi \cdot g \cdot \theta, \Pi \cdot h \cdot \vartheta\rangle^2] = \frac{1}{4}\Big\{\mathbb{E}_{\mathfrak{g},\mathfrak{h}}[M_1^2] + 2\mathbb{E}_{\mathfrak{g},\mathfrak{h}}[M_1M_2] + \mathbb{E}_{\mathfrak{g},\mathfrak{h}}[M_2^2]\Big\}.$$

Applying (108) and an argument similar to the $k = 2$ computation in the proof of Theorem 4.3.3,

$$\mathbb{E}_{\mathfrak{g},\mathfrak{h}}[M_1^2] = 2(u^{(0)}(\theta))^2(u^{(0)}(\vartheta))^2 + 2\sum_{l=0}^{L}|u^{(l)}(\theta)|^2|u^{(l)}(\vartheta)|^2,$$
$$\mathbb{E}_{\mathfrak{g},\mathfrak{h}}[M_1M_2] = 4(u^{(0)}(\theta))^2(u^{(0)}(\vartheta))^2,$$
$$\mathbb{E}_{\mathfrak{g},\mathfrak{h}}[M_2^2] = 2(u^{(0)}(\theta))^2(u^{(0)}(\vartheta))^2 + 2\sum_{l=0}^{L}|u^{(l)}(\theta)|^2|u^{(l)}(\vartheta)|^2.$$

Then, separating the $l = 0$ terms from these sums, $\mathbb{E}_{g,h}[\langle \Pi \cdot g \cdot \theta, \Pi \cdot h \cdot \vartheta\rangle^2] = 4(\theta^{(0)})^2(\vartheta^{(0)})^2 + \sum_{l=1}^{L} r_l(\theta)^2 r_l(\vartheta)^2$, so by (114),

$$\tilde{s}_2(\theta) = \Big((\theta^{(0)})^2 - (\theta_*^{(0)})^2\Big)^2 + \frac{1}{4}\sum_{l=1}^{L}\Big(r_l(\theta)^2 - r_l(\theta_*)^2\Big)^2. \tag{117}$$

Case $k = 3$: Taking the expected cube on both sides of (115), we have

$$\mathbb{E}_{g,h}[\langle \Pi \cdot g \cdot \theta, \Pi \cdot h \cdot \vartheta\rangle^3] = \frac{1}{8}\Big\{\mathbb{E}_{\mathfrak{g},\mathfrak{h}}[M_1^3] + 3\mathbb{E}_{\mathfrak{g},\mathfrak{h}}[M_1^2M_2] + 3\mathbb{E}_{\mathfrak{g},\mathfrak{h}}[M_1M_2^2] + \mathbb{E}_{\mathfrak{g},\mathfrak{h}}[M_2^3]\Big\}.$$

Applying (108) and an argument similar to the $k = 3$ computation in the proof of Theorem 4.3.3,

$$\mathbb{E}_{\mathfrak{g},\mathfrak{h}}[M_1^3] = 2(u^{(0)}(\theta))^3(u^{(0)}(\vartheta))^3 + 3\sum_{\substack{l,l',l''=0\\ l=l'+l''}}^{L} u^{(l)}(\theta)\overline{u^{(l')}(\theta)u^{(l'')}(\theta)}u^{(l)}(\vartheta)\overline{u^{(l')}(\vartheta)u^{(l'')}(\vartheta)}$$
$$+ 3\sum_{\substack{l,l',l''=0\\ l=l'+l''}}^{L} \overline{u^{(l)}(\theta)}u^{(l')}(\theta)u^{(l'')}(\theta)\overline{u^{(l)}(\vartheta)}u^{(l')}(\vartheta)u^{(l'')}(\vartheta),$$
$$\mathbb{E}_{\mathfrak{g},\mathfrak{h}}[M_1^2M_2] = \mathbb{E}_{\mathfrak{g},\mathfrak{h}}[M_1M_2^2] = 8(u^{(0)}(\theta))^3(u^{(0)}(\vartheta))^3 + 4u^{(0)}(\theta)u^{(0)}(\vartheta)\cdot\sum_{l=1}^{L}|u^{(l)}(\theta)|^2|u^{(l)}(\vartheta)|^2,$$
$$\mathbb{E}_{\mathfrak{g},\mathfrak{h}}[M_2^3] = 2(u^{(0)}(\theta))^3(u^{(0)}(\vartheta))^3 + 3\sum_{\substack{l,l',l''=0\\ l=l'+l''}}^{L} u^{(l)}(\theta)\overline{u^{(l')}(\theta)u^{(l'')}(\theta)u^{(l)}(\vartheta)}u^{(l')}(\vartheta)u^{(l'')}(\vartheta)$$
$$+ 3\sum_{\substack{l,l',l''=0\\ l=l'+l''}}^{L} \overline{u^{(l)}(\theta)}u^{(l')}(\theta)u^{(l'')}(\theta)u^{(l)}(\vartheta)\overline{u^{(l')}(\vartheta)u^{(l'')}(\vartheta)}.$$

In these expressions for $\mathbb{E}_{\mathfrak{g},\mathfrak{h}}[M_1^3]$ and $\mathbb{E}_{\mathfrak{g},\mathfrak{h}}[M_2^3]$, separating out the three cases of $l = l' = l'' = 0$,

only $l' = 0$ and $l = l'' \geq 1$, and only $l'' = 0$ and $l = l' \geq 1$, this gives

$$
\begin{aligned}
&\mathbb{E}_{g,h}[\langle \Pi \cdot g \cdot \theta, \Pi \cdot h \cdot \vartheta \rangle^3] \\
&= 8(u^{(0)}(\theta))^3 (u^{(0)}(\vartheta))^3 + 6u^{(0)}(\theta)u^{(0)}(\vartheta) \cdot \sum_{l=1}^{L} |u^{(l)}(\theta)|^2 |u^{(l)}(\vartheta)|^2 \\
&+ \frac{3}{8} \sum_{\substack{l,l',l''=1 \\ l=l'+l''}}^{L} u^{(l)}(\theta)\overline{u^{(l')}(\theta)u^{(l'')}(\theta)}u^{(l)}(\vartheta)\overline{u^{(l')}(\vartheta)u^{(l'')}(\vartheta)} + \overline{u^{(l)}(\theta)}u^{(l')}(\theta)u^{(l'')}(\theta)\overline{u^{(l)}(\vartheta)}u^{(l')}(\vartheta)u^{(l'')}(\vartheta) \\
&+ \frac{3}{8} \sum_{\substack{l,l',l''=1 \\ l=l'+l''}}^{L} u^{(l)}(\theta)\overline{u^{(l')}(\theta)u^{(l'')}(\theta)u^{(l)}(\vartheta)}u^{(l')}(\vartheta)u^{(l'')}(\vartheta) + \overline{u^{(l)}(\theta)}u^{(l')}(\theta)u^{(l'')}(\theta)u^{(l)}(\vartheta)\overline{u^{(l')}(\vartheta)u^{(l'')}(\vartheta)}.
\end{aligned}
$$

Applying this to (114) using $(x^2+\bar{x}^2)-2(xx_*+\bar{x}\bar{x}_*)+(x_*^2+\bar{x}_*^2) = (x-x_*)^2+(\bar{x}-\bar{x}_*)^2 = 2\,\mathrm{Re}[(x-x_*)^2]$, and writing as shorthand $u^{(l)} = u^{(l)}(\theta)$, $u_*^{(l)} = u^{(l)}(\theta_*)$ and similarly for $r_l, \lambda_l, r_{l,l',l''}, \lambda_{l,l',l''}$,

$$
\begin{aligned}
\tilde{s}_3(\theta) &= \frac{2}{3}\Big((u^{(0)})^3 - (u_*^{(0)})^3\Big)^2 + \frac{1}{2}\sum_{l=1}^{L}\Big(u^{(0)}|u^{(l)}|^2 - u_*^{(0)}|u_*^{(l)}|^2\Big)^2 \\
&\quad + \frac{1}{16}\sum_{\substack{l,l',l''=1 \\ l=l'+l''}}^{L}\Big|u^{(l)}\overline{u^{(l')}u^{(l'')}} - u_*^{(l)}\overline{u_*^{(l')}u_*^{(l'')}}\Big|^2 + \mathrm{Re}\Big[\Big(u^{(l)}\overline{u^{(l')}u^{(l'')}} - u_*^{(l)}\overline{u_*^{(l')}u_*^{(l'')}}\Big)^2\Big] \\
&= \frac{2}{3}\Big((\theta^{(0)})^3 - (\theta_*^{(0)})^3\Big)^2 + \frac{1}{2}\sum_{l=1}^{L}\Big(\theta^{(0)}r_l^2 - \theta_*^{(0)}r_{*,l}^2\Big)^2 \\
&\quad + \frac{1}{16}\sum_{\substack{l,l',l''=1 \\ l=l'+l''}}^{L} r_{l,l',l''}^2 + r_{*,l,l',l''}^2 - 2r_{l,l',l''}r_{*,l,l',l''}\cos(\lambda_{*,l,l',l''} - \lambda_{l,l',l''}) \\
&\qquad + r_{l,l',l''}^2\cos(2\lambda_{l,l',l''}) + r_{*,l,l',l''}^2\cos(2\lambda_{*,l,l',l''}) - 2r_{l,l',l''}r_{*,l,l',l''}\cos(\lambda_{*,l,l',l''} + \lambda_{l,l',l''}).
\end{aligned}
$$

□

Lemma C.3.1. *Let $H \in \mathbb{R}^{n\times n}$ and $n = n_1 + n_2$ with $n_1, n_2 \geq 1$. Suppose H can be decomposed as the sum of two positive semidefinite matrices A and B with*

$$
A = \begin{pmatrix} A_{11} & 0 \\ 0 & 0 \end{pmatrix} \quad \text{and} \quad B = \begin{pmatrix} B_{11} & B_{12} \\ B_{21} & B_{22} \end{pmatrix},
$$

where $A_{11}, B_{11} \in \mathbb{R}^{n_1\times n_1}, B_{12} \in \mathbb{R}^{n_1\times n_2}, B_{21} \in \mathbb{R}^{n_2\times n_1}$, and $B_{22} \in \mathbb{R}^{n_2\times n_2}$. Then

$$
\mathrm{rank}(H) \geq \mathrm{rank}(A_{11}) + \mathrm{rank}(B_{22}).
$$

Proof. Since A and B are positive semidefinite, so are A_{11}, B_{11}, B_{22}. There are $\operatorname{rank}(A_{11})$ linearly independent vectors $v \in \mathbb{R}^{n_1}$ where $v^\top A_{11} v > 0$ strictly. Then $(v,0)^\top H(v,0) > 0$ strictly for each such vector v. There are also $\operatorname{rank}(B_{22})$ linearly independent vectors $w \in \mathbb{R}^{n_2}$ where $w^\top B_{22} w > 0$ strictly. Then $(0,w)^\top H(0,w) > 0$ strictly for each such vector w. Thus $u^\top H u > 0$ for $\operatorname{rank}(A_{11}) + \operatorname{rank}(B_{22})$ linearly independent vectors $u \in \mathbb{R}^n$, so $\operatorname{rank}(H) \geq \operatorname{rank}(A_{11}) + \operatorname{rank}(B_{22})$. □

Proof of Theorem 4.3.5. As in Theorem 4.3.1, we have $\tilde{d}_0 = 1$ and $\operatorname{trdeg} \mathcal{R}^{\mathsf{G}} = 2L$. We compute $\operatorname{trdeg}(\widetilde{\mathcal{R}}^{\mathsf{G}}_{\leq k})$ for $k = 1, 2, 3$ by applying Lemma 4.2.6 at a generic point $\theta_* \in \mathbb{R}^d$ with $r_l(\theta_*) > 0$ for each $l = 1, \ldots, L$. Recall from the proof of Theorem 4.3.1 the map

$$\zeta(\theta) = (\theta_0, r_1, \ldots, r_L, t_1, \ldots, t_L), \qquad \zeta_* = \zeta(\theta_*),$$

with inverse function $\theta(\zeta)$ in a local neighborhood of θ_*. Then the same arguments as in the proof of Theorem 4.3.1 show

$$\begin{aligned}
\operatorname{trdeg}(\widetilde{\mathcal{R}}^{\mathsf{G}}_{\leq 1}) &= \operatorname{rank}\left(\nabla^2_\zeta \tilde{s}_1(\theta(\zeta))\Big|_{\zeta=\zeta_*}\right) = 1, \\
\operatorname{trdeg}(\widetilde{\mathcal{R}}^{\mathsf{G}}_{\leq 2}) &= \operatorname{rank}\left(\nabla^2_\zeta \tilde{s}_1(\theta(\zeta)) + \nabla^2_\zeta \tilde{s}_2(\theta(\zeta))\Big|_{\zeta=\zeta_*}\right) = L + 1,
\end{aligned}$$

and $\operatorname{trdeg}(\widetilde{\mathcal{R}}^{\mathsf{G}}_{\leq 3}) = \operatorname{rank}(\widetilde{H}(\zeta_*))$ for the Hessian

$$\widetilde{H}(\zeta_*) = \nabla^2_\zeta \tilde{s}_1(\theta(\zeta)) + \nabla^2_\zeta \tilde{s}_2(\theta(\zeta)) + \nabla^2_\zeta \tilde{s}_3(\theta(\zeta))\Big|_{\zeta=\zeta_*}.$$

Writing this Hessian in the block decomposition according to (r, t), and noting that $\tilde{s}_1, \tilde{s}_2$ depend only on r and not on t, we have the decomposition

$$\widetilde{H}(\zeta_*) = \begin{pmatrix} \nabla^2_r \tilde{s}_1(\theta(\zeta)) + \nabla^2_r \tilde{s}_2(\theta(\zeta))\big|_{\zeta=\zeta_*} & 0 \\ 0 & 0 \end{pmatrix} + \begin{pmatrix} \nabla^2_r \tilde{s}_3(\theta(\zeta))\big|_{\zeta=\zeta_*} & \nabla^2_{rt} \tilde{s}_3(\theta(\zeta))\big|_{\zeta=\zeta_*} \\ \nabla^2_{tr} \tilde{s}_3(\theta(\zeta))\big|_{\zeta=\zeta_*} & \nabla^2_t \tilde{s}_3(\theta(\zeta))\big|_{\zeta=\zeta_*} \end{pmatrix}$$

The second matrix is positive semidefinite by Lemma 4.2.6, and the first matrix has $\nabla^2_r \tilde{s}_1(\theta(\zeta)) + \nabla^2_r \tilde{s}_2(\theta(\zeta))|_{\zeta=\zeta_*} \succ 0$ strictly by the analysis of $\operatorname{trdeg}(\widetilde{\mathcal{R}}^{\mathsf{G}}_{\leq 2})$, with rank exactly $L+1$. Then by Lemma C.3.1,

$$\operatorname{rank}(\widetilde{H}(\zeta_*)) \geq L + 1 + \operatorname{rank}(\nabla^2_t \tilde{s}_3(\theta(\zeta))|_{\zeta=\zeta_*}). \tag{118}$$

As in the proof of Theorem 4.3.1, let us show $\operatorname{rank}(\nabla^2_t \tilde{s}_3(\theta(\zeta))|_{\zeta=\zeta_*}) \geq L - 1$ for generic $\theta_* \in \mathbb{R}^d$ by

exhibiting a single point θ_* where this holds.

We may write the expression for $\tilde{s}_3(\theta)$ in Theorem 4.3.7 as

$$\tilde{s}_3(\theta(\zeta)) = f(r) + \frac{1}{16}\sum_{\substack{l,l',l''=1\\ l=l'+l''}}^{L} -2r_{l,l',l''}r_{*,l,l',l''}\cos(\lambda_{l,l',l''} - \lambda_{*,l,l',l''}) + r_{l,l',l''}^2\cos(2\lambda_{l,l',l''}) \\ - 2r_{l,l',l''}r_{*,l,l',l''}\cos(\lambda_{l,l',l''} + \lambda_{*,l,l',l''}),$$

for a function $f(r)$ depending only on r and not t. We pick θ_* such that $\theta_*^{(0)} = 1$ and $r_{*,l} = 1$ for all $l = 1, \dots, L$. Then, recalling $t_l = \lambda_l - \lambda_{*,l}$ and $\lambda_{l,l',l''} = \lambda_l - \lambda_{l'} - \lambda_{l''}$, and differentiating twice in t at $(r,t) = (r_*, t_*) = (r_*, 0)$,

$$\begin{aligned}\nabla_t^2 \tilde{s}_3(\theta(\zeta))\Big|_{\zeta=\zeta_*} &= \frac{1}{16}\nabla_t^2\Bigg(\sum_{\substack{l,l',l''=1\\ l=l'+l''}}^{L} -2\cos(t_l - t_{l'} - t_{l''}) + \cos(2t_l - 2t_{l'} - 2t_{l''} + 2\lambda_{*,l} - 2\lambda_{*,l'} - 2\lambda_{*,l''}) \\ &\qquad - 2\cos(t_l - t_{l'} - t_{l''} + 2\lambda_{*,l} - 2\lambda_{*,l'} - 2\lambda_{*,l''})\Bigg)\Bigg|_{t=0} \\ &= \frac{1}{16}\sum_{\substack{l,l',l''=1\\ l=l'+l''}}^{L}\Big(2 - 4\cos(2\lambda_{*,l,l',l''}) + 2\cos(2\lambda_{*,l,l',l''})\Big)\cdot w_{l,l',l''}w_{l,l',l''}^\top \\ &= \frac{1}{8}\sum_{\substack{l,l',l''=1\\ l=l'+l''}}^{L}\Big(1 - \cos(2\lambda_{*,l,l',l''})\Big)\cdot w_{l,l',l''}w_{l,l',l''}^\top,\end{aligned}$$

where $w_{l,l',l''}$ is defined as (112). Stacking $w_{l,l',l''}$ as the columns of $W \in \mathbb{R}^{L\times|\mathcal{L}|}$ as in the proof of Theorem 4.3.1, and defining the diagonal matrix $D = \operatorname{diag}(1 - \cos(2\lambda_{*,l,l',l''})) \in \mathbb{R}^{|\mathcal{L}|\times|\mathcal{L}|}$, this shows

$$\nabla_t^2 \tilde{s}_3(\theta(\zeta))\Big|_{\zeta=\zeta_*} = \frac{1}{8}WDW^\top.$$

Note that, for generic $\lambda_* = (\lambda_{*,1}, \dots, \lambda_{*,L})$, we have

$$2 - 2\cos(2\lambda_{*,l} - 2\lambda_{*,l'} - 2\lambda_{*,l''}) > 0$$

for each fixed tuple $(l, l', l'') \in \mathcal{L}$. Hence we may pick λ_* so that this holds simultaneously for all tuples $(l, l', l'') \in \mathcal{L}$. Then $\operatorname{rank}(WDW^\top) = \operatorname{rank}(WW^\top) \geq L - 1$ as shown in Theorem 4.3.1. Applying this back to (118), we have shown $\operatorname{trdeg}\widetilde{\mathcal{R}}^{\mathsf{G}}_{\leq 3} = \operatorname{rank}(\widetilde{H}(\zeta_*)) \geq 2L$. We must have also $\operatorname{trdeg}\widetilde{\mathcal{R}}^{\mathsf{G}}_{\leq 3} \leq \operatorname{trdeg}\mathcal{R}^{\mathsf{G}} = 2L$, so $\operatorname{trdeg}\widetilde{\mathcal{R}}^{\mathsf{G}}_{\leq 3} = 2L$. Then the statements about $(\tilde{d}_0, \tilde{d}_1, \tilde{d}_2, \tilde{d}_3)$ and $\widetilde{K}$ follow. □

C.3.3 Spurious local minimizers for continuous MRA

In this section, we prove Theorem 4.3.4 establishing the possible existence of spurious local minimizers for continuous MRA, when $L \geq 30$.

Proof of Theorem 4.3.4. Recall the forms of $s_1(\theta)$, $s_2(\theta)$, and $s_3(\theta)$ from Theorem 4.3.3. By definition of $s_k(\theta)$ in (4.7), each moment variety $\mathcal{V}_k(\theta_*)$ is the intersection of the global minimizers of $s_1(\theta), \dots, s_k(\theta)$. Then

$$\mathcal{V}_1(\theta_*) = \{\theta : \theta^{(0)} = \theta_*^{(0)}\}, \quad \mathcal{V}_2(\theta_*) = \{\theta : \theta^{(0)} = \theta_*^{(0)},\ r_l(\theta) = r_l(\theta_*) \text{ for each } l = 1, \dots, L\}.$$

On $\mathcal{V}_0(\theta_*) = \mathbb{R}^d$, we have $\nabla s_1(\theta)|_{\mathcal{V}_0(\theta_*)} = \theta^{(0)} - \theta_*^{(0)}$, and this vanishes exactly when $\theta \in \mathcal{V}_1(\theta_*)$. Differentiating in the coordinates $\{(\theta_1^{(l)}, \theta_2^{(l)}) : l = 1, \dots, L\}$ that parametrize $\mathcal{V}_1(\theta_*)$, and applying $r_l(\theta)^2 = (\theta_1^{(l)})^2 + (\theta_2^{(l)})^2$, we have

$$\nabla s_2(\theta)|_{\mathcal{V}_1(\theta_*)} = \frac{1}{2}\Big((r_l(\theta)^2 - r_l(\theta_*)^2) \cdot (\theta_1^{(l)}, \theta_2^{(l)}) : l = 1, \dots, L\Big).$$

Suppose θ_* satisfies the generic condition $r_l(\theta_*) > 0$ for each $l = 1, \dots, L$. Then $\nabla s_2(\theta)|_{\mathcal{V}_1(\theta_*)} = 0$ if and only if, for each $l = 1, \dots, L$, either $r_l(\theta) = r_l(\theta_*)$ or $(\theta_1^{(l)}, \theta_2^{(l)}) = (0, 0)$. If the latter holds for any $l = 1, \dots, L$, then differentiating in $(\theta_1^{(l)}, \theta_2^{(l)})$ a second time shows that the Hessian of $s_2(\theta)$ in $(\theta_1^{(l)}, \theta_2^{(l)})$ is negative-definite at $(\theta_1^{(l)}, \theta_2^{(l)}) = (0, 0)$, and hence $\lambda_{\min}(\nabla^2 s_2(\theta)|_{\mathcal{V}_1(\theta_*)}) < 0$. On the other hand, if $r_l(\theta) = r_l(\theta_*)$ for every $l = 1, \dots, L$, then $\theta \in \mathcal{V}_2(\theta_*)$ and θ is a global minimizer of $s_2(\theta)$. Thus, the minimizations of $s_1(\theta)$ and $s_2(\theta)$ on $\mathcal{V}_0(\theta_*)$ and $\mathcal{V}_1(\theta_*)$ are globally benign.

We now take $L \geq 30$, and construct the example of θ_* where $s_3(\theta)$ has a spurious local minimizer in $\mathcal{V}_2(\theta_*)$ that is nondegenerate up to orbit. Consider θ_* such that $r_{*,l} := r_l(\theta_*) > 0$ for each $l = 1, \dots, L$. Then $\mathcal{V}_2(\theta_*)$ may be smoothly parametrized by the coordinates $t = (t_1, \dots, t_L)$ where $t_l = \lambda_l(\theta) - \lambda_l(\theta_*)$. The function $8s_3(\theta)$ restricted to $\mathcal{V}_2(\theta_*)$ is given as a function of t by

$$s(t) = -\sum_{\substack{l,l',l''=1 \\ l=l'+l''}}^{L} r_{*,l}^2 r_{*,l'}^2 r_{*,l''}^2 \cos(t_l - t_{l'} - t_{l''}) + \text{constant}.$$

The orbit $\mathcal{O}_{\theta_*} \cap \mathcal{V}_2(\theta_*)$ is defined by

$$\big\{(t_1, \dots, t_L) : t_l \equiv \tau \cdot l \bmod 2\pi \text{ for all } l = 1, \dots, L \text{ and some } \tau \in \mathbb{R}\big\}, \tag{119}$$

where $\tau = 0$ corresponds to the point θ_* itself. Thus, our goal is to exhibit a point θ_* for which

$$\nabla s(\hat{t}) = 0, \qquad \nabla^2 s(\hat{t}) \succeq 0, \qquad \text{and} \qquad \operatorname{rank}(\nabla^2 s(\hat{t})) = L - 1 \tag{120}$$

at some $\hat{t}$ *not* belonging to this orbit (119). Then the corresponding point $\theta \in \mathbb{R}^d$ where $\theta^{(0)} = \theta_*^{(0)}$, $r_l(\theta) = r_{*,l}$, and $t_l(\theta) = \hat{t}_l$ for each $l = 1, \dots, L$ is our desired spurious local minimizer for $s_3(\theta)$. Note that the condition (120) depends on θ_* only via $r_* = (r_{*,1}, \dots, r_{*,L})$, so equivalently, our goal is to construct an appropriate such vector r_*.

We split the construction into two steps: First, we construct $\tilde{r}_*$ for which $\hat{t} = (\pi, 0, \dots, 0)$ satisfies

$$\nabla s(\hat{t}) = 0, \qquad \nabla^2 s(\hat{t}) \succeq 0, \qquad \operatorname{rank}(\nabla^2 s(\hat{t})) = L - 2.$$

This Hessian $\nabla^2 s(\hat{t})$ will have a dimension-2 null space spanned by the vectors $e_3 = (0, 0, 1, 0, \dots, 0)$ and $e = (1, 2, \dots, L)$. Second, we make a small perturbation of the third coordinate of $\tilde{r}_*$, to eliminate the null vector e_3 while preserving $\nabla s(\hat{t}) = 0$ and $\nabla^2 s(\hat{t}) \succeq 0$. This yields r_* satisfying (120).

Step I. Clearly $\hat{t} = (\pi, 0, \dots, 0)$ satisfies $\nabla s(\hat{t}) = 0$ for any choice of r_*, because $\sin(k\pi) = 0$ for any integer k. The Hessian of $s(t)$ is given by

$$\nabla^2 s(t) = \sum_{\substack{l,l',l''=1 \\ l=l'+l''}}^{L} r_{*,l}^2 r_{*,l'}^2 r_{*,l''}^2 \cos(t_l - t_{l'} - t_{l''})(e_l - e_{l'} - e_{l''})(e_l - e_{l'} - e_{l''})^\top,$$

where e_l is the l^{th} standard basis vector. Then for the above choice of $\hat{t}$ and for any vector $v \in \mathbb{R}^L$,

$$v^\top \nabla^2 s(\hat{t}) v = \sum_{\substack{l,l',l''=1 \\ l=l'+l''}}^{L} r_{*,l}^2 r_{*,l'}^2 r_{*,l''}^2 (v_l - v_{l'} - v_{l''})^2 \times \begin{cases} -1 & \text{if exactly one of } l', l'' \text{ equals 1,} \\ 1 & \text{otherwise.} \end{cases} \tag{121}$$

Consider $\tilde{r}_* = (\tilde{r}_{*,1}, \tilde{r}_{*,2}, \tilde{r}_{*,3}, \tilde{r}_{*,4}, \dots, \tilde{r}_{*,L}) = (1, L^{\kappa/2}, 0, 1, \dots, 1)$ where $\tilde{r}_{*,\ell} = 1$ for all $\ell \geq 4$, and for a constant $\kappa > 0$ to be determined later. Then from (121) applied with $v = e_3$ and $v = e = (1, 2, \dots, L)$, it is immediate that these two vectors belong to the null space of $\nabla^2 s(\hat{t})$.

We now check that for any other unit vector $v \in \mathbb{R}^L$ orthogonal to both e_3 and e, we have

$v^\top \nabla^2 s(\hat{t}) v > 0$ strictly. Observe from (121) that for $r_* = \tilde{r}_*$,

$$v^\top \nabla^2 s(\hat{t}) v = \sum_{\substack{l,l',l''=4 \\ l=l'+l''}}^{L} (v_l - v_{l'} - v_{l''})^2 + L^\kappa (v_2 - 2v_1)^2 + L^{2\kappa}(v_4 - 2v_2)^2 + 2L^\kappa \sum_{l=4}^{L-2} (v_{l+2} - v_l - v_2)^2 - 2\sum_{l=4}^{L-1} (v_{l+1} - v_l - v_1)^2. \quad (122)$$

Note that only the last term is negative. Denote $\epsilon = \sqrt{6} L^{\frac{1-\kappa}{2}}$. We consider two cases:

Case 1: Any one of $|v_2 - 2v_1|$, $|v_4 - 2v_2|$, $\{|v_{l+2} - v_l - v_2| : l \geq 4\}$ is larger than ϵ. Then let us upper bound the last term of (122) by

$$2\sum_{l=4}^{L-1} (v_{l+1} - v_l - v_1)^2 \leq 6 \sum_{l=4}^{L-1} (v_{l+1}^2 + v_l^2 + v_1^2) \leq 6L,$$

where the last inequality follows from $\|v\|_2^2 = 1$. Then

$$v^\top \nabla^2 s(\hat{t}) v > L^\kappa \epsilon^2 - 2\sum_{l=4}^{L-1} (v_{l+1} - v_l - v_1)^2 \geq 0.$$

Case 2: We have instead

$$|v_2 - 2v_1| \leq \epsilon, \qquad |v_4 - 2v_2| \leq \epsilon, \qquad |v_{l+2} - v_l - v_2| \leq \epsilon \quad \text{for} \quad l \geq 4. \quad (123)$$

In this case, we aim to show that the first term in (122) is large enough to compensate for the negative last term of (122).

For all $m \geq 1$, the second and third inequalities of (123) imply $|v_{2m} - m v_2| \leq (m-1)\epsilon$. Similarly, for all $m \geq 0$, the last inequality implies $|v_{2m+5} - v_5 - m v_2| \leq m\epsilon$. Combining with $|m v_2 - 2m v_1| \leq m\epsilon$ by the first inequality of (123), we obtain

$$|v_{2m} - 2m v_1| \leq L\epsilon \quad \text{for} \quad 1 \leq m \leq L/2, \quad |v_{2m+5} - v_5 - 2m v_1| \leq L\epsilon \quad \text{for} \quad 0 \leq m \leq (L-5)/2. \quad (124)$$

For the summands of the first term in (122), if $l' = 2m' + 5$ and $l'' = 2m'' + 5$ are both odd where $m', m' \geq 0$, then $l = 2m + 10$ for $m = m' + m''$, and we have

$$|v_l - v_{l'} - v_{l''}| \geq |10 v_1 - 2v_5| - 3L\epsilon$$

by (124) and the triangle inequality

$$|v_l - v_{l'} - v_{l''}| + |-v_l + (2m+10)v_1| + |v_{l'} - v_5 - 2m'v_1| + |v_{l''} - v_5 - 2m''v_1| \geq |10v_1 - 2v_5|.$$

For any even $l = 2m + 10$ with $m \geq 0$, the number of odd pairs $l', l'' \geq 5$ where $l' + l'' = 2m + 10$ is $m + 1$. Then the total number of tuples (l, l', l'') in the first term of (122) where l', l'' are odd is

$$\sum_{m=0}^{\lfloor L/2 \rfloor - 5} (m+1) = \frac{1}{2}(\lfloor L/2 \rfloor - 3)(\lfloor L/2 \rfloor - 4) \geq \frac{1}{8}(L-8)(L-10).$$

Hence, we may lower bound the first term in (122) by

$$\sum_{\substack{l,l',l''=4 \\ l=l'+l''}}^{L} (v_l - v_{l'} - v_{l''})^2 \geq \frac{1}{8}(L-8)(L-10)\Big(|10v_1 - 2v_5| - 3L\epsilon\Big)_+^2. \tag{125}$$

Similarly, the summands of the last term in (122) for $l \geq 4$ are upper bounded as

$$|v_{l+1} - v_l - v_1| \leq |5v_1 - v_5| + 2L\epsilon \tag{126}$$

again by (124) and the triangle inequality. (This may be checked separately in the cases where l is odd and even.) The number of summands in this last term is $L - 4$. Then, combining (125) and (126) gives

$$v^\top \nabla^2 s(\hat{t}) v \geq \frac{1}{8}(L-8)(L-10)\Big(|10v_1 - 2v_5| - 3L\epsilon\Big)_+^2 - 2(L-4)\Big(|5v_1 - v_5| + 2L\epsilon\Big)^2 \tag{127}$$

We now claim that for sufficiently large $\kappa > 0$, we must have

$$|5v_1 - v_5| > 5L\epsilon. \tag{128}$$

To show this claim, since $v \perp e_3$ and $v \perp e$,

$$0 = -3v_3 = \sum_{\substack{l=1 \\ l \neq 3}}^{L} l\, v_l = v_1 + 5v_5 + \sum_{m=1}^{\lfloor L/2 \rfloor} 2m \cdot v_{2m} + \sum_{m=1}^{\lfloor (L-5)/2 \rfloor} (2m+5) \cdot v_{2m+5}.$$

Denote $a_{2m} = v_{2m} - 2m \cdot v_1$ and $a_{2m+5} = v_{2m+5} - v_5 - 2m \cdot v_1$ for $m \geq 1$, where these satisfy

$|a_l| \le L\epsilon$ by (124). Let us define

$$M_1 = 1 + \sum_{m=1}^{\lfloor L/2 \rfloor} 4m^2 + \sum_{m=1}^{\lfloor (L-5)/2 \rfloor} 2m(2m+5), \qquad M_5 = 5 + \sum_{m=1}^{\lfloor (L-5)/2 \rfloor} (2m+5).$$

Then we may write the above as

$$\begin{aligned} 0 &= v_1 + 5v_5 + \sum_{m=1}^{\lfloor L/2 \rfloor} 2m \cdot (a_{2m} + 2m \cdot v_1) + \sum_{m=1}^{\lfloor (L-5)/2 \rfloor} (2m+5) \cdot (a_{2m+5} + v_5 + 2m \cdot v_1) \\ &= M_1 v_1 + M_5 v_5 + \sum_{\substack{l=1 \\ l \neq 1,3,5}}^{L} l\, a_l. \end{aligned}$$

This may be rearranged as

$$v_1 = \frac{M_5(5v_1 - v_5) - \sum_{l: l \neq 1,3,5} l\, a_l}{M_1 + 5M_5}.$$

Now suppose by contradiction that $|5v_1 - v_5| \le 5L\epsilon$. Then this implies

$$|v_1| \le \frac{5M_5 L + L^2(L+1)/2}{M_1 + 5M_5}\epsilon < C\epsilon,$$

where the second inequality holds for a universal constant $C > 0$ and any $L \ge 1$. Then $|v_5| \le |5v_1| + 5L\epsilon < 5(L+C)\epsilon$, and combining with (124) gives

$$|v_l| \le C' L\epsilon \text{ for all } l \in \{1, \dots, L\} \setminus \{3\}$$

and a different universal constant $C' > 0$. Recalling $v_3 = 0$ and $\epsilon = \sqrt{6} L^{\frac{1-\kappa}{2}}$, this contradicts that $\|v\|_2 = 1$ for sufficiently large $\kappa > 0$. Thus, (128) holds.

Finally, this bound (128) implies $|10v_1 - 2v_5| - 3L\epsilon > |5v_1 - v_5| + 2L\epsilon > 0$. For $L \ge 30$, we have $(L-8)(L-10)/8 \ge 2(L-4)$. Applying these to (127) yields $v^\top s(\hat{t}) v > 0$ as desired.

Step II. We now show that making a small positive perturbation to $\tilde{r}_{*,3}$ yields a point r_* which satisfies (120) at $\hat{t} = (\pi, 0, \dots, 0)$. Denote $q_* = r_{*,3}^2$ and set $\tilde{q}_* = \tilde{r}_{*,3}^2 = 0$. Let $\Pi \in \mathbb{R}^{L \times (L-1)}$ have orthonormal columns spanning the orthogonal complement of $e = (1, 2, \dots, L)$, and consider the projected Hessian

$$H(q_*) = \Pi^\top \nabla^2 s(\hat{t}) \Pi \in \mathbb{R}^{(L-1)\times(L-1)}$$

now as a function of q_*. By the result of Step I, $H(\tilde{q}_*) \succeq 0$, and $H(\tilde{q}_*)$ has a simple eigenvalue $\mu = 0$ with eigenvector $v = \Pi^\top e_3 / \|\Pi^\top e_3\|$. Then this eigenvalue $\mu = \mu(q_*)$ is differentiable in q_*, with derivative given by $\partial_{q_*}\mu(q_*) = v^\top \partial_{q_*} H(q_*) v$. Applying $\Pi \cdot \Pi^\top = \mathrm{Id} - ee^\top/\|e\|^2$ and the fact that $e = (1, 2, \ldots, L)$ belongs to the null space of $\nabla_t^2 s(\hat{t})$ for any q_*, this is

$$\partial_{q_*}\mu(q_*) = \frac{e_3^\top(\mathrm{Id} - ee^\top/\|e\|^2) \cdot \partial_{q_*}\nabla_t^2 s(\hat{t}) \cdot (\mathrm{Id} - ee^\top/\|e\|^2)e_3}{e_3^\top(\mathrm{Id} - ee^\top/\|e\|^2)e_3} = \frac{e_3^\top \cdot \partial_{q_*}\nabla_t^2 s(\hat{t}) \cdot e_3}{e_3^\top(\mathrm{Id} - ee^\top/\|e\|^2)e_3}.$$

By (121) applied with $v = e_3$, for general r_*, we have

$$e_3^\top \nabla_t^2 s(\hat{t}) e_3 = -2r_{*,1}^2 r_{*,2}^2 r_{*,3}^2 - 2r_{*,1}^2 r_{*,3}^2 r_{*,4}^2 + 2\sum_{l=2}^{L-3} r_{*,3}^2 r_{*,l}^2 r_{*,l+3}^2 (1 + \mathbf{1}\{l = 3\}).$$

Then differentiating in $q_* = r_{*,3}^2$ and evaluating at $\tilde{r}_* = (1, L^\kappa, 0, 1, \ldots, 1)$,

$$e_3^\top \cdot \partial_{q_*}\nabla_t^2 s(\hat{t}) \cdot e_3 \Big|_{q_* = \tilde{q}_*} = -2L^{2\kappa} - 2 + 2L^{2\kappa} + 2(L-6) > 0.$$

Thus, for some sufficiently small $\delta > 0$, setting $q_* = \delta$ yields $\mu(\delta) > 0$, and hence $H(\delta) \succ 0$ strictly. Then at the point $r_* = (1, L^\kappa, \delta, 1, \ldots, 1)$, we obtain that (120) holds.

Combining Steps I and II, we have shown that θ_* given by $(r_1(\theta_*), \ldots, r_L(\theta_*)) = (1, L^\kappa, \delta, 1, \ldots, 1)$ and (say) $\theta_*^{(0)} = 0$ and $(\lambda_1(\theta_*), \ldots, \lambda_L(\theta_*)) = 0$ satisfies (120). Then (120) holds also in a sufficiently small open neighborhood U of θ_*, by continuity. For any $\theta_* \in U$, the function $s_3(\theta)$ has a spurious local minimizer $\theta \in \mathcal{V}_2(\theta_*)$ that is non-degenerate up to orbit, where $\theta^{(0)} = \theta_*^{(0)}$, $r_l(\theta) = r_l(\theta_*)$ for all $l \geq 1$, $\lambda_1(\theta) = \lambda_1(\theta_*) + \pi$, and $\lambda_l(\theta) = \lambda_l(\theta_*)$ for all $l \geq 2$. This concludes the proof. □

C.4 Analyses of function estimation under an $\mathsf{SO}(3)$ rotation

This appendix collects the proofs of the results in Section 4.4, on estimating a function in 2 or 3 dimensions under an $\mathsf{SO}(3)$ rotation of its domain.

Appendix C.4.1 first reviews the complex spherical harmonic basis, and the associated calculus of Wigner D-matrices and Clebsch-Gordan coefficients. Appendix C.4.2 proves the results of Section 4.4.1 on spherical registration. Appendix C.4.3 provides the details of the basis construction and proves the results of Section 4.4.2 for the unprojected cryo-EM model. Appendix C.4.3 contains the analogous details and proofs for the projected cryo-EM model of Section 4.4.3.

C.4.1 Calculus of spherical harmonics

We first fix notations for some special functions related to the action of $\mathsf{SO}(3)$ and present some identities between them which will appear in the proofs.

Complex spherical harmonics

Let $P_{lm}(x)$ denote the associated Legendre polynomials (without Cordon-Shortley phase)

$$P_{lm}(x) = \frac{1}{2^l l!}(1-x^2)^{m/2}\frac{d^{l+m}}{dx^{l+m}}(x^2-1)^l \quad \text{for } m = -l, -l+1, \ldots, l-1, l. \tag{129}$$

Let $\mathcal{S}^2 \subset \mathbb{R}^3$ be the unit sphere, parametrized by the latitude $\phi_1 \in [0, \pi]$ and longitude $\phi_2 \in [0, 2\pi)$. The complex spherical harmonics basis on $\mathcal{S}^2$ is given by (see (Rose, 1995, Eq. (III.20)))

$$y_{lm}(\phi_1, \phi_2) = (-1)^m \sqrt{\frac{2l+1}{4\pi} \cdot \frac{(l-m)!}{(l+m)!}} \cdot P_{lm}(\cos\phi_1) e^{\mathbf{i}m\phi_2} \text{ for } l \geq 0 \text{ and } m = -l, \ldots, l. \tag{130}$$

The index l is the frequency, and there are $2l+1$ basis functions at each frequency l. These functions are orthonormal in $L_2(\mathcal{S}^2, \mathbb{C})$ with respect to the surface area measure $\sin\phi_1 \, \mathrm{d}\phi_1 \, \mathrm{d}\phi_2$, and satisfy the conjugation symmetry (see (Rose, 1995, Eq. (III.23)))

$$\overline{y_{lm}(\phi_1, \phi_2)} = (-1)^m y_{l,-m}(\phi_1, \phi_2). \tag{131}$$

Lemma C.4.1. *For all m, the associated Legendre polynomials in (129) satisfy*

$$P_{lm}(0) = \mathbf{1}\{l+m \text{ is even}\} \cdot \frac{(-1)^{(l-m)/2}}{2^l l!} \binom{l}{(l+m)/2} (l+m)!$$

Proof. This follows from applying a binomial expansion of $(x^2-1)^l$, and then differentiating in x—see also (Bandeira et al., 2017, Eq. (14)). □

Wigner D-matrices

Let $f \in L_2(\mathcal{S}^2, \mathbb{C})$. Then f may be decomposed in the complex spherical harmonics basis (130) as

$$f = \sum_{l=0}^{\infty} \sum_{m=-l}^{l} u_m^{(l)} y_{lm}.$$

Writing $u^{(l)} = \{u_m^{(l)} : -l \le m \le l\}$, the rotation $f \mapsto f_{\mathfrak{g}}$ given by $f_{\mathfrak{g}}(\phi_1, \phi_2) = f(\mathfrak{g}^{-1} \cdot (\phi_1, \phi_2))$ is described by the map of spherical harmonic coefficients (see (Rose, 1995, Eq. (4.28a)))

$$u^{(l)} \mapsto D^{(l)}(\mathfrak{g})u^{(l)} \text{ for each } l = 0, 1, 2, \ldots,$$

where $D^{(l)}(\mathfrak{g}) \in \mathbb{C}^{(2l+1)\times(2l+1)}$ is the *complex Wigner D-matrix* at frequency l corresponding to $\mathfrak{g}$.

Our computations will not require the explicit forms of $D^{(l)}(\mathfrak{g})$, but only the following moment identities when $\mathfrak{g} \in \mathsf{SO}(3)$ is a Haar-uniform random rotation (see (Rose, 1995, Section 16) and (Bandeira et al., 2017, Appendix A.3)):

(1) Mean identity:

$$D^{(0)}(\mathfrak{g}) = 1, \qquad \mathbb{E}_{\mathfrak{g}}[D^{(l)}(\mathfrak{g})] = 0 \text{ for all } l \ge 1. \tag{132}$$

(2) Orthogonality: for any $l, l' \ge 0$ and $-l \le q, m \le l$ and $-l' \le q', m' \le l'$,

$$\mathbb{E}_{\mathfrak{g}}\left[D^{(l)}_{qm}(\mathfrak{g})D^{(l')}_{q'm'}(\mathfrak{g})\right] = \frac{(-1)^{m+q}}{2l+1}\mathbf{1}\{l = l', q = -q', m = -m'\}. \tag{133}$$

(3) Third order identity: for any $l, l', l'' \ge 0$ and $-l \le q, m \le l$ and $-l' \le q', m' \le l'$ and $-l'' \le q'', m'' \le l''$,

$$\begin{aligned}\mathbb{E}_{\mathfrak{g}}\left[D^{(l)}_{qm}(\mathfrak{g})D^{(l')}_{q'm'}(\mathfrak{g})D^{(l'')}_{q''m''}(\mathfrak{g})\right] = \mathbf{1}\{q + q' = -q''\}\cdot\mathbf{1}\{m + m' = -m''\}\cdot\mathbf{1}\{|l - l'| \le l'' \le l + l'\} \\ \cdot \frac{(-1)^{m''+q''}}{2l''+1}\langle l, q; l', q'|l'', -q''\rangle\langle l, m; l', m'|l'', -m''\rangle,\end{aligned} \tag{134}$$

where $\langle l, m; l', m'|l'', m''\rangle$ is a Clebsch-Gordan coefficient, defined in the following section.

Clebsch-Gordan coefficients

The Clebsch-Gordan coefficients $\langle l, m; l', m'|l'', m''\rangle$ are defined for integer arguments l, l', l'', m, m', m'' where

$$|m| \le l, \quad |m'| \le l', \quad |m''| \le l'' \quad \text{and} \quad |l - l'| \le l'' \le l + l'. \tag{135}$$

The latter condition $|l - l'| \le l'' \le l + l'$ is equivalent to the three symmetric triangle inequality conditions $l + l' \ge l''$, $l + l'' \ge l'$, and $l' + l'' \ge l$. For such arguments, $\langle l, m; l', m'|l'', m''\rangle$ is given

explicitly by (see (Böhm, 2013, Eq. (2.41)) and (Bandeira et al., 2017, Appendix A.2))

$$\begin{aligned}
&\langle l, m; l', m' | l'', m'' \rangle \\
&= \mathbf{1}\{m'' = m + m'\} \times \sqrt{\frac{(2l''+1)(l+l'-l'')!(l+l''-l')!(l'+l''-l)!}{(l+l'+l''+1)!}} \\
&\quad \times \sqrt{(l-m)!(l+m)!(l'-m')!(l'+m')!(l''-m'')!(l''+m'')!} \\
&\quad \times \sum_k \frac{(-1)^k}{k!(l+l'-l''-k)!(l-m-k)!(l'+m'-k)!(l''-l'+m+k)!(l''-l-m'+k)!}
\end{aligned} \tag{136}$$

where the summation is over all integers k for which the argument of every factorial is nonnegative. We extend the definition to all integer arguments by

$$\langle l, m; l', m' | l'', m' \rangle = 0 \quad \text{if (135) does not hold.} \tag{137}$$

We will use the notational shorthand

$$C^{l,l',l''}_{m,m',m''} = \langle l, m; l', m' | l'', m'' \rangle.$$

These coefficients satisfy the sign symmetry (see (Rose, 1995, Eq. (3.16a)) and (Böhm, 2013, Eq. (2.47)))

$$C^{l,l',l''}_{m,m',m''} = (-1)^{l+l'+l''} C^{l,l',l''}_{-m,-m',-m''}. \tag{138}$$

Note that we may have $C^{l,l',l''}_{m,m',m''} = 0$ even if (135) holds and $m'' = m+m'$. For example, $C^{3,2,2}_{2,-1,1} = 0$. In our later proofs, we will require that certain Clebsch-Gordan coefficients are *non-zero*, and the following lemma provides a sufficient condition for this to hold.

Lemma C.4.2. *Let l, l', l'', m, m', m'' satisfy (135), where $m'' = m + m'$. In addition, suppose the following conditions all hold:*

- *$l \geq l'$ and $l \geq l'' + 1$.*
- *$|m'| \in \{l' - 1, l'\}$ and $|m''| \in \{l'' - 1, l''\}$.*
- *We do not have $|m| = l - 1$, $|m'| = l' - 1$, $|m''| = l'' - 1$, and $l' = l''$.*

Then

$$C^{l,l',l''}_{m,m',m''} \neq 0.$$

Proof. Applying the sign symmetry (138), we may assume $m' \in \{-l', -l'+1\}$. We consider separately these cases.

Case I: $m' = -l'$**.** Then $m = m'' - m' = m'' + l'$. The condition that k and $l' + m' - k$ are both nonnegative in (136) requires $k = 0$, so the sum in (136) consists of just this single term. The remaining factorials in (136) are also nonnegative, because $l + l' - l'' \geq 0$, $l - m \geq 0$, $l'' - l' + m = l'' + m'' \geq 0$, and $l'' - l - m' = l'' + l' - l \geq 0$. Thus (136) is non-zero.

Case II: $m' = -l' + 1$**.** Then $m = m'' + l' - 1$. The condition that k and $l' + m' - k$ are both nonnegative then requires $k \in \{0, 1\}$. Substituting $m' = -l' + 1$ and $m = m'' + l' - 1$, these two terms in (136) for $k \in \{0, 1\}$ are

$$\frac{1}{(l+l'-l'')!(l-m)!(l''+m''-1)!(l'+l''-l-1)!} - \frac{1}{(l+l'-l''-1)!(l-m-1)!(l''+m'')!(l'+l''-l)!}$$

where each term is understood as 0 if an argument to one of its factorials is negative. Here $l+l'-l'' \geq l + l' - l'' - 1 \geq 0$ always, because $l \geq l'' + 1$.

- If $m = l$, then the second term is 0. Also $l'' + m'' - 1 = l'' + (m + m') - 1 = l'' + l - l' \geq 0$ and $l' + l'' - l - 1 = (m - m'' + 1) + l'' - l - 1 = l'' - m'' \geq 0$, so the first term is non-zero.
- If $m < l$ but $m'' = -l''$ or $l = l' + l''$, then the first term is 0, but the second term is non-zero.

It remains to consider $m < l$, $m'' \in \{-l'' + 1, l'' - 1, l''\}$, and $l < l' + l''$. Then both terms are non-zero, and their sum is

$$\frac{1}{(l+l'-l'')!(l-m)!(l''+m'')!(l'+l''-l)!} \left((l'' + m'')(l' + l'' - l) - (l + l' - l'')(l - m)\right).$$

We now consider the three cases of m'':

- $m'' = l''$ is not possible, because this would imply $m = l' + l'' - 1 \geq l$, contradicting $m < l$.
- If $m'' = l'' - 1$, then $m = l' + l'' - 2 \geq l - 1$. Hence we must have the equalities $m = l - 1$ and $l' + l'' - 1 = l$. Then

  $$(l'' + m'')(l' + l'' - l) - (l + l' - l'')(l - m) = (2l'' - 1) - (2l' - 1),$$

  which is non-zero because our third given condition implies $l' \neq l''$ when $|m| = l - 1$, $|m'| = l' - 1$, and $|m''| = l'' - 1$.

- If $m'' = -l'' + 1$, then

$$(l'' + m'')(l' + l'' - l) - (l + l' - l'')(l - m) = (l' + l'' - l) - (l + l' - l'')(l - m).$$

  This is non-zero because $l - m \geq 1$ and $l + l' - l'' > l' + l'' - l$ strictly.

Thus we obtain that (136) is non-zero in all cases. □

C.4.2 Spherical registration

In this section, we give proofs of our results relating to spherical registration.

Function basis

We describe the real spherical harmonic basis in this example, and prove Lemma 4.4.1.

The real spherical harmonic basis $\{h_{lm} : l \geq 0,\, m \in \{-l, \ldots, l\}\}$ used in Section 4.4.1 is related to the complex spherical harmonic basis (130) by

$$h_{lm} = \begin{cases} \frac{1}{\sqrt{2}}\big(y_{l,-m} + (-1)^m y_{lm}\big) & \text{if } m > 0 \\ y_{l0} & \text{if } m = 0 \\ \frac{\mathbf{i}}{\sqrt{2}}\big(y_{lm} - (-1)^m y_{l,-m}\big) & \text{if } m < 0. \end{cases}$$

It may be checked from (131) that these functions $\{h_{lm}\}$ are real-valued and form an orthonormal basis for $L_2(\mathcal{S}^2, \mathbb{R})$. For any function $f \in L_2(\mathcal{S}^2, \mathbb{C})$, writing its orthogonal decompositions in the bases $\{y_{lm}\}$ and $\{h_{lm}\}$ as

$$f = \sum_{l=0}^{\infty} \sum_{m=-l}^{l} u_m^{(l)} y_{lm} = \sum_{l=0}^{\infty} \sum_{m=-l}^{l} \theta_m^{(l)} h_{lm},$$

the coefficients $\{u_m^{(l)}\}$ and $\{\theta_m^{(l)}\}$ are then related by the unitary transformation (4.22). If f is real-valued, then $\{\theta_m^{(l)}\}$ are real, and hence $\{u_m^{(l)}\}$ satisfy the sign symmetry (4.23).

Proof of Lemma 4.4.1. As described in Appendix C.4.1, the rotation by $\mathfrak{g} \in \mathsf{SO}(3)$ acts on the complex spherical harmonic coefficients $u \in \mathbb{C}^d$ by

$$u \mapsto D(\mathfrak{g})u,$$

where $D(\mathfrak{g})$ is the block-diagonal matrix defined in (4.24). Since u and θ are related by the unitary transformations $u = V^*\theta$ and $\theta = Vu$, the action on θ is then given by $\theta \mapsto V \cdot D(\mathfrak{g}) \cdot V^*\theta$. □

Terms of the high-noise series expansion

We prove Theorem 4.4.4 on the forms of $s_1(\theta)$, $s_2(\theta)$, and $s_3(\theta)$.

Proof of Theorem 4.4.4. Recall by Lemma C.1.1 that

$$s_k(\theta) = \frac{1}{2(k!)}\mathbb{E}_g\left[\langle\theta, g\cdot\theta\rangle^k - 2\langle\theta, g\cdot\theta_*\rangle^k + \langle\theta_*, g\cdot\theta_*\rangle^k\right]. \tag{139}$$

Consider two different real spherical harmonic coefficient vectors $\theta, \vartheta \in \mathbb{R}^d$, and the corresponding complex coefficients $u = V^*\theta \in \mathbb{C}^d$ and $v = V^*\vartheta \in \mathbb{C}^d$. We compute $\mathbb{E}_g[\langle\theta, g\cdot\vartheta\rangle^k]$ for $k = 1, 2, 3$.

Case $k = 1$: By Lemma 4.4.1, for any $g \in \mathsf{G}$,

$$\langle\theta, g\cdot\vartheta\rangle = \langle\theta, VD(\mathfrak{g})V^*\vartheta\rangle = \langle u, D(\mathfrak{g})v\rangle.$$

From the block-diagonal form for $D(\mathfrak{g})$ in (4.24), we obtain

$$\langle\theta, g\cdot\vartheta\rangle = \sum_{l=0}^{L}\langle u^{(l)}, D^{(l)}(\mathfrak{g})v^{(l)}\rangle = \sum_{l=0}^{L}\sum_{q,m=-l}^{l}\overline{u_q^{(l)}}D^{(l)}_{qm}(\mathfrak{g})v^{(l)}_m. \tag{140}$$

Applying the identities (132) yields

$$\mathbb{E}_g[\langle\theta, g\cdot\vartheta\rangle] = \overline{u_0^{(0)}}v_0^{(0)}.$$

Write the shorthands $u^{(0)} = u_0^{(0)}$ and $v^{(0)} = v_0^{(0)}$, and recall from (4.23) that $u^{(0)}, v^{(0)}$ are real. Then applying this to (139),

$$s_1(\theta) = \frac{1}{2}\mathbb{E}_g[\langle\theta, g\cdot\theta\rangle] - \mathbb{E}_g[\langle\theta_*, g\cdot\theta\rangle] + \frac{1}{2}\mathbb{E}_g[\langle\theta_*, g\cdot\theta_*\rangle] = \frac{1}{2}\Big(u^{(0)}(\theta) - u^{(0)}(\theta_*)\Big)^2.$$

Case $k = 2$: We take the expected square on both sides of (140), applying (4.23) and the relation

(133). Then

$$\mathbb{E}_g[\langle\theta, g\cdot\vartheta\rangle^2] = \sum_{l=0}^{L}\sum_{q,m=-l}^{l}\frac{(-1)^{m+q}}{2l+1}\overline{u_q^{(l)}u_{-q}^{(l)}}v_m^{(l)}v_{-m}^{(l)}$$
$$= \sum_{l=0}^{L}\sum_{q,m=-l}^{l}\frac{1}{2l+1}\overline{u_q^{(l)}}u_q^{(l)}v_m^{(l)}\overline{v_m^{(l)}} = \sum_{l=0}^{L}\frac{1}{2l+1}\|u^{(l)}\|^2\cdot\|v^{(l)}\|^2.$$

Applying this to (139),

$$s_2(\theta) = \frac{1}{4}\mathbb{E}_g[\langle\theta, g\cdot\theta\rangle^2] - \frac{1}{2}\mathbb{E}_g[\langle\theta_*, g\cdot\theta\rangle^2] + \frac{1}{4}\mathbb{E}_g[\langle\theta_*, g\cdot\theta_*\rangle^2]$$
$$= \sum_{l=0}^{L}\frac{1}{4(2l+1)}\left(\|u^{(l)}(\theta)\|^2 - \|u^{(l)}(\theta_*)\|^2\right)^2.$$

Case $k=3$: We now take the expected cube on both sides of (140), applying the relation (134). Recall the convention (137). Then

$$\mathbb{E}_g[\langle\theta, g\cdot\vartheta\rangle^3]$$
$$= \sum_{\substack{l,l',l''=0\\ |l-l'|\le l''\le l+l'}}^{L}\sum_{q,m=-l}^{l}\sum_{q',m'=-l'}^{l'}\frac{(-1)^{m+m'+q+q'}}{2l''+1}\cdot C_{q,q',q+q'}^{l,l',l''}C_{m,m',m+m'}^{l,l',l''}\overline{u_q^{(l)}u_{q'}^{(l')}u_{-q-q'}^{(l'')}}v_m^{(l)}v_{m'}^{(l')}v_{-m-m'}^{(l'')}$$
$$= \sum_{\substack{l,l',l''=0\\ |l-l'|\le l''\le l+l'}}^{L}\sum_{q,m=-l}^{l}\sum_{q',m'=-l'}^{l'}\frac{1}{2l''+1}\cdot C_{q,q',q+q'}^{l,l',l''}C_{m,m',m+m'}^{l,l',l''}\overline{u_q^{(l)}u_{q'}^{(l')}}u_{q+q'}^{(l'')}v_m^{(l)}v_{m'}^{(l')}\overline{v_{m+m'}^{(l'')}}.$$

Recall that

$$B_{l,l',l''}(\theta) = \sum_{m=-l}^{l}\sum_{m'=-l'}^{l'}C_{m,m',m+m'}^{l,l',l''}\overline{u_m^{(l)}u_{m'}^{(l')}}u_{m+m'}^{(l'')}, \qquad u = V^*\theta.$$

Then the above may be written as

$$\mathbb{E}_g[\langle\theta, g\cdot\vartheta\rangle^3] = \sum_{\substack{l,l',l''=0\\ |l-l'|\le l''\le l+l'}}^{L}\frac{1}{2l''+1}B_{l,l',l''}(\theta)\overline{B_{l,l',l''}(\vartheta)}.$$

Changing indices $(m, m') \mapsto (-m, -m')$ and applying the symmetries (138) and (4.23), we have

$$\begin{aligned} B_{l,l',l''}(\theta) &= \sum_{m=-l}^{l} \sum_{m'=-l'}^{l'} C^{l,l',l''}_{-m,-m',-m-m'} \overline{u^{(l)}_{-m} u^{(l')}_{-m'}} u^{(l'')}_{-m-m'} \\ &= \sum_{m=-l}^{l} \sum_{m'=-l'}^{l'} (-1)^{l+l'+l''} C^{l,l',l''}_{m,m',m+m'} \cdot (-1)^{m+m'+(m+m')} u^{(l)}_{m} u^{(l')}_{m'} \overline{u^{(l'')}_{m+m'}} \\ &= (-1)^{l+l'+l''} \overline{B_{l,l',l''}(\theta)}. \end{aligned}$$

Thus $B_{l,l',l''}(\theta)$ is real-valued if $l + l' + l''$ is even and pure imaginary if $l + l' + l''$ is odd. Applying this to (139),

$$\begin{aligned} s_3(\theta) &= \frac{1}{12}\mathbb{E}_g[\langle \theta, g \cdot \theta \rangle^3] - \frac{1}{6}\mathbb{E}_g[\langle \theta_*, g \cdot \theta \rangle^3] + \frac{1}{12}\mathbb{E}_g[\langle \theta_*, g \cdot \theta_* \rangle^3] \\ &= \frac{1}{12} \sum_{\substack{l,l',l''=0 \\ |l-l'| \le l'' \le l+l'}}^{L} \frac{1}{2l''+1} \left(B_{l,l',l''}(\theta) - B_{l,l',l''}(\theta_*)\right) \left(\overline{B_{l,l',l''}(\theta)} - \overline{B_{l,l',l''}(\theta_*)}\right) \\ &= \frac{1}{12} \sum_{\substack{l,l',l''=0 \\ |l-l'| \le l'' \le l+l'}}^{L} \frac{1}{2l''+1} \left|B_{l,l',l''}(\theta) - B_{l,l',l''}(\theta_*)\right|^2. \end{aligned}$$

□

Transcendence degrees

We now prove Theorem 4.4.2 on the sequences of transcendence degrees.

Proof of Theorem 4.4.2. For generic values $(\theta^{(1)}_{-1}, \theta^{(1)}_0, \theta^{(1)}_1) \in \mathbb{R}^3$ of the coefficients of θ at spherical frequency $l = 1$, the action of $\{D^{(1)}(\mathfrak{g}) : \mathfrak{g} \in \mathsf{SO}(3)\}$ on $(\theta^{(1)}_{-1}, \theta^{(1)}_0, \theta^{(1)}_1)$ has trivial stabilizer $\{\mathrm{Id}\}$. Thus for any $L \ge 1$, the full action of G on $\theta \in \mathbb{R}^d$ also has trivial stabilizer, so $\operatorname{trdeg} \mathcal{R}^{\mathsf{G}} = d - \dim(\mathsf{G}) = d - \dim(\mathsf{SO}(3)) = d - 3$, and $d_0 = 3$.

We compute $\operatorname{trdeg}(\mathcal{R}^{\mathsf{G}}_{\le k})$ for $k = 1, 2, 3$ using Lemma 4.2.6. Recall the forms of $s_1(\theta)$ and $s_2(\theta)$ in Theorem 4.4.4, where $u^{(0)}(\theta) = \theta^{(0)}_0$ and $\|u^{(l)}(\theta)\|^2 = \|\theta^{(l)}\|^2$ for $\theta^{(l)} = (\theta^{(l)}_m : m = -l, \dots, l)$. Then we obtain directly that for generic $\theta_* \in \mathbb{R}^d$,

$$\begin{aligned} \operatorname{trdeg}(\mathcal{R}^{\mathsf{G}}_{\le 1}) &= \operatorname{rank}\left(\nabla^2 s_1(\theta_*)\right) = 1 \\ \operatorname{trdeg}(\mathcal{R}^{\mathsf{G}}_{\le 2}) &= \operatorname{rank}\left(\nabla^2 s_1(\theta_*) + \nabla^2 s_2(\theta_*)\right) = L + 1. \end{aligned}$$

It remains to show $\operatorname{trdeg}(\mathcal{R}^{\mathsf{G}}_{\le 3}) = d - 3$. Note that $\operatorname{trdeg}(\mathcal{R}^{\mathsf{G}}_{\le 3}) \le \operatorname{trdeg}(\mathcal{R}^{\mathsf{G}}) = d - 3$, so it suffices to show the lower bound $\operatorname{trdeg}(\mathcal{R}^{\mathsf{G}}_{\le 3}) \ge d - 3$.

By Lemma 4.2.6 and the fact that each Hessian $\nabla^2 s_k(\theta_*)$ is positive semidefinite,

$$\operatorname{trdeg}(\mathcal{R}^{\mathsf{G}}_{\leq 3}) \geq \operatorname{rank}\big(\nabla^2 s_3(\theta_*)\big).$$

Writing the index set

$$\mathcal{J} = \Big\{(l,l',l'') : 0 \leq l,l',l'' \leq L,\ |l-l'| \leq l'' \leq l+l'\Big\}, \tag{141}$$

we have by Theorem 4.4.4

$$s_3(\theta) = \frac{1}{12}\sum_{(l,l',l'')\in\mathcal{J}} \frac{1}{2l''+1}\big(B_{l,l',l''}(\theta) - B_{l,l',l''}(\theta_*)\big)\big(\overline{B_{l,l',l''}(\theta)} - \overline{B_{l,l',l''}(\theta_*)}\big).$$

Let us denote

$$B(\theta) = \Big(B_{l,l',l''}(\theta) :\ (l,l',l'') \in \mathcal{J}\Big), \qquad B : \mathbb{R}^d \to \mathbb{C}^{|\mathcal{J}|},$$

and write $\mathrm{d}B(\theta) \in \mathbb{C}^{|\mathcal{J}|\times d}$ for its the derivative in θ. Then, applying the chain rule to differentiate $s_3(\theta)$ twice at $\theta = \theta_*$, we obtain

$$\nabla^2 s_3(\theta_*) = \mathrm{d}B(\theta_*)^\top \cdot \operatorname{diag}\left(\frac{1}{6(2l''+1)} : (l,l',l'') \in \mathcal{J}\right) \cdot \overline{\mathrm{d}B(\theta_*)}.$$

The diagonal matrix in the middle has full rank, so

$$\operatorname{rank}\Big(\nabla^2 s_3(\theta_*)\Big) = \operatorname{rank}\Big(\mathrm{d}B(\theta_*)\Big). \tag{142}$$

To analyze this rank, recall the complex parametrization $u = V^*\theta \in \mathbb{C}^d$ from (4.22), satisfying the symmetry (4.23). Let us write the real and imaginary parts of u as

$$u^{(l)}_m = v^{(l)}_m + \mathbf{i} w^{(l)}_m$$

so that this symmetry (4.23) is equivalent to

$$v^{(l)}_{-m} = (-1)^m v^{(l)}_m, \qquad w^{(l)}_{-m} = (-1)^{m+1} w^{(l)}_m. \tag{143}$$

Note that for $m = 0$, this implies $w_0^{(l)} = 0$. Then, setting

$$\eta^{(l)}(\theta) = (v_0^{(l)}, v_1^{(l)}, w_1^{(l)}, v_2^{(l)}, w_2^{(l)}, \dots, v_l^{(l)}, w_l^{(l)}),$$

these coordinates $\eta^{(l)} \in \mathbb{R}^{2l+1}$ provide a (linear) invertible reparametrization of $\theta^{(l)}$. This defines a reparametrization

$$\eta(\theta) = \Big(\eta^{(l)}(\theta) : 0 \le l \le L\Big) \in \mathbb{R}^d$$

with inverse function $\theta(\eta)$. Writing as shorthand $\eta_* = \eta(\theta_*)$ and $B(\eta) \equiv B(\theta(\eta))$, and denoting by $\mathrm{d}_\eta B(\eta)$ the derivative of B in the new variables η, (142) is equivalent to

$$\operatorname{rank}\Big(\nabla^2 s_3(\theta_*)\Big) = \operatorname{rank}\Big(\mathrm{d}_\eta B(\eta_*)\Big).$$

Denote

$$\tilde{B}(\eta) = \Big(B_{l,l',l''}(\eta) : (l,l',l'') \in \mathcal{J},\ \max(l,l',l'') \le 10\Big).$$

Let us group the columns and rows of $\mathrm{d}_\eta B$ into blocks indexed by $\{\sim, 11, 12, \dots, L\}$ as follows: The column block $\sim$ corresponds to $\mathrm{d}_{\eta^{(0)},\dots,\eta^{(10)}}$. The row block $\sim$ corresponds to $\tilde{B}(\eta)$. For $l \ge 11$, the column block l corresponds to $\mathrm{d}_{\eta^{(l)}}$, and the row block l corresponds to $B^{(l)}$ as defined below in Lemma C.4.3. (These blocks $\tilde{B}$ and $B^{(l)}$ for $l \ge 11$ are disjoint by definition, and we may discard the remaining rows of $\mathrm{d}_\eta B$ not corresponding to any such block to produce a lower bound for its rank.) Ordering the blocks by $\sim, 11, 12, \dots, L$, the resulting matrix $\mathrm{d}_\eta B$ is block lower-triangular, because each $B^{(l)}$ does not depend on the variables $\eta^{(l+1)}, \dots, \eta^{(L)}$. Thus $\operatorname{rank}(\mathrm{d}_\eta B)$ is lower-bounded by the sum of ranks of all diagonal blocks, i.e.

$$\operatorname{rank}(\mathrm{d}_\eta B(\eta_*)) \ge \operatorname{rank}\Big(\mathrm{d}_{\eta^{(0)},\dots,\eta^{(10)}} \tilde{B}(\eta_*)\Big) + \sum_{l=11}^{L} \operatorname{rank}(\mathrm{d}_{\eta^{(l)}} B^{(l)}(\eta_*)).$$

A direct numerical evaluation of the matrix $\mathrm{d}_{\eta^{(0)},\dots,\eta^{(10)}} \tilde{B}(\eta_*)$ verifies that for $\eta_* \in \mathbb{R}^d$ with all entries of $\eta_*^{(0)}, \dots, \eta_*^{(10)}$ equal to 1, we have[8]

$$\operatorname{rank}\Big(\mathrm{d}_{\eta^{(0)},\dots,\eta^{(10)}} \tilde{B}(\eta_*)\Big) = \sum_{l=0}^{10} (2l+1) - 3 = 118.$$

8. An equivalent statement was verified in (Bandeira et al., 2017, Theorem 5.5) corresponding to the case $F = 10$, using exact-precision numerical arithmetic.

Then also for generic $\eta_* \in \mathbb{R}^d$, by lower-semicontinuity of rank,

$$\operatorname{rank}\left(\mathrm{d}_{\eta^{(0)},\ldots,\eta^{(10)}}\tilde{B}(\eta_*)\right) \geq \sum_{l=0}^{10}(2l+1) - 3 = 118.$$

In particular, this establishes the desired result that $\operatorname{rank}(\nabla^2 s_3(\theta_*)) = \operatorname{rank}(\mathrm{d}_\eta B(\eta_*)) \geq d-3$ for $L = 10$. If $L \geq 11$, then by Lemma C.4.3 below, we also have for generic $\eta_* \in \mathbb{R}^d$,

$$\sum_{l=11}^{L} \operatorname{rank}(\mathrm{d}_{\eta^{(l)}} B^{(l)}(\eta_*)) = \sum_{l=11}^{L}(2l+1).$$

Combining these above,

$$\operatorname{rank}(\nabla^2 s_3(\theta_*)) = \operatorname{rank}(\mathrm{d}_\eta B(\eta_*)) \geq \sum_{l=0}^{10}(2l+1) - 3 + \sum_{l=11}^{L}(2l+1) = d-3,$$

which completes the proof that $\operatorname{trdeg}(\mathcal{R}^{\mathsf{G}}_{\leq 3}) = d-3$. The remaining statements about (d_0, d_1, d_2, d_3) and K directly follow. □

Lemma C.4.3. *Suppose $L \geq 11$. For each $l \in \{11, \ldots, L\}$, let $\mathcal{J}^{(l)}$ be the set of tuples $(l, l', l'') \in \mathcal{J}$ where l takes this fixed value, and where $l' \leq l$ and $l'' \leq l$. Denote*

$$B^{(l)}(\eta) = \left(B_{l,l',l''}(\eta) : (l,l',l'') \in \mathcal{J}^{(l)}\right) \in \mathbb{C}^{|\mathcal{J}^{(l)}|}$$

and let $\mathrm{d}_{\eta^{(l)}} B^{(l)} \in \mathbb{C}^{|\mathcal{J}^{(l)}| \times (2l+1)}$ be the submatrix of $\mathrm{d}_\eta B$ corresponding to the derivative of $B^{(l)}$ in $\eta^{(l)}$. Then for all generic $\eta_* \in \mathbb{R}^d$,

$$\operatorname{rank}\left(\mathrm{d}_{\eta^{(l)}} B^{(l)}(\eta_*)\right) = 2l+1.$$

Proof. It suffices to show $\operatorname{rank}(\mathrm{d}_{\eta^{(l)}} B^{(l)}(\eta_*)) = 2l+1$ for a single point $\eta_* \in \mathbb{R}^d$. Our strategy is to choose η_* with many coordinates equal to 0, such that $\mathrm{d}_{\eta^{(l)}} B^{(l)}(\eta_*)$ has a sparse structure and its rank may be explicitly analyzed. Specifically, we choose η_* so that

$$\begin{aligned}
&\text{For } l' \in \{l-1, l\} : v^{(l')}_{*,m'}, w^{(l')}_{*,m'} = 0 \text{ unless } m' = l-1 \\
&\text{For } l' \in \{0, 1, 4, 5, \ldots, l-2\} : v^{(l')}_{*,m'}, w^{(l')}_{*,m'} = 0 \text{ unless } m' = l' \\
&\text{For } l' \in \{2, 3\} : v^{(l')}_{*,m'}, w^{(l')}_{*,m'} = 0 \text{ unless } m' \in \{l', l'-1\}.
\end{aligned} \tag{144}$$

We choose the values of the non-zero coordinates of η_* to be generic. The rest of this proof checks

that $\operatorname{rank}(\mathrm{d}_{\eta^{(l)}} B^{(l)}(\eta_*)) = 2l+1$ holds under this choice.

Recall the form of $B_{l,l',l''}$ from (4.25). We first compute $\mathrm{d}_{\eta^{(l)}} B_{l,l',l''}$ in the two cases: (i) $l', l'' < l$ and (ii) $l' = l$ and $l'' < l$.

Case I: $l', l'' < l$. For each $k = 0, \dots, l$, the derivatives $\partial_{v_k^{(l)}}, \partial_{w_k^{(l)}}$ apply only to the terms $\overline{u_m^{(l)}}$ in (4.25) for $m \in \{+k, -k\}$. We have $u_m^{(l)} = v_m^{(l)} + \mathbf{i} w_m^{(l)} = (-1)^m v_{-m}^{(l)} - \mathbf{i} \cdot (-1)^m w_{-m}^{(l)}$ where the second equality applies the sign symmetry (160). Thus (relabeling k by m), for $m > 0$ strictly,

$$\partial_{v_m^{(l)}} B_{l,l',l''} = \sum_{m'=-l'}^{l'} C^{l,l',l''}_{m,m',m+m'} \overline{u_{m'}^{(l')}} u_{m+m'}^{(l'')} + (-1)^m C^{l,l',l''}_{-m,m',-m+m'} \overline{u_{m'}^{(l')}} u_{-m+m'}^{(l'')}$$

$$\partial_{w_m^{(l)}} B_{l,l',l''} = \sum_{m'=-l'}^{l'} -\mathbf{i} \cdot C^{l,l',l''}_{m,m',m+m'} \overline{u_{m'}^{(l')}} u_{m+m'}^{(l'')} + (-1)^m \cdot \mathbf{i} \cdot C^{l,l',l''}_{-m,m',-m+m'} \overline{u_{m'}^{(l')}} u_{-m+m'}^{(l'')}.$$

Re-indexing $m' \mapsto -m'$ for the summations of the second terms, and applying the symmetries (138) and (4.23), we obtain

$$\partial_{v_m^{(l)}} B_{l,l',l''} = \sum_{m'=-l'}^{l'} 2C^{l,l',l''}_{m,m',m+m'} \times \begin{cases} \operatorname{Re} \overline{u_{m'}^{(l')}} u_{m+m'}^{(l'')} & \text{if } l+l'+l'' \text{ is even} \\ \mathbf{i} \cdot \operatorname{Im} \overline{u_{m'}^{(l')}} u_{m+m'}^{(l'')} & \text{if } l+l'+l'' \text{ is odd,} \end{cases} \tag{145}$$

$$\partial_{w_m^{(l)}} B_{l,l',l''} = \sum_{m'=-l'}^{l'} 2C^{l,l',l''}_{m,m',m+m'} \times \begin{cases} \operatorname{Im} \overline{u_{m'}^{(l')}} u_{m+m'}^{(l'')} & \text{if } l+l'+l'' \text{ is even} \\ (-\mathbf{i}) \cdot \operatorname{Re} \overline{u_{m'}^{(l')}} u_{m+m'}^{(l'')} & \text{if } l+l'+l'' \text{ is odd.} \end{cases} \tag{146}$$

For $m = 0$, we have similarly

$$\partial_{v_0^{(l)}} B_{l,l',l''} = \sum_{m'=-l'}^{l'} C^{l,l',l''}_{0,m',m'} \overline{u_{m'}^{(l')}} u_{m'}^{(l'')}. \tag{147}$$

Case II: $l' = l$ and $l'' < l$. An additional contribution to each derivative $\partial_{v_k^{(l)}}, \partial_{w_k^{(l)}}$ arises from differentiating $u_{m'}^{(l')}$ in (4.25). By symmetry of (4.25) with respect to interchanging l and l', this has the effect of doubling each of the above expressions. So for $m > 0$, we have

$$\partial_{v_m^{(l)}} B_{l,l,l''} = \sum_{m'=-l}^{l} 4C^{l,l,l''}_{m,m',m+m'} \times \begin{cases} \operatorname{Re} \overline{u_{m'}^{(l)}} u_{m+m'}^{(l'')} & \text{if } l'' \text{ is even} \\ \mathbf{i} \cdot \operatorname{Im} \overline{u_{m'}^{(l)}} u_{m+m'}^{(l'')} & \text{if } l'' \text{ is odd,} \end{cases} \tag{148}$$

$$\partial_{w_m^{(l)}} B_{l,l,l''} = \sum_{m'=-l}^{l} 4C^{l,l,l''}_{m,m',m+m'} \times \begin{cases} \operatorname{Im} \overline{u_{m'}^{(l)}} u_{m+m'}^{(l'')} & \text{if } l'' \text{ is even} \\ (-\mathbf{i}) \cdot \operatorname{Re} \overline{u_{m'}^{(l)}} u_{m+m'}^{(l'')} & \text{if } l'' \text{ is odd.} \end{cases} \tag{149}$$

For $m = 0$ we have

$$\partial_{v_0^{(l)}} B_{l,l,l''} = \sum_{m'=-l}^{l} 2C_{0,m',m'}^{l,l,l''} \overline{u_{m'}^{(l)}} u_{m'}^{(l'')}. \tag{150}$$

Now specializing these derivatives to η_* of the form (144), we observe for example the following: If $l' \in \{l-1, l\}$ and $l'' \in \{4, \ldots, l-2\}$, then $\partial_{v_m^{(l)}} B_{l,l',l''}, \partial_{w_m^{(l)}} B_{l,l',l''}$ are 0 unless $|m+m'| = l''$ for either $m' = l-1$ or $m' = -(l-1)$. Since $0 \le m \le l$, this occurs for only the single index $m = (l-1) - l''$. Thus, only two entries in the row $\mathrm{d}_{\eta^{(l)}} B_{l,l',l''}$ are non-zero, corresponding to $\partial_{v_m^{(l)}}, \partial_{w_m^{(l)}}$ for this m. More generally, let us write the condition (144) succinctly as

$$\mathrm{Type}(0), \mathrm{Type}(1), \mathrm{Type}(4), \ldots, \mathrm{Type}(l-2), \mathrm{Type}(l-1) = 0, \quad \mathrm{Type}(l) = 1, \quad \mathrm{Type}(2,3) = \{0,1\}$$

where $\mathrm{Type}(l') = i$ means that $v_{*,m'}^{(l')}, w_{*,m'}^{(l')} = 0$ except for $m' \in l' - i$. Then for $\partial_{v_m^{(l)}} B_{l,l',l''}, \partial_{w_m^{(l)}} B_{l,l',l''}$ to be non-zero, we require $|m+m'| \in l'' - \mathrm{Type}(l'')$ for some m' satisfying $|m'| \in l' - \mathrm{Type}(l')$. This occurs for the indices

$$m \in \Big\{ \big|(l' - \mathrm{Type}(l')) - (l'' - \mathrm{Type}(l''))\big|,\ (l' - \mathrm{Type}(l')) + (l'' - \mathrm{Type}(l'')) \Big\} \cap \{0, \ldots, l\} \tag{151}$$

where we use the set notations $|A| = \{|a| : a \in A\}$, $A - B = \{a - b : a \in A, b \in B\}$, and $A + B = \{a + b : a \in A, b \in B\}$.

For the given value of l, note that

$$\mathcal{J}^{(l)} = \Big\{ (l, l', l'') : 0 \le l' \le l,\ 0 \le l'' \le l,\ l' + l'' \ge l \Big\}.$$

We label rows of $\mathrm{d}_{\eta^{(l)}} B^{(l)}(\eta_*)$ by the pairs (l', l'') where $(l, l', l'') \in \mathcal{J}^{(l)}$. We now choose $2l+1$ such rows (l', l'') and check that the corresponding square $(2l+1) \times (2l+1)$ submatrix is non-singular. These rows are indicated in the left column of the below table. The right column displays all values of m satisfying (151), i.e. for which $\partial_{v_m^{(l)}}, \partial_{w_m^{(l)}}$ are non-zero in that row.

(l', l'')	Values of m
$(l-1, l-1)$ if l is even or $(l, l-1)$ if l is odd	0
$(l, l-2)$	1
$(l-1, l-2)$	1
$(l, l-3)$	2
$(l-1, l-3)$	2

$\vdots$	$\vdots$
$(l,4)$	$l-5$
$(l-1,4)$	$l-5$
$(l-5,5)$	$l-10$ and l
$(l-4,4)$	$l-8$ and l
$(l,1)$	l and $l-2$
$(l-1,1)$	l and $l-2$
$(l,2)$	l, $l-2$, and $l-3$
$(l-1,2)$	l, $l-2$, and $l-3$
$(l,3)$	$l-3$ and $l-4$
$(l-1,3)$	$l-3$ and $l-4$
$(l-3,3)$	$l-6$, $l-5$, l, and $l-1$
$(l-2,2)$	$l-4$, $l-3$, l, and $l-1$

To verify that this selected $(2l+1)\times(2l+1)$ submatrix of $\mathrm{d}_{\eta^{(l)}}B^{(l)}(\eta_*)$ is non-singular, let us order its rows in the order of the above table, and its columns according to the ordering of variables

$$v_0^{(l)}, v_1^{(l)}, w_1^{(l)}, \ldots, v_{l-5}^{(l)}, w_{l-5}^{(l)}, v_l^{(l)}, w_l^{(l)}, v_{l-2}^{(l)}, w_{l-2}^{(l)}, v_{l-3}^{(l)}, w_{l-3}^{(l)}, v_{l-4}^{(l)}, w_{l-4}^{(l)}, v_{l-1}^{(l)}, w_{l-1}^{(l)}$$

as they appear in the right column above. Then the table implies that this $(2l+1)\times(2l+1)$ submatrix has a block lower-triangular structure with respect to $2l+1 = 1+2+\ldots+2$. So it suffices to check that each 1×1 and 2×2 diagonal block is non-singular. It is tedious but straightforward to verify this explicitly, by computing their forms:

Block corresponding to $v_0^{(l)}$: For even l, we have that $l+(l-1)+(l-1)$ is even. Then applying (147) and the symmetries (138) and (4.23), this 1×1 matrix is

$$\partial_{v_0^{(l)}} B_{l,l-1,l-1}(\eta_*) = \Big(C^{l,l-1,l-1}_{0,l-1,l-1} + C^{l,l-1,l-1}_{0,-(l-1),-(l-1)}\Big)|u^{(l-1)}_{*,l-1}|^2 = 2C^{l,l-1,l-1}_{0,l-1,l-1}|u^{(l-1)}_{*,l-1}|^2.$$

For odd l, we have that $l+l+(l-1)$ is even. Then applying instead (150), this 1×1 matrix is

$$\begin{aligned}\partial_{v_0^{(l)}} B_{l,l,l-1}(\eta_*) &= 2C^{l,l,l-1}_{0,l-1,l-1}\overline{u^{(l)}_{*,l-1}}u^{(l-1)}_{*,l-1} + 2C^{l,l,l-1}_{0,-(l-1),-(l-1)}u^{(l)}_{*,l-1}\overline{u^{(l-1)}_{*,l-1}} \\ &= 4C^{l,l,l-1}_{0,l-1,l-1}\,\mathrm{Re}\,\overline{u^{(l)}_{*,l-1}}u^{(l-1)}_{*,l-1}.\end{aligned}$$

These two coefficients $C^{l,l-1,l-1}_{0,l-1,l-1}$ and $C^{l,l,l-1}_{0,l-1,l-1}$ are non-zero by Lemma C.4.2, so this block is non-zero for generic values of the non-zero coordinates $v^{(l-1)}_{*,l-1}, w^{(l-1)}_{*,l-1}, v^{(l)}_{*,l-1}, w^{(l)}_{*,l-1}$ of η_*.

Blocks corresponding to $(v^{(l)}_1, w^{(l)}_1), \ldots, (v^{(l)}_{l-2}, w^{(l)}_{l-2})$: The calculations for all these blocks are similar. We demonstrate the case $v^{(l)}_{l-3}, w^{(l)}_{l-3}$: Applying (145–146) and (148–149), this 2×2 block is

$$\begin{aligned}
&\partial_{v^{(l)}_{l-3}, w^{(l)}_{l-3}} \Big(B_{l,l,2}, B_{l,l-1,2} \Big)(\eta_*) \\
&= \begin{pmatrix} 4C^{l,l,2}_{l-3,-(l-1),-2} \cdot \operatorname{Re} \overline{u^{(l)}_{*,-(l-1)}} u^{(2)}_{*,-2} & 4C^{l,l,2}_{l-3,-(l-1),-2} \cdot \operatorname{Im} \overline{u^{(l)}_{*,-(l-1)}} u^{(2)}_{*,-2} \\ 2\mathbf{i} C^{l,l-1,2}_{l-3,-(l-1),-2} \cdot \operatorname{Im} \overline{u^{(l-1)}_{*,-(l-1)}} u^{(2)}_{*,-2} & -2\mathbf{i} C^{l,l-1,2}_{l-3,-(l-1),-2} \cdot \operatorname{Re} \overline{u^{(l-1)}_{*,-(l-1)}} u^{(2)}_{*,-2} \end{pmatrix} \\
&= \begin{pmatrix} 4C^{l,l,2}_{l-3,-(l-1),-2} & 0 \\ 0 & 2\mathbf{i} C^{l,l-1,2}_{l-3,-(l-1),-2} \end{pmatrix} \begin{pmatrix} \operatorname{Re} \overline{u^{(l)}_{*,-(l-1)}} u^{(2)}_{*,-2} & \operatorname{Im} \overline{u^{(l)}_{*,-(l-1)}} u^{(2)}_{*,-2} \\ \operatorname{Im} \overline{u^{(l-1)}_{*,-(l-1)}} u^{(2)}_{*,-2} & -\operatorname{Re} \overline{u^{(l-1)}_{*,-(l-1)}} u^{(2)}_{*,-2} \end{pmatrix}
\end{aligned}$$

The coefficients $C^{l,l,2}_{l-3,-(l-1),-2}$ and $C^{l,l-1,2}_{l-3,-(l-1),-2}$ are both non-zero by Lemma C.4.2, so the first matrix of this product is non-singular. It is direct to check that the determinant of the second matrix is a non-zero polynomial of the six non-zero coordinates $v^{(l)}_{*,l-1}, w^{(l)}_{*,l-1}, v^{(l-1)}_{*,l-1}, w^{(l-1)}_{*,l-1}, v^{(2)}_{*,2}, w^{(2)}_{*,2}$ of η_*. Then for generic values of these six coordinates, the determinant is non-zero, and this matrix is also non-singular.

Blocks corresponding to $(v^{(l)}_{l-1}, w^{(l)}_{l-1}), (v^{(l)}_l, w^{(l)}_l)$: Applying (145–146), these 2×2 matrices are

$$\begin{aligned}
&\partial_{v^{(l)}_{l-1}, w^{(l)}_{l-1}} \Big(B_{l,l-3,3}, B_{l,l-2,2} \Big)(\eta_*) \\
&= \begin{pmatrix} 2C^{l,l-3,3}_{l-1,-(l-3),2} \cdot \operatorname{Re} \overline{u^{(l-3)}_{*,-(l-3)}} u^{(3)}_{*,2} & 2C^{l,l-3,3}_{l-1,-(l-3),2} \cdot \operatorname{Im} \overline{u^{(l-3)}_{*,-(l-3)}} u^{(3)}_{*,2} \\ 2C^{l,l-2,2}_{l-1,-(l-2),1} \cdot \operatorname{Re} \overline{u^{(l-2)}_{*,-(l-2)}} u^{(2)}_{*,1} & 2C^{l,l-2,2}_{l-1,-(l-2),1} \cdot \operatorname{Im} \overline{u^{(l-2)}_{*,-(l-2)}} u^{(2)}_{*,1} \end{pmatrix}, \\
&\partial_{v^{(l)}_l, w^{(l)}_l} \Big(B_{l,l-5,5}, B_{l,l-4,4} \Big)(\eta_*) \\
&= \begin{pmatrix} 2C^{l,l-5,5}_{l,-(l-5),5} \cdot \operatorname{Re} \overline{u^{(l-5)}_{*,-(l-5)}} u^{(5)}_{*,5} & 2C^{l,l-5,5}_{l,-(l-5),5} \cdot \operatorname{Im} \overline{u^{(l-5)}_{*,-(l-5)}} u^{(5)}_{*,5} \\ 2C^{l,l-4,4}_{l,-(l-4),4} \cdot \operatorname{Re} \overline{u^{(l-4)}_{*,-(l-4)}} u^{(4)}_{*,4} & 2C^{l,l-4,4}_{l,-(l-4),4} \cdot \operatorname{Im} \overline{u^{(l-4)}_{*,-(l-4)}} u^{(4)}_{*,4} \end{pmatrix}.
\end{aligned}$$

The coefficients $C^{l,l-3,3}_{l-1,-(l-3),2}$,$C^{l,l-2,2}_{l-1,-(l-2),1}$,$C^{l,l-5,5}_{l,-(l-5),5}$,$C^{l,l-4,4}_{l,-(l-4),4}$ are non-zero by Lemma C.4.2. Then the determinant of the first matrix is a non-zero polynomial of the eight coordinates

$$v^{(l-3)}_{*,l-3}, w^{(l-3)}_{*,l-3}, v^{(l-2)}_{*,l-2}, w^{(l-2)}_{*,l-2}, v^{(2)}_{*,1}, w^{(2)}_{*,1}, v^{(3)}_{*,2}, w^{(3)}_{*,2},$$

and that of the second matrix is a non-zero polynomial of the eight coordinates

$$v_{*,l-5}^{(l-5)}, w_{*,l-5}^{(l-5)}, v_{*,l-4}^{(l-4)}, w_{*,l-4}^{(l-4)}, v_{*,5}^{(5)}, w_{*,5}^{(5)}, v_{*,4}^{(4)}, w_{*,4}^{(4)}.$$

(Note that these eight coordinates are distinct when $l \geq 11$.) Thus for generic values of these coordinates, these matrices are non-singular.

Combining these cases, we have shown that each 1×1 and 2×2 diagonal block of this $(2l+1) \times (2l+1)$ submatrix is nonsingular for generic choices of the non-zero coordinates of η_*. Then they are also simultaneously nonsingular for generic choices of these coordinates, so in particular there exists $\eta_* \in \mathbb{R}^d$ where $\mathrm{d}_{\eta^{(l)}} B^{(l)}(\eta_*)$ has full column rank $2l+1$. Then $\mathrm{d}_{\eta^{(l)}} B^{(l)}(\eta_*)$ must also have full column rank $2l+1$ for all generic $\eta_* \in \mathbb{R}^d$, concluding the proof. □

C.4.3 Unprojected cryo-EM

In this section, we give proofs of our results relating to unprojected cryo-EM.

Function basis

We describe the choice of function basis for this example, and prove Lemma 4.4.5.

For $f \in L_2(\mathbb{R}^3, \mathbb{C})$, denote its Fourier transform

$$\hat{f}(k_1, k_2, k_3) = \int_{\mathbb{R}^3} e^{-2\pi \mathbf{i}(k_1 x_1 + k_2 x_2 + k_3 x_3)} f(x_1, x_2, x_3) \mathrm{d}x_1 \, \mathrm{d}x_2 \, \mathrm{d}x_3. \tag{152}$$

We reparametrize $k = (k_1, k_2, k_3) \in \mathbb{R}^3$ in the Fourier domain by spherical coordinates (ρ, ϕ_1, ϕ_2), and write with a slight abuse of notation $\hat{f}(\rho, \phi_1, \phi_2)$ for this parametrization.

Let $\hat{j}_{lsm}$ be as defined in (4.26), where y_{lm} are the complex spherical harmonics in (130) and $\{z_s : s \geq 1\}$ are any functions $z_s : [0, \infty) \to \mathbb{R}$ satisfying the orthogonality relation (4.27). By the spherical change-of-coordinates $\mathrm{d}k_1 \, \mathrm{d}k_2 \, \mathrm{d}k_3 = \rho^2 \sin\phi_1 \, \mathrm{d}\rho \, \mathrm{d}\phi_1 \, \mathrm{d}\phi_2$, these functions $\{\hat{j}_{lsm}\}$ are orthonormal in $L_2(\mathbb{R}^3, \mathbb{C})$. Then so are their inverse Fourier transforms $\{j_{lsm}\}$, by the Parseval relation.

Recall the space of $(L, S_0, \ldots, S_L)$-bandlimited functions (4.29). By linearity of the Fourier transform, the basis representation (4.29) is equivalent to

$$\hat{f} = \sum_{(l,s,m) \in \mathcal{I}} u_m^{(ls)} \hat{j}_{lsm} \tag{153}$$

in the Fourier domain. A function $f \in L_2(\mathbb{R}^3, \mathbb{C})$ is real-valued if and only if

$$\hat{f}(\rho, \phi_1, \phi_2) = \overline{\hat{f}(\rho, \pi - \phi_1, \pi + \phi_2)},$$

where $(\rho, \pi - \phi_1, \pi + \phi_2)$ are the coordinates for the reflection of (ρ, ϕ_1, ϕ_2) about the origin. Applying $P_{lm}(x) = (-1)^{l+m} P_{lm}(-x)$ by (129) and hence $y_{lm}(\pi - \phi_1, \pi + \phi_2) = (-1)^l y_{lm}(\phi_1, \phi_2) = (-1)^{l+m} \overline{y_{l,-m}(\phi_1, \phi_2)}$ by (130) and (131), it may be checked that this condition is equivalent to the sign symmetry

$$u_m^{(ls)} = (-1)^{l+m} \overline{u_{-m}^{(ls)}} \tag{154}$$

in the basis representations (4.29) and (153). We may then define a real basis $\{h_{lsm}\}$ by

$$h_{lsm} = \begin{cases} \frac{1}{\sqrt{2}} \big(j_{ls,-m} + (-1)^{l+m} j_{lsm} \big) & \text{if } m > 0 \\ \mathbf{i}^l \cdot j_{ls0} & \text{if } m = 0 \\ \frac{\mathbf{i}}{\sqrt{2}} \big(j_{lsm} - (-1)^{l+m} j_{ls,-m} \big) & \text{if } m < 0. \end{cases} \tag{155}$$

Note that by this definition, h_{lsm} satisfies (154) for its coefficients $u_m^{(ls)}$ in the basis $\{j_{lsm}\}$, and hence is real-valued. Thus $\{h_{lsm}\}$ forms an orthonormal basis for $L_2(\mathbb{R}^3, \mathbb{R})$. For any function $f \in L_2(\mathbb{R}^3, \mathbb{R})$, writing its orthogonal decompositions

$$f = \sum_{(l,s,m) \in \mathcal{I}} u_m^{(ls)} \cdot j_{lsm} = \sum_{(l,s,m) \in \mathcal{I}} \theta_m^{(ls)} \cdot h_{lsm},$$

the coefficients $\{u_m^{(ls)}\}$ and $\{\theta_m^{(ls)}\}$ are then related by a unitary transform $u = \hat{V}^* \theta$ defined as

$$u_m^{(ls)} = \begin{cases} \frac{(-1)^{l+m}}{\sqrt{2}} (\theta_{|m|}^{(ls)} - \mathbf{i} \theta_{-|m|}^{(ls)}) & \text{if } m > 0 \\ \mathbf{i}^l \cdot \theta_0^{(ls)} & \text{if } m = 0 \\ \frac{1}{\sqrt{2}} (\theta_{|m|}^{(ls)} + \mathbf{i} \theta_{-|m|}^{(ls)}) & \text{if } m < 0. \end{cases} \tag{156}$$

Here, the sign symmetry (154) and transform $\hat{V}$ are different from (4.23) and the transform V defined by (4.22) in the example of spherical registration, because we are modeling the Fourier transform $\hat{f}$ rather than f in the spherical harmonics basis, but we assume that f rather than $\hat{f}$ is real-valued.

Proof of Lemma 4.4.5. Note that if $f_{\mathfrak{g}}(x) = f(\mathfrak{g} \cdot x)$, then its Fourier transform undergoes the same

rotation $\hat{f}_{\mathfrak{g}}(k) = \hat{f}(\mathfrak{g} \cdot k)$, by (152). Writing

$$\hat{f}(\rho, \phi_1, \phi_2) = \sum_{l=0}^{L} \sum_{s=1}^{S_l} z_s(\rho) \cdot \hat{f}_{ls}(\phi_1, \phi_2), \qquad \hat{f}_{ls}(\phi_1, \phi_2) = \sum_{m=-l}^{l} u_m^{(ls)} y_{lm}(\phi_1, \phi_2),$$

each function $\hat{f}_{ls}$ is defined on the unit sphere, and the rotation by $\mathfrak{g}$ acts separately on each such function $\hat{f}_{ls}$ via the map $u^{(ls)} \mapsto D^{(l)}(\mathfrak{g})u^{(ls)}$ described in Appendix C.4.1. Thus rotation by $\mathfrak{g}$ induces the transformation $u \mapsto D(\mathfrak{g})u$ on the complex coefficient vector u, for $D(\mathfrak{g})$ as defined in (4.32). Applying the unitary relations $u = \hat{V}^*\theta$ and $\theta = \hat{V}u$, this rotation then induces the transformation $\theta \mapsto \hat{V} \cdot D(\mathfrak{g}) \cdot \hat{V}^*\theta$ on the real coefficients θ. □

Terms of the high-noise series expansion

We prove Theorem 4.4.8 on the forms of $s_1(\theta)$, $s_2(\theta)$, and $s_3(\theta)$.

Proof of Theorem 4.4.8. Similar to the proof of Theorem 4.4.4, consider two different real coefficient vectors $\theta, \vartheta \in \mathbb{R}^d$, with corresponding complex coefficients $u = \hat{V}^*\theta$ and $v = \hat{V}^*\vartheta$. We compute $\mathbb{E}_g[\langle \theta, g \cdot \vartheta \rangle^k]$ for $k = 1, 2, 3$.

Case $k = 1$: By Lemma 4.4.5, for any $g \in \mathsf{G}$,

$$\langle \theta, g \cdot \vartheta \rangle = \langle \theta, \hat{V} D(\mathfrak{g}) \hat{V}^* \vartheta \rangle = \langle u, D(\mathfrak{g}) v \rangle.$$

From the block-diagonal form of $D(\mathfrak{g})$ in (4.32), we obtain

$$\langle \theta, g \cdot \vartheta \rangle = \sum_{l=0}^{L} \sum_{s=1}^{S_l} \langle u^{(ls)}, D^{(l)}(\mathfrak{g}) v^{(ls)} \rangle = \sum_{l=0}^{L} \sum_{s=1}^{S_l} \sum_{q,m=-l}^{l} \overline{u_q^{(ls)}} D_{qm}^{(l)}(\mathfrak{g}) v_m^{(ls)}. \tag{157}$$

Applying the identities (132) yields

$$\mathbb{E}_g[\langle \theta, g \cdot \vartheta \rangle] = \sum_{s=1}^{S_0} \overline{u_0^{(0s)}} v^{(0s)}.$$

Write as shorthand $u^{(0s)} = u_0^{(0s)}$, $v^{(0s)} = v_0^{(0s)}$, and observe from (154) that these are real-valued. Then applying this to (139), we have

$$s_1(\theta) = \frac{1}{2}\mathbb{E}_g[\langle \theta, g \cdot \theta \rangle] - \mathbb{E}_g[\langle \theta_*, g \cdot \theta \rangle] + \frac{1}{2}\mathbb{E}_g[\langle \theta_*, g \cdot \theta_* \rangle] = \frac{1}{2} \sum_{s=1}^{S_0} \left(u^{(0s)}(\theta) - u^{(0s)}(\theta_*) \right)^2.$$

Case $k = 2$: We take the expected square on both sides of (157), applying (154) and the relation (133). Then

$$\begin{aligned}\mathbb{E}_g[\langle\theta, g\cdot\vartheta\rangle^2] &= \sum_{l=0}^{L}\sum_{s,s'=1}^{S_l}\sum_{q,m=-l}^{l}\frac{(-1)^{m+q}}{2l+1}\overline{u_q^{(ls)}u_{-q}^{(ls')}}v_m^{(ls)}v_{-m}^{(ls')}\\ &= \sum_{l=0}^{L}\sum_{s,s'=1}^{S_l}\sum_{q,m=-l}^{l}\frac{1}{2l+1}\overline{u_q^{(ls)}}u_q^{(ls')}v_m^{(ls)}\overline{v_m^{(ls')}}\\ &= \sum_{l=0}^{L}\frac{1}{2l+1}\sum_{s,s'=1}^{S_l}\langle u^{(ls)}, u^{(ls')}\rangle\cdot\overline{\langle v^{(ls)}, v^{(ls')}\rangle}.\end{aligned}$$

Note that from the isometry $\langle u^{(ls)}, u^{(ls')}\rangle = \langle\theta^{(ls)}, \theta^{(ls')}\rangle$, the inner-products on the last line are real. Then applying this to (139),

$$\begin{aligned}s_2(\theta) &= \frac{1}{4}\mathbb{E}_g[\langle\theta, g\cdot\theta\rangle^2] - \frac{1}{2}\mathbb{E}_g[\langle\theta_*, g\cdot\theta\rangle^2] + \frac{1}{4}\mathbb{E}_g[\langle\theta_*, g\cdot\theta_*\rangle^2]\\ &= \sum_{l=0}^{L}\frac{1}{4(2l+1)}\sum_{s,s'=1}^{S_l}\Big(\langle u^{(ls)}(\theta), u^{(ls')}(\theta)\rangle - \langle u^{(ls)}(\theta_*), u^{(ls')}(\theta_*)\rangle\Big)^2.\end{aligned}$$

Case $k = 3$: We now take the expected cube on both sides of (157) and apply the relations (134) and (154). Then

$$\begin{aligned}\mathbb{E}_g[\langle\theta, g\cdot\vartheta\rangle^3] = \sum_{\substack{l,l',l''=0\\ |l-l'|\le l''\le l+l'}}^{L}\sum_{s=1}^{S_l}\sum_{s'=1}^{S_{l'}}\sum_{s''=1}^{S_{l''}}\sum_{q,m=-l}^{l}\sum_{q',m'=-l'}^{l'}\frac{1}{2l''+1}\\ \cdot C^{l,l',l''}_{q,q',q+q'}C^{l,l',l''}_{m,m',m+m'}\overline{u_q^{(ls)}u_{q'}^{(l's')}}u_{q+q'}^{(l''s'')}v_m^{(ls)}v_{m'}^{(l's')}\overline{v_{m+m'}^{(l''s'')}}.\end{aligned}$$

Recall that

$$B_{(l,s),(l',s'),(l'',s'')}(\theta) = \sum_{m=-l}^{l}\sum_{m'=-l'}^{l'}C^{l,l',l''}_{m,m',m+m'}\overline{u_m^{(ls)}u_{m'}^{(l's')}}u_{m+m'}^{(l''s'')}, \qquad u = \hat{V}^*\theta$$

with the convention (137). Changing indices $(m, m') \mapsto (-m, -m')$ and applying the symmetries

(138) and (154), we have

$$\begin{aligned}
B_{(l,s),(l',s'),(l'',s'')}(\theta) &= \sum_{m=-l}^{l} \sum_{m'=-l'}^{l'} C^{l,l',l''}_{-m,-m',-m-m'} \overline{u^{(ls)}_{-m} u^{(l's')}_{-m'}} u^{(l''s'')}_{-m-m'} \\
&= \sum_{m=-l}^{l} \sum_{m'=-l'}^{l'} (-1)^{l+l'+l''} C^{l,l',l''}_{m,m',m+m'} \cdot (-1)^{l+l'+l''+m+m'+(m+m')} u^{(ls)}_{m} u^{(l's')}_{m'} \overline{u^{(l''s'')}_{m+m'}} \\
&= \overline{B_{(l,s),(l',s'),(l'',s'')}(\theta)}.
\end{aligned}$$

Thus (in contrast to spherical registration in Section 4.4.1 and Appendix C.4.2) $B_{(l,s),(l',s'),(l'',s'')}(\theta)$ is always real-valued. Then the above may be written as

$$\mathbb{E}_g[\langle \theta, g \cdot \vartheta \rangle^3] = \sum_{\substack{l,l',l''=0 \\ |l-l'| \le l'' \le l+l'}}^{L} \frac{1}{2l''+1} \sum_{s=1}^{S_l} \sum_{s'=1}^{S_{l'}} \sum_{s''=1}^{S_{l''}} B_{(l,s),(l',s'),(l'',s'')}(\theta) B_{(l,s),(l',s'),(l'',s'')}(\vartheta).$$

Then applying this to (139),

$$\begin{aligned}
s_3(\theta) &= \frac{1}{12}\mathbb{E}_g[\langle \theta, g \cdot \theta \rangle^3] - \frac{1}{6}\mathbb{E}_g[\langle \theta_*, g \cdot \theta \rangle^3] + \frac{1}{12}\mathbb{E}_g[\langle \theta_*, g \cdot \theta_* \rangle^3] \\
&= \frac{1}{12} \sum_{\substack{l,l',l''=0 \\ |l-l'| \le l'' \le l+l'}}^{L} \frac{1}{2l''+1} \sum_{s=1}^{S_l} \sum_{s'=1}^{S_{l'}} \sum_{s''=1}^{S_{l''}} \left(B_{(l,s),(l',s'),(l'',s'')}(\theta) - B_{(l,s),(l',s'),(l'',s'')}(\theta_*) \right)^2 . \quad (158)
\end{aligned}$$

□

Transcendence degrees

We now prove Theorem 4.4.6 on the sequences of transcendence degrees.

Proof of Theorem 4.4.6. As in Theorem 4.4.2, considering the frequencies $(l, s) = (1, 1)$, for generic $(\theta^{(11)}_{-1}, \theta^{(11)}_0, \theta^{(11)}_1) \in \mathbb{R}^3$ the action of $\{D^{(1)}(\mathfrak{g}) : \mathfrak{g} \in \mathsf{SO}(3)\}$ on $(\theta^{(11)}_{-1}, \theta^{(11)}_0, \theta^{(11)}_1)$ has trivial stabilizer. Then $\operatorname{trdeg} \mathcal{R}^{\mathsf{G}} = d - \dim(\mathsf{G}) = d - 3$, and $d_0 = 3$.

We now compute $\operatorname{trdeg}(\mathcal{R}^{\mathsf{G}}_{\le k})$ for $k = 1, 2, 3$ using Lemma 4.2.6. Recall the forms of $s_1(\theta)$ and $s_2(\theta)$ in Theorem 4.4.8. For $k = 1$, differentiating twice at $\theta = \theta_*$ yields

$$\nabla^2 s_1(\theta_*) = \sum_{s=1}^{S_0} \nabla u^{(0s)}(\theta_*) \nabla u^{(0s)}(\theta_*)^\top.$$

Recalling $u^{(0s)}(\theta) = \theta_0^{(0s)}$, these vectors $\{\nabla u^{(0s)}(\theta_*)\}_{s=1}^{S_0}$ are S_0 different standard basis vectors, so

$$\operatorname{trdeg}(\mathcal{R}^{\mathsf{G}}_{\leq 1}) = \operatorname{rank}\Big(\nabla^2 s_1(\theta_*)\Big) = S_0.$$

For $k = 2$, differentiating twice at $\theta = \theta_*$ yields

$$\nabla^2 s_1(\theta_*) + \nabla^2 s_2(\theta_*) = \sum_{s=1}^{S_0} \nabla u^{(0s)}(\theta_*) \nabla u^{(0s)}(\theta_*)^\top + \sum_{l=0}^{L} \frac{1}{2(2l+1)} \sum_{s,s'=1}^{S_l} \nabla[\langle u^{(ls)}(\theta), u^{(ls')}(\theta)\rangle] \nabla[\langle u^{(ls)}(\theta), u^{(ls')}(\theta)\rangle]^\top \Big|_{\theta=\theta_*}.$$

Defining matrices G^0 and G with the columns

$$\begin{aligned} G^0_s &:= \nabla u^{(0s)}(\theta_*) \qquad \text{for } 1 \leq s \leq S_0 \\ G_{lss'} &:= \frac{1}{\sqrt{2(2l+1)}} \nabla[\langle u^{(ls)}(\theta), u^{(ls')}(\theta)\rangle]\Big|_{\theta=\theta_*} \qquad \text{for } 0 \leq l \leq L,\ 1 \leq s, s' \leq S_l, \end{aligned}$$

this may be written as

$$\nabla^2 s_1(\theta_*) + \nabla^2 s_2(\theta_*) = G^0 (G^0)^\top + G G^\top = [G \mid G^0][G \mid G^0]^\top.$$

For generic θ_*, the column span of G^0 coincides with the span of columns $\{G_{0ss} : s = 1, \ldots, S_0\}$ of G. Thus

$$\operatorname{trdeg}(\mathcal{R}^{\mathsf{G}}_{\leq 2}) = \operatorname{rank}(\nabla^2 s_1(\theta_*) + \nabla^2 s_2(\theta_*)) = \operatorname{rank}([G \mid G^0]) = \operatorname{rank}(G).$$

Applying the isometry $\langle u^{(ls)}(\theta), u^{(ls')}(\theta)\rangle = \langle \theta^{(ls)}, \theta^{(ls')}\rangle$, Lemma C.4.4 below shows that

$$\operatorname{rank}(G) = \sum_{l=0}^{L} \begin{cases} \frac{S_l(S_l+1)}{2} & \text{if } S_l < 2l+1, \\ (2l+1)(S_l - l) & \text{if } S_l \geq 2l+1, \end{cases}$$

establishing the desired form for $k = 2$.

For $k = 3$, we have $\operatorname{trdeg}(\mathcal{R}^{\mathsf{G}}_{\leq 3}) \leq \operatorname{trdeg}(\mathcal{R}^{\mathsf{G}}) = d-3$, so it suffices to show $\operatorname{rank}(\nabla^2 s_3(\theta_*)) \geq d-3$. Writing the index set

$$\mathcal{K} = \Big\{((l,s),(l',s'),(l'',s'')) : 0 \leq l, l', l'' \leq L,\ |l-l'| \leq l'' \leq l+l',\ 1 \leq s \leq S_l,\ 1 \leq s' \leq S_{l'},\ 1 \leq s'' \leq S_{l''}\Big\},$$

by Theorem 4.4.8 we have

$$s_3(\theta) = \sum_{((l,s),(l',s'),(l'',s''))\in\mathcal{K}} \frac{1}{12}\cdot\frac{1}{2l''+1}\cdot\left(B_{(l,s),(l',s'),(l'',s'')}(\theta) - B_{(l,s),(l',s'),(l'',s'')}(\theta_*)\right)^2$$

for the function $B_{(l,s),(l',s'),(l'',s'')}(\theta)$ defined in (4.34). Recall from the proof of Theorem 4.4.8 that $B_{(l,s),(l',s'),(l'',s'')}(\theta)$ is real-valued. Let us denote

$$B(\theta) = \Big(B_{(l,s),(l',s'),(l'',s'')}(\theta) :\ ((l,s),(l',s'),(l'',s''))\in\mathcal{K}\Big), \qquad B:\mathbb{R}^d\to\mathbb{R}^{|\mathcal{K}|},$$

and write $\mathrm{d}B(\theta)\in\mathbb{R}^{|\mathcal{K}|\times d}$ for its the derivative in θ. Then, applying the chain rule to differentiate $s_3(\theta)$ twice at $\theta=\theta_*$, we obtain

$$\nabla^2 s_3(\theta_*) = \mathrm{d}B(\theta_*)^\top\cdot\mathrm{diag}\left(\frac{1}{6(2l''+1)} : ((l,s),(l',s'),(l'',s''))\in\mathcal{K}\right)\cdot\mathrm{d}B(\theta_*).$$

The diagonal matrix in the middle has full rank, so

$$\mathrm{rank}\left(\nabla^2 s_3(\theta_*)\right) = \mathrm{rank}\left(\mathrm{d}B(\theta_*)\right). \tag{159}$$

To analyze this rank, recall the complex parametrization $u=\hat{V}^*\theta\in\mathbb{C}^d$ from (156), where u satisfies the symmetry (154). Let us write the real and imaginary parts of u as

$$u_m^{(ls)} = v_m^{(ls)} + \mathbf{i}w_m^{(ls)}$$

so that this symmetry (154) is equivalent to

$$v_{-m}^{(ls)} = (-1)^{l+m}v_m^{(ls)}, \qquad w_{-m}^{(ls)} = (-1)^{l+m+1}w_m^{(ls)}. \tag{160}$$

Note that for $m=0$, this implies $v_0^{(ls)}=0$ when l is odd and $w_0^{(ls)}=0$ when l is even. Then, setting

$$\eta^{(ls)}(\theta) = \begin{cases} (v_0^{(ls)}, v_1^{(ls)}, w_1^{(ls)}, \ldots, v_l^{(ls)}, w_l^{(ls)}) & \text{if } l \text{ is even} \\ (w_0^{(ls)}, v_1^{(ls)}, w_1^{(ls)}, \ldots, v_l^{(ls)}, w_l^{(ls)}) & \text{if } l \text{ is odd,} \end{cases} \tag{161}$$

these coordinates $\eta^{(ls)}\in\mathbb{R}^{2l+1}$ provide a (linear) invertible reparametrization of $\theta^{(ls)}$. This defines a reparametrization

$$\eta(\theta) = \Big(\eta^{(ls)}(\theta) : 0\le l\le L, 1\le s\le S_l\Big)\in\mathbb{R}^d \tag{162}$$

with inverse function $\theta(\eta)$. Writing as shorthand $\eta_* = \eta(\theta_*)$ and $B(\eta) \equiv B(\theta(\eta))$, and denoting by $\mathrm{d}_\eta B(\eta)$ the derivative of B in the new variables η, (159) is equivalent to

$$\operatorname{rank}\left(\nabla^2 s_3(\theta_*)\right) = \operatorname{rank}(\mathrm{d}_\eta B(\eta_*)). \tag{163}$$

Let us group the columns and rows of $\mathrm{d}_\eta B$ into blocks indexed by (l, s), where the (l, s) column block corresponds to $\mathrm{d}_{\eta^{(ls)}}$ and the (l, s) row block corresponds to $B^{(ls)}$ as defined below in Lemma C.4.5. (These blocks $B^{(ls)}$ are disjoint by definition, and we may discard the remaining rows of $\mathrm{d}_\eta B$ not belonging to any such block to produce a lower bound for its rank.) Ordering the pairs (l, s) as in Lemma C.4.5, the resulting matrix $\mathrm{d}_\eta B$ is block lower-triangular. Thus its rank is lower-bounded by the total rank of all blocks along the diagonal, i.e.

$$\operatorname{rank}(\mathrm{d}_\eta B(\eta_*)) \geq \sum_{l=0}^{L} \sum_{s=1}^{S_l} \operatorname{rank}(\mathrm{d}_{\eta^{(ls)}} B^{(ls)}(\eta_*)).$$

Lemma C.4.5 shows that for generic $\eta_* \in \mathbb{R}^d$,

$$\begin{aligned}
\sum_{l=2}^{L} \sum_{s=1}^{S_l} \operatorname{rank}(\mathrm{d}_{\eta^{(ls)}} B^{(ls)}(\eta_*)) &= \sum_{l=2}^{L} \sum_{s=1}^{S_l} (2l+1) = \sum_{l=2}^{L} (2l+1) S_l, \\
\sum_{s=1}^{S_1} \operatorname{rank}(\mathrm{d}_{\eta^{(1s)}} B^{(1s)}(\eta_*)) &\geq 1 + 2 + \sum_{s=3}^{S_1} 3 = 3S_1 - 3 \\
\sum_{s=1}^{S_0} \operatorname{rank}(\mathrm{d}_{\eta^{(0s)}} B^{(0s)}(\eta_*)) &= S_0.
\end{aligned}$$

Combining these,

$$\operatorname{trdeg} \mathcal{R}^{\mathsf{G}}_{\leq 3} = \operatorname{rank}(\nabla^2 s_3(\theta_*)) = \operatorname{rank}(\mathrm{d}_\eta B(\eta_*)) \geq \left(\sum_{l=0}^{L} (2l+1) S_l \right) - 3 = d - 3.$$

Thus $\operatorname{trdeg} \mathcal{R}^{\mathsf{G}}_{\leq 3} = d - 3$. The values of (d_0, d_1, d_2, d_3) directly follow. We may check that when $L = 1$, we have $\operatorname{trdeg} \mathcal{R}^{\mathsf{G}}_{\leq 2} = d - 3$ and hence $K = 2$. For all other L, we have $\operatorname{trdeg} \mathcal{R}^{\mathsf{G}}_{\leq 2} < d - 3$ strictly, so $K = 3$. □

Lemma C.4.4. *For any $l \geq 0$ and $S \geq 2$, consider $\theta^{(1)}, \ldots, \theta^{(S)} \in \mathbb{R}^{2l+1}$ and the Jacobian matrix of all their pairwise inner-products with respect to $\theta = (\theta^{(1)}, \ldots, \theta^{(S)}) \in \mathbb{R}^{(2l+1)S}$,*

$$\mathrm{d}_\theta[\langle \theta^{(s)}, \theta^{(s')} \rangle : 1 \leq s \leq s' \leq S] \in \mathbb{R}^{\frac{S(S+1)}{2} \times (2l+1)S}.$$

At generic $\theta_* \in \mathbb{R}^{(2l+1)S}$, this matrix has rank

$$\operatorname{rank}\left(\mathrm{d}_\theta[\langle\theta^{(s)},\theta^{(s')}\rangle : 1 \le s \le s' \le S]\Big|_{\theta=\theta_*}\right) = \begin{cases} \frac{S(S+1)}{2} & S < 2l+1 \\ (2l+1)(S-l) & S \ge 2l+1. \end{cases}$$

Proof. Let $q = \min(2l+1, S)$ and consider the rows of the Jacobian for pairs (s, s') given by

$$(1,1),(1,2),\dots,(1,S),(2,2),(2,3),\dots,(2,S),\dots(q,q),\dots,(q,S).$$

It may be checked that the number of such rows is exactly the desired formula for the rank. Consider θ_* where $\theta^{(1)}_{*,1} = \theta^{(2)}_{*,2} = \cdots = \theta^{(q)}_{*,q} = 1$, and all other coordinates are 0. For this θ_*, the entries of the Jacobian are given by

$$\partial_{\theta^{(p)}_m}[\langle\theta^{(s)},\theta^{(s')}\rangle]\Big|_{\theta=\theta_*} = \mathbf{1}\{p=s\}\cdot\theta^{(s')}_{*,m} + \mathbf{1}\{p=s'\}\cdot\theta^{(s)}_{*,m} = \mathbf{1}\{p=s, m=s'\} + \mathbf{1}\{p=s', m=s\}.$$

Thus for each row (s, s') above where $s \le q \le 2l+1$ and $s' \le S$, there are either 1 or 2 non-zero entries, in the column $\partial_{\theta^{(s')}_s}$ and also in the column $\partial_{\theta^{(s)}_{s'}}$ if $s' \le 2l+1$. These columns are distinct for different rows (s, s'), so the submatrix of these columns has full row rank. This shows

$$\operatorname{rank}\left(\mathrm{d}_\theta[\langle\theta^{(s)},\theta^{(s')}\rangle : 1 \le s \le s' \le S]\Big|_{\theta=\theta_*}\right) \ge \begin{cases} \frac{S(S+1)}{2} & S < 2l+1 \\ (2l+1)(S-l) & S \ge 2l+1 \end{cases}$$

for this choice of θ_*, and hence also at any generic θ_*.

For the corresponding upper bound, for $S < 2l+1$ this follows because the Jacobian has only $S(S+1)/2$ rows. For $S \ge 2l+1$, consider the action of $\mathsf{SO}(2l+1)$ on θ by simultaneous rotation of the vectors $\theta^{(1)},\dots,\theta^{(S)}$. At generic θ_* and for $S \ge 2l+1$, this action is injective. Hence θ_* has trivial stabilizer, and $\dim(\mathcal{O}_{\theta_*}) = \dim(\mathsf{SO}(2l+1)) = (2l+1)l$ where $\mathcal{O}_{\theta_*}$ is the orbit of θ_* under this action. Since $\langle\theta^{(s)},\theta^{(s')}\rangle$ is constant on $\mathcal{O}_{\theta_*}$, for each vector v in the dimension-$(2l+1)l$ tangent space to $\mathcal{O}_{\theta_*}$, we have

$$\mathrm{d}_\theta[\langle\theta^{(s)},\theta^{(s')}\rangle : 1 \le s \le s' \le S]\big|_{\theta=\theta_*}\cdot v = 0.$$

Thus the column rank of the Jacobian is at most $(2l+1)S - (2l+1)l = (2l+1)(S-l)$, as desired. □

Lemma C.4.5. *Suppose $L \ge 1$ and $S_0,\dots,S_L \ge 2$. Order the pairs (l,s) by $(l,s) < (l',s')$ if $l < l'$ or if $l = l'$ and $s < s'$. Fix any $l \in \{1,\dots,L\}$ and $s \in \{1,\dots,S_l\}$, and let $\mathcal{K}^{(ls)}$ be the set of tuples*

$((l,s),(l',s'),(l'',s''))\in\mathcal{K}$ *where* (l,s) *take these fixed values, and* $(l',s')\le(l,s)$ *and* $(l'',s'')\le(l,s)$. *Denote*

$$B^{(ls)}(\eta)=\Big(B_{(l,s),(l',s'),(l'',s'')}(\eta):\ ((l,s),(l',s'),(l'',s''))\in\mathcal{K}^{(ls)}\Big)\in\mathbb{R}^{|\mathcal{K}^{(ls)}|}$$

and let $\mathrm{d}_{\eta^{(ls)}}B^{(ls)}\in\mathbb{R}^{|\mathcal{K}^{(ls)}|\times(2l+1)}$ *be its Jacobian in* $\eta^{(ls)}$. *Then for any generic* $\eta_*\in\mathbb{R}^d$*:*

(a) If $l\ge 2$, *then* $\operatorname{rank}(\mathrm{d}_{\eta^{(ls)}}B^{(ls)}(\eta_*))=2l+1$.

(b) If $l\ge 1$ *and* $s\ge 3$, *then also* $\operatorname{rank}(\mathrm{d}_{\eta^{(ls)}}B^{(ls)}(\eta_*))=2l+1=3$. *Furthermore for* $s=2$, *removing* $w_0^{(12)}$ *from* $\eta^{(12)}$, *we have* $\operatorname{rank}(\mathrm{d}_{v_1^{(12)},w_1^{(12)}}B^{(12)}(\eta_*))=2$. *For* $s=1$, *removing* $w_0^{(11)},w_1^{(11)}$ *from* $\eta^{(11)}$, *we have* $\operatorname{rank}(\mathrm{d}_{v_1^{(11)}}B^{(11)}(\eta_*))=1$.

(c) If $l=0$, *then* $\operatorname{rank}(\mathrm{d}_{\eta^{(0s)}}B^{(0s)}(\eta_*))=1$.

Proof. The strategy is similar to the proof of Lemma C.4.3. For each statement, it suffices to exhibit a single point $\eta_*\in\mathbb{R}^d$ where the rank equality holds. We choose η_* having most coordinates 0, to allow an explicit computation of the rank.

Recall the form of $B_{(l,s),(l',s'),(l'',s'')}$ from (4.34). We first compute $\mathrm{d}_{\eta^{(ls)}}B_{(l,s),(l',s'),(l'',s'')}$: If $(l',s'),(l'',s'')<(l,s)$ strictly, then the derivative $\mathrm{d}_{\eta^{(ls)}}$ applies to only the term $\overline{u_m^{(ls)}}$ in (4.34). A computation analogous to (145–146) using the sign symmetry (154) shows, for $m>0$ strictly,

$$\partial_{v_m^{(ls)}}B_{(l,s),(l',s'),(l'',s'')}=\sum_{m'=-l'}^{l'}2C^{l,l',l''}_{m,m',m+m'}\cdot\operatorname{Re}\overline{u_{m'}^{(l's')}}u_{m+m'}^{(l''s'')}\tag{164}$$

$$\partial_{w_m^{(ls)}}B_{(l,s),(l',s'),(l'',s'')}=\sum_{m'=-l'}^{l'}2C^{l,l',l''}_{m,m',m+m'}\cdot\operatorname{Im}\overline{u_{m'}^{(l's')}}u_{m+m'}^{(l''s'')}.\tag{165}$$

For $m=0$, recalling that $\eta_0^{(ls)}=v_0^{(ls)}$ if l is even and $\eta_0^{(ls)}=w_0^{(ls)}$ if l is odd, we also have

$$\partial_{\eta_0^{(ls)}}B_{(l,s),(l',s'),(l'',s'')}=\sum_{m'=-l'}^{l'}C^{l,l',l''}_{0,m',m'}\overline{u_{m'}^{(l's')}}u_{m'}^{(l''s'')}\times\begin{cases}1 & \text{if } l \text{ is even}\\ -\mathbf{i} & \text{if } l \text{ is odd.}\end{cases}\tag{166}$$

If $(l',s')=(l,s)$ and $(l'',s'')<(l,s)$ strictly, an additional contribution to the derivatives arise

from differentiating $u_{m'}^{(l's')}$. This doubles the above expressions, and we have

$$\partial_{v_m^{(ls)}} B_{(l,s),(l,s),(l'',s'')} = \sum_{m'=-l}^{l} 4C^{l,l,l''}_{m,m',m+m'} \cdot \mathrm{Re}\, \overline{u_{m'}^{(ls)}} u_{m+m'}^{(l''s'')} \tag{167}$$

$$\partial_{w_m^{(ls)}} B_{(l,s),(l,s),(l'',s'')} = \sum_{m'=-l}^{l} 4C^{l,l,l''}_{m,m',m+m'} \cdot \mathrm{Im}\, \overline{u_{m'}^{(ls)}} u_{m+m'}^{(l''s'')} \tag{168}$$

$$\partial_{\eta_0^{(ls)}} B_{(l,s),(l,s),(l'',s'')} = \sum_{m'=-l}^{l} 2C^{l,l,l''}_{0,m',m'} \overline{u_{m'}^{(ls)}} u_{m'}^{(l''s'')} \times \begin{cases} 1 & \text{if } l \text{ is even} \\ -\mathbf{i} & \text{if } l \text{ is odd.} \end{cases} \tag{169}$$

We now use a different construction of η_* for different values of (l, s):

Part (a), $l \geq 4$: Let us fix two radial frequencies $(A, B) = (1, 2)$. (We use here the condition $S_0, \ldots, S_L \geq 2$, so that these frequencies exist for each $l = 0, \ldots, L$.) We choose η_* such that for all $l' \in \{1, \ldots, l-1\}$ and $m' \in \{0, \ldots, l'\}$,

$$v_{*,m'}^{(l'A)} = w_{*,m'}^{(l'A)} = 0 \text{ unless } m' = l', \qquad v_{*,m'}^{(l'B)} = w_{*,m'}^{(l'B)} = 0 \text{ unless } m' = l' - 1.$$

We choose the non-zero coordinates of η_* to be generic. Using similar notation as in Lemma C.4.3, we write this as

$$\mathrm{Type}(l', A) = 0, \qquad \mathrm{Type}(l', B) = 1 \qquad \text{for all} \qquad l' = 1, \ldots, l-1,$$

where $\mathrm{Type}(l', s') = i$ indicates that $v_{*,m}^{(l's')}, w_{*,m}^{(l's')} = 0$ unless $m = l' - i$. (In contrast to Lemma C.4.3, here $\mathrm{Type}(\cdot)$ is a single integer rather than a set.) For $\partial_{v_m^{(ls)}} B_{(l,s),(l',s'),(l'',s'')}, \partial_{w_m^{(ls)}} B_{(l,s),(l',s'),(l'',s'')}$ to be non-zero, we require $|m + m'| = l'' - \mathrm{Type}(l'', s'')$ and $|m'| = l' - \mathrm{Type}(l', s')$. This requires analogously to (151)

$$m \in \Big\{ \big| (l' - \mathrm{Type}(l', s')) - (l'' - \mathrm{Type}(l'', s'')) \big|, (l' - \mathrm{Type}(l', s')) + (l'' - \mathrm{Type}(l'', s'')) \Big\}. \tag{170}$$

Rows of $\mathrm{d}_{\eta^{(ls)}} B^{(ls)}(\eta_*)$ may be indexed by $(l', s'), (l'', s'')$ for which $((l, s), (l', s'), (l'', s'')) \in \mathcal{K}^{(ls)}$. We select $2l + 1$ such rows, given by the left column of the following table. Note that when $l \geq 4$, these rows satisfy the requirement $l' + l'' \geq l$ in the definition of $\mathcal{K}$. For each row, the right column indicates the values of m satisfying (170), for which $\partial_{v_m^{(ls)}}, \partial_{w_m^{(ls)}}$ are non-zero.

(l', s') and (l'', s'')	Values of m
$(l-1, A)$ and $(l-1, A)$ if l is even; $(l-2, A)$ and $(l-1, B)$ if l is odd	0
$(l-1, B)$ and $(l-1, A)$	1
$(l-2, A)$ and $(l-1, A)$	1
$(l-2, B)$ and $(l-1, A)$	2
$(l-3, A)$ and $(l-1, A)$	2
$\vdots$	$\vdots$
$(3, B)$ and $(l-1, A)$	$l-3$
$(2, A)$ and $(l-1, A)$	$l-3$
$(3, B)$ and $(l-1, B)$	$l-4$ and l
$(2, A)$ and $(l-1, B)$	$l-4$ and l
$(2, B)$ and $(l-1, B)$	$l-3$ and $l-1$
$(1, A)$ and $(l-1, B)$	$l-3$ and $l-1$
$(2, B)$ and $(l-1, A)$	l and $l-2$
$(1, A)$ and $(l-1, A)$	l and $l-2$

To verify that this selected $(2l+1) \times (2l+1)$ submatrix of $\mathrm{d}_{\eta^{(ls)}} B^{(ls)}(\eta_*)$ is non-singular, we order its rows as in the above table, and its columns by the ordering of variables

$$\eta_0^{(ls)}, v_1^{(ls)}, w_1^{(ls)}, \ldots, v_{l-3}^{(ls)}, w_{l-3}^{(ls)}, v_l^{(ls)}, w_l^{(ls)}, v_{l-1}^{(ls)}, w_{l-1}^{(ls)}, v_{l-2}^{(ls)}, w_{l-2}^{(ls)}$$

as they appear in the right column above. Then this $(2l+1) \times (2l+1)$ submatrix is block lower-triangular in the decomposition $2l+1 = 1+2+2+\ldots+2$. It suffices to check that each 1×1 and 2×2 diagonal block is non-singular.

Block corresponding to $\eta_0^{(l)}$: Applying (166) and the symmetries (138) and (154), the first 1×1 diagonal block is

$$\partial_{\eta_0}^{(ls)} B_{(l,s),(l-1,A),(l-1,A)}(\eta_*) = 2C_{0,l-1,l-1}^{l,l-1,l-1} \cdot \left|u_{*,l-1}^{(l-1,A)}\right|^2 \text{ for even } l$$
$$\partial_{\eta_0}^{(ls)} B_{(l,s),(l-2,A),(l-1,B)}(\eta_*) = 2C_{0,l-2,l-2}^{l,l-2,l-1} \cdot \operatorname{Im} \overline{u_{*,l-2}^{(l-2,A)}} u_{*,l-2}^{(l-1,B)} \text{ for odd } l.$$

By Lemma C.4.2, these Clebsch-Gordan coefficients are non-zero, so this block is generically non-zero.

Blocks corresponding to $(v_1^{(ls)}, w_1^{(ls)}), \ldots, (v_{l-3}^{(ls)}, w_{l-3}^{(ls)})$: The arguments for these blocks are

similar, so we consider only $v_{l-3}^{(ls)}, w_{l-3}^{(ls)}$. Applying (164–165), this 2×2 block is

$$\partial_{v_{l-3}^{(ls)}, w_{l-3}^{(ls)}} \Big(B_{(l,s),(3,B),(l-1,A)}, B_{(l,s),(2,A),(l-1,A)} \Big)(\eta_*)$$
$$= \begin{pmatrix} 2C_{l-3,2,l-1}^{l,3,l-1} \cdot \operatorname{Re} \overline{u_{*,2}^{(3,B)}} u_{*,l-1}^{(l-1,A)} & 2C_{l-3,2,l-1}^{l,3,l-1} \cdot \operatorname{Im} \overline{u_{*,2}^{(3,B)}} u_{*,l-1}^{(l-1,A)} \\ 2C_{l-3,2,l-1}^{l,2,l-1} \cdot \operatorname{Re} \overline{u_{*,2}^{(2,A)}} u_{*,l-1}^{(l-1,A)} & 2C_{l-3,2,l-1}^{l,2,l-1} \cdot \operatorname{Im} \overline{u_{*,2}^{(2,A)}} u_{*,l-1}^{(l-1,A)} \end{pmatrix}$$

These Clebsch-Gordan coefficients are again non-zero by Lemma C.4.2, so the determinant of this matrix is a non-zero polynomial in the six coefficients of η_*

$$v_{*,2}^{(3,B)}, w_{*,2}^{(3,B)}, v_{*,2}^{(2,A)}, w_{*,2}^{(2,A)}, v_{*,l-1}^{(l-1,A)}, w_{*,l-1}^{(l-1,A)}.$$

(These coefficients are distinct for $l \geq 4$.) Hence this determinant is generically non-zero.

Blocks corresponding to $(v_l^{(ls)}, w_l^{(ls)}), (v_{l-1}^{(ls)}, w_{l-1}^{(ls)}), (v_{l-2}^{(ls)}, w_{l-2}^{(ls)})$: Applying (164–165), these 2×2 blocks are

$$\partial_{v_l^{(ls)}, w_l^{(ls)}} \Big(B_{(l,s),(3,B),(l-1,B)}, B_{(l,s),(2,A),(l-1,B)} \Big)(\eta_*)$$
$$= \begin{pmatrix} 2C_{l,-2,l-2}^{l,3,l-1} \cdot \operatorname{Re} \overline{u_{*,-2}^{(3,B)}} u_{*,l-2}^{(l-1,B)} & 2C_{l,-2,l-2}^{l,3,l-1} \cdot \operatorname{Im} \overline{u_{*,-2}^{(3,B)}} u_{*,l-2}^{(l-1,B)} \\ 2C_{l,-2,l-2}^{l,2,l-1} \cdot \operatorname{Re} \overline{u_{*,-2}^{(2,A)}} u_{*,l-2}^{(l-1,B)} & 2C_{l,-2,l-2}^{l,2,l-1} \cdot \operatorname{Im} \overline{u_{*,-2}^{(2,A)}} u_{*,l-2}^{(l-1,B)} \end{pmatrix}$$
$$\partial_{v_{l-1}^{(ls)}, w_{l-1}^{(ls)}} \Big(B_{(l,s),(2,B),(l-1,B)}, B_{(l,s),(1,A),(l-1,B)} \Big)(\eta_*)$$
$$= \begin{pmatrix} 2C_{l-1,-1,l-2}^{l,2,l-1} \cdot \operatorname{Re} \overline{u_{*,-1}^{(2,B)}} u_{*,l-2}^{(l-1,B)} & 2C_{l-1,-1,l-2}^{l,2,l-1} \cdot \operatorname{Im} \overline{u_{*,-1}^{(2,B)}} u_{*,l-2}^{(l-1,B)} \\ 2C_{l-1,-1,l-2}^{l,1,l-1} \cdot \operatorname{Re} \overline{u_{*,-1}^{(1,A)}} u_{*,l-2}^{(l-1,B)} & 2C_{l-1,-1,l-2}^{l,1,l-1} \cdot \operatorname{Im} \overline{u_{*,-1}^{(1,A)}} u_{*,l-2}^{(l-1,B)} \end{pmatrix}$$
$$\partial_{v_{l-2}^{(ls)}, w_{l-2}^{(ls)}} \Big(B_{(l,s),(2,B),(l-1,A)}, B_{(l,s),(1,A),(l-1,A)} \Big)(\eta_*)$$
$$= \begin{pmatrix} 2C_{l-2,1,l-1}^{l,2,l-1} \cdot \operatorname{Re} \overline{u_{*,1}^{(2,B)}} u_{*,l-1}^{(l-1,A)} & 2C_{l-2,1,l-1}^{l,2,l-1} \cdot \operatorname{Im} \overline{u_{*,1}^{(2,B)}} u_{*,l-1}^{(l-1,A)} \\ 2C_{l-2,1,l-1}^{l,1,l-1} \cdot \operatorname{Re} \overline{u_{*,1}^{(1,A)}} u_{*,l-1}^{(l-1,A)} & 2C_{l-2,1,l-1}^{l,1,l-1} \cdot \operatorname{Im} \overline{u_{*,1}^{(1,A)}} u_{*,l-1}^{(l-1,A)} \end{pmatrix}$$

The Clebsch-Gordan coefficients here are non-zero by Lemma C.4.2 (for the term $C_{l-1,-1,l-2}^{l,2,l-1}$ of the second matrix, this uses the condition $2 \neq l-1$ when $l \geq 4$). Then the determinants of all three matrices are non-zero polynomials of six distinct coordinates of η_*, except in the case of the first matrix for $l = 4$. In this case, $u_2^{(3,B)}$ and $u_{l-2}^{(l-1,B)}$ coincide, and the determinant may be checked to be a non-zero polynomial of the four distinct coordinates $v_{*,2}^{(3,B)}, w_{*,2}^{(3,B)}, v_{*,2}^{(2,A)}, w_{*,2}^{(2,A)}$.

Combining these cases shows that $\mathrm{d}_{\eta^{(ls)}} B^{(ls)}(\eta_*)$ has full column rank $2l+1$ as desired.

Part (a), $l = 3$: We again fix $(A, B) = (1, 2)$, and specialize to a point η_* such that

$$\mathrm{Type}(3, A), \mathrm{Type}(2, A), \mathrm{Type}(1, A) = 0, \qquad \mathrm{Type}(2, B), \mathrm{Type}(1, B) = 1.$$

We then pick 7 rows of $\mathrm{d}_{\eta^{(3s)}} B^{(3s)}(\eta_*)$, indicated by the left column of the below table. Applying (170), the derivatives in $(v_m^{(3s)}, w_m^{(3s)})$ are non-zero for only the values of m in the right column.

(l', s') and (l'', s'')	Values of m
$(1, B)$ and $(2, B)$	1
$(3, A)$ and $(2, A)$	1
$(1, B)$ and $(2, A)$	2
$(3, A)$ and $(1, A)$	2
$(1, A)$ and $(2, A)$	1 and 3
$(2, B)$ and $(2, A)$	1 and 3
$(1, A)$ and $(2, B)$	2 and 0

Ordering the columns by $v_1^{(3s)}, w_1^{(3s)}, v_2^{(3s)}, w_2^{(3s)}, v_3^{(3s)}, w_3^{(3s)}, w_0^{(3s)}$, this 7×7 submatrix has a block lower-triangular structure in the decomposition $7 = 2 + 2 + 2 + 1$. If $s \neq A$, then applying (164–166) and (167–168), its diagonal blocks are given explicitly by

$$\partial_{v_1^{(3s)}, w_1^{(3s)}} \Big(B_{(3,s),(1,B),(2,B)}, B_{(3,s),(3,A),(2,A)} \Big)(\eta_*) = \begin{pmatrix} 2C^{3,1,2}_{1,0,1} \cdot \mathrm{Re}\, \overline{u^{(1B)}_{*,0}} u^{(2B)}_{*,1} & 2C^{3,1,2}_{1,0,1} \cdot \mathrm{Im}\, \overline{u^{(1B)}_{*,0}} u^{(2B)}_{*,1} \\ 2C^{3,3,2}_{1,-3,-2} \cdot \mathrm{Re}\, \overline{u^{(3A)}_{*,-3}} u^{(2A)}_{*,-2} & 2C^{3,3,2}_{1,-3,-2} \cdot \mathrm{Im}\, \overline{u^{(3A)}_{*,-3}} u^{(2A)}_{*,-2} \end{pmatrix}$$

$$\partial_{v_2^{(3s)}, w_2^{(3s)}} \Big(B_{(3,s),(1,B),(2,A)}, B_{(3,s),(3,A),(1,A)} \Big)(\eta_*) = \begin{pmatrix} 2C^{3,1,2}_{2,0,2} \cdot \mathrm{Re}\, \overline{u^{(1B)}_{*,0}} u^{(2A)}_{*,2} & 2C^{3,1,2}_{2,0,2} \cdot \mathrm{Im}\, \overline{u^{(1B)}_{*,0}} u^{(2A)}_{*,2} \\ 2C^{3,3,1}_{2,-3,-1} \cdot \mathrm{Re}\, \overline{u^{(3A)}_{*,-3}} u^{(1A)}_{*,-1} & 2C^{3,3,1}_{2,-3,-1} \cdot \mathrm{Im}\, \overline{u^{(3A)}_{*,-3}} u^{(1A)}_{*,-1} \end{pmatrix}$$

$$\partial_{v_3^{(3s)}, w_3^{(3s)}} \Big(B_{(3,s),(1,A),(2,A)}, B_{(3,s),(2,B),(2,A)} \Big)(\eta_*) = \begin{pmatrix} 2C^{3,1,2}_{3,-1,2} \cdot \mathrm{Re}\, \overline{u^{(1A)}_{*,-1}} u^{(2A)}_{*,2} & 2C^{3,1,2}_{3,-1,2} \cdot \mathrm{Im}\, \overline{u^{(1A)}_{*,-1}} u^{(2A)}_{*,2} \\ 2C^{3,2,2}_{3,-1,2} \cdot \mathrm{Re}\, \overline{u^{(2B)}_{*,-1}} u^{(2A)}_{*,2} & 2C^{3,2,2}_{3,-1,2} \cdot \mathrm{Im}\, \overline{u^{(2B)}_{*,-1}} u^{(2A)}_{*,2} \end{pmatrix}$$

$$\partial_{w_0^{(3s)}} B_{(3,s),(1,A),(2,B)}(\eta_*) = 2C^{3,1,2}_{0,1,1} \cdot \mathrm{Im}\, \overline{u^{1A}_{*,1}} u^{2B}_{*,1}$$

Here $u^{(1B)}_{*,0} = \mathbf{i} w^{(1B)}_{*,0}$ depends on only one rather than two non-zero coordinate of η_*; nonetheless, one may still check that the determinants of the above three matrices are generically non-zero. If $s = A$, then the second rows of the first two matrices above have coefficients 4 instead of 2, from applying (167–168) in place of (164–165), but this does not affect their ranks. Thus these blocks are generically non-singular, so $\mathrm{d}_{\eta^{(3s)}} B^{(3s)}(\eta_*)$ has full column rank 7.

Part (a), $l = 2$: We specialize to a point η_* such that

$$\mathrm{Type}(2, A), \mathrm{Type}(1, A), \mathrm{Type}(0, A) = 0, \qquad \mathrm{Type}(2, B), \mathrm{Type}(1, B) = 1.$$

(Here $\mathrm{Type}(0, A) = 0$ means simply that $v_{*,0}^{(0A)}$ is non-zero.) We pick the following 5 rows of $\mathrm{d}_{\eta^{(2s)}} B^{(2s)}(\eta_*)$, for which the derivatives in $(v_m^{(2s)}, w_m^{(2s)})$ are non-zero for only the following corresponding values of m.

(l', s') and (l'', s'')	Values of m
$(1, B)$ and $(1, B)$	0
$(1, B)$ and $(1, A)$	1
$(2, B)$ and $(0, A)$	1
$(2, A)$ and $(0, A)$	2
$(1, A)$ and $(1, A)$	0 and 2

Ordering the columns by $v_0^{(2s)}, v_1^{(2s)}, w_1^{(2s)}, v_2^{(2s)}, w_2^{(2s)}$, this 5×5 submatrix has a block lower-triangular structure in the decomposition $5 = 1 + 2 + 2$. If $s \notin \{A, B\}$, these blocks are

$$\partial_{v_0^{(2s)}} B_{(2,s),(1,B),(1,B)}(\eta_*) = C_{0,0,0}^{2,1,1} \cdot \left| u_{*,0}^{(1B)} \right|^2$$

$$\partial_{v_1^{(2s)}, w_1^{(2s)}} \Big(B_{(2,s),(1,B),(1,A)}, B_{(2,s),(2,B),(0,A)} \Big)(\eta_*) = \begin{pmatrix} 2C_{1,0,1}^{2,1,1} \cdot \mathrm{Re}\, \overline{u_{*,0}^{(1B)}} u_{*,1}^{(1A)} & 2C_{1,0,1}^{2,1,1} \cdot \mathrm{Im}\, \overline{u_{*,0}^{(1B)}} u_{*,1}^{(1A)} \\ 2C_{1,-1,0}^{2,2,0} \cdot \mathrm{Re}\, \overline{u_{*,-1}^{(2B)}} u_{*,0}^{(0A)} & 2C_{1,-1,0}^{2,2,0} \cdot \mathrm{Im}\, \overline{u_{*,-1}^{(2B)}} u_{*,0}^{(0A)} \end{pmatrix}$$

$$\partial_{v_2^{(2s)}, w_2^{(2s)}} \Big(B_{(2,s),(2,A),(0,A)}, B_{(2,s),(1,A),(1,A)} \Big)(\eta_*) = \begin{pmatrix} 2C_{2,-2,0}^{2,2,0} \cdot \mathrm{Re}\, \overline{u_{*,-2}^{(2A)}} u_{*,0}^{(0A)} & 2C_{2,-2,0}^{2,2,0} \cdot \mathrm{Im}\, \overline{u_{*,-2}^{(2A)}} u_{*,0}^{(0A)} \\ 2C_{2,-1,1}^{2,1,1} \cdot \mathrm{Re}\, \overline{u_{*,-1}^{(1A)}} u_{*,1}^{(1A)} & 2C_{2,-1,1}^{2,1,1} \cdot \mathrm{Im}\, \overline{u_{*,-1}^{(1A)}} u_{*,1}^{(1A)} \end{pmatrix}$$

If $s = A$ or $s = B$, then the first row of the third matrix or second row of the second matrix should have coefficient 4 in place of 2, but this does not affect their ranks. These blocks are generically non-singular, so $\mathrm{d}_{\eta^{(2s)}} B^{(2s)}(\eta_*)$ has full column rank 5.

Part (b), $l = 1$, $s \geq 3$: Note that $(A, B, s) = (1, 2, s)$ are distinct indices because $s \geq 3$. We specialize to a point η_* such that

$$\mathrm{Type}(1, s), \mathrm{Type}(1, A), \mathrm{Type}(0, A), \mathrm{Type}(0, B) = 0, \qquad \mathrm{Type}(1, B) = 1.$$

We pick the following 3 rows of $\mathrm{d}_{\eta^{(1s)}} B^{(1s)}(\eta_*)$, for which the derivatives in $(v_m^{(1s)}, w_m^{(1s)})$ are non-zero for only the following corresponding values of m.

(l',s') and (l'',s'')	Values of m
$(1,s)$ and $(0,A)$	1
$(1,A)$ and $(0,B)$	1
$(1,B)$ and $(0,B)$	0

Ordering the columns by $v_1^{(1s)}, w_1^{(1s)}, w_0^{(1s)}$, this 3×3 submatrix has a block lower-triangular structure in the decomposition $3 = 2+1$, with diagonal blocks

$$\partial_{v_1^{(1s)},w_1^{(1s)}}\Big(B_{(1,s),(1,s),(0,A)}, B_{(1,s),(1,A),(0,B)}\Big)(\eta_*) = \begin{pmatrix} 4C^{1,1,0}_{1,-1,0}\cdot\mathrm{Re}\,\overline{u^{(1s)}_{*,-1}}u^{(0A)}_{*,0} & 4C^{1,1,0}_{1,-1,0}\cdot\mathrm{Im}\,\overline{u^{(1s)}_{*,-1}}u^{(0A)}_{*,0} \\ 2C^{1,1,0}_{1,-1,0}\cdot\mathrm{Re}\,\overline{u^{(1A)}_{*,-1}}u^{(0B)}_{*,0} & 2C^{1,1,0}_{1,-1,0}\cdot\mathrm{Im}\,\overline{u^{(1A)}_{*,-1}}u^{(0B)}_{*,0}\end{pmatrix}$$

$$\partial_{w_0^{(1s)}} B_{(1,s),(1,B),(0,B)}(\eta_*) = -\mathbf{i}C^{1,1,0}_{0,0,0}\cdot\overline{u^{(1B)}_{*,0}}u^{(0A)}_{*,0}$$

These blocks are generically non-singular (where we use that s and A are distinct for the first block), so $\mathrm{d}_{\eta^{(1s)}}B^{(1s)}(\eta_*)$ has full column rank 3.

Part (b), $l=1$, $s=2$: Consider the two columns of $\mathrm{d}_{\eta^{(12)}}B^{(12)}$ corresponding to $\partial_{v_1^{(12)},w_1^{(12)}}$ and the two rows corresponding to $B_{(1,2),(1,1),(0,1)}, B_{(1,2),(1,2),(0,1)}$. This 2×2 submatrix is (for any η_*)

$$\partial_{v_1^{(12)},w_1^{(12)}}\Big(B_{(1,2),(1,1),(0,1)}, B_{(1,2),(1,2),(0,1)}\Big)(\eta_*) = \begin{pmatrix} 2C^{1,1,0}_{1,-1,0}\cdot\mathrm{Re}\,\overline{u^{(11)}_{*,-1}}u^{(01)}_{*,0} & 2C^{1,1,0}_{1,-1,0}\cdot\mathrm{Im}\,\overline{u^{(11)}_{*,-1}}u^{(01)}_{*,0} \\ 4C^{1,1,0}_{1,-1,0}\cdot\mathrm{Re}\,\overline{u^{(12)}_{*,-1}}u^{(01)}_{*,0} & 4C^{1,1,0}_{1,-1,0}\cdot\mathrm{Im}\,\overline{u^{(12)}_{*,-1}}u^{(01)}_{*,0}\end{pmatrix}$$

This is generically non-singular, so $\mathrm{d}_{v_1^{(12)},w_1^{(12)}}B^{(12)}(\eta_*)$ has full column rank 2.

Part (b), $l=1$, $s=1$: Consider the column and row of $\mathrm{d}_{\eta^{(11)}}B^{(11)}$ corresponding to

$$\partial_{v_1^{(11)}} B_{(1,1),(1,1),(0,1)}(\eta_*) = 4C^{1,1,0}_{1,-1,0}\,\mathrm{Re}\,\overline{u^{(11)}_{*,-1}}u^{(01)}_{*,0}.$$

This is generically non-zero, so $\mathrm{d}_{v_1^{(11)}}B^{(11)}(\eta_*)$ has full column rank 1.

Part (c), $l=0$: For any $s\in\{1,\dots,S_0\}$, $\eta^{(0s)} = v_0^{(0s)}$ is a single real variable. Applying $\langle 0,0;0,0|0,0\rangle = 1$, we have from (4.34) that

$$\partial_{\eta^{(0s)}} B_{(0,s),(0,s),(0,s)}(\eta_*) = \partial_{v_0^{(0s)}}(v^{(0s)}_{*,0})^3 = 3(v^{(0s)}_{*,0})^2,$$

which is generically non-zero. Thus $\mathrm{d}_{\eta^{(0s)}}B^{(0s)}(\eta_*)$ has full column rank 1. □

C.4.4 Projected cryo-EM

In this section, we give proofs of our results relating to projected cryo-EM.

Function basis

We describe the choices of function bases and the associated projection operator.

Let $\hat{j}_{lsm}$ and $\hat{j}_{sm}$ be defined by (4.36) and (4.37), where y_{lm} are the complex spherical harmonics (130),

$$b_m(\phi_2) = (2\pi)^{-1/2} e^{\mathbf{i}m\phi_2},$$

and $\{\tilde{z}_s : s \geq 1\}$ are any functions $\tilde{z}_s : [0, \infty) \to \mathbb{R}$ satisfying the orthogonality (4.41). Let j_{lsm} and j_{sm} be their inverse Fourier transforms. The polar change-of-coordinates $\mathrm{d}k_1\mathrm{d}k_2 = \rho \sin\phi_2 \, \mathrm{d}\rho \, \mathrm{d}\phi_2$ shows that $\{\hat{j}_{sm}\}$ are orthonormal in $L_2(\mathbb{R}^2, \mathbb{C})$, and hence so are $\{j_{sm}\}$.

For $f \in L_2(\mathbb{R}^3, \mathbb{C})$, let (152) be its Fourier transform, and let

$$\widehat{\Pi \cdot f}(k_1, k_2) = \int_{\mathbb{R}^2} e^{-2\pi\mathbf{i}(k_1x_1 + k_2x_2)} (\Pi \cdot f)(x_1, x_2) \mathrm{d}x_1 \mathrm{d}x_2$$

be the 2-D Fourier transform of its tomographic projection. By the Fourier-slice relation,

$$\widehat{\Pi \cdot f}(k_1, k_2) = \hat{f}(k_1, k_2, 0). \tag{171}$$

We reparametrize $k = (k_1, k_2, k_3) \in \mathbb{R}^3$ by spherical coordinates (ρ, ϕ_1, ϕ_2), and $\tilde{k} = (k_1, k_2) \in \mathbb{R}^2$ by polar coordinates (ρ, ϕ_2). Then (171) corresponds to the restriction $\phi_1 = \pi/2$. This restriction of each complex spherical harmonic y_{lm} in (130) is given by

$$y_{lm}(\pi/2, \phi_2) = p_{lm} \cdot b_m(\phi_2)$$

where b_m is the function defined above, and

$$\begin{aligned} p_{lm} &= (-1)^m \sqrt{\frac{(2l+1)}{2} \frac{(l-m)!}{(l+m)!}} \cdot P_{lm}(0) \\ &= \mathbf{1}\{l+m \text{ is even}\} \times \frac{(-1)^{(l+m)/2} \sqrt{(2l+1)/2}}{2^l l!} \binom{l}{(l+m)/2} \sqrt{(l-m)!(l+m)!} \end{aligned} \tag{172}$$

the second equality applying Lemma C.4.1. Note that these coefficients p_{lm} satisfy a sign symmetry

$$p_{lm} = (-1)^m p_{l,-m}. \tag{173}$$

For any $(L, S_0, \ldots, S_L)$-bandlimited function f as in (4.38), its projection is then defined by (4.39) where

$$\tilde{u}_m^{(s)} = \sum_{l:\, S_l \geq s} p_{lm} \cdot u_m^{(ls)}.$$

This may be written as $\tilde{u} = \Pi^{\mathbb{C}} u$ for the map $\Pi^{\mathbb{C}}$ in (4.40).

We pass from the complex basis $\{j_{lsm}\}$ for $L_2(\mathbb{R}^3, \mathbb{C})$ to a real basis $\{h_{lsm}\}$ via (155), and recall that the coefficients $u_m^{(ls)}$ for the former and $\theta_m^{(ls)}$ for the latter are related by $u = \hat{V}^* \theta$ defined in (156). Similarly, we pass from the complex basis $\{j_{sm}\}$ for $L_2(\mathbb{R}^2, \mathbb{C})$ to a real basis

$$h_{sm} = \begin{cases} \frac{1}{\sqrt{2}}\big(j_{s,-m} + (-1)^m j_{sm}\big) & \text{if } m > 0 \\ j_{s0} & \text{if } m = 0 \\ \frac{\mathbf{i}}{\sqrt{2}}\big(j_{sm} - (-1)^m j_{s,-m}\big) & \text{if } m < 0. \end{cases}$$

The two basis representations (4.39) are related by a unitary transform $\tilde{u} = \widetilde{V}^* \tilde{\theta}$ defined as

$$\tilde{u}_m^{(s)} = \begin{cases} \frac{(-1)^m}{\sqrt{2}}(\tilde{\theta}_{|m|}^{(s)} - \mathbf{i}\tilde{\theta}_{-|m|}^{(s)}) & \text{if } m > 0 \\ \tilde{\theta}_0^{(s)} & \text{if } m = 0 \\ \frac{1}{\sqrt{2}}(\tilde{\theta}_{|m|}^{(s)} + \mathbf{i}\tilde{\theta}_{|m|}^{(s)}) & \text{if } m < 0. \end{cases} \tag{174}$$

The projection $\theta \mapsto \tilde{\theta}$ then takes the form of a linear map $\Pi = \widetilde{V} \cdot \Pi^{\mathbb{C}} \cdot \hat{V}^*$ as described in (4.40).

Since $\Pi \cdot f$ is real-valued, its Fourier transform satisfies

$$\widehat{\Pi \cdot f}(\rho, \phi_2) = \overline{\widehat{\Pi \cdot f}(\rho, \pi + \phi_2)}$$

where $(\rho, \pi + \phi_2)$ is the reflection of (ρ, ϕ_2) about the origin. Then the coefficients $\tilde{u}_m^{(s)}$ of $\widehat{\Pi \cdot f}$ in the basis $\{\hat{j}_{sm}\}$ must satisfy the sign symmetry, analogously to (154),

$$\tilde{u}_m^{(s)} = (-1)^m \overline{\tilde{u}_{-m}^{(s)}}. \tag{175}$$

If $S_1 = \ldots = S_L = S$, these actions of rotation and projection on the basis coefficients θ and $\tilde{\theta}$ are the same as described in (Bandeira et al., 2017, Appendix A.4) in the context of S "spherical shells".

Terms of the high noise series expansion

We prove Theorem 4.4.11 on the forms of $\tilde{s}_1(\theta)$, $\tilde{s}_2(\theta)$, and $\tilde{s}_3(\theta)$.

Proof of Theorem 4.4.11. Recall from Lemma C.1.1 that

$$\tilde{s}_k(\theta) = \frac{1}{2(k!)}\mathbb{E}_{g,h}\left[\langle \Pi g\theta, \Pi h\theta\rangle^k - 2\langle \Pi g\theta, \Pi h\theta_*\rangle^k + \langle \Pi g\theta_*, \Pi h\theta_*\rangle^k\right]. \tag{176}$$

Consider two different real coefficient vectors $\theta, \vartheta \in \mathbb{R}^d$, with corresponding complex coefficients $u = \hat{V}^*\theta$ and $v = \hat{V}^*\vartheta$.

Case $k = 1$: Notice that

$$\langle \Pi g\theta, \Pi h\vartheta\rangle = \left\langle (\widetilde{V}^*\Pi\hat{V})(\hat{V}^*g\hat{V})u, (\widetilde{V}^*\Pi\hat{V})(\hat{V}^*h\hat{V})v\right\rangle = \langle D(\mathfrak{g})u, (\Pi^{\mathbb{C}})^*\Pi^{\mathbb{C}}D(\mathfrak{h})v\rangle,$$

where $D(\mathfrak{g}), D(\mathfrak{h})$ are the block-diagonal matrices in (4.32). The form of $\Pi^{\mathbb{C}}$ from (4.40) yields

$$(\Pi^{\mathbb{C}^*}\Pi^{\mathbb{C}})_{lsm,l's'm'} = \mathbf{1}\{s = s'\}\cdot\mathbf{1}\{m = m'\}p_{lm}p_{l'm'}$$

so that

$$\langle \Pi g\theta, \Pi h\vartheta\rangle = \sum_{k,l=0}^{L}\sum_{s=1}^{S_k\wedge S_l}\sum_{m,q=-k}^{k}\sum_{n,r=-l}^{l}\overline{D^{(k)}_{qm}(\mathfrak{g})u^{(ks)}_m}\cdot\mathbf{1}\{q = r\}p_{kq}p_{lr}\cdot D^{(l)}_{rn}(\mathfrak{h})v^{(ls)}_n. \tag{177}$$

Applying (132) to take the expectation, we preserve only the terms for $k = l = m = q = n = r = 0$, yielding

$$\mathbb{E}_{g,h}[\langle \Pi g\theta, \Pi h\vartheta\rangle] = \sum_{s=1}^{S_0}p_{00}^2\overline{u_0^{(0s)}}v_0^{(0s)}.$$

Recalling that $u^{(0s)} = u_0^{(0s)}$ and $v^{(0s)} = v_0^{(0s)}$ are real-valued by (156), and substituting into (176), we obtain

$$\tilde{s}_1(\theta) = \frac{p_{00}^2}{2}\sum_{s=1}^{S_0}\left(u^{(0s)}(\theta) - u^{(0s)}(\theta_*)\right)^2.$$

Case $k=2$: We square both sides of (177) and apply the relations (133), (154), and (173) to get

$$\begin{aligned}
&\mathbb{E}_{g,h}[\langle \Pi g\theta, \Pi h\vartheta\rangle^2] \\
&= \sum_{k,l=0}^{L} \sum_{s,s'=1}^{S_k\wedge S_l} \sum_{m,q=-k}^{k} \sum_{n,r=-l}^{l} \frac{(-1)^{m+q+n+r}}{(2k+1)(2l+1)} \overline{u_m^{(ks)} u_{-m}^{(ks')}} \cdot \mathbf{1}\{q=r\} p_{kq} p_{k,-q} p_{lr} p_{l,-r} \cdot v_n^{(ls)} v_{-n}^{(ls')} \\
&= \sum_{k,l=0}^{L} \sum_{s,s'=1}^{S_k\wedge S_l} \sum_{m,q=-k}^{k} \sum_{n,r=-l}^{l} \frac{(-1)^{k+l}}{(2k+1)(2l+1)} \overline{u_m^{(ks)}} u_m^{(ks')} \cdot \mathbf{1}\{q=r\} p_{kq}^2 p_{lr}^2 \cdot v_n^{(ls)} \overline{v_n^{(ls')}} \\
&= \sum_{k,l=0}^{L} \frac{(-1)^{k+l}}{(2k+1)(2l+1)} \sum_{s,s'=1}^{S_k\wedge S_l} \langle u^{(ks)}, u^{(ks')}\rangle \cdot \overline{\langle v^{(ls)}, v^{(ls')}\rangle} \sum_{q=-(k\wedge l)}^{k\wedge l} p_{kq}^2 p_{lq}^2 \\
&= \sum_{k,l=0}^{L} Q_{kl} \sum_{s,s'=1}^{S_k\wedge S_l} \langle u^{(ks)}, u^{(ks')}\rangle \cdot \overline{\langle v^{(ls)}, v^{(ls')}\rangle}.
\end{aligned}$$

By the isometry $\langle u^{(ks)}, u^{(ks')}\rangle = \langle \theta^{(ks)}, \theta^{(ks')}\rangle$, both inner products on the last line are real. Then applying this to (176),

$$\begin{aligned}
\tilde{s}_2(\theta) = \frac{1}{4} \sum_{k,l=0}^{L} Q_{kl} \sum_{s,s'=1}^{S_k\wedge S_l} &\Big(\langle u^{(ks)}(\theta), u^{(ks')}(\theta)\rangle - \langle u^{(ks)}(\theta_*), u^{(ks')}(\theta_*)\rangle\Big) \\
&\times \Big(\langle u^{(ls)}(\theta), u^{(ls')}(\theta)\rangle - \langle u^{(ls)}(\theta_*), u^{(ls')}(\theta_*)\rangle\Big).
\end{aligned}$$

Case $k=3$: We cube both sides of (177) and apply the relation (134) to obtain

$$\begin{aligned}
&\mathbb{E}_{g,h}[\langle \Pi g\theta, \Pi h\vartheta\rangle^3] \\
&= \sum_{\substack{k,k',k'',l,l',l''=0 \\ |k-k'|\le k''\le k+k',\ |l-l'|\le l''\le l+l'}}^{L} \sum_{s=1}^{S_k\wedge S_l} \sum_{s'=1}^{S_{k'}\wedge S_{l'}} \sum_{s''=1}^{S_{k''}\wedge S_{l''}} \sum_{m,q=-k}^{k} \sum_{m',q'=-k'}^{k'} \sum_{n,r=-l}^{l} \sum_{n',r'=-l'}^{l'} \\
&\quad \frac{(-1)^{m+m'+q+q'+n+n'+r+r'}}{(2k''+1)(2l''+1)} C_{q,q',q+q'}^{k,k',k''} C_{m,m',m+m'}^{k,k',k''} C_{r,r',r+r'}^{l,l',l''} C_{n,n',n+n'}^{l,l',l''} \mathbf{1}\{q=r\}\mathbf{1}\{q'=r'\} \\
&\quad \times \overline{u_m^{(ks)} u_{m'}^{(k's')} u_{-m-m'}^{(k''s'')}} v_n^{(ls)} v_{n'}^{(l's')} v_{-n-n'}^{(l''s'')} p_{kq} p_{k'q'} p_{k'',-q-q'} p_{lr} p_{l'r'} p_{l'',-r-r'}.
\end{aligned}$$

Let us apply, by (154) and (173),

$$\overline{u_{-m-m'}^{(k''s'')}} = (-1)^{m+m'+k''} u_{m+m'}^{(k''s'')}, \qquad \overline{v_{-n-n'}^{(l''s'')}} = (-1)^{n+n'+l''} v_{n+n'}^{(l''s'')},$$

$$p_{k'',-q-q'} = (-1)^{q+q'} p_{k'',q+q'}, \qquad p_{l'',-r-r'} = (-1)^{r+r'} p_{l'',r+r'}.$$

Recalling $B_{(l,s),(l',s'),(l'',s'')}(\theta)$ from (4.34), which is real-valued, the above may be written succinctly

as

$$\mathbb{E}_{g,h}[\langle \Pi g\theta, \Pi h\vartheta\rangle^3] = \sum_{\substack{k,k',k'',l,l',l''=0 \\ |k-k'|\le k''\le k+k',\ |l-l'|\le l''\le l+l'}}^{L} M_{k,k',k'',l,l',l''} \cdot \sum_{s=1}^{S_k\wedge S_l}\sum_{s'=1}^{S_{k'}\wedge S_{l'}}\sum_{s''=1}^{S_{k''}\wedge S_{l''}} B_{(k,s),(k',s'),(k'',s'')}(\theta) B_{(l,s),(l',s'),(l'',s'')}(\vartheta).$$

Then by (176), we find

$$\tilde{s}_3(\theta) = \frac{1}{12} \sum_{\substack{k,k',k'',l,l',l''=0 \\ |k-k'|\le k''\le k+k',\ |l-l'|\le l''\le l+l'}}^{L} M_{k,k',k'',l,l',l''} \sum_{s=1}^{S_k\wedge S_l}\sum_{s'=1}^{S_{k'}\wedge S_{l'}}\sum_{s''=1}^{S_{k''}\wedge S_{l''}} \Big(B_{(k,s),(k',s'),(k'',s'')}(\theta) - B_{(k,s),(k',s'),(k'',s'')}(\theta_*)\Big)\Big(B_{(l,s),(l',s'),(l'',s'')}(\theta) - B_{(l,s),(l',s'),(l'',s'')}(\theta_*)\Big).$$

□

Transcendence degrees

We now prove Theorem 4.4.9 on the sequences of transcendence degrees.

Proof of Theorem 4.4.9. We compute $\mathrm{trdeg}(\widetilde{\mathcal{R}}^{\mathsf{G}}_{\le m})$ for $m = 1, 2, 3$ using Lemma 4.2.6. For $m = 1$,

$$\nabla^2 \tilde{s}_1(\theta_*) = p_{00}^2 \sum_{s=1}^{S_0} \nabla u^{(0s)}(\theta_*) \nabla u^{(0s)}(\theta_*)^\top.$$

Since $p_{00} \neq 0$, this shows $\mathrm{trdeg}(\widetilde{\mathcal{R}}^{\mathsf{G}}_{\le 1}) = \mathrm{rank}(\nabla^2 \tilde{s}_1(\theta_*)) = S_0$ as in Theorem 4.4.6.

For $m = 2$,

$$\nabla^2 \tilde{s}_1(\theta_*) + \nabla^2 \tilde{s}_2(\theta_*) = p_{00}^2 \sum_{s=1}^{S_0} \nabla u^{(0s)}(\theta_*) \nabla u^{(0s)}(\theta_*)^\top + \frac{1}{2}\sum_{k,l=0}^{L} Q_{kl} \sum_{s,s'=1}^{S_k\wedge S_l} \nabla[\langle u^{(ks)}(\theta), u^{(ks')}(\theta)\rangle] \nabla[\langle u^{(ls)}(\theta), u^{(ls')}(\theta)\rangle]^\top\Big|_{\theta=\theta_*}.$$

Recall the form of Q_{kl} from (4.42). Then, defining matrices G^0 and G with the columns

$$G^0_s := p_{00} \nabla u^{(0s)}(\theta_*) \qquad \text{for } 1 \le s \le S_0$$
$$G_{krr'} := \nabla[\langle u^{(kr)}(\theta), u^{(kr')}(\theta)\rangle]\Big|_{\theta=\theta_*} \qquad \text{for } 0 \le k \le L,\ 1 \le r, r' \le S_k$$

and defining a square matrix D with the entries

$$D_{krr',qss'} := \frac{(-1)^k}{2k+1} \frac{p_{kq}^2}{\sqrt{2}\mathbf{1}_{q=0} + \mathbf{1}_{q>0}} \mathbf{1}_{s=r} \mathbf{1}_{s'=r'} \mathbf{1}_{q \le k} \quad \text{for } 0 \le q \le L,\ 0 \le k \le L,\ 1 \le s, s', r, r' \le S_k,$$

we have

$$\begin{aligned}
&\nabla^2 \tilde{s}_1(\theta_*) + \nabla^2 \tilde{s}_2(\theta_*) \\
&= G^0 (G^0)^\top + \sum_{k=0}^{L} \sum_{r,r'=1}^{S_k} \sum_{l=0}^{L} \sum_{s,s'=1}^{S_l} \frac{1}{2} Q_{kl} \mathbf{1}\{r = r'\} \mathbf{1}\{s = s'\} G_{krr'} G_{lss'}^\top \\
&= G^0 (G^0)^\top + \sum_{k=0}^{L} \sum_{r,r'=1}^{S_k} \sum_{l=0}^{L} \sum_{s,s'=1}^{S_l} \frac{(-1)^k}{2k+1} \frac{(-1)^l}{2l+1} \left(\frac{1}{2} p_{k0}^2 p_{l0}^2 + \sum_{q=1}^{k \wedge l} p_{kq}^2 p_{lq}^2 \right) \mathbf{1}\{r = r'\} \mathbf{1}\{s = s'\} G_{krr'} G_{lss'}^\top \\
&= [GD \mid G^0][GD \mid G^0]^\mathsf{T}.
\end{aligned}$$

Here D is lower triangular with non-zero diagonal because $p_{kk} \neq 0$ for any $k = 0, \ldots, L$. Then, since the column span of G^0 is contained in that of G for generic θ_*, we conclude that

$$\operatorname{trdeg}(\widetilde{\mathcal{R}}_{\le 2}^{\mathsf{G}}) = \operatorname{rank}(\nabla^2 \tilde{s}_1(\theta_*) + \nabla^2 \tilde{s}_2(\theta_*)) = \operatorname{rank}\Big([GD \mid G_0]\Big) = \operatorname{rank}(G).$$

Then $\operatorname{trdeg}(\widetilde{\mathcal{R}}_{\le 2}^{\mathsf{G}}) = \operatorname{trdeg}(\mathcal{R}_{\le 2}^{\mathsf{G}})$ as in Theorem 4.4.6.

For $m = 3$, we have $\operatorname{trdeg}(\mathcal{R}_{\le 3}^{\mathsf{G}}) \le \operatorname{trdeg}(\mathcal{R}^{\mathsf{G}}) = d - 3$, so it suffices to show $\operatorname{rank}(\nabla^2 \tilde{s}_3(\theta_*)) \ge d - 3$. For this, we first write a more convenient form for $\tilde{s}_3(\theta)$ and its Hessian at $\theta = \theta_*$. Recall $S = \max_{l=0}^{L} S_l$ and define the index sets

$$\begin{aligned}
\mathcal{Q} &= \Big\{ ((q,r),(q',r'),(q'',r'')) :\ -L \le q, q', q'' \le L,\ \ q + q' + q'' = 0,\ \ 1 \le r, r', r'' \le S \Big\} \\
\mathcal{H} &= \Big\{ ((l,s),(l',s'),(l'',s'')) : 0 \le l, l', l'' \le L, |l - l'| \le l'' \le l + l', 1 \le s \le S_l, 1 \le s' \le S_{l'}, 1 \le s'' \le S_{l''} \Big\}.
\end{aligned}$$

Define a matrix $N \in \mathbb{R}^{|\mathcal{Q}| \times |\mathcal{H}|}$ entrywise by

$$\begin{aligned}
N_{(q,r),(q',r'),(q'',r'')}^{(l,s),(l',s'),(l'',s'')} = \mathbf{1}\{r = s, r' = s', r'' = s''\} \cdot \mathbf{1}\{|q| \le l, |q'| \le l', |q''| \le l''\} \\
\cdot \frac{(-1)^{l''+q''}}{2l''+1} \cdot \langle l, q; l', q' | l'', -q'' \rangle p_{lq} p_{l'q'} p_{l''q''},
\end{aligned} \tag{178}$$

where the subscript is the row index in $\mathcal{Q}$ and the superscript is the column index in $\mathcal{H}$. In the

expression (4.43) for $M_{k,k',k'',l,l',l''}$, let us flip the sign of q'' and apply (173) to write this as

$$M_{k,k',k'',l,l',l''} = \frac{(-1)^{k''+q''}}{2k''+1}\frac{(-1)^{l''+q''}}{2l''+1}\sum_{|q|\le k\wedge l}\sum_{\substack{|q'|\le k'\wedge l'\\ q+q'+q''=0}}\sum_{|q''|\le k''\wedge l''} \langle k,q;k',q'|k'',-q''\rangle\langle l,q;l',q'|l'',-q''\rangle p_{kq}p_{k'q'}p_{k''q''}p_{lq}p_{l'q'}p_{l''q''}.$$

Then

$$\tilde{s}_3(\theta) = \frac{1}{12}\big(B(\theta)-B(\theta_*)\big)^\top N^\top N\big(B(\theta)-B(\theta_*)\big)$$

Applying the chain rule to differentiate this twice at $\theta=\theta_*$, we obtain

$$\nabla^2\tilde{s}_3(\theta_*) = \frac{1}{6}\mathrm{d}B(\theta_*)^\top N^\top N\mathrm{d}B(\theta_*),$$

so $\operatorname{rank}\big(\nabla^2\tilde{s}_3(\theta_*)\big) = \operatorname{rank}\big(N\cdot\mathrm{d}B(\theta_*)\big)$.

Recall the linear reparametrization by the coordinates $\eta(\theta)$ in (161) and (162). Then equivalently

$$\operatorname{rank}\big(\nabla^2\tilde{s}_3(\theta_*)\big) = \operatorname{rank}\big(N\cdot\mathrm{d}_\eta B(\eta_*)\big)$$

The proof of Theorem 4.4.6 verified that $\operatorname{rank}(\mathrm{d}_\eta B(\eta_*)) = d-3$ for generic $\eta_*\in\mathbb{R}^d$. In fact, let

$$D(\eta_*) = \text{submatrix of } \mathrm{d}_\eta B(\eta_*) \text{ with columns } \partial_{w_0^{(12)}}, \partial_{w_1^{(11)}}, \partial_{w_0^{(11)}} \text{ removed.}$$

Then Lemma C.4.5 shows that $D(\eta_*)$ has full column rank $d-3$ for generic $\eta_*\in\mathbb{R}^d$. Applying

$$\operatorname{rank}(N\cdot\mathrm{d}_\eta B(\eta_*)) \ge \operatorname{rank}(N\cdot D(\eta_*)),$$

it then suffices to show that $N\cdot D(\eta_*)$ also has full column rank $d-3$ for generic $\eta_*\in\mathbb{R}^d$.

For this, we define the following submatrices of N and $D(\eta_*)$. For each $k\in\{0,1,\dots,L\}$, define

the index sets

$$\begin{aligned}
\mathcal{H}^{(k)} &= \Big\{((l,s),(l',s'),(l'',s'')) \in \mathcal{H} :\ \max(l,l',l'') = k\Big\},\\
\mathcal{Q}^{(k)} &= \Big\{((q,r),(q',r'),(q'',r'')) \in \mathcal{Q} :\ \max(|q|,|q'|,|q''|) = k\Big\},\\
\mathcal{V}^{(k)} &= \Big\{\text{coordinates } v_m^{(ls)}, w_m^{(ls)} \text{ of } \eta :\ l = k\Big\} \qquad \text{if } k \neq 1,\\
\mathcal{V}^{(1)} &= \Big\{\text{coordinates } v_m^{(1s)}, w_m^{(1s)} \text{ of } \eta\Big\} \Big\backslash \Big\{w_0^{(12)}, w_1^{(11)}, w_0^{(11)}\Big\}.
\end{aligned}$$

Let $N_k \in \mathbb{R}^{|\mathcal{Q}^{(k)}| \times |\mathcal{H}^{(k)}|}$ be the submatrix of N containing the rows in $\mathcal{Q}^{(k)}$ and columns in $\mathcal{H}^{(k)}$, and let $D_k(\eta_*) \in \mathbb{R}^{|\mathcal{H}^{(k)}| \times |\mathcal{V}^{(k)}|}$ be the submatrix of $D(\eta_*)$ containing the rows in $\mathcal{H}^{(k)}$ and columns in $\mathcal{V}^{(k)}$. Similarly, define $N_{\leq k}$ and $D_{\leq k}(\eta_*)$ to contain rows and columns of $\mathcal{Q}^{(l)}, \mathcal{H}^{(l)}, \mathcal{V}^{(l)}$ for $l \leq k$. Note that $D_k(\eta_*)$ and $D_{\leq k}(\eta_*)$ depend only on the coordinates of $v_m^{(ls)}$ and $w_m^{(ls)}$ where $l \leq k$, by the definition of $\mathcal{H}^{(k)}$ and the form of each function $B_{(l,s),(l',s'),(l'',s'')}$.

We prove by induction on L the claim that $N \cdot D(\eta_*)$ has full column rank for generic $\eta_* \in \mathbb{R}^d$. Lemma C.4.6(a) below shows that for $L = 1$, there exists some η_* where $N \cdot D(\eta_*)$ has full column rank. Then $N \cdot D(\eta_*)$ has full column rank also for generic η_*, establishing the base case $L = 1$.

For the inductive step, we establish a block structure on N and $D(\eta_*)$. Block the rows and columns of N by $(\mathcal{Q} \setminus \mathcal{Q}^{(L)}, \mathcal{Q}^{(L)})$ and $(\mathcal{H} \setminus \mathcal{H}^{(L)}, \mathcal{H}^{(L)})$, and those of $D(\eta_*)$ by $(\mathcal{H} \setminus \mathcal{H}^{(L)}, \mathcal{H}^{(L)})$ and $(\eta \setminus \mathcal{V}^{(L)}, \mathcal{V}^{(L)})$. Note that $N^{(l,s),(l',s'),(l'',s'')}_{(q,r),(q',r'),(q'',r'')} = 0$ unless $\max(|q|,|q'|,|q''|) \leq \max(l,l',l'')$, and also $B_{(l,s),(l',s'),(l'',s'')}$ does not depend on any variable $v_m^{(ks)}$ or $w_m^{(ks)}$ where $k > \max(l,l',l'')$. Thus N and $D(\eta_*)$ have the block structures

$$N = \begin{pmatrix} A & B \\ 0 & N_L \end{pmatrix}, \qquad D(\eta_*) = \begin{pmatrix} X(\eta_*) & 0 \\ Y(\eta_*) & D_L(\eta_*) \end{pmatrix}$$

for some matrices $A, B, X(\eta_*), Y(\eta_*)$.

Let us now specialize to $\eta_* \in \mathbb{R}^d$ where

$$v_{*,m}^{(Ls)} = w_{*,m}^{(Ls)} = 0 \text{ for all } s = 1, \ldots, S_L \text{ and } m = -L, \ldots, L. \tag{179}$$

The above matrix $Y(\eta_*)$ contains the derivatives in variables $\{v_m^{(ks)}, w_m^{(ks)} : k < L\}$ of the functions $B_{(l,s),(l',s'),(l'',s'')}$ where $\max(l,l',l'') = L$. By the form of $B_{(l,s),(l',s'),(l'',s'')}$, any such derivative

vanishes for η_* satisfying (179), so $Y(\eta_*) = 0$ and

$$N \cdot D(\eta_*) = \begin{pmatrix} A \cdot X(\eta_*) & B \cdot D_L(\eta_*) \\ 0 & N_L \cdot D_L(\eta_*) \end{pmatrix}.$$

The induction hypothesis for $L-1$ is exactly the statement that the upper-left block $A \cdot X(\eta_*)$ has full column rank for all generic values of the coordinates $\{v_{*,m}^{(ks)}, w_{*,m}^{(ks)} : k \leq L-1\}$. Applying Lemma C.4.6(b) below, also for generic values of $\{v_{*,m}^{(ks)}, w_{*,m}^{(ks)} : k \leq L-1\}$, the lower-right block $N_L \cdot D_L(\eta_*)$ has full column rank. Then there exists a point $\eta_* \in \mathbb{R}^d$ satisfying (179) where $N \cdot D(\eta_*)$ has full column rank. Then $N \cdot D(\eta_*)$ has full column rank also for generic $\eta_* \in \mathbb{R}^d$, completing the induction and the proof. □

Lemma C.4.6. *If $S_l \geq 4$ for $0 \leq l \leq L$, then we have the following.*

(a) There exists a point $\eta_* \in \mathbb{R}^d$ such that $N_{\leq 1} \cdot D_{\leq 1}(\eta_*)$ has full column rank.

(b) For each $k \geq 2$, there exists a point $\eta_* \in \mathbb{R}^d$ such that $v_{*,m}^{(ks)} = w_{*,m}^{(ks)} = 0$ for all $s \in \{1, \ldots, S_k\}$ and $m \in \{-k, \ldots, k\}$, and $N_k \cdot D_k(\eta_*)$ has full column rank.

Proof of Lemma C.4.6. **Part (a):** Recall from the form of p_{lm} in (172) that $p_{lm} = 0$ if $l + m$ is odd and $p_{lm} \neq 0$ if $l + m$ is even. Then, for $\max\{l, l', l''\} \leq 1$, the non-vanishing of Clebsch-Gordon coefficients in Lemma C.4.2 and the definition of N in (178) imply that

$$N_{(q,r),(q',r'),(q'',r'')}^{(l,s),(l',s'),(l'',s'')} \neq 0 \text{ if and only if } l = |q|, l' = |q'|, l'' = |q''|, r = s, r' = s', r'' = s''. \tag{180}$$

For each $((l,s),(l',s'),(l'',s'')) \in \mathcal{H}^{(0)} \cup \mathcal{H}^{(1)}$ where $l = l' + l''$, take the row $((-l,s),(l',s'),(l'',s'')) \in \mathcal{Q}^{(0)} \cup \mathcal{Q}^{(1)}$ of $N_{\leq 1}$. It suffices to exhibit η_* such that the submatrix of corresponding rows of $N_{\leq 1} \cdot D_{\leq 1}(\eta_*)$ has full column rank. Observation (180) implies that each such row of $N_{\leq 1}$ has exactly one non-zero entry, which is given by $N_{(-l,s),(l',s'),(l'',s'')}^{(l,s),(l',s'),(l'',s'')}$. Then it suffices to show that the submatrix of $D_{\leq 1}(\eta_*)$ consisting of the rows $((l,s),(l',s'),(l'',s'')) \in \mathcal{H}^{(0)} \cup \mathcal{H}^{(1)}$ where $l = l' + l''$ has full column rank. But this has been exhibited already in Lemma C.4.5, because the proof of Lemma C.4.5(b–c) in fact only used rows of $\mathrm{d}_{\eta^{(0s)}} B^{(0s)}$ and $\mathrm{d}_{\eta^{(1s)}} B^{(1s)}$ for which $(l, l', l'') = (0,0,0)$ or $(1,1,0)$, both satisfying $l = l' + l''$. This completes the proof of (a).

Part (b), $k = 2$ and $k = 3$. The argument is similar to part (a). Observe first that when η_* satisfies $v_{*,m}^{(ks)} = w_{*,m}^{(ks)} = 0$ for all s and m, the rows of $D_k(\eta_*)$ indexed by $((l,s),(l',s'),(l'',s'')) \in \mathcal{H}^{(k)}$

having more than one index l, l', l'' equal to k are identically 0. Let $D_k(\eta_*)'$ be the submatrix of $D_k(\eta_*)$ with these rows removed, and let N_k' be the submatrix of N_k with the corresponding columns removed. Then $N_k \cdot D_k(\eta_*) = N_k' \cdot D_k(\eta_*)'$.

For each remaining tuple $((l,s),(l',s'),(l'',s'')) \in \mathcal{H}^{(k)}$ where $l = l' + l''$, consider the row $((-l,s),(l',s'),(l'',s'')) \in \mathcal{Q}^{(k)}$ of N_k'. Note that we must have $(l,l',l'') = (2,1,1)$ if $k = 2$, and $(l,l',l'') = (3,1,2)$ or $(3,2,1)$ if $k = 3$. Each such row has the non-zero entry $N^{(l,s),(l',s'),(l'',s'')}_{(-l,s),(l',s'),(l'',s'')}$ as above, and this is the only non-zero entry in the row: Indeed, if $((j,r),(j',r'),(j'',r''))$ is a column of N_k' where $N^{(j,r),(j',r'),(j'',r'')}_{(-l,s),(l',s'),(l'',s'')} \neq 0$, then by definition of N in (178) we must have $(s,s',s'') = (r,r',r'')$, $j \geq l$, $j' \geq l'$, $j'' \geq l''$, and each of $j - l$, $j' - l'$, $j'' - l''$ is even. Columns of N_k' must satisfy $(j,j',j'') \in \{(2,1,1),(3,1,2),(3,2,1)\}$, and this forces $(j,j',j'') = (l,l',l'')$. So the non-zero entry in this row of N_k' is unique, as claimed.

Then it suffices to check that the submatrix of rows of $D_k(\eta_*)$ indexed by $((l,s),(l',s'),(l'',s'')) \in \mathcal{H}^{(k)}$ where $l', l'' < k$ and $k = l = l' + l''$ has full column rank. This was not exhibited in the proof of Lemma C.4.5 (which used rows where $l' + l'' > l$ strictly) but we may show this here by a similar argument, assuming now the availability of 4 different spherical frequencies: Fix spherical frequencies $(A,B,C,D) = (1,2,3,4)$, and consider η_* satisfying

$$\mathrm{Type}(l',A), \mathrm{Type}(l',B) = 0, \quad \mathrm{Type}(l',C), \mathrm{Type}(l',D) = 1 \quad \text{for all} \quad l' \in \{1,\dots,k-1\}.$$

Recall that this means $v^{(l'A)}_{*,m}, w^{(l'A)}_{*,m}, v^{(l'B)}_{*,m}, w^{(l'B)}_{*,m} = 0$ unless $m = l'$, and $v^{(l'C)}_{*,m}, w^{(l'C)}_{*,m}, v^{(l'D)}_{*,m}, w^{(l'D)}_{*,m} = 0$ unless $m = l' - 1$. Then, for $\partial_{v^{(ls)}_m} B_{(l,s),(l',s'),(l'',s'')}, \partial_{w^{(ls)}_m} B_{(l,s),(l',s'),(l'',s'')}$ to be non-zero, this requires as in (170)

$$m \in \Big\{ \big|(l' - \mathrm{Type}(l',s')) - (l'' - \mathrm{Type}(l'',s''))\big|, (l' - \mathrm{Type}(l',s')) + (l'' - \mathrm{Type}(l'',s'')) \Big\}. \quad (181)$$

For $k = 2$, we choose the following 5 rows of $D_k(\eta_*)$, with the following corresponding values of m satisfying (181):

(l',s') and (l'',s'')	Values of m
$(1,C)$ and $(1,C)$	0
$(1,A)$ and $(1,A)$	0, 2
$(1,B)$ and $(1,B)$	0, 2
$(1,A)$ and $(1,C)$	1
$(1,B)$ and $(1,D)$	1

Ordering the columns by $v_0^{(2s)}, v_2^{(2s)}, w_2^{(2s)}, v_1^{(2s)}, w_1^{(2s)}$, the resulting 5×5 submatrix is block lower-triangular with diagonal blocks

$$\partial_{v_0^{(2s)}} B_{(2,s),(1,C),(1,C)}(\eta_*) = C^{2,1,1}_{0,0,0} \cdot \left| u^{(1C)}_{*,0} \right|^2$$

$$\partial_{v_2^{(2s)},w_2^{(2s)}} \Big(B_{(2,s),(1,A),(1,A)}, B_{(2,s),(1,B),(1,B)} \Big)(\eta_*) = \begin{pmatrix} 2C^{2,1,1}_{2,-1,1} \cdot \mathrm{Re}\, \overline{u^{(1A)}_{*,-1}} u^{(1A)}_{*,1} & 2C^{2,1,1}_{2,-1,1} \cdot \mathrm{Im}\, \overline{u^{(1A)}_{*,-1}} u^{(1A)}_{*,1} \\ 2C^{2,1,1}_{2,-1,1} \cdot \mathrm{Re}\, \overline{u^{(1B)}_{*,-1}} u^{(1B)}_{*,1} & 2C^{2,1,1}_{2,-1,1} \cdot \mathrm{Im}\, \overline{u^{(1B)}_{*,-1}} u^{(1B)}_{*,1} \end{pmatrix}$$

$$\partial_{v_1^{(2s)},w_1^{(2s)}} \Big(B_{(2,s),(1,A),(1,C)}, B_{(2,s),(1,B),(1,D)} \Big)(\eta_*) = \begin{pmatrix} 2C^{2,1,1}_{1,-1,0} \cdot \mathrm{Re}\, \overline{u^{(1A)}_{*,-1}} u^{(1C)}_{*,0} & 2C^{2,1,1}_{1,-1,0} \cdot \mathrm{Im}\, \overline{u^{(1A)}_{*,-1}} u^{(1C)}_{*,0} \\ 2C^{2,1,1}_{1,-1,0} \cdot \mathrm{Re}\, \overline{u^{(1B)}_{*,-1}} u^{(1D)}_{*,0} & 2C^{2,1,1}_{1,-1,0} \cdot \mathrm{Im}\, \overline{u^{(1B)}_{*,-1}} u^{(1D)}_{*,0} \end{pmatrix}$$

These blocks are generically non-singular, so this submatrix of $D_2(\eta_*)$ has full column rank.

For $k = 3$, we choose the following 7 rows of $D_k(\eta_*)$, with the following corresponding values of m satisfying (181):

(l', s') and (l'', s'')	values of m
$(1, D)$ and $(2, B)$	2
$(1, C)$ and $(2, A)$	2
$(1, C)$ and $(2, C)$	1
$(1, D)$ and $(2, D)$	1
$(1, A)$ and $(2, A)$	1, 3
$(1, B)$ and $(2, B)$	1, 3
$(1, A)$ and $(2, C)$	2, 0

Ordering the columns by $v_2^{(3s)}, w_2^{(3s)}, v_1^{(3s)}, w_1^{(3s)}, v_3^{(3s)}, w_3^{(3s)}, w_0^{(3s)}$, the resulting 7×7 submatrix is block lower-triangular with diagonal blocks

$$\partial_{v_2^{(3s)},w_2^{(3s)}} \Big(B_{(3,s),(1,D),(2,B)}, B_{(3,s),(1,C),(2,A)} \Big)(\eta_*) = \begin{pmatrix} 2C^{3,1,2}_{2,0,2} \cdot \mathrm{Re}\, \overline{u^{(1D)}_{*,0}} u^{(2B)}_{*,2} & 2C^{3,1,2}_{2,0,2} \cdot \mathrm{Im}\, \overline{u^{(1D)}_{*,0}} u^{(2B)}_{*,2} \\ 2C^{3,1,2}_{2,0,2} \cdot \mathrm{Re}\, \overline{u^{(1C)}_{*,0}} u^{(2A)}_{*,2} & 2C^{3,1,2}_{2,0,2} \cdot \mathrm{Im}\, \overline{u^{(1C)}_{*,0}} u^{(2A)}_{*,2} \end{pmatrix}$$

$$\partial_{v_1^{(3s)},w_1^{(3s)}} \Big(B_{(3,s),(1,C),(2,C)}, B_{(3,s),(1,D),(2,D)} \Big)(\eta_*) = \begin{pmatrix} 2C^{3,1,2}_{1,0,1} \cdot \mathrm{Re}\, \overline{u^{(1C)}_{*,0}} u^{(2C)}_{*,1} & 2C^{3,1,2}_{1,0,1} \cdot \mathrm{Im}\, \overline{u^{(1C)}_{*,0}} u^{(2C)}_{*,1} \\ 2C^{3,1,2}_{1,0,1} \cdot \mathrm{Re}\, \overline{u^{(1D)}_{*,0}} u^{(2D)}_{*,1} & 2C^{3,1,2}_{1,0,1} \cdot \mathrm{Im}\, \overline{u^{(1D)}_{*,0}} u^{(2D)}_{*,1} \end{pmatrix}$$

$$\partial_{v_3^{(3s)},w_3^{(3s)}} \Big(B_{(3,s),(1,A),(2,A)}, B_{(3,s),(1,B),(2,B)} \Big)(\eta_*) = \begin{pmatrix} 2C^{3,1,2}_{3,-1,2} \cdot \mathrm{Re}\, \overline{u^{(1A)}_{*,-1}} u^{(2A)}_{*,2} & 2C^{3,1,2}_{3,-1,2} \cdot \mathrm{Im}\, \overline{u^{(1A)}_{*,-1}} u^{(2A)}_{*,2} \\ 2C^{3,1,2}_{3,-1,2} \cdot \mathrm{Re}\, \overline{u^{(1B)}_{*,-1}} u^{(2B)}_{*,2} & 2C^{3,1,2}_{3,-1,2} \cdot \mathrm{Im}\, \overline{u^{(1B)}_{*,-1}} u^{(2B)}_{*,2} \end{pmatrix}$$

$$\partial_{w_0^{(3s)}} B_{(3,s),(1,A),(2,C)}(\eta_*) = 2C^{3,1,2}_{0,1,1} \cdot \mathrm{Im}\, \overline{u^{(1A)}_{*,1}} u^{2C}_{*,1}$$

These blocks are again generically non-singular, so this submatrix of $D_3(\eta_*)$ has full column rank.

This verifies that $N_k \cdot D_k(\eta_*)$ has full column rank for $k = 2, 3$.

Part (b), $k \geq 4$. As above, we fix $(A, B, C, D) = (1, 2, 3, 4)$ and consider η_* satisfying both

$v_{*,m}^{(ks)}, w_{*,m}^{(ks)} = 0$ for all m, s and

$$\text{Type}(l', A), \text{Type}(l', B) = 0, \quad \text{Type}(l', C), \text{Type}(l', D) = 1 \quad \text{for all} \quad l' \in \{1, \dots, k-1\}. \tag{182}$$

Columns of $D_k(\eta_*)$ correspond to derivatives in the coordinates $\mathcal{V}^{(k)}$. We partition these coordinates into blocks $s = 1, \dots, S_k$ and write

$$D_k(\eta_*) = [D_k^{(s)}(\eta_*) : s = 1, \dots, S_k],$$

where columns of each $D_k^{(s)}(\eta_*)$ are indexed by $\eta_0^{(ks)}, v_1^{(ks)}, w_1^{(ks)}, \dots, v_k^{(ks)}, w_k^{(ks)}$. It suffices to show that $N_k \cdot D_k^{(s)}(\eta_*)$ has full column rank $2k+1$ for generic η_* satisfying (182), for each fixed s. We do this by choosing $2k+1$ rows of N_k—call this submatrix N_k'—and verifying that the corresponding $(2k+1) \times (2k+1)$ submatrix $N_k' \cdot D_k^{(s)}(\eta_*)$ is non-singular.

The argument for verifying non-singularity is different from our preceding approaches in Lemmas C.4.3 and C.4.5. Let us first explain the high-level idea: Rather than exhibiting a sparse structure for $N_k' \cdot D_k^{(s)}(\eta_*)$ where the rank may be explicitly checked, we study the determinant

$$P(\eta_*) = \det[N_k' \cdot D_k^{(s)}(\eta_*)] \tag{183}$$

and show that this is not identically 0 as a polynomial of the non-zero coordinates of η_*. We introduce a special degree-$(2k+1)$ monomial

$$M = \left(w_0^{(1C)} w_0^{(1D)} v_1^{(1A)} v_1^{(1B)}\right)^2 \left(\prod_{j=2}^{\lfloor k/2 \rfloor - 1} v_j^{(jA)} v_j^{(jB)} v_{j-1}^{(jC)} v_{j-1}^{(jD)}\right) v_{\lfloor k/2 \rfloor - 1}^{(\lfloor k/2 \rfloor C)} \left(v_{\lfloor k/2 \rfloor}^{(\lfloor k/2 \rfloor A)} v_{\lfloor k/2 \rfloor - 1}^{(\lfloor k/2 \rfloor D)}\right)^{\mathbf{1}\{k \text{ odd}\}}, \tag{184}$$

where all variables appearing in M are coordinates of η_* which are not fixed to be zero. We then write

$$P = (P/M) \cdot M + Q \tag{185}$$

where Q are the terms of P not divisible by M, $(P/M) \cdot M$ are the terms which *are* divisible by M, and P/M denotes their quotient by M. It suffices to show that P/M is not identically 0.

We now describe the choice of $2k+1$ rows of N_k' that allows us to verify this claim $P/M \neq 0$. We restrict to rows $((-k, s), (q', s'), (q'', s'')) \in \mathcal{Q}^{(k)}$ of N_k where the first pair is fixed to be $(-k, s)$, and where $q' \in \{1, \dots, \lfloor k/2 \rfloor\}$. This requires $-k + q' + q'' = 0$, so $q'' = k - q' \in \{k-1, \dots, \lceil k/2 \rceil\}$. We index such rows by $(q', s'), (q'', s'')$. For any such row $(q', s'), (q'', s'')$, we apply the following two

observations:

- By definition of N in (178), each non-zero entry in this row of N_k belongs to a column $((k,s),(l',s'),(l'',s'')) \in \mathcal{H}^{(k)}$ where $l', l'' \in \{1,\dots,k-1\}$ and

$$l' \geq q', \qquad l'' \geq q'', \qquad l'-q', l''-q'' \text{ are even.} \tag{186}$$

- As in (170), for this row $((k,s),(l',s'),(l'',s'')) \in \mathcal{H}^{(k)}$ of $D_k^{(s)}(\eta_*)$, the entries in the columns $\partial_{v_m^{(ks)}}, \partial_{w_m^{(ks)}}$ can be non-zero only when

$$m \in \Big\{ \big|(l'-\mathrm{Type}(l',s')) - (l''-\mathrm{Type}(l'',s''))\big|, (l'-\mathrm{Type}(l',s')) + (l''-\mathrm{Type}(l'',s'')) \Big\}. \tag{187}$$

Combined, these yield the important observation that, fixing a row $(q',s'),(q'',s'')$ of $N_k \cdot D_k^{(s)}(\eta_*)$ and a pair of columns $\partial_{v_m^{(ks)}}, \partial_{w_m^{(ks)}}$ (or a single column in the case $m=0$) for a specific index $m \in \{0,\dots,k\}$, these two entries (or one entry) of $N_k \cdot D_k^{(s)}(\eta_*)$ are homogenous degree-2 polynomials, whose degree-2 monomials are each a product of some variable $v_\cdot^{l'\cdot}, w_\cdot^{l'\cdot}$ and some variable $v_\cdot^{l''\cdot}, w_\cdot^{l''\cdot}$ where l', l'' satisfy both conditions (186) and (187).

The following table now explicitly chooses $2k+1$ rows $(q',s'),(q'',s'')$ of N_k to form N_k', and indicates which columns $\partial_{v_m^{(ks)}}, \partial_{w_m^{(ks)}}$ of each corresponding row of $N_k \cdot D_k^{(s)}(\eta_*)$ can depend on some variable $v_\cdot^{q'\cdot}, w_\cdot^{q'\cdot}$ with the same spherical frequency as the first row index q'. For example: If $(s',s'',q',q'') = (A,A,1,k-1)$, then (186) forces $l''=k-1$. In order for a term of this row to depend on $v_\cdot^{1\cdot}, w_\cdot^{1\cdot}$, we must then have $l'=1$. Then $\mathrm{Type}(l',s')=1$ and $\mathrm{Type}(l'',s'')=k-1$, so the condition (187) implies that only columns corresponding to $m \in \{k,k-2\}$ can depend on such variables $v_\cdot^{1\cdot}, w_\cdot^{1\cdot}$. This yields the first row of the table. If $(s',s'',q',q'') = (C,C,3,k-3)$, then (186) forces $l'' \in \{k-3,k-1\}$. For this row to depend on $v_\cdot^{3\cdot}, w_\cdot^{3\cdot}$, we must have $l'=3$. Then $\mathrm{Type}(l',s')=2$ and $\mathrm{Type}(l'',s'') \in \{k-4,k-2\}$, so $m \in \{k-6,k-4,k-2,k\}$, and this yields the 13^{th} row of the table. The remaining rows are deduced by the same type of reasoning. (The sequences $(2,4,\dots)$, $(3,5,\dots)$, etc. below denote some sequences of consecutive even and odd integers, whose exact last elements will not be important for our later arguments.)

	s'	s''	q'	q''	m s.t. $\partial_{v_m^{(ks)}}, \partial_{w_m^{(ks)}}$ can depend on $v_\cdot^{q'\cdot}, w_\cdot^{q'\cdot}$
	A	A	1	$k-1$	$k, k-2$
	B	B	1	$k-1$	$k, k-2$
	C	C	1	$k-1$	$k-2$
	D	D	1	$k-1$	$k-2$
	A	C	1	$k-1$	$k-1, k-3$
	B	D	1	$k-1$	$k-1, k-3$
	C	A	1	$k-1$	$k-1$
	D	B	1	$k-1$	$k-1$
	C	C	2	$k-2$	$k-4$ and $k-2$
	D	D	2	$k-2$	$k-4$ and $k-2$
	A	C	2	$k-2$	$k-5$ and $k-1$
	B	D	2	$k-2$	$k-5$ and $k-1$
	C	C	3	$k-3$	$k-6, k-4, k-2$ and k
	D	D	3	$k-3$	$k-6, k-4, k-2$ and k
	A	C	3	$k-3$	$k-7, k-5$ and $k-1$
	B	D	3	$k-3$	$k-7, k-5$ and $k-1$
			$\vdots$	$\vdots$	$\vdots$
	C	C	$\lfloor k/2 \rfloor - 1$	$\lceil k/2 \rceil + 1$	$2, 4, \ldots$ and $k-2, k$ if k even; $3, 5, \ldots$ and $k-2, k$ if k odd
	D	D	$\lfloor k/2 \rfloor - 1$	$\lceil k/2 \rceil + 1$	$2, 4, \ldots$ and $k-2, k$ if k even; $3, 5, \ldots$ and $k-2, k$ if k odd
	A	C	$\lfloor k/2 \rfloor - 1$	$\lceil k/2 \rceil + 1$	$1, 3, \ldots$ and $k-1$ if k even; $2, 4, \ldots$ and $k-1$ if k odd
	B	D	$\lfloor k/2 \rfloor - 1$	$\lceil k/2 \rceil + 1$	$1, 3, \ldots$ and $k-1$ if k even; $2, 4, \ldots$ and $k-1$ if k odd
	C	C	$\lfloor k/2 \rfloor$	$\lceil k/2 \rceil$	$0, 2, \ldots$ and $k-2, k$ if k even; $1, 3, \ldots$ and $k-2, k$ if k odd
(if k odd)	D	D	$\lfloor k/2 \rfloor$	$\lceil k/2 \rceil$	$1, 3, \ldots$ and $k-2, k$
(if k odd)	A	C	$\lfloor k/2 \rfloor$	$\lceil k/2 \rceil$	$0, 2, \ldots$ and $k-1$

Order the rows of $N'_k \cdot D_k^{(s)}(\eta_*)$ as above, and the columns in the ordering of *decreasing* m

$$v_k^{(ks)}, w_k^{(ks)}, v_{k-1}^{(ks)}, w_{k-1}^{(ks)}, v_{k-2}^{(ks)}, w_{k-2}^{(ks)} \ldots, v_1^{(ks)}, w_1^{(ks)}, \eta_0^{(ks)}.$$

Consider the block decomposition for both rows and columns of $N'_k \cdot D_k^{(s)}(\eta_*)$ with respect to

$$2k+1 = 8+4+4+\ldots+4+\begin{cases}1 & \text{if } k \text{ even}\\ 3 & \text{if } k \text{ odd.}\end{cases}$$

Let $P = \det(N'_k \cdot D_k^{(s)}(\eta_*))$ as defined in (183), and let $P_1, P_2, \ldots, P_{\lfloor k/2 \rfloor}$ be the determinants of the diagonal blocks in this decomposition. Recall that we wish to show $P/M \neq 0$. Let us factor M in (184) correspondingly as $M = M_1 M_2 \ldots M_{\lfloor k/2 \rfloor}$ where

$$\begin{aligned} M_1 &= (w_0^{(1C)} w_0^{(1D)} v_1^{(1A)} v_1^{(1B)})^2 \\ M_j &= v_j^{(jA)} v_j^{(jB)} v_{j-1}^{(jC)} v_{j-1}^{(jD)} \quad \text{for } j = 2, \ldots, \lfloor k/2 \rfloor - 1 \\ M_{\lfloor k/2 \rfloor} &= v_{\lfloor k/2 \rfloor - 1}^{(\lfloor k/2 \rfloor C)} \left(v_{\lfloor k/2 \rfloor}^{(\lfloor k/2 \rfloor A)} v_{\lfloor k/2 \rfloor - 1}^{(\lfloor k/2 \rfloor D)} \right)^{\mathbf{1}\{k \text{ odd}\}}. \end{aligned}$$

The degrees of $M_1, M_2, M_3, \ldots$ coincide with the above block sizes $8, 4, 4, \ldots$. Furthermore, each M_j depends on only variables $v_\cdot^{j\cdot}, w_\cdot^{j\cdot}$ having spherical frequency j.

Observe now that:

- Only the 8×8 upper-left diagonal block of $N'_k \cdot D_k^{(s)}(\eta_*)$ has entries depending on variables $v_\cdot^{1\cdot}, w_\cdot^{1\cdot}$. This is because all monomials in rows 9 onwards are a product of some $v_\cdot^{l'\cdot}, w_\cdot^{l'\cdot}$ with some $v_\cdot^{l''\cdot}, w_\cdot^{l''\cdot}$ where $l' \geq q' \geq 2$ and $l'' \geq q'' \geq 2$. In the first 8 rows, the table indicates that only the first 8 columns (corresponding to $m = k, k-1, k-2, k-3$) can depend on $v_\cdot^{1\cdot}, w_\cdot^{1\cdot}$.

- Furthermore, any degree-2 monomial in this 8×8 block that depends on $v_\cdot^{1\cdot}, w_\cdot^{1\cdot}$ must have as its second variable $v_\cdot^{l''\cdot}, w_\cdot^{l''\cdot}$ for some $l'' \geq k-1 > \lfloor k/2 \rfloor$ strictly.

- Removing this first row block and column block of size 8, only the 4×4 upper-left diagonal block of the remaining matrix has entries depending on $v_\cdot^{2\cdot}, w_\cdot^{2\cdot}$, by the same reasoning. Furthermore, any degree-2 monomial in this 4×4 block that depends on $v_\cdot^{2\cdot}, w_\cdot^{2\cdot}$ must have as its second variable $v_\cdot^{l''\cdot}, w_\cdot^{l''\cdot}$ for some $l'' \geq k-2 > \lfloor k/2 \rfloor$ strictly.

- Removing also this second row block and column block of size 4, only the 4×4 upper-left remaining diagonal block has entries depending on $v_\cdot^{3\cdot}, w_\cdot^{3\cdot}$, etc. This argument can be continued inductively until the last block.

These observations imply that the terms of P divisible by M must have the factorization

$$P/M = (P_1/M_1)(P_2/M_2)\dots(P_{\lfloor k/2\rfloor}/M_{\lfloor k/2\rfloor}), \tag{188}$$

where, analogously to (185), each factor P_j/M_j is the polynomial that is the quotient by M_j of those terms of P_j which are exactly divisible by M_j.

To complete the proof, we check by direct computation that each polynomial P_j/M_j on the right side of (188) is non-zero.

Verification that $P_1/M_1 \neq 0$: Consider, as an example, the entry in the first row $(A, A, 1, k-1)$ and first column $\partial_{v_k^{(ks)}}$ of $N'_k \cdot D_k^{(s)}(\eta_*)$. This entry is the inner product

$$\begin{aligned}\big(N_{(-k,s),(1,A),(k-1,A)}\big)^\top \big(\partial_{v_k^{(ks)}} B(\eta_*)\big) \\ = \sum_{((k,s),(l',s'),(l'',s''))\in\mathcal{H}^{(k)}} N^{(k,s),(l',s'),(l'',s'')}_{(-k,s),(1,A),(k-1,A)} \cdot \partial_{v_k^{(ks)}} B_{(k,s),(l',s'),(l'',s'')}(\eta_*).\end{aligned}$$

Importantly, only the single term indexed by $((k,s),(l',s'),(l'',s'')) = ((k,s),(1,A),(k-1,A))$ of this sum depends on any variable appearing in the monomial M_1. This is because, from the definition of N in (178), all other non-zero entries $N^{(k,s),(l',s'),(l'',s'')}_{(-k,s),(1,A),(k-1,A)}$ of this row of N have $l' \geq 3$ and $l'' = k-1$. We introduce the shorthand

$$Y_q = N^{(k,s),(q,s'),(k-q,s'')}_{(-k,s),(q,s'),(k-q,s'')},$$

where this notation fixes k and uses that this value does not actually depend on (s, s', s''). Note that by (178) and the non-vanishing of Clebsch-Gordan coefficients in Lemma C.4.2, $Y_q \neq 0$ for every $q = 0, 1, \dots, k$. Then, applying (164), (182), and the sign symmetry (154), the above single term is

$$\begin{aligned}N^{(k,s),(1,A),(k-1,A)}_{(-k,s),(1,A),(k-1,A)} \cdot \partial_{v_k^{(ks)}} B_{(k,s),(1,A),(k-1,A)}(\eta_*) &= Y_1 \cdot 2C^{k,1,k-1}_{k,-1,k-1} \operatorname{Re}\overline{u_{-1}^{(1A)}} u_{k-1}^{(k-1,A)} \\ &= 2Y_1 C^{k,1,k-1}_{k,-1,k-1}\Big(v_1^{(1A)} v_{k-1}^{(k-1,A)} - w_1^{(1A)} w_{k-1}^{(k-1,A)}\Big).\end{aligned}$$

Only the first of these two summands depends on a variable in M_1, namely $v_1^{(1A)}$. We write its quotient by this variable $v_1^{(1A)}$ in the upper-left entry of the first table below.

As a second example, consider the entry in row $(C, C, 1, k-1)$ and column $\partial_{v_{k-2}^{(ks)}}$ of $N'_k \cdot D_k^{(s)}(\eta_*)$.

By the same reasoning as above, the only term of this entry which depends on a variable in M_1 is

$$N^{(k,s),(1,C),(k-1,C)}_{(-k,s),(1,C),(k-1,C)} \cdot \partial^{(ks)}_{v_{k-2}} B_{(k,s),(1,C),(k-1,C)} = Y_1 \cdot 2C^{k,1,k-1}_{k-2,0,k-2} \cdot \operatorname{Re}\overline{u_0^{(1C)}} u_{k-2}^{(k-1,C)}$$
$$= 2Y_1 C^{k,1,k-1}_{k-2,0,k-2} \cdot w_0^{(1C)} w_{k-2}^{(k-1,C)}.$$

Its quotient by the variable $w_0^{(1C)}$ appearing in M_1 is the $(3,3)$ entry of the first table below.

The entries of the 8×8 block for P_1 which depend on some variable in M_1 are contained within two 4×4 submatrices, corresponding to the below two tables. Similar to the above computations, each entry of each submatrix has at most 1 term depending on some variable in M_1. We indicate the quotient of this term by the corresponding variable of M_1 in the two tables below. For entries that have no dependence on variables of M_1, we write this quotient as 0.

	v_k^{ks}	w_k^{ks}	$v_{k-2}^{k,s}$	$w_{k-2}^{k,s}$
$A,A,1,k-1$	$2Y_1 C^{k,1,k-1}_{k,-1,k-1} v_{k-1}^{k-1,A}$	$2Y_1 C^{k,1,k-1}_{k,-1,k-1} w_{k-1}^{k-1,A}$	$2Y_1 C^{k,1,k-1}_{k-2,1,k-1} v_{k-1}^{k-1,A}$	$2Y_1 C^{k,1,k-1}_{k-2,1,k-1} w_{k-1}^{k-1,A}$
$B,B,1,k-1$	$2Y_1 C^{k,1,k-1}_{k,-1,k-1} v_{k-1}^{k-1,B}$	$2Y_1 C^{k,1,k-1}_{k,-1,k-1} w_{k-1}^{k-1,B}$	$2Y_1 C^{k,1,k-1}_{k-2,1,k-1} v_{k-1}^{k-1,B}$	$2Y_1 C^{k,1,k-1}_{k-2,1,k-1} w_{k-1}^{k-1,B}$
$C,C,1,k-1$	0	0	$2Y_1 C^{k,1,k-1}_{k-2,0,k-2} w_{k-2}^{k-1,C}$	$-2Y_1 C^{k,1,k-1}_{k-2,0,k-2} v_{k-2}^{k-1,C}$
$D,D,1,k-1$	0	0	$2Y_1 C^{k,1,k-1}_{k-2,0,k-2} w_{k-2}^{k-1,D}$	$-2Y_1 C^{k,1,k-1}_{k-2,0,k-2} v_{k-2}^{k-1,D}$

	$v_{k-1}^{k,s}$	$w_{k-1}^{k,s}$	$v_{k-3}^{k,s}$	$w_{k-3}^{k,s}$
$A,C,1,k-1$	$2Y_1 C^{k,1,k-1}_{k-1,-1,k-2} v_{k-2}^{k-1,C}$	$2Y_1 C^{k,1,k-1}_{k-1,-1,k-2} w_{k-2}^{k-1,C}$	$2Y_1 C^{k,1,k-1}_{k-3,1,k-2} v_{k-2}^{k-1,C}$	$2Y_1 C^{k,1,k-1}_{k-3,1,k-2} w_{k-2}^{k-1,C}$
$B,D,1,k-1$	$2Y_1 C^{k,1,k-1}_{k-1,-1,k-2} v_{k-2}^{k-1,D}$	$2Y_1 C^{k,1,k-1}_{k-1,-1,k-2} w_{k-2}^{k-1,D}$	$2Y_1 C^{k,1,k-1}_{k-3,1,k-2} v_{k-2}^{k-1,D}$	$2Y_1 C^{k,1,k-1}_{k-3,1,k-2} w_{k-2}^{k-1,D}$
$C,A,1,k-1$	$2Y_1 C^{k,1,k-1}_{k-1,0,k-1} w_{k-1}^{k-1,A}$	$-2Y_1 C^{k,1,k-1}_{k-1,0,k-1} v_{k-1}^{k-1,A}$	0	0
$D,B,1,k-1$	$2Y_1 C^{k,1,k-1}_{k-1,0,k-1} w_{k-1}^{k-1,B}$	$-2Y_1 C^{k,1,k-1}_{k-1,0,k-1} v_{k-1}^{k-1,B}$	0	0

Now P_1/M_1 is the product of determinants of the above two 4×4 matrices. By Lemma C.4.2, each Clebsch-Gordan coefficient here is non-zero. Then the determinant of each 4×4 matrix is the product of two 2×2 determinants, each of which is a non-vanishing quadratic, so $P_1/M_1 \neq 0$.

Verification that $P_j/M_j \neq 0$ for $j = 2, \ldots, \lfloor k/2 \rfloor - 1$: Consider, as an example, the entry of row $(C,C,3,k-3)$ and column $\partial^{(ks)}_{w_{k-6}}$. This entry is the inner product

$$\left(N_{(-k,s),(3,C),(k-3,C)}\right)^\top \left(\partial_{w_{k-6}^{(ks)}} B(\eta_*)\right).$$

The non-zero entries $N^{(k,s),(l',C),(l'',C)}_{(-k,s),(3,C),(k-3,C)}$ of this row of N must have $l' \geq 3$ odd and $l'' \in \{k-1, k-3\}$. We must then have $l' = 3$ in order for the corresponding entry $\partial_{w_{k-6}^{(ks)}} B_{(k,s),(l',C),(l'',C)}(\eta_*)$ to depend on some variable of M_3, which would be $v_2^{(3C)}$. Recalling the form of this derivative in (165), this forces $|m'| = 2$ for the summation index of (165) corresponding to any term depends on $v_2^{(3C)}$. Then

$m + m' \in \{k-8, k-4\}$, since $m = k-6$. Applying our specialization (187) to the derivative (165), this requires $l'' \in \{k-7, k-3\}$ in order for this term to be non-zero. Combining with the above condition $l'' \in \{k-1, k-3\}$, we must have $l'' = k-3$. Thus, to summarize, again only a single term of the sum constituting the above inner-product depends on the variable $v_2^{(3C)}$ of M_3. This term is

$$N^{(k,s),(3,C),(k-3,C)}_{(-k,s),(3,C),(k-3,C)} \cdot \partial_{w_{k-6}^{(ks)}} B_{(k,s),(3,C),(k-3,C)}(\eta_*) = Y_3 \cdot 2C^{k,3,k-3}_{k-6,2,k-4} \operatorname{Im} \overline{u_2^{(3C)}} u_{k-4}^{(k-3,C)}$$
$$= 2Y_3 C^{k,3,k-3}_{k-6,2,k-4} \Big(v_2^{(3C)} w_{k-4}^{(k-3,C)} - w_2^{(3C)} v_{k-4}^{(k-3,C)} \Big).$$

Only the first summand depends on $v_2^{(3C)}$, and its quotient by $v_2^{(3C)}$ is recorded in row 1 and column 2 of the table below, corresponding to $j = 3$.

By the same reasoning, a similar simplification occurs for every $j = 2, \ldots, \lfloor k/2 \rfloor - 1$ and every entry of P_j/M_j. For general j, we may compute each entry of this 4×4 block that depends on a variable of M_j, and the table records the quotient of this entry by the corresponding variable of M_j.

	$v_{k-2j}^{k,s}$	$w_{k-2j}^{k,s}$	$v_{k-2j-1}^{k,s}$	$w_{k-2j-1}^{k,s}$
$C, C, j, k-j$	$2Y_j C^{k,j,k-j}_{k-2j,j-1,k-j-1} v_{k-j-1}^{k-j,C}$	$2Y_j C^{k,j,k-j}_{k-2j,j-1,k-j-1} w_{k-j-1}^{k-j,C}$	0	0
$D, D, j, k-j$	$2Y_j C^{k,j,k-j}_{k-2j,j-1,k-j-1} v_{k-j-1}^{k-j,D}$	$2Y_j C^{k,j,k-j}_{k-2j,j-1,k-j-1} w_{k-j-1}^{k-j,D}$	0	0
$A, C, j, k-j$	0	0	$2Y_j C^{k,j,k-j}_{k-2j-1,j,k-j-1} v_{k-j-1}^{k-j,C}$	$2Y_j C^{k,j,k-j}_{k-2j-1,j,k-j-1} w_{k-j-1}^{k-j,C}$
$B, D, j, k-j$	0	0	$2Y_j C^{k,j,k-j}_{k-2j-1,j,k-j-1} v_{k-j-1}^{k-j,D}$	$2Y_j C^{k,j,k-j}_{k-2j-1,j,k-j-1} w_{k-j-1}^{k-j,D}$

Then P_j/M_j is the determinant of this 4×4 matrix, which is a product of two 2×2 determinants. By Lemma C.4.2, these Clebsch-Gordan coefficients are non-zero, so each 2×2 determinant is a non-vanishing quadratic, and $P_j/M_j \neq 0$.

Verification that $P_{\lfloor k/2 \rfloor}/M_{\lfloor k/2 \rfloor} \neq 0$: If k is even, we have $\eta_0^{(ks)} = v_0^{(ks)}$, and

$$P_{k/2}(\eta_*) = \big(N_{(-k,s),(k/2,C),(k/2,C)}\big)^\top \big(\partial_{v_0^{(ks)}} B(\eta_*)\big).$$

The non-zero elements $N^{(k,s),(l',C),(l'',C)}_{(-k,s),(k/2,C),(k/2,C)}$ have $l' \geq k/2$ and $l'' \geq k/2$ with $l' - k/2$ and $l' - k/2$ both even. From (166) and the specialization (187), the only term of this inner-product depending on $M_{k/2} = v_{(k/2)-1}^{(k/2)C}$ arises from $l' = l'' = k/2$, and this term is

$$N^{(k,s),(k/2,C),(k/2,C)}_{(-k,s),(k/2,C),(k/2,C)} \cdot \partial_{v_0^{(ks)}} B_{(k,s),(k/2,C),(k/2,C)}(\eta_*)$$
$$= Y_{k/2} C^{k,k/2,k/2}_{0,k/2-1,k/2-1} \left| u_{k/2-1}^{(k/2)C} \right|^2 = Y_{k/2} C^{k,k/2,k/2}_{0,k/2-1,k/2-1} \left((v_{k/2-1}^{(k/2)C})^2 + (w_{k/2-1}^{(k/2)C})^2 \right).$$

So $P_{k/2}/M_{k/2} = Y_{k/2} C^{k,k/2,k/2}_{0,k/2-1,k/2-1} \cdot v_{k/2-1}^{(k/2)C}$, which is non-zero.

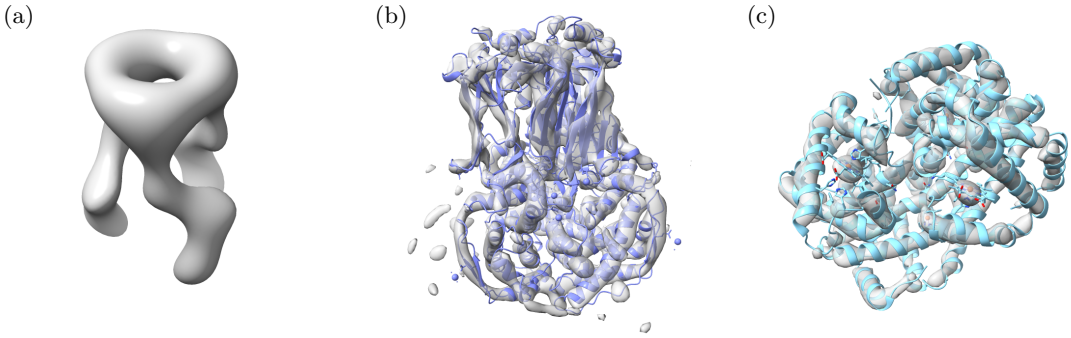

Figure C.1: (a) 24.6Å-resolution and (b) 8.2Å-resolution low-pass filtered maps for the rotavirus VP6 trimer, prior to performing basis approximation as depicted in Figure 4.1. (c) 7.0Å-resolution low-pass filtered map for hemoglobin, prior to performing basis approximation as depicted in Figure 4.2.

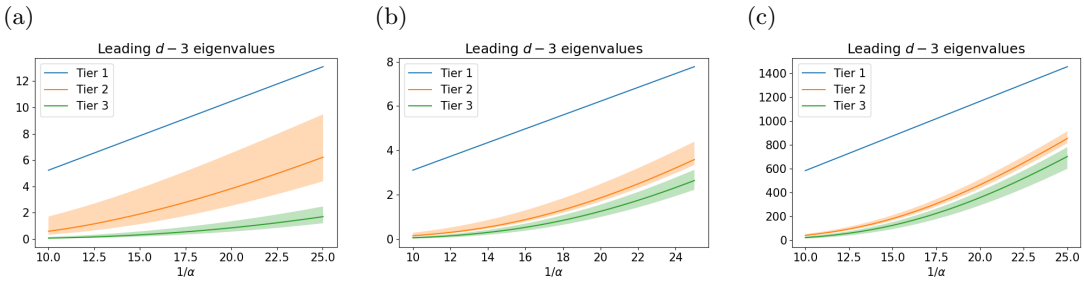

Figure C.2: Leading $d-3$ eigenvalues of the observed Fisher information matrices depicted in Figures 4.1 and 4.2, plotted against a common scaling $1/\alpha \propto \sigma^{-2}$, for (a) the 405-dimensional approximation for rotavirus VP6, (b) the 4410-dimensional approximation for rotavirus VP6, and (c) the 3528-dimensional approximation for hemoglobin. Lines depict the median within each of the three tiers, and bands depict the 10th to 90th percentiles.

If k is odd, then $\eta_0^{(ks)} = w_0^{(ks)}$. In the 3×3 submatrix corresponding to $P_{\lfloor k/2 \rfloor}$, again each entry has at most 1 term depending on some variable of $M_{\lfloor k/2 \rfloor}$. The below table records the quotient of this term by the corresponding variable.

	$v_1^{k,s}$	$w_1^{k,s}$	$w_0^{k,s}$
$C, C, \lfloor k/2 \rfloor, \lceil k/2 \rceil$	$2Y_{\lfloor k/2 \rfloor} C^{k,\lfloor k/2 \rfloor,\lceil k/2 \rceil}_{1,\lfloor k/2 \rfloor-1,\lceil k/2 \rceil-1} v^{\lceil k/2 \rceil,C}_{\lceil k/2 \rceil-1}$	$2Y_{\lfloor k/2 \rfloor} C^{k,\lfloor k/2 \rfloor,\lceil k/2 \rceil}_{1,\lfloor k/2 \rfloor-1,\lceil k/2 \rceil-1} w^{\lceil k/2 \rceil,C}_{\lceil k/2 \rceil-1}$	0
$D, D, \lfloor k/2 \rfloor, \lceil k/2 \rceil$	$2Y_{\lfloor k/2 \rfloor} C^{k,\lfloor k/2 \rfloor,\lceil k/2 \rceil}_{1,\lfloor k/2 \rfloor-1,\lceil k/2 \rceil-1} v^{\lceil k/2 \rceil,D}_{\lceil k/2 \rceil-1}$	$2Y_{\lfloor k/2 \rfloor} C^{k,\lfloor k/2 \rfloor,\lceil k/2 \rceil}_{1,\lfloor k/2 \rfloor-1,\lceil k/2 \rceil-1} w^{\lceil k/2 \rceil,D}_{\lceil k/2 \rceil-1}$	0
$A, C, \lfloor k/2 \rfloor, \lceil k/2 \rceil$	0	0	$2Y_{\lfloor k/2 \rfloor} C^{k,\lfloor k/2 \rfloor,\lceil k/2 \rceil}_{0,\lfloor k/2 \rfloor,\lfloor k/2 \rfloor} w^{\lceil k/2 \rceil,C}_{\lceil k/2 \rceil-1}$

Then $P_{\lfloor k/2 \rfloor}/M_{\lfloor k/2 \rfloor}$ is the determinant of this 3×3 matrix, which is non-zero.

Combining the above, we have shown $P/M \neq 0$ as desired. This completes the proof of part (b) also for $k \geq 4$. □

C.5 Details of the numerical simulations

We used rotavirus VP6 and hemoglobin maps publicly available on EMDB (EMDB-1461 and EMDB-3650). We recentered the rotavirus map EMDB-1461 to have center-of-mass at the origin, and zero-padded it into a cubical volume of dimensions $141 \times 141 \times 141$. The hemoglobin volume EMDB-3650 is already cubical. We centered the values of both maps to have mean value 0.

Fourier quadrature. We computed the Fourier transform $\hat{f}$ of both maps over a spherical grid in the Fourier domain, using the FINUFFT library developed in Barnett et al. (2019). Parametrizing Fourier space by spherical coordinates (ρ, ϕ_1, ϕ_2), we computed $\hat{f}$ on a linearly spaced grid of $150 \times 250 \times 250$ points $(\rho, \phi_1, \phi_2) \in [0, 1/R] \times [0, \pi] \times [0, 2\pi)$, where R is the spatial-domain distance from the origin to the boundary of the cubical volume. All integrals in the Fourier domain were computed using the weighted quadrature defined by this discrete grid with weight proportional to $\rho^2 \sin \phi_1$.

Low-pass filter and basis approximation. For each frequency threshold v, we performed low-pass filtering by simple truncation of the Fourier transform to radii $\rho \in [0, v]$. We then iteratively defined radial functions $z_1, \ldots, z_S : [0, v] \to \mathbb{R}$ satisfying the orthogonality (4.27), so that for each $s = 1, \ldots, S$, the partial basis $\{z_1, \ldots, z_s\}$ maximizes the total power of the projection of the Fourier transform $\hat{f}$ onto the function space

$$\Big\{ z_1(\rho)h_1(\phi_1, \phi_2) + \ldots + z_s(\rho)h_s(\phi_1, \phi_2) : h_1, \ldots, h_s \in L_2(\mathcal{S}^2, \mathbb{C}) \Big\}.$$

In detail, let us denote $u = (\phi_1, \phi_2)$, and $\mathrm{d}u = \sin \phi_1 \, \mathrm{d}\phi_1 \, \mathrm{d}\phi_2$ as the surface area measure on $\mathcal{S}^2$. Then the projection of $\hat{f}$ onto the above space is defined explicitly by

$$h_i(u) = \int_0^v \hat{f}(\rho, u)\overline{z_i(\rho)} \cdot \rho^2 \mathrm{d}\rho \quad \text{for each } i = 1, \ldots, s.$$

The projected power is then

$$\begin{aligned}\text{Power} &= \int_{\mathcal{S}^2}\int_0^v \left|\sum_{i=1}^s z_i(\rho)h_i(u)\right|^2 \cdot \rho^2 \,\mathrm{d}\rho\,\mathrm{d}u = \int_{\mathcal{S}^2}\sum_{i=1}^s |h_i(u)|^2\,\mathrm{d}u \\ &= \int_0^v\int_0^v \sum_{i=1}^s \overline{z_i(\rho)}C(\rho,\rho')z_i(\rho')\cdot\rho^2\,\mathrm{d}\rho\cdot\rho'^2\,\mathrm{d}\rho'\end{aligned}$$

where we have defined the cross-covariance of $\hat{f}(\rho,\cdot)$ and $\hat{f}(\rho',\cdot)$ as

$$C(\rho,\rho') = \int_{\mathcal{S}^2}\hat{f}(\rho,u)\overline{\hat{f}(\rho',u)}\mathrm{d}u.$$

From the orthogonality (4.27), the maximizing functions $z_1,\ldots,z_S$ are such that $\{\rho\, z_1(\rho),\ldots,\rho\, z_S(\rho)\}$ are the S leading eigenfunctions (orthogonal with respect to the standard unweighted L_2-inner-product) of the weighted cross-covariance kernel

$$K(g,h) = \int_0^v\int_0^v \overline{g(\rho)}C(\rho,\rho')h(\rho)\cdot\rho\,\mathrm{d}\rho\cdot\rho'\mathrm{d}\rho'.$$

We approximated this kernel K by its $M\times M$ matrix discretization $K_{\text{mat}} = (C(\rho,\rho')\rho\,\rho')_{\rho,\rho'}$ where M is the number of radial quadrature points $\rho\in[0,v]$. We approximated its eigenfunctions by the eigenvectors of K_{mat}, and divided these eigenvectors by ρ to obtain the values of the radial basis functions $z_1,\ldots,z_S$ along the above radial quadrature.

The final function basis over $\mathbb{R}^3$ was obtained as a product of $\{z_s : s=1,\ldots,S\}$ with the spherical harmonics as described in Section 4.4.2. We used the implementation of the spherical harmonics provided by the `sph_harm` function in scipy. Finally, basis coefficients θ_* were computed by integration in the Fourier domain using the above Fourier quadrature.

$\mathsf{SO}(3)$ quadrature. We computed the empirical Hessian $\nabla^2 R_n(\theta_*)$ by approximating the integral over $\mathsf{SO}(3)$ in the definition of the log-likelihood using a weighted discrete quadrature on $\mathsf{SO}(3)$. Parametrizing $\mathsf{SO}(3)$ by the Euler angles (α,β,γ), we used a discrete grid of $40\times40\times40$ values $(\alpha,\beta,\gamma)\in[0,2\pi)\times[0,\pi]\times[0,2\pi)$, with linearly-spaced grid points and equal weights for (α,γ). For β we also used linearly-spaced points $\beta_1,\ldots,\beta_{40}$, with weights $w_1,\ldots,w_{40}$ computed by numerically solving the equations

$$\sum_{i=1}^{40} w_i D^{(l)}_{0,0}\left((0,\beta_i,0)\right) = \begin{cases}1, & \text{if } l=0\\ 0, & \text{otherwise}\end{cases} \tag{189}$$

for $0 \leq l < 40$. Here $D^{(l)}_{0,0}((0, \beta_i, 0))$ is the middle element of the Wigner-D matrix $D^{(l)}(\mathfrak{g})$, evaluated at $\mathfrak{g} \in \mathsf{SO}(3)$ having Euler angles $(0, \beta_i, 0)$. With proper normalization, this yields an approximate quadrature for band-limited functions over $\mathsf{SO}(3)$.

We note that computing $\nabla^2 R_n(\theta_*)$ for many samples is quite computationally intensive, scaling as $O(nd^2 \cdot |\text{quad}|)$ where $|\text{quad}|$ is the number of quadrature points, and we were consequently limited in the size of this quadrature. Since this quadrature may provide an imperfect approximation to integration over true Haar measure on $\mathsf{SO}(3)$, to mitigate some of the discretization effects, we generated samples $y_1, \ldots, y_n$ using random rotations also drawn from the weighted discrete distribution over $\mathsf{SO}(3)$ defined by this quadrature, rather than from the Haar measure. This does not fully address the numerical inaccuracy, but at least ensures that the true rotation for each sample y_i belongs to our discretization of $\mathsf{SO}(3)$.

We translated this rotational grid in $\mathsf{SO}(3)$ to rotational elements in $\mathsf{O}(d)$ via the Wigner-D representation described in Lemma 4.4.1. We used the implementation of Wigner-D matrices provided by the third-party `quaternion` and `spherical_functions` Python libraries. Finally, these rotational elements in $\mathsf{O}(d)$ were applied to θ_* to generate the samples $y_1, \ldots, y_n$, and also to compute the empirical Hessian $\nabla^2 R_n(\theta_*)$.

Visualizations. The molecular graphics in Figures 4.1 and 4.2 were rendered using the UCSF ChimeraX software Pettersen et al. (2021). We used atomic structures publicly available on PDB (PDB:1QHD and PDB:5NI1). We aligned the rotavirus VP6 structure PDB:1QHD to the 8.2Å-resolution map depicted in Figure C.1(a) using the ChimeraX "Fit in Map" tool. The hemoglobin structure PDB:5NI1 is already pre-aligned to the analyzed map.

C.6 Cryogenic Electron Microscopy (Cryo-EM)

Cryo-EM is a technology for determining the spatial structure of macromolecules. In recent years, cryo-EM has become increasingly popular in structural biology. Thanks to technological advancement in hardware and algorithms in the last decade, cryo-EM now allows scientists to routinely recover structures at near-atomic resolutions. Unlike popular X-ray crystallography techniques for structure determination, cryo-EM does not require the samples to be crystallized. This gives cryo-EM an advantage, in particular, for molecules that are difficult to crystallize, and in heterogeneous samples.

In a typical cryo-EM study, a solution with the molecule of interest is flash-frozen in a thin layer of ice. The particles are sufficiently sparse and the layer sufficiently thin so that when viewed from above, the molecules rarely overlap. Each particle is trapped in the ice at an unknown random orientation. The sample is then inserted into the microscope; an electron beam is transmitted through the sample and then recorded by a camera. A detailed description of the procedure can be found, inter alia, in Glaeser et al. (2021).

The procedure produces a 2D tomographic projection of each particle. For simplicity, in this work we have omitted some effects such as the filters applied in the process (i.e. the contrast transfer function) and the problem of centering the particles, which is less crucial at lower resolutions. In addition, we assume the experimental distribution of viewing directions is uniform. A more comprehensive description can be found in Glaeser et al. (2021), and a more detailed mathematical description can be found in Bendory et al. (2020a). The simplified imaging model is summarized by the equation

$$I(r_1, r_2) = \int_{\mathbb{R}} f(\mathfrak{g}^{-1}\boldsymbol{r})\mathrm{d}r_3 = \int_{\mathbb{R}} (\mathfrak{g} \cdot f)\left((r_1, r_2, r_3)\right)\mathrm{d}r_3, \tag{190}$$

where $\boldsymbol{r} = (r_1, r_2, r_3)$, the function $f : \mathbb{R}^3 \to \mathbb{R}$ is the electric potential, and $\mathfrak{g} \in \mathsf{SO}(3)$ is a rotation. We have expressed this equivalently in the main text as (4.35). In other words, the image is obtained by integrating the z axis of the volume rotated to viewing direction $\mathfrak{g}$ (which is not known to us). The interactions of the electrons with the sample lead to rapid deterioration in the quality of the sample, and very few electrons can be used to record the images before the sample becomes unusable. Therefore, the measurements are characterized by low signal-to-noise ratios.

Taking the Fourier transform of Eq. (190) with appropriate normalization yields

$$\hat{I}(\omega_1, \omega_2) = \left(\mathfrak{g} \cdot \hat{f}\right)\left((\omega_1, \omega_2, 0)\right), \tag{191}$$

where $\hat{I}$ is the Fourier transform of the image and $\hat{f}$ is the Fourier transform of the density map. In other words, in the Fourier domain, the tomographic projection can be conveniently described as taking a slice of the Fourier transform of the volume, at the plane that passes through the origin and is perpendicular to the viewing direction. We have expressed this relation in our analysis as (171), which is characterized in our specific function bases by the projection operator $\Pi^{\mathbb{C}}$ in (4.40).

C.6.1 Cryo-Electron Tomography (Cryo-ET, "Unprojected Cryo-EM")

Cryo-ET is based on the same technology as cryo-EM. However, in cryo-ET several images are taken of each particle, with the sample tilted in a different direction for every image. As in the classic cryo-EM problem above, the relative rotation angles of the different particles are unknown. However, the relative tilt angles of images of *the same particle* are known. By the Fourier-slice relation (191), each image is a slice of the Fourier domain, and thus a dense set of slices from different viewing directions of *the same particle* can be used to reconstruct an entire 3D volume. Unfortunately, due to physical limitations, the tilt angles cannot cover all viewing directions, and a series of cryo-ET tilt images is typically noisier than a cryo-EM image. Thus cryo-ET provides a method of obtaining noisy 3D maps of individual particles, whose relative rotations across different particles are unknown as in the cryo-EM problem. Cryo-ET is more commonly used to study larger samples (e.g. entire cells), but is also used in the study of smaller particles. For additional information, see Eisenstein et al. (2019); Turk and Baumeister (2020). In the main text, we have referred to this problem of reconstructing a map from *unprojected* and rotated 3D volumes also as the "unprojected cryo-EM" model.

A simplified model of cryo-ET, after the tilt series has been reassembled to a 3D function, has the form:

$$f_{\mathfrak{g}}(\omega) = (\mathfrak{g} \cdot f)(\omega) = f(\mathfrak{g}^{-1} \cdot \omega), \tag{192}$$

or, in the Fourier domain:

$$\hat{f}_{\mathfrak{g}}(\omega) = \left(\mathfrak{g} \cdot \hat{f}\right)(\omega) = \hat{f}(\mathfrak{g}^{-1} \cdot \omega). \tag{193}$$

The (projected) cryo-EM model, is related to the cryo-ET model ("unprojected cryo-EM") through the tomographic projection operator Π; in the Fourier domain, Π has the form

$$\left(\Pi \hat{f}\right)(\omega_1, \omega_2) = \hat{f}(\omega_1, \omega_2, 0). \tag{194}$$